Universidad de Málaga
Escuela Técnica Superior de Ingeniería de Telecomunicación

TESIS DOCTORAL

Modulation and Multiple Access Techniques for Indoor Broadband Power-Line Communications

Autor:

José Antonio Cortés Arrabal

Directores:

Luis Díez del Río
José Tomás Entrambasaguas Muñoz

MENÚ SALIR

UNIVERSIDAD DE MÁLAGA

DEPARTAMENTO DE
INGENIERÍA DE COMUNICACIONES

E.T.S. INGENIERÍA DE TELECOMUNICACIÓN
Campus Universitario de Teatinos, E-29071 Málaga (SPAIN)
Tlf.: +34 952131440 - Fax: +34 952132027

D. José Tomás Entrambasaguas Muñoz y D. Luis Díez del Río, profesores doctores del Departamento de Ingeniería de Comunicaciones

CERTIFICAN:

Que D. José Antonio Cortés Arrabal, Ingeniero de Telecomunicación, ha realizado en el Departamento de Ingeniería de Comunicaciones de la Universidad de Málaga, bajo nuestra dirección, el trabajo de investigación correspondiente a su TESIS DOCTORAL titulada: *Modulation and Multiple Access Techniques for Indoor Broadband Power-Line Communications*.

En dicho trabajo se han propuesto aportaciones originales sobre el uso de la modulación DMT para comunicaciones de banda ancha por la red eléctrica del interior de los edificios. Entre ellas cabe destacar las siguientes: métodos analíticos para el cálculo de la distorsión; determinación de los parámetros óptimos de la modulación; diseño de técnicas de recuperación del sincronismo de muestra; estudio del uso compartido de la red mediante acceso múltiple por división en frecuencia. Estas aportaciones han dado lugar a varias publicaciones nacionales e internacionales.

Por todo ello, consideramos que esta Tesis es apta para su presentación a trámite de lectura. Y para que conste a efectos de lo establecido en la normativa reguladora de los Estudios de Tercer Ciclo, AUTORIZAMOS su presentación en la Universidad de Málaga.

Málaga, a 17 de Junio de 2007

Fdo.: Dr. D. Luis Díez del Río

Fdo.: Dr. D. José Tomás Entrambasaguas Muñoz

MENÚ SALIR

UNIVERSIDAD DE MÁLAGA
ESCUELA TÉCNICA SUPERIOR DE INGENIERÍA DE TELECOMUNICACIÓN

Reunido el tribunal examinador en el día de la fecha, constituido por:

Presidente: Dr. D. _____

Secretario: Dr. D. _____

Vocales: Dr. D. _____

Dr. D. _____

Dr. D. _____

para juzgar la Tesis Doctoral titulada *Modulation and Multiple Access Techniques for Indoor Broadband Power-Line Communications* realizada por D. José Antonio Cortés Arrabal y dirigida por los Dres. D. Luis Díez del Río y D. José Tomás Entrambasaguas Muñoz, acordó por

_____ otorgar la calificación de

_____ y para que conste, se extiende firmada por los componentes del tribunal la presente diligencia.

Málaga, a _____ de _____ del _____

El presidente: El secretario:

Fdo.: _____ Fdo.: _____

El vocal: El vocal: El vocal:

Fdo.: _____ Fdo.: _____ Fdo.: _____

MENÚ SALIR

A mis padres
por su amor y sacrificio sin límites

MENÚ SALIR

Si vas a emprender el viaje hacia Ítaca
pide que tu camino sea largo
rico en experiencias y en conocimiento[...]
Ten siempre a Ítaca en la memoria.
Llegar allí es tu meta.
Mas no apresures el viaje.
Mejor que se extienda largos años;
y en tu vejez arribes a la isla
con cuanto hayas ganado en el camino[...]
Ítaca te regaló un hermoso viaje.
Sin ella el camino no hubieras emprendido.
Mas ninguna otra cosa puede darte.

K. Kavafis

MENÚ SALIR

Agradecimientos

En este viaje hacia Ítaca que emprendí hace ya algunos años, he tenido el privilegio de poder aprender de muchos *sabios*. Luis Díez, cuyo ingenio y paciencia nunca han dejado de sorprenderme. Puedo asegurar que la alegría de ver el final de esta etapa no empaña la sinceridad de mi agradecimiento. Tomás Entrambasaguas, cuya organización, rigor y capacidad para reducir los grandes problemas a una sucesión de pequeños obstáculos se han convertido en un auténtico modelo.

Afortunadamente, en la lucha contra los *Lestrigones y Cíclopes* del camino no he estado solo. Desde el primer momento tuve la fortuna de poder contar con Francisco Javier Cañete. En los comienzos fue casi un maestro para mí, y con el paso del tiempo se ha convertido en un compañero inseparable. Su amistad es un lujo del que espero poder seguir disfrutando muchos años. La generosa ayuda de Eduardo Martos, oráculo de la sincronización, y las horas de discusión que hemos compartido son una de las más preciadas *mercancías* que he logrado atesorar.

Las numerosas singladuras se han hecho siempre mucho más llevaderas en la grata compañía de Jesús López, Unai Fernández, José Paris y Nacho Herrero. Su sentido del humor y su compañerismo no caben, me temo, en tan pocas palabras. También las conversaciones con Javier Poncela, implacable ejemplo de honestidad y racionalismo, y la energía desbordante de Mari Carmen Aguayo me han acompañado en este viaje.

Igualmente, durante este periplo ha habido dos personas que me han regalado su valioso tiempo. Lorenzo José Tardón, con quien he tenido el placer de compartir despacho estos años, y Carlos Camacho, cuya puerta ha estado abierta siempre que la he necesitado.

Por fortuna, el devenir del trayecto me ha llevado a otros lugares que me han hecho más *rico en saber y en vida*. Responsables de ello son, en buena medida, Ove Edfors, de la Universidad de Lund, y Andrea Tonello, de la Universidad de Udine.

Ahora bien, si ha habido un verdadero viento de popa en todo este tiempo, ese ha sido el de mis padres. Su amor y sacrificio desinteresado nunca podrán ser correspondidos, y mucho menos con unas líneas en este humilde trabajo. Del mismo modo he sentido el cariño y el apoyo de mi tía Josefa y mi abuela María, quien seguro que intentará leer esta tesis.

Y siempre a mi lado en estos años, Ana. Regalándome su generosidad, su amor y su sonrisa que alegra el alma. Su compañía es el único equipaje que necesito para el resto del viaje.

Este trabajo ha sido subvencionado en parte por la Comisión Interministerial de Ciencia y Tecnología mediante los proyectos TIC2000-1110 y TIC2003-06842.

MENÚ SALIR

Contents

Resumen

A lo largo de la última década ha habido un interés creciente en el uso de las redes de distribución eléctrica para comunicaciones de banda ancha. Se han propuesto tres aplicaciones principales. La primera es emplear las líneas de baja tensión como tecnología de acceso alternativa al bucle de abonado. La segunda es utilizar la red eléctrica del interior de los edificios a modo de red de área local que permita el establecimiento de conexiones de alta velocidad entre ordenadores, periféricos y equipos multimedia. En la tercera el objetivo es usar el cableado que distribuye la corriente en los vehículos como medio de comunicación entre los distintos dispositivos electrónicos del mismo.

Esta tesis se centra en la segunda aplicación y, en concreto, en el estudio de los principales aspectos relacionados con el empleo de la modulación DMT (*Discrete MulTitone*) para dicho propósito. Esta modulación multiportadora está considerada, junto a OFDM (*Orthogonal Frequency Division Multiplexing*), como la técnica de transmisión más apropiada para las comunicaciones por la red eléctrica. Adicionalmente, este trabajo también realiza algunas aportaciones novedosas en el ámbito de la caracterización del canal, del que se proporcionan parámetros que tienen una aplicación directa en el diseño de sistemas de comunicaciones digitales.

En primera instancia se presentan las principales características del canal. Una vez hecho esto se acomete la optimización y el análisis de prestaciones de la modulación DMT en un escenario monousuario. Para tal fin se propone el empleo de un método que permite el cálculo analítico de la distorsión debida tanto a la selectividad espectral como temporal del canal. Con él se determinan los valores óptimos de número de portadoras y longitud del prefijo cíclico. Finalmente se analiza la idoneidad de la igualación temporal mediante un estudio de las ganancias de régimen binario proporcionadas y del incremento en el coste computacional asociado.

La modulación DMT se emplea habitualmente con pulsos rectangulares. El reducido confinamiento espectral de estos pulsos ocasiona un incremento de la interferencia entre portadoras en los entornos monousuario y de la interferencia de acceso múltiple (MAI-*Multiple Access Interference*) en los multiusuario. Del mismo modo, el uso de pulsos rectangulares en recepción aumenta la potencia de fuera de banda captada por el receptor. Es por ello que en esta tesis también se evalúa la conveniencia de usar pulsos no rectangulares tanto en el transmisor como en el receptor de sistemas que operan en escenarios monousuario y multiusuario.

Una vez que se han determinado los parámetros más apropiados para la modulación DMT se investigan los beneficios obtenidos cuando la constelación transmitida se va adaptando a las condiciones instantáneas del canal. Para ello se desarrollan algoritmos de *bit-loading* sujetos

a la clásica restricción de tasa de error media pero aplicados solo en la dimensión temporal o espectral. Además, y para explotar las variaciones periódicas del canal, también se propone un algoritmo de *bit-loading* en el que el promediado se efectúa en ambas dimensiones. Con todo ello se determinan y comparan los regímenes binarios que pueden obtenerse con esquemas de modulación adaptativa y fija sujetos a distintas restricciones de tasa de error.

La sincronización es un aspecto que también se aborda en esta tesis. Si bien se trata de un aspecto fundamental en cualquier sistema de comunicaciones, en el caso de los sistemas que emplean la red eléctrica interior existen dos elementos que lo hacen particularmente importante. El primero es que las características del canal permiten alcanzar eficiencias espectrales elevadas. Por tanto, y para evitar degradar estas prestaciones potenciales, es necesario que el sistema de sincronización se diseñe con especial cuidado. El segundo elemento es la naturaleza variante con el tiempo del canal. La estructura que se propone en esta tesis consiste en un muestreo no sincronizado con corrección en el dominio del tiempo y un esquema de recuperación del sincronismo ayudado por la decisión. El trabajo presentado se centra en este último bloque. En primer lugar se identifican las principales perturbaciones y, a continuación, se proponen soluciones específicas que tienen en cuenta las peculiaridades del canal.

Por último, se analiza la viabilidad de compartir la red interior entre los distintos usuarios empleando un esquema de multiplexación por división en frecuencia. Este esquema es especialmente eficiente cuando se usa DMT, ya que las bandas asignadas a los distintos usuarios se solapan. Además, los flujos de información de los distintos usuarios pueden separarse mediante la transformada discreta de Fourier sin necesidad de un filtrado analógico. En su contra, cabe decir que este esquema es muy sensible a la MAI, que es particularmente dañina en una red no sincronizada. Así pues, en primer lugar se evalúa la importancia de los distintos tipos de MAI. Una vez hecho esto se estudia si mediante el uso combinado de pulsos no rectangulares y la asignación de grupos de portadoras contiguas es posible implementar una red no sincronizada. Finalmente, se determina el número de bits que se requieren en el conversor analógico-digital para llevar a cabo la separación digital de bandas.

Abstract

In the last decade, there has been a growing interest in the use of existing power distribution lines for broadband communications. Three main applications have been proposed. The first one is to employ the low voltage distribution lines as a *last-mile* technology. The second one is to utilize the power distribution grid inside the buildings as a local area network (LAN) to provide high-speed data connections between computers, peripherals and multimedia equipment. In the third one, the in-vehicle power lines are used to communicate the onboard electronic devices.

This thesis is focused on the second application and, in particular, in the study of the major issues concerned with the utilization of Discrete MultiTone (DMT) modulation for this purpose. This multicarrier modulation, along with Orthogonal Frequency Division Multiplexing (OFDM), is currently considered to be one of the most suitable transmission techniques for broadband power-line communications (PLC). In addition, this work provides some novel channel characterization results with straight application to the design of digital communication systems.

In a first instance, the key characteristics of the channel are presented. Afterwards, performance analysis and optimization of DMT in a single-user scenario are addressed. To this end, an analytical method for the calculation of the distortion caused by the frequency and time selectivity of the channel is proposed. This ground is employed to determine the optimum number of carriers and cyclic prefix length. The suitability of time equalization is also studied by assessing the provided bit-rate gain and the increment in the implementation complexity.

DMT is usually employed with rectangular pulse shapes. This is responsible for a reduced spectral containment of the transmitted signal, which leads to an increased intercarrier interference (ICI) in a single-user environment and to multiple access interference (MAI) in a multiuser scenario. Similarly, rectangular pulses increase the out-of-band power captured by the receiver. Hence, this thesis also evaluates the enhancement obtained by using non-rectangular pulses at both ends in a single-user and in a multiuser scenario.

Once the DMT system is properly parameterized, benefits obtained by adapting the transmitted constellation to the instantaneous channel conditions are investigated. To this aim, bit-loading algorithms subject to the classical average bit error rate (BER) criteria, performed only in the time or the frequency dimension, are developed. Additionally, to take advantage of the periodical behavior of the channel, a bit-loading strategy in which the averaging is accomplished in both dimensions is also proposed. Based on this framework, bit-rates obtained with adaptive and fixed modulation schemes subject to different BER criteria are determined and compared.

Synchronization aspects are also tackled in this thesis. Although this is a fundamental issue in any digital communication system, there are two facts that make it especially challenging in indoor power-line scenarios. The first one is that the existing channel conditions allow to achieve large spectral efficiencies. Therefore, the synchronization system must be thoroughly designed. The second one is the time-varying nature of the channel. The proposed structure consists of a non-synchronized sampling with timing correction in the time domain and a data-aided decision-directed timing recovery scheme. The presented work focuses on the latter block. In a first instance, main impairments are identified and, afterwards, ad hoc solutions based on the peculiarities of the channel are proposed.

Finally, this thesis studies the suitability of sharing the indoor network between different users by means of a frequency division multiple access (FDMA) scheme. When using DMT modulation this is a particularly appropriate strategy because the bands assigned to the different users overlap. Hence, the multiplexing process is efficiently accomplished. In addition, users can be separated without the need for analog filtering by means of the receiver DFT. However, this strategy is prone to MAI, which is remarkably harmful in a non-synchronized network. Firstly, the importance of the different MAI sources is assessed. Afterwards, and in order to implement a non-synchronized network, the combined use of non-rectangular pulses and resource allocation schemes in which carriers are assigned on a group basis is analyzed. To conclude, the number of bits required in the analog-to-digital converter (ADC) to perform the digital band separation is determined.

List of Acronyms

ABER	Average Bit Error Rate
AC	Alternating Current
ADC	Analog-to-Digital Converter
AWGN	Additive White Gaussian Noise
BER	Bit Error Rate
BICM	Bit-Interleaved Coded Modulation
BPSK	Binary Phase-Shift Keying
CDF	Cummulative Distribution Function
CDMA	Code Division Multiple Access
CENELEC	Comité Européen de Normalisation Electrotechnique
CSMA/CA	Carrier Sense Multiple Access/Collision Avoidance
DC	Direct Current
DFT	Discrete Fourier Transform
DMT	Discrete MultiTone
DSL	Digial Subscriber Line
DWMT	Discrete Wavelet MultiTone
EMC	ElectroMagnetic Compatibility
ETSI	European Telecommunications Standards Institute
FDD	Frequency Division Duplexing
FDMA	Frequency Division Multiple Access
FEQ	Frequency EQualizer
FFT	Fast Fourier Transform
FIR	Finite Impulse Response
FMT	Filtered MultiTone
IBER	Instantaneous Bit Error Rate
ICI	InterCarrier Interference
IEEE	Institute of Electrical and Electronic Engineering
IP	Integer Programming
ISI	InterSymbol Interference
LAN	Local Area Network
LFEQ	Long-term Frequency EQualizer
LP	Linear Programming
LPTV	Linear Periodically Time-Variying

LS	Least-Squares
LTI	Linear Time-Invariant
LTV	Linear Time-Variant
LV	Low Voltage
MA	Margin Adaptive criterion for the bit-loading
MAC	Medium Access Control
MAI	Multiple Access Interference
MMSE	Minimum Mean-Squared Error
MSE	Mean-Squared Error
MV	Medium Voltage
OFDM	Orthogonal Frequency Division Multiplexing
PDF	Probability Density Function
PLC	Power-line Communications
PLT	PowerLine Telecommunications
PSD	Power Spectral Density
QAM	Quadrature Amplitude Modulation
RA	Rate Adaptive criterion for the bit-loading
RMS	Root Mean Square
SCR	Silicon Controlled Rectifier
SER	Symbol Error Probability
SFEQ	Short-term Frequency EQualizer
SNDR	Signal-to-Noise and Distortion Ratio
SNR	Signal-to-Noise Ratio
SOHO	Small Office-Home Office
TDD	Time Division Duplexing
TDMA	Time Division Multiple Access
TEQ	Time EQualizer
VDSL	Very-high Digital Subscriber Line

List of Symbols

$ABER_f(q)$	Average Bit Error Rate over the frequency dimension
$ABER_t(k)$	Average Bit Error Rate over the time dimension
$ABER_{tf}$	Average Bit Error Rate computed in the time and frequency dimensions
$\mathbf{ABER}_{\Delta b}$	QxN matrix with the average Bit Error Rate when subchannel (q,k) is assigned the immediately higher constellation
$\mathbf{ABER}_{\nabla b}$	QxN matrix with the average Bit Error Rate when subchannel (q,k) is assigned the immediately smaller constellation
$\mathbf{b}$	Matrix with the number of bits per symbol allocated to each subchannel
b_k	Number of bits per symbol transmitted in carrier k
b_k^i	Number of bits per symbol transmitted in carrier k of the i-th link of a multiuser scenario
$b_{q,k}$	Number of bits per symbol transmitted in subchannel (q,k)
B	ADC number of bits
$B_C(t)$	Coherence bandwidth (at 0.9) of a continuous-time LPTV channel at time instant t
$B_D(f)$	Doppler spread of a continuous-time LPTV channel at frequency f
B_Drms	RMS value of the Doppler spread of a continuous-time LPTV channel
$IBER(q,k)$	Bit error rate in subchannel (q,k) of an adaptive DMT system
c_k^i	Coefficient that indicates if the k-th carrier is allocated to the i-th link of a multiuser scenario
cp	Cyclic prefix length, in samples
C	Channel capacity
$d(t)$	Mean excess delay of the impulse response of a continuous-time LPTV system at time instant t
D	Sample index of the beginning of the channel impulse response $(cp+1)$-samples window with highest energy
$D_{\ell,k}$	Distortion at the k-th output of the DFT for the ℓ-th received symbol
$e_\ell(t)$	Limiting error in the analog-to-digital conversion process
E[·]	Mathematical expectation
f	Continuous time frequency
f_0	Mains frequency
f_s	Sampling frequency

F	Confinement of the composite impulse response of the TEQ and the channel
FEQ_k	Value of the frequency equalizer tap for carrier k
$FFT(x[n], N, k)$	k-th output of the N-point Fast Fourier Transform of $x[n]$
$h(t, \tau)$	Response of a continuous-time LPTV channel at time t to an impulse applied at $t - \tau$
$h[n, m]$	Response of a discrete-time LPTV channel at time n to an impulse applied at $n - m$
$h[n]$	Discrete-time impulse response of an LTI system
$h_{ij}[n]$	Discrete-time impulse response of the LTI channel from the transmitter of the i-th link to the receiver of the j-th link of a multiuser scenario
$h_\ell[n]$	Time-invariant term of the channel impulse response at the n-th sample of the ℓ-th symbol
$h_c[n]$	Composite impulse response of the TEQ and the discrete-time LTI channel
$h_{teq}[n]$	Impulse response of the TEQ
$H(t, f)$	Frequency response of a continuous-time LPTV channel
$H(f)$	Time-averaged value of the continuous-time LTPV channel frequency response $H(t, f)$. Alternatively, frequency response of an LTI channel
H_k	Frequency response of a discrete-time LTI channel
$H_{q,k}$	Response of a discrete-time LTPV channel at the frequency of carrier k at the time instant corresponding to the q-th transmitted symbol in each mains cycle
$\measuredangle \widetilde{H}_{q,k}$	Phase of the compensated (by the LFEQ) channel frequency response at the frequency of the k-th carrier of the q-th symbol transmitted in each mains cycle
$H_\ell[k]$	Fourier Transform of $h_\ell[n]$
$H^\alpha(f)$	Order-α coefficient of the Fourier Series decomposition of $H(t, f)$
$H_{pp}(f)$	Peak excursion of the frequency response of a continuous-time LPTV channel
$\widetilde{H}_{pp}(f)$	Normalized value (with respect to the average attenuation) of the peak excursion of the frequency response of a continuous-time LPTV channel
$\measuredangle H(f)_{pp}$	Peak excursion of the frequency response phase of a continuous-time LPTV channel
$Hrms$	RMS value of $\lvert H(f)\rvert$ in logarithmic scale
ICI_z	Power of the ICI suffered by carrier z due to the frequency selectivity of the channel
ISI_z	Power of the ISI in carrier z
k, z	Carrier index
K	Set of carriers employed in a certain operation
ℓ, m, q	Discrete-time symbol index
L	DMT symbol length in samples
L_h	Length of a discrete-time impulse response h[n]
$LFEQ_k$	Long-term FEQ in carrier k
$\mathscr{L}(f)$	Single-Sideband Phase Noise Spectrum

M	Number of notch filters introduced in the timing recovery loop
MSE_q^r	Phase estimation MSE for the q-th symbol transmitted in the r-th mains cycle
n	Discrete time index
N	Number of carriers of the DMT system
$p_k[n]$	DMT transmitter pulse for carrier k
P	Number of regularly distributed samples (within the mains cycle) employed in the measurement of the channel frequency response and of the instantaneous PSD of the received noise
P_e	Bit error probability
$P(t,\tau)$	Power delay profile of an LPTV system
$q_k[n]$	DMT receiver pulse for carrier k
r	Mains cycle index
R	Bit-rate
$R(t,\Delta f)$	Spaced-frequency correlation function of an LPTV channel
$R_U(t,u)$	Autocorrelation function of the cyclostationary signal $U(t)$
$S_s(f)$	Oscillator PSD
$S_a(f)$	Aperture phase noise PSD
$S_U(t,f)$	Instantaneous PSD of of the cyclostationary signal $U(t)$
$S_U(f)$	Time-averaged value of the instantaneous PSD of the cyclostationary signal $U(t)$. Alternatively, PSD of the stationary signal $U(t)$
$S_{U_{pp}}(f)$	Peak excursion of the instantaneous PSD $S_U(t,f)$
$S_{\phi_o}(f)$	Oscillator phase noise PSD
SNR_k	Signal-to-noise ratio in carrier k
$SNR_{q,k}$	Signal-to-noise ratio in carrier k of the q-th symbol transmitted in each mains cycle
t	Continuous time variable
$\mathbf{T}$	Transmission matrix of a DMT system in an LTI channel
$T_{\ell+i,k}^{z,I}$, $T_{\ell+i,k}^{z,Q}$	Complex coefficients by which the respective in-phase and quadrature components of the $(\ell+i)$-th transmitted symbol in carrier k appears at the ℓ-th output of carrier z
T_0	Mains period
T_{DMT}	DMT symbol duration
$U_{\ell,k}$	Noise at the k-th output of the DFT corresponding to the ℓ-th received symbol
$U_{q,k}^r$	Noise at the k-th output of the DFT corresponding to the q-th received symbol in the r-th mains cycle
$w_L[n]$	Rectangular window with L non-zero samples
$w_{RX}[n]$	Window employed in the windowing process of the DMT receiver
$w_{TX}[n]$	Window employed in the pulse-shaping process of the DMT transmitter
$x_\ell[n]$	Discrete-time expression of the ℓ-th transmitted DMT symbol
X_ℓ	Limiting value in the analog-to-digital conversion process
$X_{\ell,k}$	Complex value transmitted in carrier k of the ℓ-th symbol of a DMT system

$X^r_{q,k}$	Complex value transmitted in carrier k of the q-th symbol transmitted in the r-th mains cycle
$X^I_{\ell,k}$, $X^Q_{\ell,k}$	In-phase and quadrature components of the ℓ-th QAM symbol transmitted in carrier k
$Y_{\ell,k}$	k-th output of the DFT for the ℓ-th received symbol
$\widetilde{Y}_{\ell,k}$	k-th output of the FEQ for the ℓ-th received symbol
$Z(t,f)$	Periodially time-varying impedance
α	Length, in samples, of the shaped region at each side of the transmitted DMT symbol
α	Parameter of the timing recovery loop filter
β	Lenght, in samples, of the shaped region in the windowing process
β	Parameter of the timing recovery loop filter
Γ_k	*SNR gap* in carrier k
γ^p_n	Coeffient employed to obtain the n-th sample of the LPTV impulse response by means of the linear interpolation of the impulse response values measured at the p-th and $(p+1)$-th intervals within the mains cycle
Δ	Sample index of the beginning of the confinement window in the TEQ design process
$\Delta b_{q,k}$, $\nabla b_{q,k}$	Number of bits that can be added, or removed, from subchannel (q,k)
$\Delta h^n_\ell[m]$	Time variation of the channel impulse response at the n-th sample of the ℓ-th symbol with respect to $h_\ell[n]$
$\Delta h_\ell[m]$	Magnitude of the channel impulse response variation along the ℓ-th symbol
$\Delta H_\ell[k]$	Fourier Transform of $\Delta h_\ell[m]$
Δf	Frequency offset between the transmitter and the receiver clocks
Δf	Frequency resolution employed in the measurement of $H(t,f)$
Δn	Misalignment, in samples, between the desired and the interferer symbols
$\Delta S_U(f)$	Rate of change of the instantaneous PSD $S_U(t,f)$
Δt	Time resolution employed in the measurement of $H(t,f)$
θ_m	Phase error caused by the uncorrected timing error in the first carrier of the m-th symbol
θ^r_q	Phase error caused by the uncorrected timing error in the first carrier of the q-th symbol of the r-th cycle
$\phi_a(t)$	ADC aperture phase noise
$\phi_o(t)$	Oscillator phase noise
$\phi^r_{q,k}$	Total phase error in the k-th carrier of the q-th symbol transmitted in the r-th mains cycle
ν	Lenght, in samples, of the measured channel impulse response
ξ	Damping ratio of the notch filters introduced in the timing recovery loop
$\sigma(t)$	Delay spread of an LPTV channel at time instant t
σ_a	ADC aperture jitter
σ_{e_ℓ}	RMS value of the limiting error in the analog-to-digital conversion process
σ_{e_q}	RMS value of the quantization error in the analog-to-digital conversion process
σ_o	Oscillator integrated jitter
σ_{rms}	RMS value of the delay spread of an LPTV channel

$\sigma_{z,I}$, $\sigma_{z,Q}$	RMS value of the in-phase and quadrature components of the transmitted values in carrier z
σ_{U_k}	RMS value of the noise at the output of the DFT corresponding to carrier k
$\sigma_{\varphi_{q,k}}$	RMS value of $\varphi_{q,k}$
$\tau_\ell[n]$	Uncorrected timing error in the n-th sample of the ℓ-th symbol entering the receiver DFT
$\tau_o(t)$	Oscillator timing jitter
$\varphi^r_{q,k}$	Phase error in the k-th carrier of the q-th symbol transmitted in the r-th mains cycle due to the channel noise
$\omega_{z,i}$	Frequency (rad/s) of the i-th notch introduced in the timing recovery loop
$\omega_{o,i}$	Natural frequency (rad/s) of the i-th notch filter introduced in the timing recovery loop
$\Re[\cdot]$	Real part
$\Im[\cdot]$	Imaginary part
$\lvert\cdot\rvert$	Modulus
$(\cdot)^*$	Complex conjugate
$\measuredangle(\cdot)$	Angle of the inner function
$<\cdot>$	Time averaging of the inner function
$\overline{\cdot}$	Ensemble average of the inner set
$*$	Convolution
$\lfloor\cdot\rfloor$	Integer part
$\widehat{\cdot}$	Estimated value

Chapter 1

Introduction

1.1 Power-line communications

The utilization of power lines as an information transmission medium dates back to the early 1900's [1]. For many years, their use has been restricted to narrowband systems. In the outdoor part they were firstly employed by utility companies for remote meter reading and telecontrol applications. In the indoor network they were almost restricted to home automation applications [2], [3]. In Europe, these systems exploit the CENELEC band, which extends from 3kHz up to 148.5kHz [4], using rather simple modulation schemes. However, the use of power lines for broadband applications was dismissed because the channel was considered too noise and unpredictable.

The end of European telecommunication monopolies in the late 1990's, along with the advances in digital transmission techniques, opened new business possibilities for power-line communications (PLC). In a first instance, the existing distribution grid from the medium-to-low voltage (MV/LV) transformers to the user premises was proposed as a *last-mile* access to wide area networks. In some cases, this also covered the utilization of the MV network as a backbone to connect LV transformers. Many utility companies all over the world started deployment plans [5]. However, in developed countries, there is a strong competition from digital subscriber lines (DSL) and cable services and the number of actual PLC costumers is not fulfilling expectations. This has caused many companies, like the Spanish utility Endesa [6], to abandon the business. Nevertheless, still there others that go on with the service [7], [8] and outdoor PLC seems to have a promising future in developing countries.

At the same time, the increasing demand for networking applications in the so-called Small Office-Home Office (SOHO) environments focused the attention on indoor PLC. The objective is to utilize the in-building power distribution grid to implement a local area network (LAN). This LAN is not restricted to computer interconnection and also extends to entertainment equipment such as DVD players or high definition TV. In fact, the recent offering of the commonly named triple play service (video, telephony and internet access) by telecom operators, makes PLC an alternative solution for carrying the broadband data connection from the residential gateway

to the television set top box and the computer. In this way, users can share files, printers or even a common internet connection provided by PLC or any other technology. Paradoxically, the high penetration of DSL services that is slowing-down the deployment of outdoor PLC is widening the possibilities of indoor applications. Nevertheless, PLC also has strong contenders in this scenario: in business areas it has to compete against well established solutions, such as Ethernet, and in residential scenarios against wireless networks [9].

In recent years, additional applications of PLC have been proposed. One of these is the use of the in-vehicle power lines for communication purposes [10]. The objective is to communicate the increasing number of electronic devices (on-board computers, sensors, multimedia equipment, etc.) employing the direct-current (DC) cables. By doing so, the vehicle weight could be considerably reduced. Another one suggests that the DC-powered traction network of mass transit systems can also act as a communication channel for train automation purposes [11].

Electromagnetic compatibility (EMC) with existing services is a major concern in PLC. Since power lines were designed for carrying a low frequency signal, at 30MHz wires behave as more or less efficient antennas that radiate the communication signal. Existing EMC regulations in Europe distinguish frequencies below and above 148.5kHz. In the former band, PLC is regulated by the EN-50065 [4]. In the U.S., limits for these systems are established in the FCC Part 15 [12], which extends the available band up to 490kHz. In Japan, PLC are only allowed in the frequency band from 10kHz to 450kHz.

Unfortunately, for frequencies above 500kHz, PLC systems are currently considered as unintentional interferers and the EN-55022 [13] or its equivalent, the CISPR 22 [14], apply. These specifications distinguish between communication and mains ports. Limits for the latter are much rigorous. Since in the particular case of PLC systems one port has both functionalities, it is not clear which one must be complied. In addition, conducted limits are too stringent for communication purposes. At this moment, the European Telecommunications Standards Institute (ETSI) has fixed the frequency range for broadband PLC between 1.6MHz and 30MHz [15]. It differentiates between first and second generation systems. In the former case, there exists a strict frequency band allocation: outdoor systems have been assigned the frequency band from 1.6MHz up to 10MHz, and the band from 10MHz up to 30MHz is designated for indoor ones. The reasons for this assignment are that outdoor links are longer than indoor ones and that cables attenuation increases with frequency. In second generation systems, the aforementioned allocation should be taken as the priority band for each system, but a flexible sharing of the band is allowed. On the other hand, despite an ETSI PLT (Powerline Telecommunications) liaison with CENELEC SC205A has been working in the allowable EMC limits for many years, still there is no regulation for neither the injected power nor the power spectral density (PSD) to be used by PLC systems. However, it seems that the primary restriction will be on the PSD and that multiple transmission gaps will be imposed to the ETSI frequency band [16]. According to [17], [18], reasonable values would be in the range from -35dBm/kHz to -10dBm/kHz.

In addition to the aforementioned regulation effort, the Institute of Electrical and Electronic

MENÚ SALIR

Engineering (IEEE) has recently set up a working group on PLC that includes EMC aspects [19].

PLC transmission systems technology has experienced an enormous change in the last few years. Former standardized narrowband systems like CEBus [20] and EHS [3] achieved maximum bit-rates of about 7kbit/s employing single-carrier modulations with rather simple frequency or amplitude shift keying signals. However, newer proprietary systems attain more than 150kbit/s by employing multicarrier modulations [21].

Similarly, commercial high speed indoor PLC systems have evolved from first generation products at 14Mbit/s [22], to recent ones at 200Mbit/s [23], [24]. Two leading systems achieve this notable performance. One of these has been developed by the Spanish company DS2 [24], while the other is the result of the *HomePlug Powerline Alliance* [25]. Both of them employ Orthogonal Frequency Division Multiplexing (OFDM) with more than 1000 carriers in their physical layers. Constellation in each carrier is selected according to the channel conditions in its frequency band. They both use time division multiple access (TDMA) with time division duplexing (TDD) and a centralized medium access control (MAC). The DS2 system uses the frequency from 1MHz up to 34MHz with a PSD of -20dBm/kHz and with three possible signal bandwidths: 10, 20 and 30MHz. On the other hand, the HomePlug system uses the frequency range from 2MHz up to 28MHz. Pulse-shaping is used to achieve higher spectral confinement. Both systems include coexistence mechanisms with similar devices, but they are not interoperable with each other. Currently, an standardization activity is ongoing at the IEEE with the objective of developing a physical and MAC specifications for outdoor and indoor PLC [26].

1.2 Indoor power-line as a broadband transmission medium

Indoor power lines are quite a hostile medium for broadband communications. Network topology varies with countries [27], although the tree-like arrangement is the most common one [28]. This branched structure is composed of a set of wires with different sections and ended in open circuits or in connected appliances. Since impedances presented by the appliances are quite diverse (absolute values range from a few ohms up to kilo-ohms), a multipath propagation phenomena appear due to the reflections that the signal suffers in every branch, empty socket, or load encountered along the direct path from transmitter to receiver. More than the link distance, the relevant factors in the variation of attenuation with frequency are the number of branches and their relative situation, lengths, and loads. The resultant impulse response of the channel consists of several delayed echoes, which lead to a frequency response with deep notches at a priori unknown position [29]. Time dispersion of the impulse response energy is usually characterized by means of the delay spread [30]. Performed measurements indicate that maximum delay spread values in this environment are around 1.75μs [31], [32]. As a reference, typical values in cellular telephony channels range from 0.2μs in open areas to 3μs in urban ones.

In addition, indoor power-line channel response exhibits a time variation with a twofold origin. The first is a long-term variation caused by the connection and disconnection of the electrical devices [33]. This causes a change in the channel response, usually frequency selective (i.e., not in the entire band) and more remarkable the nearer to the receiver the device is. The second is a short-term variation, synchronous with the mains, due to the dependence of the impedance presented by electrical devices on the mains voltage [34]. These frequency selective periodic variations have gone unnoticed for many years due to the non-synchronized averaging performed in the measurement process, which was designed for linear and time-invariant (LTI) systems. Time variations in the channel response are usually characterized by measuring the spectral broadening experienced by a sinusoid after traversing the channel. In mobile radio channels this figure is usually referred to as Doppler spread, and typical values in current cellular telephony systems range from 1Hz to 100Hz. Measurements carried out in PLC scenarios show that values higher than 100Hz are quite common.

Noise in the indoor power-line environment is one of the most challenging aspects of this channel. It is mainly generated by the electrical devices connected to the power grid, although external noise sources are also coupled to the indoor network via radiation or via conduction. It does not certainly follow the classical additive white Gaussian noise (AWGN) model. Besides narrowband interferences, it is composed of three major terms. One is a cyclostationary component, synchronous with mains, caused by the dependence of the electrical devices behavior on the instantaneous alternating current (AC) value. It typically takes the form of periodical damped sinusoids impulses. This cyclostationary nature has been well-known for many years [35]. In fact, the X10 system [2], exploited the low noise characteristics at the zero crossings of the mains to increase the system robustness. Another component is an asynchronous and non-stationary term which is primary caused by transients due to the connection and disconnection of electrical devices. Finally, there is a background stationary noise term whose PSD decays with frequency.

In the last few years, considerable PLC channel measurements and modeling efforts have been carried out [36], [37]. Two basic approaches have been followed. One is a top-down strategy that considers the communication channel as an LTI system whose frequency response is characterized by a few relevant parameters. The structure of the model is based on the underlying multipath effect, but its parameters are derived from measurements [38], [39]. The most popular model of this group was initially proposed for outdoor channels [39], although it was lately adapted by many authors for indoor scenarios. Alternative strategies following a bottom-up scheme have also been proposed [40], [41], [27]. They allow the computation of the frequency response of a given link based on the network layout, on the characteristics of the wires and on the impedances of the electrical devices connected to the grid. Provided that most of these parameters are usually unknown, the final objective of most of these models is not to exactly match a particular channel configuration, but to serve as a generator of feasible channels. In addition, channel short-term variations can be relatively easily included in these schemes [41].

Despite the aforementioned endeavor, still there are neither reference channels, as in DSL, nor appropriate statistical models, as in wireless. This work employs the bottom-up channel model proposed in [41]. According to it, putting aside the asynchronous noise components, the most

MENÚ SALIR

appropriate channel model for a static network (i.e. without long-term changes) is comprised of a linear periodically time-varying (LPTV) filter plus a cyclostationary noise term.

1.3 Modulation and multiple access techniques

To cope with PLC channel impairments, several transmission schemes have been investigated [42]. This section provides a succinct description of the most common ones.

Single-carrier modulations are the straightest approach. However, their use is precluded by two main factors. Firstly, because of the severe intersymbol interference (ISI) caused by the strong dependence of the attenuation with frequency, which obliges to employ complex equalization and detection structures. Moreover, the classical Viterbi sequence detector is not appropriate because its computational complexity increases exponentially with the impulse response length, which is quite large in power-line channels. In addition, the short symbol periods needed to attain high bit rates makes these modulations extremely vulnerable to impulsive noise. Furthermore, since spectral resources are disperse because of EMC constraints, a single-carrier modulation is not the best suited scheme to make the most from the channel.

Spread spectrum modulations and their natural multiple access technique, Code Division Multiple Access (CDMA), have aroused considerable interest in the last years [43], [44], [45]. Indeed, commercial solutions using these strategies are currently available [46]. The low PSD of the transmitted signal, required to comply with the EMC regulations, and their greater immunity to multipath fading, compared to single-carrier systems, make them adequate candidates for PLC. On the other hand, they do not take advantage of the spectral shaping of the power-line channel, in which signal-to-noise ratio (SNR) differences among bands may be up to 40dB. Powerful equalization schemes are also required. In addition, orthogonal codes and perfect synchronization are needed to avoid the near-far effect that arises in multiuser environments, where the desired signal received from a distant user may be completely hidden by the interference caused by a closer transmitter. Spread spectrum modulations seem to be an interesting solution, in terms of implementation complexity, for moderate to low data rates.

Multicarrier modulations are considered to be the most appropriate transmission techniques for broadband PLC [42]. Accordingly, leading modem manufacturers in this area have selected OFDM, one of their two most common forms along with Discrete MultiTone (DMT), for their physical layers implementation [23], [24]. The basic principle is to divide the available spectrum into subbands or subchannels. Hence, a frequency selective channel is transformed into a set of parallel flat channels in which equalization is easily accomplished by means of a one-tap frequency equalizer (FEQ) [47]. By using the so-called bit-loading, the constellation employed in each subband can be chosen independently according to its particular channel conditions. Those subbands with EMC problems or deep notches are left unused. Therefore, spectral resources can be fully exploited even if they are sparse. An additional consequence of the division into parallel subchannels is that the symbol length becomes longer. Hence, their sensitivity to impulsive noise and ISI is reduced. On the other hand, the decoding delay increases (although it still remains acceptable for most applications) and, as the resulting signal is the sum of a large number of independent components, it exhibits a large peak-to-

average ratio (PAR). Furthermore, considerable interference may also arise in an asynchronous multiuser environment.

Two main multiple access schemes have been proposed to employ OFDM and DMT in a multiuser environment. The straightest one is to use a TDMA scheme with a random access algorithm, similar to the carrier sense multiple access with collision avoidance (CSMA/CA) used in the IEEE 802.11 wireless LAN standard. This scheme is very simple but, since it does not take into consideration link characteristics, it may result in a quite unfair sharing of the medium. In addition, it does not provide the quality of service (QoS) required by multimedia applications. To avoid this end, centralized TDMA schemes have been investigated [48]. The basic idea is to establish special time intervals in which users exchange information about their profiles (e.g. performance of their channels, requested bit rate and priority) and, according to an allocation algorithm, a central node computes the time slot distribution. Alternative hybrid solutions with both CSMA and contention free periods have also been proposed [23]. Nevertheless, since unused carriers in a certain link (because of low SNR) may experience acceptable SNR in other links, the preceding schemes actually waste capacity. Hence, a straightforward extension would be to allow a *secondary* user to utilize the remaining carriers [49]. The price to be paid is the increment in the signaling among users and the multiple access interference (MAI) that the *secondary* user may cause on the *primary* one.

The above strategy is just an intermediate step towards a frequency division division multiple access (FDMA). This process is particularly efficient when employing OFDM or DMT because bands assigned to different users overlap. In the particular case of DMT, carriers allocated to different users can be theoretically separated without the need for an analog filtering by means of the DFT. This process is sometimes referred to as digital band separation and is done at the cost of increasing the number of bits of the ADC. Despite this fact, DMT-FDMA has some additional drawbacks. Firstly, synchronization among users is required to avoid severe MAI [50]. Furthermore, even in the case of synchronized transmissions, the frequency selectivity of the channel causes MAI. Secondly, the optimum carrier allocation scheme is a non-linear optimization problem with thousands of unknowns [51]. Although this problem is usually tackled by means of suboptimal linear programming approaches [52], the MAI dependence on the carrier assignment may require the use of iterative resource allocation procedures. Moreover, the amount of signalling between the users and the centralized manager is considerably high, since per-carrier information must be exchanged. Before the awareness of the channel short-term changes, this was a point in favor of TDMA. However, to cope with these periodic variations, TDMA users must divide the mains cycle into a relatively high number of regions and indicate the bit-rate achieved in these regions to the central node. Hence, this previous advantage of TDMA vanishes in a periodically time-varying channel.

Both TDMA and FDMA can be employed with a time division duplexing (TDD) or a frequency division duplexing (FDD) scheme. Traditionally, traffic asymmetries between both communication directions have been more easily accomplished with the former technique. However, the same flexibility can be obtained with the latter strategy when it is performed by means of the digital band separation. On the other hand, the receiver has to deal with severe echo levels. This is due to the low isolation values provided by the directional coupler employed in the two-

wire to four-wire conversion, which in turns is due to the wide range of input impedance values presented by the power grid. As a consequence, the required resolution of the analog-to-digital converter (ADC) might be notably increased [53].

1.4 Objectives and outline of the thesis

1.4.1 Objectives of the thesis

Performance of indoor PLC systems have experienced significant improvements in a relatively short time period. First generation modems were designed with considerable ignorance of the channel features. Hence, they basically adapted solutions that were known to perform well in other scenarios, mainly DSL and wireless [22]. Latest systems are more tuned to the peculiarities of indoor power-line channels, however, still there is room for advances on many aspects. In addition, most of the academic research effort performed up to now has been concentrated in channel modeling aspects [36], [37]. Therefore, the suitability of some disregarded alternatives have not been sufficiently justified or even considered.

The **main objective** of this thesis is to perform a **comprehensive study** of the main issues related with the utilization **of DMT for PLC**: modulation parameters, adaptive modulation, equalization, synchronization and multiple access techniques. The reason for selecting DMT, instead of OFDM, is because state-of-the-art ADC's easily allows the acquisition of 30MHz signals with more than 12bits of effective precision. By doing so, distortion caused in the downconversion of OFDM signals is avoided [54]. To achieve the above objective, the following partial aims have been accomplished:

- DMT parameters. The number of carriers is one of the key factors in the performance of a DMT system. Its selection involves the following trade-off. Increasing the number of carriers reduces the distortion caused by the frequency selectivity of the channel and improves the transmission efficiency, since the duration of the cyclic prefix represents a smaller percentage of the overall symbol length [28]. In addition, it reduces the out of band power captured by the side lobes of the rectangular pulses employed at the receiver, which is of particular interest in a colored noise environment. On the other hand, it enlarges the symbol length, making the system more sensitive to the channel time variations. Since time variations cause an orthogonality loss among carriers, it increases the intercarrier interference (ICI) [55].

  Values employed by actual systems seems to be driven by implementation complexity rather than by a performance criterion. Hence, one of the objectives of this thesis is to determine the number of carriers that maximizes the performance of a DMT system in the considered scenario.

- Pulse shapes. DMT is usually used with rectangular pulse shapes. This leads to individual carrier spectra that decay only as f^{-2}. In a severe frequency-selective channel with colored

noise, pulse shapes with much faster falls would be desirable. Computationally simple techniques that allow to retain the efficient DFT-based structure of the DMT modem have been fruitfully proven in DSL scenarios [56]. These schemes are also an interesting solution for reducing the MAI in a multiuser FDMA environment. The price to be paid is a reduction in the symbol rate. Parameterization and performance evaluation of these techniques for indoor PLC are also objectives of this thesis.

- Equalization. Equalization in DMT is commonly carried out using a threefold approach. Firstly, a time equalizer (TEQ) is employed to shorten the channel impulse response [57]. Secondly, a cyclic prefix is used to avoid the ISI and ICI caused by the frequency selectivity of the shortened channel impulse response [47]. Finally, channel attenuation suffered by each carrier is compensated in the frequency domain by means of the FEQ [47]. The first approach is successfully employed in DSL systems [58], but it has not been tested in indoor PLC environments. The selection of an appropriate cyclic prefix length is also an important issue. Increasing its length reduces the distortion caused by the frequency selectivity of the channel, but also reduces the transmission efficiency. To the author knowledge, there are no rigorous studies about this issue in the literature related to PLC. Hence, ascertaining the suitability of the TEQ for indoor PLC and the determination of the optimum cyclic prefix length for a given number of carriers have been selected as additional objectives of this thesis. Frequency equalization is not treated in this work. Perfect compensation of the channel frequency response is assumed throughout the study. An insight into the problem can be found in [59], [60].

- Adaptive modulation. The principle behind adaptive transmission is to vary the transmitted power level, the symbol rate, the constellation size, the coding scheme or a combination of these parameters according to the channel state [61]. The objective is to transmit at high data rates when channel conditions are favorable and to reduce the throughput when the channel gets poorer, while guaranteeing a target bit error rate (BER). In this thesis, only constellation adaptation is considered. Provided that indoor PLC channels are time-variant, there is potential room for this adaptive technique to improve the system bit-rate. Moreover, the periodical behavior of the channel opens interesting possibilities. Therefore, it is a goal of the thesis to develop bit-loading algorithms that take into account the cyclic changes of the channel characteristics and to assess their performance gain.

- Synchronization. Synchronization in a digital communication system involves two main tasks: timing recovery and timing correction. The former estimates the phase error of the received symbols and, by means of a feedback loop, computes the correction to be applied by the latter. Synchronization techniques in PLC have to cope with certainly peculiar circumstances. On the one hand, relatively high SNR can be achieved. This implies that a careful design must be done to avoid degrading the potentially high system performance. In this sense, the situation is quite similar to the one in DSL scenarios. On the other hand, the channel is time-variant. This is also the case of wireless channels, but in this environment the achievable SNR is relatively low. Hence, the requirements of the synchronization system can be relaxed. An additional difficulty is that, since indoor

PLC channel time variations can be quite fast [34], the FEQ should be adapted at a rate comparable to that of the synchronization system. This may cause interaction between both adaptive systems and their eventual divergence [62].

The timing correction task in high SNR scenarios has been studied in depth in [63]. Hence, the presented work concentrates in the timing recovery problem. In particular, it is aimed to identify the main drawbacks of already existing solutions and to propose adequate alternatives.

- Multiple access. TDMA-TDD is the multiple access scheme implemented in the current generation of broadband power-line modems [23], [64], probably due to its simplicity. Despite DMT-FDMA has many a priori potential benefits, to the author's knowledge, there is no comprehensive study about its use in an indoor power-line scenario. Hence, this thesis is also intended to analyze the performance of this strategy. To this end, the multiple MAI sources are evaluated: frequency-selectivity of the channel, symbol misalignment and frequency asynchrony. Since MAI is strongly dependent on the carrier assignment, the influence of the carrier allocation strategy on the bit-rate is also evaluated. Finally, the number of bits required in the ADC to accomplish the digital band separation is determined.

Although channel characteristics have been extensively treated in the literature [29], [32], [65], [41]. This thesis also provides some additional insight into the problem. In particular, useful channel parameters and hints for the design and simulation of communication systems are given.

1.4.2 Outline of the thesis

The study carried out to achieve the above objectives has been organized as shown in Fig. 1.1.

After this introduction, chapter 2 provides a description of the main characteristics of indoor power-line channels. Material presented in this chapter is largely based in the work by F. J. Cañete [41]. However, novel results concerning the channel time variation and the noise distribution are provided and discussed.

Chapter 3 introduces the basics of DMT modulation. Once this is done, the optimum number of carriers and cyclic prefix length are determined. To this end, analytical expressions for the distortion terms caused by the frequency and the time selectivity of the channel are firstly derived. Suitability of the time equalization procedure in the considered scenario is assessed. Performance improvements obtained by using alternative pulse shapes are evaluated and, finally, bit-rate gains obtained by using adaptive modulation strategies are investigated.

Synchronization is certainly an involved issue. Accordingly, chapter 4 has been exclusively devoted to its study. In a first instance, an appropriate analog-to-digital conversion model is proposed. Afterwards, the performance of already existing solutions is assessed and, once their

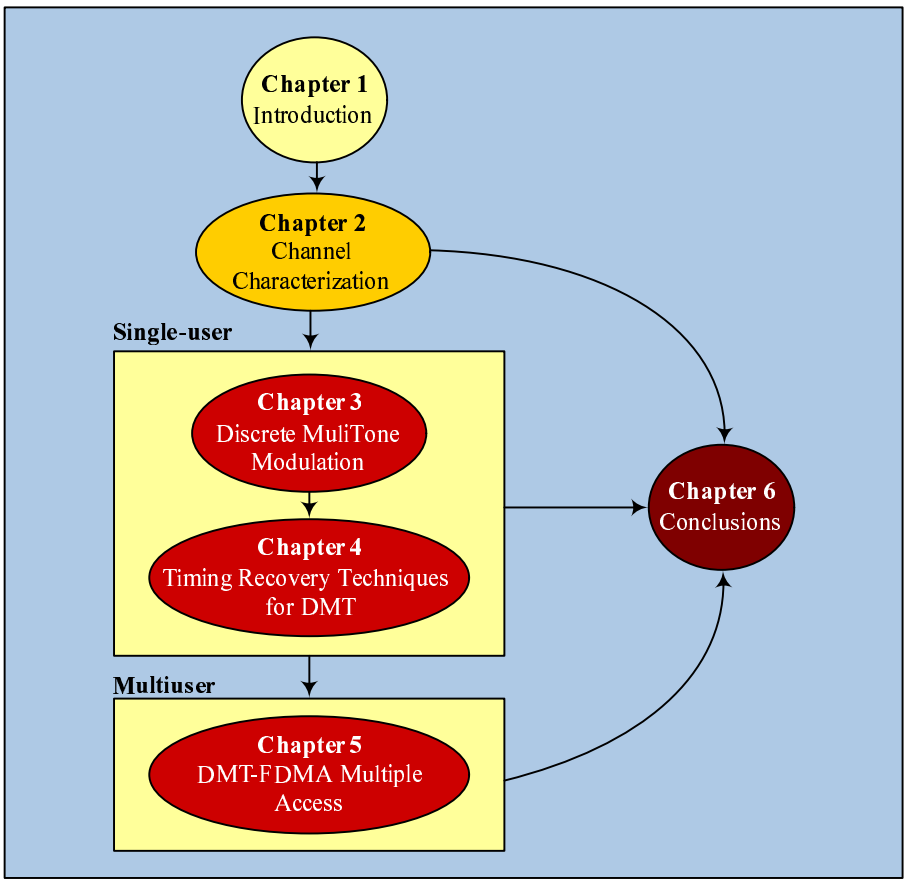

Figure 1.1: Outline of the thesis

main drawbacks have been identified, solutions matched to the peculiarities of indoor power-line channels are proposed.

Aspects discussed in chapters 3 and 4 are exclusively concerned with single-user communications. Multiuser issues are addressed in chapter 5. It starts with an introduction to the mains topics related to DMT-FDMA: MAI, carrier allocation procedures and the digital band separation problems. Afterwards, the performance of a synchronous and an asynchronous implementation of a DMT-FDMA scheme is evaluated by means of an analytical expression derived to compute the different MAI terms. To conclude, the required resolution of the ADC in an FDD and a TDD scheme with digital band separation is investigated.

Finally, main conclusions and achievements derived from the work are summarized in Chapter 6, where suggestions for further work are also discussed.

Chapter 2

Channel Characterization

2.1 Introduction

Power-line communications have been around since the beginning of the 20th century. However, it was not until the second half of the 1990s that the high frequency properties of the channel began to be studied in depth. The celebration of the first *International Symposium on Power Line Communications and its Applications* [37] marked the starting point of an intense research activity that is still ongoing [36].

Indoor power-line channels are frequency and time variant. The former phenomenon is due to the layout of the indoor power distribution network, which usually has a tree-like structure. In most countries it consists of a series of branch circuits that extend from the service panel to the different outlets, where electrical devices can be plugged. Branch circuits are usually made of wires with different diameters ended in open circuits or in connected devices with quite diverse impedance values. This causes impedance discontinuities and, consequently, signal reflections [29][33]. The time variant phenomenon is caused by some electrical devices connected to the power network, whose voltage to current relation depends on the instantaneous value of the mains. Besides this, changes in the working state of the electrical devices also causes long-term variations in the channel [28]. Electrical devices also act as broadband noise generators whose level is also dependent on the mains [32][66]. In fact, they can be considered the most important sources of the noise that reaches any point of the grid. However, there are additional disturbances originated outside by wireless systems and coupled to the wires via radiation, or generated in neighbors networks and conducted from the service panel [29].

This chapter describes the main characteristics of indoor power-line channels and presents the channel models employed in this thesis. To this end, the physical structure of the indoor power network and the behavior of typical electrical devices connected to the grid are firstly introduced. Afterwards, characteristics of the channel response and the received noise are explained. Based on this framework, channel models used throughout of this work are detailed. Finally, the capacity of a frequency and time-selective channel is discussed and approximate values for indoor power-line ones are obtained. To a great extent, results presented in this

chapter are grounded in [41] and in papers [28], [66], [31], [34], co-authored by the author of this thesis.

2.2 Indoor broadband power-line channel characteristics

In most European countries electric power is delivered from the MV/LV transformers using a three-phase scheme. The nominal frequency is 50Hz, the phase shift and the voltage difference between any two phases is 120 degrees and 400Vrms, respectively. However, homes are commonly supplied just one of this phases plus a neutral conductor with 230Vrms between them. These two wires enter the service panel, where circuit breakers and the ground fault current interrupter are located. The layout of the indoor networks is usually not precisely known but, in most countries, there are several circuits pending from the service panel and ended in open circuit outlets or in the electrical devices plugged to the grid. Fig. 2.1 shows its typical tree-like structure. In general, isolation between power lines of neighboring homes is neither guaranteed by the elements in the service panel nor by power meters. Nevertheless, in the ETSI technical report [67], statistical information about attenuation between outlet pairs located in neighbor flats and houses in Europe shows that in 80% of the cases, the attenuation is at least 50dB.

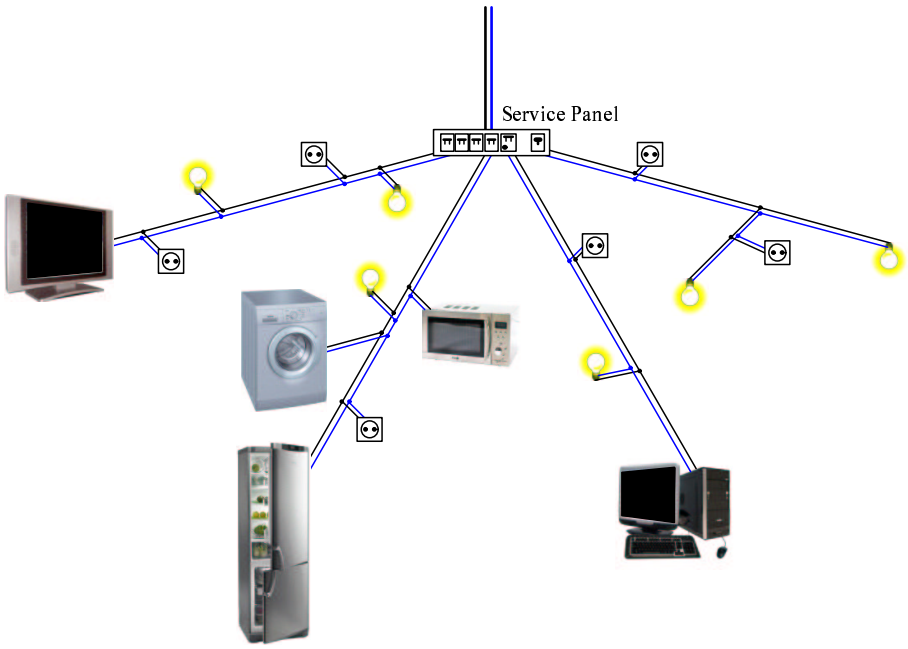

Figure 2.1: Simplified layout of an indoor power network

In power-line transmissions the link is commonly established using the line and neutral conductors. The characteristics of the channel are determined by the network structure (e.g. branch length, relative position, sort of wire, etc.) and by the behavior of the electrical appliances plugged to the grid. Impedance mismatch in the different branches, loads and empty outlets lead to a multipath propagation phenomena. The current to voltage relation of the electrical devices is responsible for a short-term variation of the channel response, which in turns is also

partially responsible for the cyclostationary nature of the received noise. In addition, changes in their working state are responsible for long-term variations of the channel.

Electrical devices can be modeled as one-port circuits consisting of a noise source and a certain load. The input signal to these devices has two components with high separation both in frequency and voltage level: the mains signal and the communications signal. During normal operation, the voltage to current relation in some devices is linear and time-invariant (LTI). Therefore, their load can be completely characterized by means of a frequency-dependent impedance. Similarly, the noise generated by some devices is stationary and can be characterized by their PSD. However, the high-frequency properties of other appliances exhibit an appreciable non-linear behavior exclusively determined by the AC waveform, since the communication signal level is negligible. This leads to a small-signal model whose parameters depend on the instantaneous value of the mains voltage and, hence, are periodic in time. It comprises a cyclostationary noise source characterized by its instantaneous PSD, $S_U(t, f)$, and a linear periodically time-varying (LPTV) load characterized by its short-term impedance, $Z(t, f)$.

Electrical devices with an LPTV load can be categorized in two groups according to their behavior during the mains cycle. The first set contains loads that present two states of impedance value and abrupt transitions between them. The impedance seems to depend on the absolute level of the mains signal, resulting in a periodicity of 100Hz (in Europe). Devices of the second group exhibit impedance values with smoother time variations, usually with the periodicity of the mains $f_0 = 1/T_0 = 50$Hz. In both cases, time variations use to have a remarkable frequency selectivity character. Fig. 2.2(a) shows the impedance of an electric shaver, that belongs to the first group. As seen, the magnitude of the short-term impedance clearly exhibits the aforementioned two-state behavior during a cycle: in the first and third quarter of the cycle there are high values around 20MHz, but they move towards low frequencies in the second and fourth quarter. There are changes of more than 500Ω between these two states at many frequencies. Correspondingly, Fig. 2.2 (b) shows the impedance of a device from the second group (an electric blanket).

The great variety of appliances connected to the grid also makes the characteristics of the associated noise sources quite diverse. Many devices introduce a non-relevant level of noise, while others are really noisy. Some of them have a simple electrical structure and can be modeled as stationary and Gaussian (but seldom white) noise sources. On the other hand, other devices have an interface to the grid that includes circuits whose behavior is strongly dependent on the instantaneous mains signal level, which causes a periodic variation of the noise source parameters. A random process $U(t)$ in which both its mean and autocorrelation are periodical in t with period T_0 is referred to as wide-sense cyclostationary. The Fourier transform of the autocorrelation function, $R_U(t, u)$, is usually referred to as the instantaneous PSD and is given by [68]

$$S_U(t, f) = \int_{-\infty}^{+\infty} R_U(t, u) e^{-j2\pi f u}\, du. \tag{2.1}$$

This function is also periodical in t and its time-averaged value over t is usually called the PSD

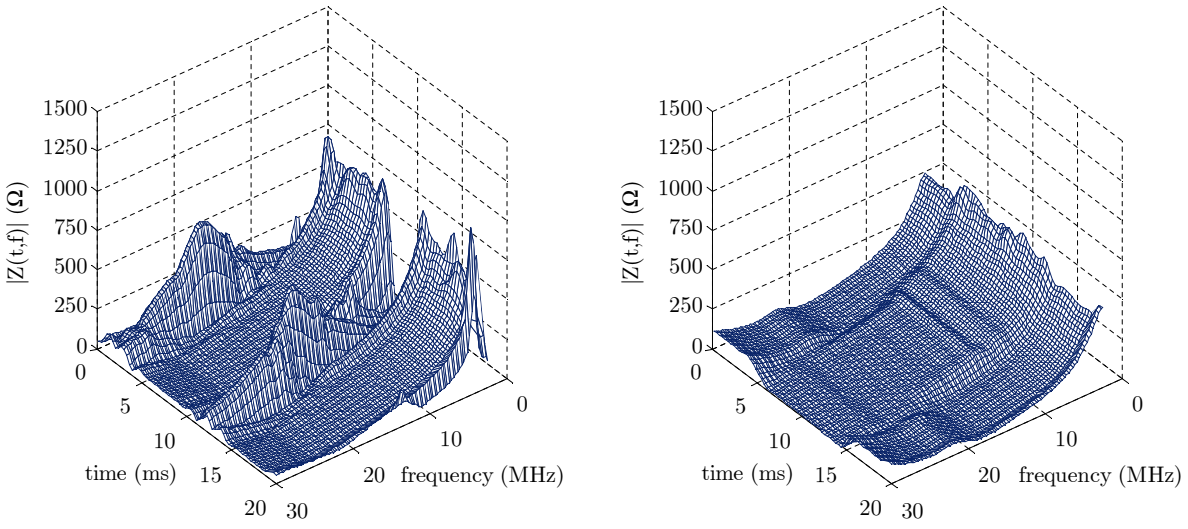

Figure 2.2: Time variant impedance of two electrical appliances with (a) 100Hz periodicity and (b) 50Hz periodicity

of the cyclostationary process,

$$S_U(f) = < S_U(t,f) > = \frac{1}{T_0} \int_{-T_0/2}^{T_0/2} S_U(t,f)\, dt. \tag{2.2}$$

The analysis of a considerable number of devices has revealed that the periodicity of the noise instantaneous PSD can also be 100Hz or 50Hz, depending on whether the devices are affected just by the absolute value of the mains voltage or also by its polarity. Fig. 2.3 shows two instantaneous PSD: (a) with a 100Hz periodicity corresponding to a low-power lamp and, (b), with a 50Hz periodicity generated by a mixer. It is worth noting the remarkable frequency selectivity of the time variations and the high excursion of the changes along the cycle, with more than 20dB at certain frequencies.

In addition to the short-term variations described up to now, changes in the working state of the electrical devices also affect the channel response and the noise level. These changes are usually frequency-selective and become more remarkable the nearer to the receiver the load is. However, their rate is much lower than the common symbol rates employed in communication systems and, hence, the channel can be assumed to have a periodical behavior between them.

2.2.1 Channel response characteristics

Since the indoor power network consists of a set of interconnected transmission lines terminated in non-linear loads, it should be described by means of a nonlinear system. However, there exists certain conditions that facilitate the channel analysis [41]. The first one is that, due to the periodic nature of the large signal component at the input (mains voltage) and its very high level, the channel can be linearized and studied as an LPTV system synchronous with

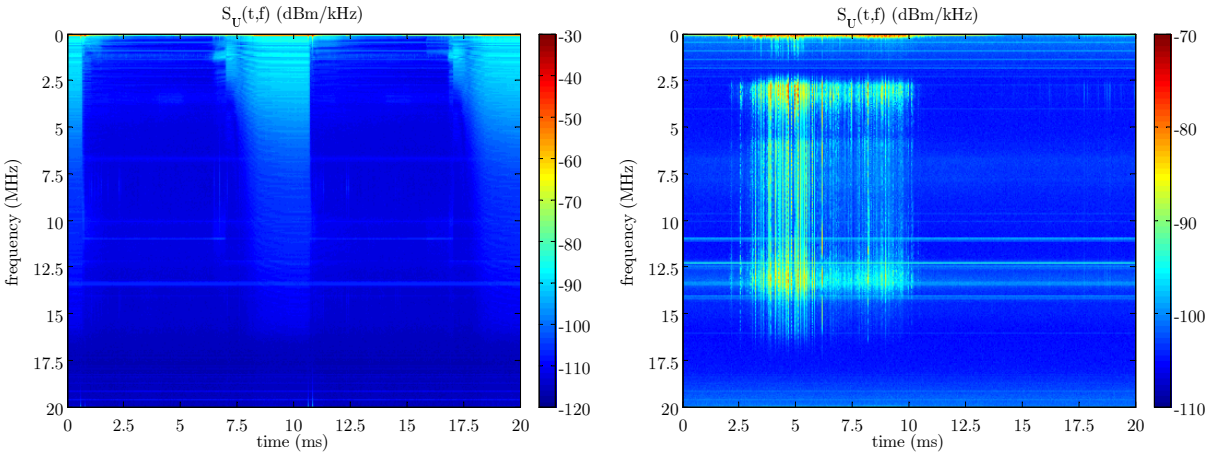

(a) (b)

Figure 2.3: Cyclostationary noise instantaneous PSD of two electrical appliances (a) 100Hz periodicity and (b) 50Hz periodicity

the mains. Its impulse response can be denoted by $h(t,\tau)$, where t is the time at which the response is observed and τ is the time elapsed since the impulse was applied. The frequency response of the system is obtained from the Fourier transform of the impulse response in the variable τ,

$$H(t,f) = \int_{-\infty}^{+\infty} h(t,\tau) e^{-j2\pi f\tau} d\tau, \tag{2.3}$$

which is also a periodical function in t with a period T_0, and thus, can be expanded in Fourier series as follows,

$$H^{\alpha}(f) = \frac{1}{T_0} \int_{-T_0/2}^{T_0/2} H(t,f) e^{-j2\pi\alpha t/T_0} dt. \tag{2.4}$$

The system output to an input signal $x(t)$ can be expressed as

$$y(t) = \int_{-\infty}^{+\infty} h(t,\tau) x(t-\tau) d\tau, \tag{2.5}$$

and its corresponding spectrum by

$$Y(f) = \sum_{\alpha=-\infty}^{+\infty} H^{\alpha}\left(f - \frac{\alpha}{T_0}\right) X\left(f - \frac{\alpha}{T_0}\right). \tag{2.6}$$

The second condition is that measurements show that PLC channels coherence time is several orders of magnitude above the effective length of the channel impulse response. Channels satisfying this criterion are usually referred to as underspread [69]. In general, it also happens that time variations of the channel are quite slow when compared with the rate of change of the communication signal. Denoting by $x_\sigma(t)$ an input signal shorter than the channel coherence time and applied at $t \approx \sigma$ (i.e. an interval around σ), the channel output can be expressed as,

$$y_\sigma(t) = \int_{-\infty}^{+\infty} h(t,\tau) x_\sigma(t-\tau) d\tau \approx \int_{-\infty}^{+\infty} h_\sigma(\tau) x_\sigma(t-\tau) d\tau. \tag{2.7}$$

As the channel impulse response does not change substantially in $t \approx \sigma$, it has been substituted by $h_\sigma(\tau) = h(t,\tau)|_{t=\sigma}$, the LTI response measured in this interval. In the frequency domain the relation can be express as,

$$Y_\sigma(f) \approx H(t,f)|_{t=\sigma} \cdot X_\sigma(f). \tag{2.8}$$

This idea can be generalized to any sort of input signal, because a longer signal can be represented by means of a set of short-time signals,

$$x(t) = \sum_{\sigma \in \Sigma} x_\sigma(t), \tag{2.9}$$

where the union of the time intervals σ define the set Σ that expands the duration of $x(t)$. Since the channel can be assumed linear for the communication signal [34], the channel output is the superposition of the short-time output signals,

$$y(t) = \sum_{\sigma \in \Sigma} y_\sigma(t). \tag{2.10}$$

To illustrate the characteristics of indoor power-line channels, Fig. 2.4 depicts the cyclic amplitude response of a channel registered in an apartment of about 80m^2. Fig. 2.4 (a) shows the magnitude of the time-averaged value of the cyclic frequency response, $|H^0(f)|$, which for simplicity will be denoted as $|H(f)|$. As seen, the frequency-selective character of the channel is clearly manifest. To appreciate the importance of the time variations Fig. 2.4 (b) depicts the magnitude of the amplitude response variations with respect to the time-averaged value,

$$\Delta H(t,f) = 20\log_{10}|H(t,f)| - 20\log_{10}|H(f)| \qquad \text{(dB)}. \tag{2.11}$$

As shown, time variations are quite frequency-selective. In this particular case, the channel response is nearly time-invariant for frequencies above 14MHz. On the other hand, variations of about 4dB occur in frequencies around 4MHz and 13MHz, and up to 10dB around 7MHz. Since the periodic behavior of the channel is caused by devices connected to the grid, the channel responses exhibit similar tendencies in their time variation to the ones of the devices impedance. Hence, there are some with progressive response variation along a cycle, and others with sharp changes between two amplitude states. Similarly, some of them exhibit a 50Hz periodicity, while others have a 100Hz periodicity, as the one in Fig. 2.4 (b).

However, changes in the frequency response affect not only to its module but also to its phase. This circumstance is clearly shown in Fig. 2.5, where the evolution of the frequency response along a cycle is depicted in the complex plane (the meaning of $\widetilde{H}_{pp}(f)$ will explained later on). It is frequent to find situations like the one in curve (b), in which the attenuation remains nearly constant while the phase experiences fluctuations of up to π rad. In other occasions, both the module and phase vary, as shown in curve (a).

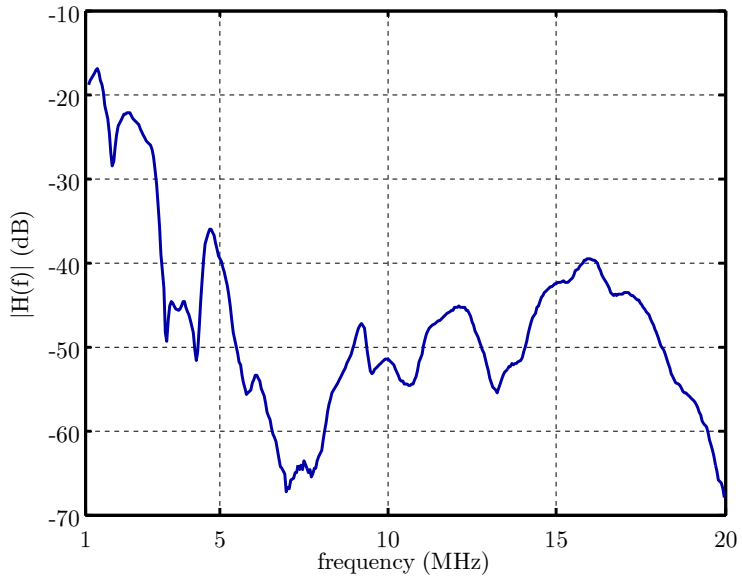

(a)

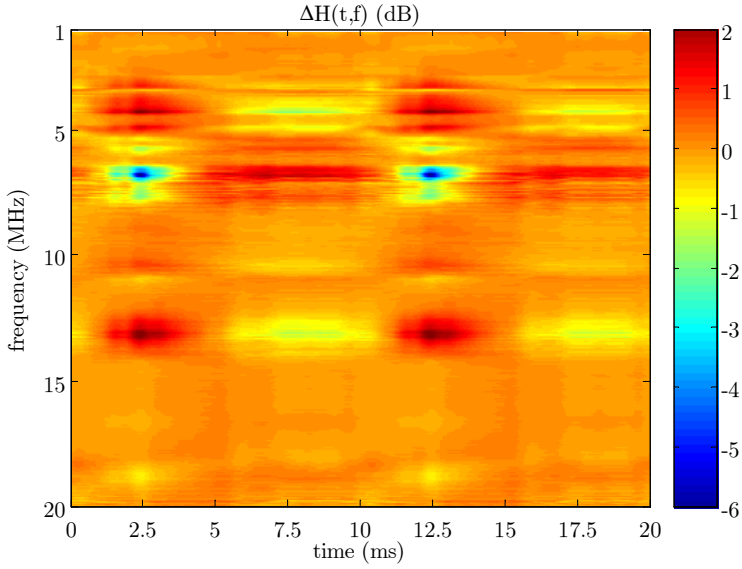

(b)

Figure 2.4: Cyclic frequency response of an apartment channel (a) time-averaged frequency response (b) frequency response variation with respect to the time-averaged value

Statistical characterization

Qualitative features of indoor power-line channels response have been already presented. However, the design of efficient communication systems requires a deeper knowledge of the channel that can only be obtained after extensive measurement campaigns. This section presents a statistical analysis derived from a set of more than fifty actual channels registered in three different scenarios: a university building (laboratories and offices), an apartment of about 80m^2 and a detached house with, approximately, 300m^2. Channels were established between randomly selected outlets with no special care about the devices connected in their neighborhood.

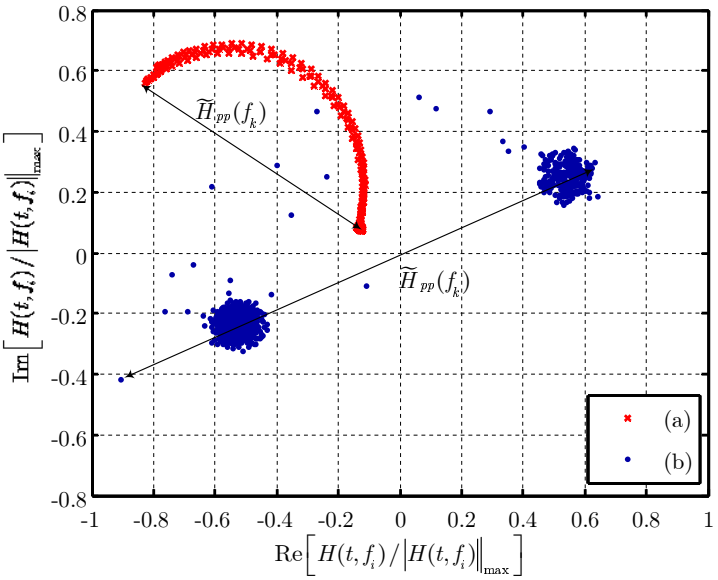

Figure 2.5: Normalized real and imaginary part of the frequency response of two channels in a 20ms time interval. (a) university laboratory at $f_k = 12.5$MHz and (b) detached house at $f_k = 1.4$MHz

A similar number of channels was measured in each scenario. The measurement procedure described in [34] was employed to sample the channel frequency response between 1MHz and 20MHz at $P = 976$ regularly distributed intervals within the mains cycle with a frequency resolution $\Delta f = 25\text{MHz}/512 \approx 48.8\text{kHz}$. Presented parameters can be grouped in three sets. The first one concerns the attenuation profile of the channel. The second one characterizes the channel impulse response and the third one is intended to characterize the short-term variation of the frequency response.

A) Attenuation Profile

In order to study the frequency selectivity of the attenuation, the modulus of each measured frequency response, $|H(t,f)|$ (dB), is computed. Then, a time averaging is performed to obtain the mean attenuation profile of each channel, $|H(f)|$ (dB). Fig. 2.6 shows the averaged $|H(f)|$ (dB), calculated over the channels of each scenario. Corresponding values obtained in the overall set of measured channels are also depicted. As expected, apartment channels are less attenuated than the ones in the detached house and in the university environment, where values below 50dB are experienced in most frequencies. The effect of the increased attenuation of the cables at high frequencies, which is neglected in some channel model proposals [70], is clearly revealed by the dashed lines. They have been obtained by using the classical cable attenuation expression given by

$$|H(f)| = a\sqrt{f} + b \qquad \text{(dB)}, \tag{2.12}$$

where a and b have been obtained according to the least-squares (LS) criterion.

However, the main cause for the higher attenuation values measured in the university building and in the detached house is the multipath effect due to the impedance mismatch and the

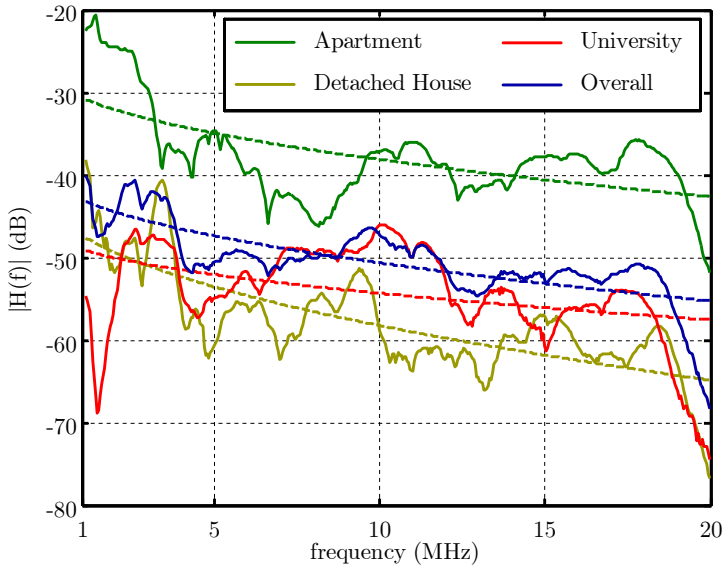

Figure 2.6: Averaged $|H(f)|$ per scenario

branched structure of the indoor power networks. This is illustrated in Fig. 2.7, where the frequency-averaged value of $|H(f)|$ (dB) of each channel, denoted by $< 20\log_{10}|H(f)| >$, is represented against its rms (root-mean square) value, computed according to

$$Hrms = \sqrt{<(20\log_{10}|H(f)| - <20\log_{10}|H(f)|>)^2>} \qquad \text{(dB)}. \tag{2.13}$$

$Hrms$ measures the frequency selectivity of the channel and, as shown in Fig. 2.7, is highly correlated with the averaged attenuation of the channel. It is worth noting that there are no channels below the red line. This indicates that high attenuated channels are very frequency-selective. Similarly, almost all channels are located below the blue line, what reveals that the amplitude response of low attenuated channels is relatively flat.

B) Delay Spread and Coherence Bandwidth

The time dispersion of the channel or, equivalently, the effective length of its impulse response is usually measured in terms of the delay spread. It has a plain application to the design of digital communication systems, since it provides an upper bound for the symbol length that can be employed while keeping ISI at reasonable levels. In the particular case of a DMT system, the delay spread gives an approximate value of the minimum cyclic prefix length that must be employed to avoid ICI and ISI. In power-line channels, due to the periodic variation of the impulse response, the delay spread will be also periodic.

The power delay profile of an LPTV system with impulse response $h(t,\tau)$ can be defined as

$$P(t,\tau) = |h(t,\tau)|^2. \tag{2.14}$$

The mean excess delay is then computed as

$$d(t) = \frac{\int_0^\infty \tau \cdot P(t,\tau)d\tau}{\int_0^\infty P(t,\tau)d\tau}, \tag{2.15}$$

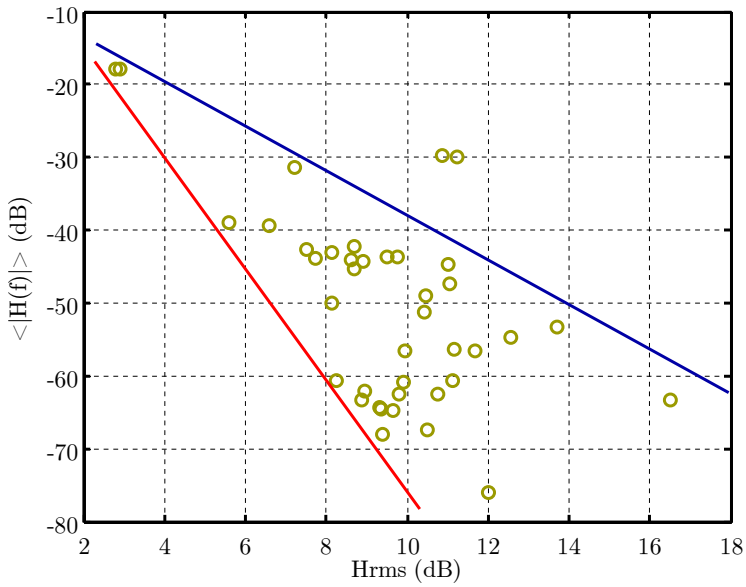

Figure 2.7: Relation between the average and rms values of the channel attenuation

and the delay spread as

$$\sigma(t) = \sqrt{\frac{\int_0^\infty [\tau - d(t)]^2 \cdot P(t,\tau) d\tau}{\int_0^\infty P(t,\tau) d\tau}}. \tag{2.16}$$

For each measured channel, $\sigma(t)$ has been computed and grouped in a subset according to the corresponding scenario (apartment, detached house and university building) in which the impulse response was measured. The cumulative distribution function (CDF) associated to each scenario is depicted in Fig. 2.8 [31]. As seen, 50% of the apartment channels experience delay spreads of about 0.3μs, while this value goes up to 0.65μs in the detached-house. Similarly, it can be observed that channels measured in the detached house experience the greatest delay spreads. The layout of this particular scenario was the larger one and had the more branched topology. As previously discussed, the more branched the network is, the higher number of reflections the signal will found in its way between the transmitter and the receiver, and the stronger time dispersion it will suffer. Results displayed in Fig. 2.8 indicate that, in order to avoid ISI and ICI in all channels, the cyclic prefix length of a DMT system must be longer than 1μs.

In order to analyze the variation of the delay spread along the mains cycle, its rms value can be calculated in each channel according to

$$\sigma_{rms} = \sqrt{<[\sigma(t) - <\sigma(t)>]^2>}, \tag{2.17}$$

where $<\sigma(t)>$ is the time-averaged delay spread, computed as

$$<\sigma(t)> = \frac{1}{T_0} \int_{-T_0/2}^{T_0/2} \sigma(t)\, dt. \tag{2.18}$$

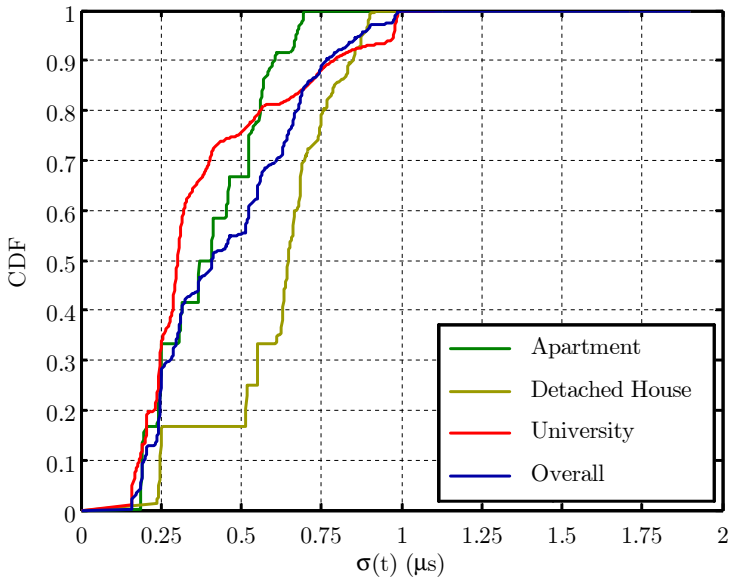

Figure 2.8: CDF of the delay spread values along the mains cycle

Fig. 2.9 depicts the CDF of the values given by (2.17) [31]. For the sake of clarity, they have been expressed as a percentage relative to $<\sigma(t)>$. Considering the overall set of measured channels, it can be seen that 80% of them experience relative variations smaller than 8%. This result shows that the effective length of the impulse response does not suffer significant variations along its period. This fact, although somewhat surprising, is the normal situation in other time varying channels like mobile radio ones. Implications derived from the curves in Fig. 2.9 may be of considerable interest for the design of a DMT system. In particular, for the cyclic prefix length, whose value is strongly dependent on the dispersion of the channel [47]. Thus, this result indicate that cyclic prefix length can be chosen without taken special care about the time instant in which the delay spread of the channel is estimated.

The delay spread is closely related to the channel coherence bandwidth, which can be loosely defined as the bandwidth in which the frequency response is essentially invariant. The coherence bandwidth, $B_C(t)$, at time t is more precisely defined as the frequency separation for which the spaced-frequency correlation function, given by [30].

$$R(t, \Delta f) = \int_{-\infty}^{\infty} H(t, f) H^*(t, f + \Delta f)\, df, \tag{2.19}$$

falls down a given threshold, usually $0.9R(t, 0)$.

The time-averaged coherence bandwidth (at 0.9), $<B_C(t)>$, is then calculated as

$$<B_C(t)>= \frac{1}{T_0} \int_{-T_0/2}^{T_0/2} B_C(t)\, dt. \tag{2.20}$$

Fig. 2.10 depicts the relation between the values of $< B_C(t) >$ and $< \sigma(t) >$ estimated in the overall set of measured channels. As seen, there is a clear correspondence that can be

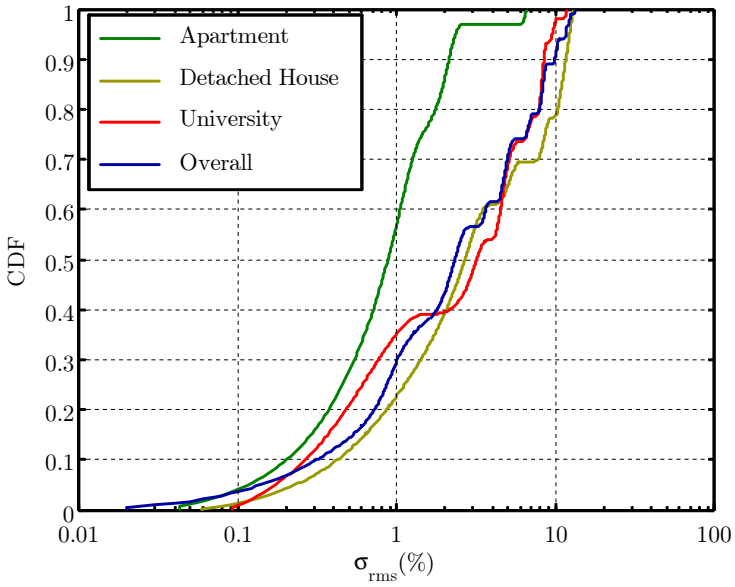

Figure 2.9: CDF of the rms delay spread expressed as a percentage

approximated by [41]

$$<\sigma(t)>\,(\mu\text{s}) \approx \frac{0.097}{<B_C(t)>\,(\text{MHz})}. \tag{2.21}$$

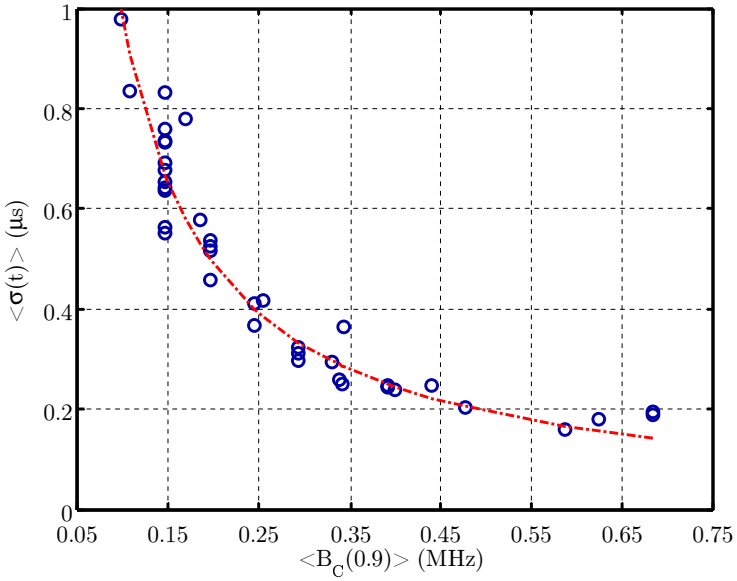

Figure 2.10: Mean delay spread versus coherence bandwidth at 0.9

In a first attempt, values of $<B_C(t)>$ shown in Fig. 2.10 can be employed to determine the minimum number of carriers in a DMT system. Selecting a carrier bandwidth smaller than the minimum coherence bandwidth, e.g. about 50kHz, ensures that carriers will experience a frequency non-selective channel. Hence, if the transmission bandwidth is fixed to 25MHz, at least 500 carriers are required.

C) Frequency Response Short-term Variation

Two parameters are employed to study the frequency response time variation: the first one reflects the peak excursion of the changes, while the second one quantifies their rate. The peak excursion is a parameter commonly employed in the characterization of real signals. This concept can be extended to a complex signal like the frequency response of the channel by defining [41],

$$H_{pp}(f) = \max_{t_1,t_2}\{|H(t_1,f) - H(t_2,f)|\}\ , \tag{2.22}$$

with $t_1, t_2 \in [0, T_0)$. However, to allow the comparison among peak excursions of different frequencies and channels, it is better to express $H_{pp}(f)$ relative to the time-averaged value of the frequency response amplitude, leading to [41]

$$\widetilde{H}_{pp}(f) = \frac{H_{pp}(f)}{|H(f)|}. \tag{2.23}$$

This parameter has a straightforward geometrical interpretation that can be observed in Fig. 2.5, where the values of $H(t,f)$ for a fixed f and $0 \leq t < T_0$ were represented. In this plot, $\widetilde{H}_{pp}(f)$ corresponds to the distance between the two points that are further away in the complex plane.

The values of $\widetilde{H}_{pp}(f)$ have been computed for all the frequencies of the whole set of measured channels. Afterwards, they have been grouped in subsets according to the scenario where their corresponding frequency response was measured. Fig. 2.11 depicts an estimate of the CDF associated to each subset and to the overall set of frequencies and channels [41]. For clarity, the values of (2.23) have been expressed as a percentage. In all the scenarios, the frequency response presents peak excursions greater than 10% in approximately 40% of the cases. However, it should be noted that due to the high frequency selectivity of time variations, the presented CDFs are biased by those frequencies in which the response is nearly invariant, i.e. significant peak excursions measured in certain bands are masked.

The second parameter in this study tries to quantify the rate of channel time variation. It has been estimated by measuring the spectral broadening at the channel output when it is excited with a sinusoid. In mobile radio channels this figure is usually referred to as Doppler spread. In an LPTV channel, the spectral broadening manifests as discrete components harmonically related to $1/T_0$ around the input frequency. In this case, a sort of Doppler spread, $B_D(f)$, can be defined as the largest non-zero Fourier series coefficient of the frequency response, $H^\alpha(f)$. However, since $H(t,f)$ is estimated from real measurements, $H^\alpha(f)$ is non-zero for all values of α. Hence, $B_D(f)$ has been taken as the frequency of the largest coefficient for which $H^\alpha(f)$ has reduced 40dB below its maximum, $H^0(f)$ [71][34].

The values of $B_D(f)$ have been computed for all the frequencies of the whole set of measured channels and grouped in subsets according to the scenario in which they were measured. Fig. 2.12 shows the estimated CDF associated to each scenario, where the quantized nature of $B_D(f)$ at multiples of $1/T_0$ is reflected in the staircase shape of the curves [34]. It is worth noting that not only in 50% of the frequencies the Doppler spread can be even greater than 100Hz, but also in 10% of the frequencies (except for the apartment channels) values are above 400Hz.

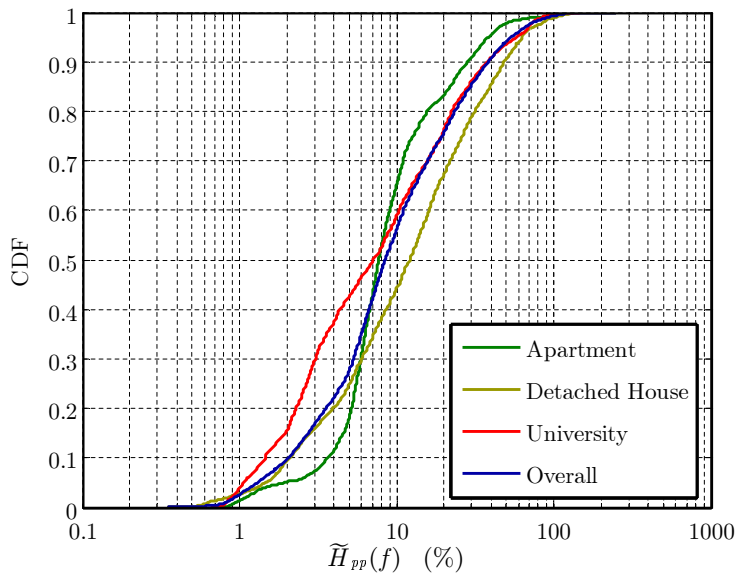

Figure 2.11: CDF of the relative peak excursion of the frequency response expressed as a percentage

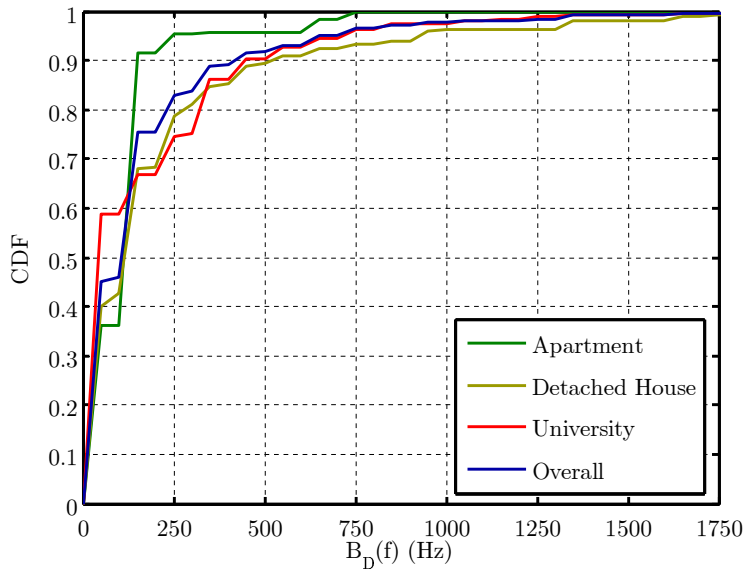

Figure 2.12: CDF of the Doppler spread

As previously suggested, cyclic variations in the channel response are generally frequency selective, i.e., $\widetilde{H}_{pp}(f)$ and $B_D(f)$ and are clearly colored functions for a given channel. This can be highlighted by calculating the rms Doppler spread of each measured channel,

$$B_D rms = \sqrt{<(B_D(f) - <B_D(f)>)^2>}, \tag{2.24}$$

where $<B_D(f)>$ denotes frequency average. Fig. 2.12 shows the estimated CDF of the values of $B_D rms$ corresponding to each channel of the three scenarios [34]. For clarity, values have been expressed normalized to the average Doppler spread of the channel, $<B_D(f)>$. As seen,

no channel experience less than 40% of relative variation, and 50% of them suffer changes up to 140%.

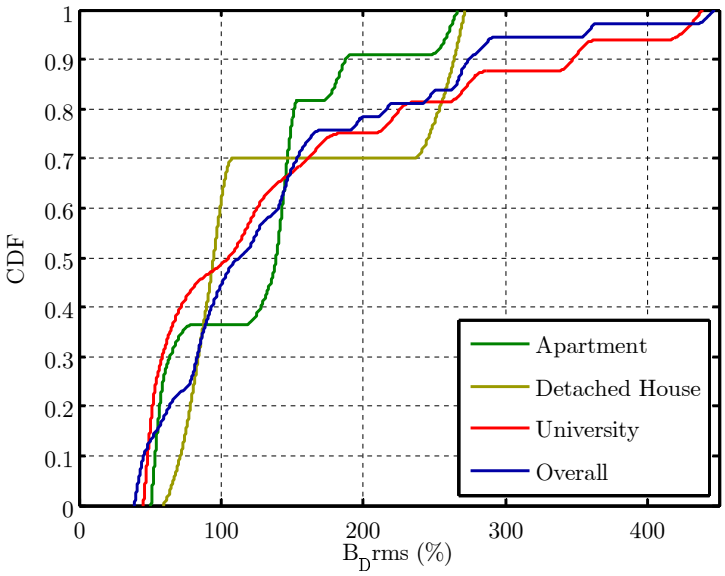

Figure 2.13: CDF of the rms Doppler spread of each measured channel

Results presented in this subsection may be of considerable interest for the design of any digital communication system and, in particular, for DMT ones. Values of $\widetilde{H}_{pp}(f)$ and $B_D(f)$ can be helpful parameters to determine the dynamic range and rate of adaptation needed for the taps of the frequency equalizer (FEQ) commonly employed in DMT. Moreover, the Doppler spread provides very useful information to determine the maximum number of carriers that still guarantees that the channel is essentially invariant during the symbol length.

2.2.2 Noise characteristics

The existent noise in power line communication is far from being the typical AWGN model. It has two main origins: noise generated by the electrical devices connected to the power grid and external noise coupled to the indoor network via radiation or via conduction. According to [65], the following classification can be established:

1. Impulsive noise. It is composed of short duration impulses (some microseconds) which can be also classified according to:

   a) Periodic impulsive noise synchronous with the mains. It is a cyclostationary noise synchronous with the mains and commonly originated by Silicon Controlled Rectifiers (SCR) in power-supplies.

   b) Periodic impulsive noise asynchronous with the mains. It takes the form of impulses with a rate between 50kHz and 200kHz and it is mainly caused by switched power supplies. In addition to this high repetition frequency, most of them also use to

exhibit a lower period equal to the mains one [41]. Hence, it can be also categorized as a cyclostationary noise.

c) Asynchronous impulsive noise. It is usually due to transients caused by the connection and disconnection of electrical devices. It is clearly a non-stationary noise associated with the channel long-term changes and will not be considered in this work.

2. Narrowband interferences. It is mostly formed by sinusoidal or modulated signals with different origins: broadcast stations, spurious caused by electrical appliances with a transmitter or a receiver, etc. Their level varies with daytime, i.e. changes are much slower than those of the communication signal, which allows to treat them as stationary.

3. Background noise. Includes the rest of noise types not included in the previous categories. Although their level depends on the number and type of electrical devices connected to the network, it can be assumed to be stationary. Its PSD decays with frequency.

To illustrate the characteristics of indoor power-line noise, Fig. 2.14 shows the time-averaged instantaneous PSD of the noise measured in an apartment and Fig. 2.15 depicts the variation of the instantaneous PSD with respect to this time-averaged value. As shown in Fig. 2.14, noise is strongly colored with narrowband components that may be caused by interferences or by periodic impulsive noise. In addition, time variations have a frequency-selective nature, as illustrated in Fig. 2.15, with changes of about 10dB in frequencies around 4MHz, 8MHz and 10MHz.

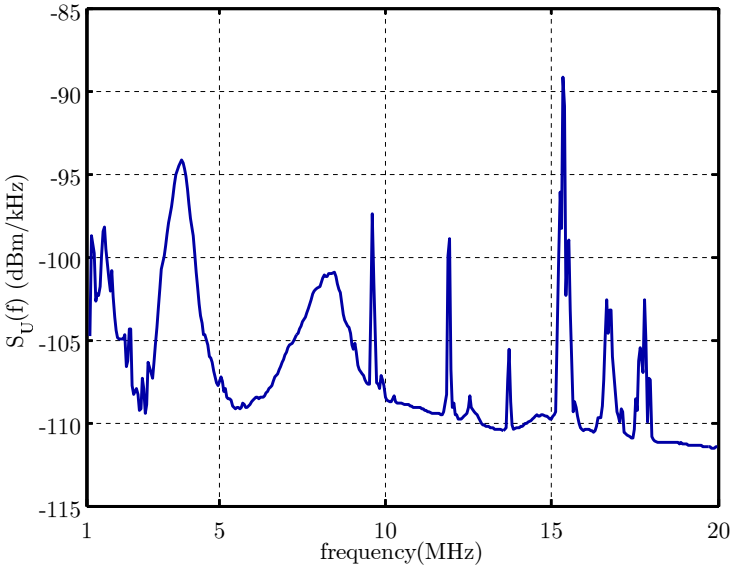

Figure 2.14: PSD of the cyclostationary noise measured in an apartment

Whereas many features of the indoor power-line noise have been extensively studied and there is quite good agreement among results presented in the literature [29], [65], [33], [72], [40], [73], [74], the probability function distribution (PDF) of the noise amplitudes is still unknown or, at least, there are no conclusive results. Broadband measurements performed up to now indicate that when the periodical behavior of the noise characteristics is ignored, the obtained PDF is not

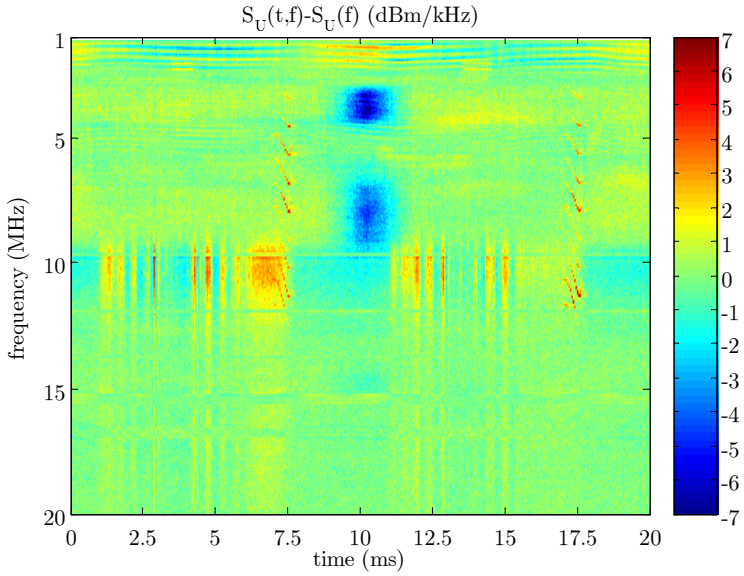

Figure 2.15: Variation of the instantaneous PSD with respect to its time-averaged value shown in Fig. 2.14

Gaussian [40], [73]. This unsurprising result is caused by the impulsive noise components. Fig. 2.16 depicts an estimation of the probability density function of the noise samples amplitude in a detached house. A Gaussian PDF of the same mean and variance has been superimposed for reference. As seen, in the low amplitudes region, both PDF's are quite similar, but the estimated PDF has flatter *tails* than the Gaussian one. This is due to the presence of high amplitude samples caused by impulsive noise components.

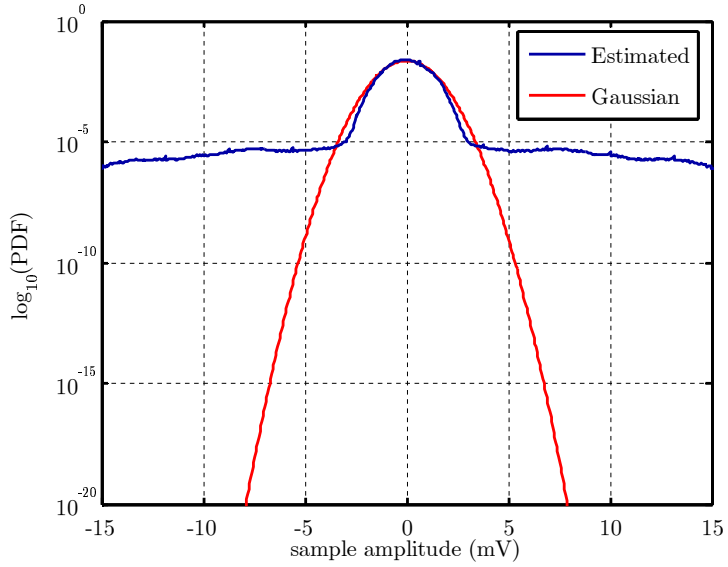

Figure 2.16: PDF of the measured noise samples amplitude and of a Gaussian one with the same mean and variance

However, based on measurements accomplished in the band up to 1.9MHz, it is stated in [74] that when the PDF is computed from noise samples measured at fixed phases within the

mains, the obtained PDF is Gaussian. Even in the absence of asynchronous impulsive noise, this conclusion does not apply to broadband noise. In this scenario, the Gaussian assumption seems to be appropriate for those phases of the mains cycle with no periodic impulsive noise terms. However, in the remaining ones, the almost deterministic nature of the impulsive components make the noise samples amplitude to exhibit a PDF with flatter *tails* than the Gaussian. Both ideas are illustrated in Fig. 2.17, where the PDF of the noise samples amplitude measured in a detached house has been estimated at different phases of the mains cycle.

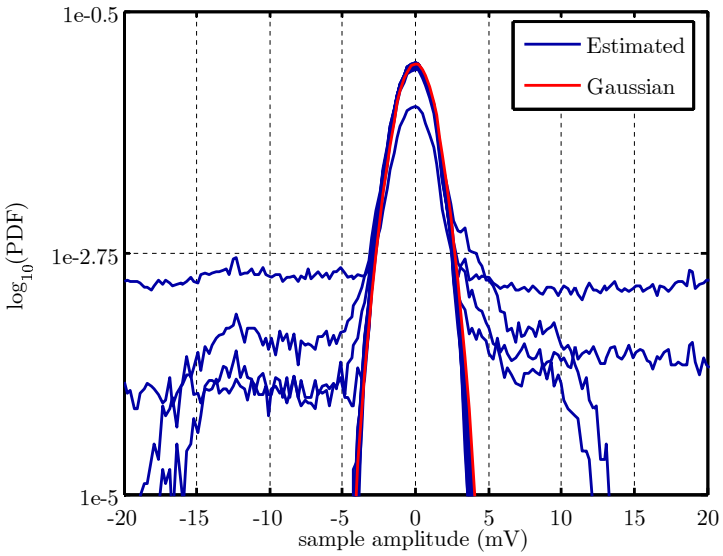

Figure 2.17: PDF of the measured noise samples amplitude at various phases of the mains cycle

Statistical characterization

This section presents a statistical characterization of the noise measured at the receiver's site of the links whose impulse and frequency response has been analyzed in the previous section. Noise is treated as a cyclostationary random process. The measurement procedure described in [34] was employed to sample the instantaneous PSD of the received noise between 1MHz and 20MHz at $P = 976$ regularly distributed intervals within the mains cycle with a frequency resolution $\Delta f = 25\text{MHz}/512 \approx 48.8\text{kHz}$. To separate both the frequency and time behavior of the noise, the PSD is analyzed in a first instance. Afterwards, the short-term variation is evaluated by determining the peak excursion of the instantaneous PSD and the rate at which these changes occur.

A) Noise PSD

In order to study the frequency characteristics of the noise, the PSD of each registered noise has been computed. Fig. 2.18 shows values obtained by averaging the PSDs obtained in each scenario. The dashed lines result from an LS approximation of the form [40]

$$S_U(f) = af^b + c \qquad \text{(dBm/kHz)}. \tag{2.25}$$

As expected, the university building shows higher noise levels and also a stronger colored PSD. This is due to the high and diverse number of electrical appliances connected to its power network. On the other hand, the detached house exhibit much lower levels at nearly all frequencies. The reason is that, while the number of electrical devices is similar to the one in the apartment, the layout is composed of longer and more branched circuits. Hence, noise generated by each device reaches the receiver point through a high attenuated channel (see Fig. 2.6).

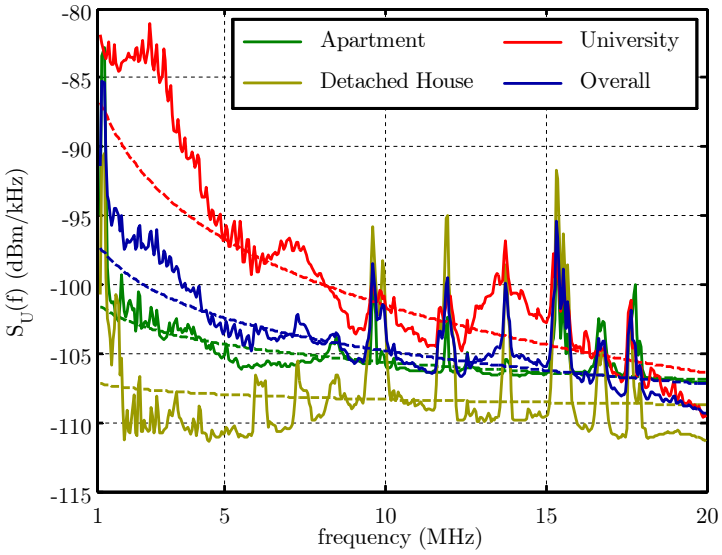

Figure 2.18: Averaged $S_U(f)$ per scenario

B) Noise instantaneous PSD

To characterize the magnitude of the short-term changes in the noise, the peak excursion of the instantaneous PSD is defined according to [34]

$$S_{U_{pp}}(f) = \max_t\{10\log_{10}[S_U(t,f)]\} - \min_t\{10\log_{10}[S_U(t,f)]\} \quad \text{(dB)}, \tag{2.26}$$

with $t \in [0, T_0)$. Similarly, to quantify the velocity of these changes, the rate of change of the noise instantaneous PSD can be defined as [34]

$$\Delta S_U(f) = \max_t\{|10\log_{10}[S_U(t+\Delta t,f)] - 10\log_{10}[S_U(t,f)]|\} \quad \text{(dB)}, \tag{2.27}$$

with $t \in [0, T_0)$ and $\Delta t = T_0/976 \approx 20.5\mu$s [34]. The estimated CDF of the values given by (2.26) and (2.27) have been plotted in Fig. 2.19 and Fig. 2.20, respectively. As seen, approximately in 20% of the situations, the noise peak excursion exceeds 10dB, of which up to 3dB may occur in just 20.5μs. Furthermore, it is also worth noting that the laboratory and the apartment are the environments with the highest values of both parameters for most percentiles. As previously mentioned, in the university site this can be due to the high number of devices connected to the grid. In the apartment, channels are established over shorter and less branched links than in the detached house, due to its smaller size. Therefore, cyclostationary noise components reach most outlets with a level that clearly exceeds the one of the background stationary noise.

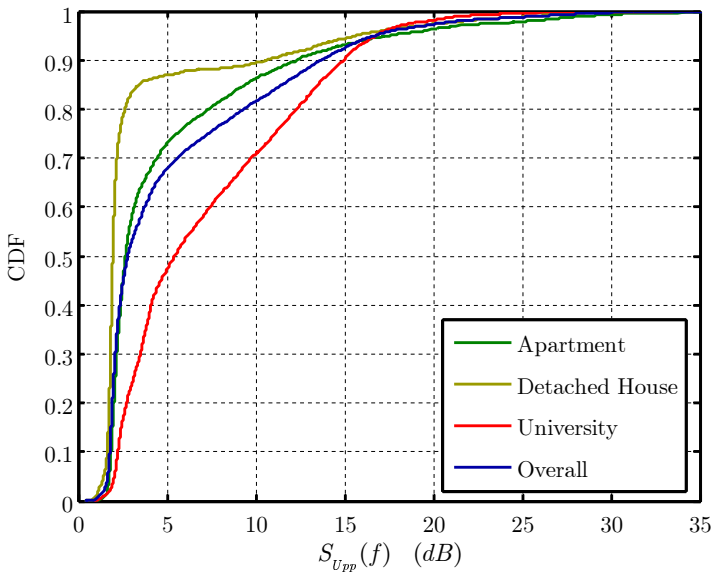

Figure 2.19: CDF of the peak excursion of the noise instantaneous PSD

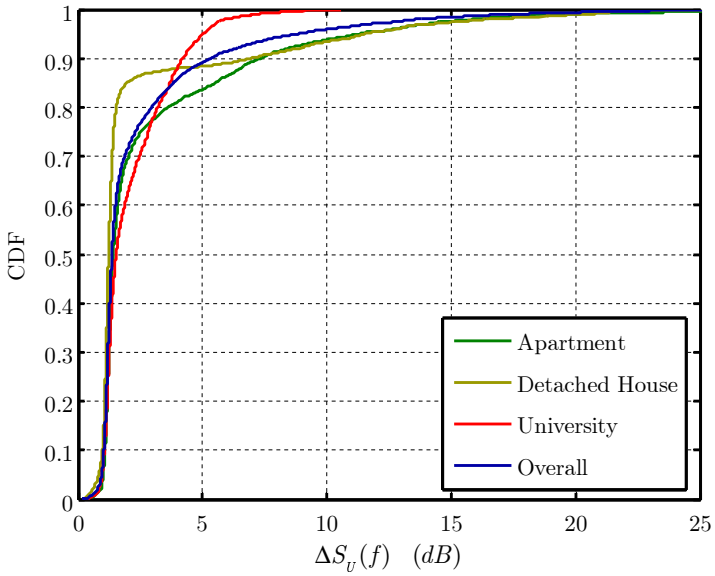

Figure 2.20: CDF of the rate of change of the noise instantaneous PSD

2.3 Channel models

The design of efficient communication systems requires the use of channel models that reflect those characteristics that are relevant for the considered problem. Contrary to what happens in wireless or DSL scenarios, still there are neither appropriate statistical models nor reference channels for broadband PLC. Except for the asynchronous impulsive noise, a suitable model is composed of an LPTV filter plus a cyclostationary noise term [41]. However, the particular behavior of the channel make this model unnecessarily detailed for the analysis of certain aspects of a DMT system. For instance, it has been shown in the previous section that the effective

length of the impulse response remains essentially constant throughout the mains cycle. Hence, in order to determine the performance of a TEQ or to select the cyclic prefix length, there is no need for including the channel time variation in the study.

Based on the above considerations, two channel models are employed in this work. The first one reflects both the frequency and time-selective nature of the channel and is composed of an LPTV filter plus a cyclostationary noise term, as shown in Fig. 2.21 (a). The frequency response of the LPTV filter and the instantaneous noise PSD are taken from the measurements whose statistical characterization has been shown in the previous section. The employed frequency band extends from 1MHz up to 20MHz. The second model only reflects the frequency-selective properties of the channel and is comprised of an LTI filter and a stationary noise term, as depicted in Fig. 2.21 (b). In this case the frequency band extends up to 30MHz, and the utilized frequency response and noise PSD are obtained using the time-invariant version of the channel simulator proposed in [41]. Concretely, the simulator is configured with the layout of an apartment of about 70m^2. This approach has several advantages over the more straighter one in which $H(f)$ and $S_U(f)$ are obtained by means of a time averaging of the frequency responses and instantaneous noise PSD used in the first model. Firstly, since the layout is perfectly known, it is relatively easy to determine those channels with the best and worst transmission characteristics. Hence, upper and lower bounds for the expected performance of indoor PLC systems can be obtained. Secondly, the possibility of placing many transmitters and receivers at the same time, along with the layout knowledge, makes the channel simulator a very useful tool for the generation of multiuser environments.

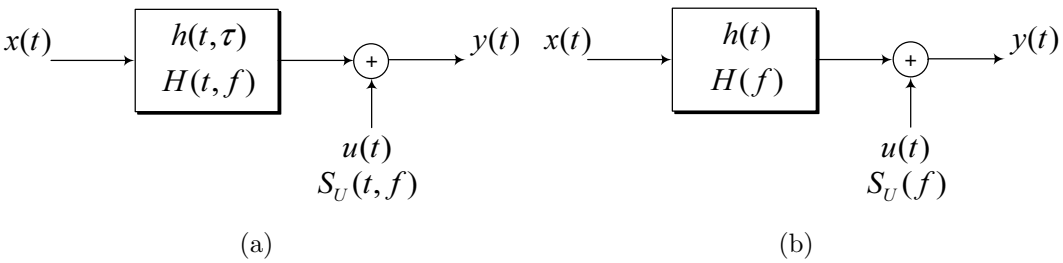

Figure 2.21: Channel models employed in this work (a) cyclic (b) time-invariant

The noise is assumed to have a Gaussian nature both in the cyclic and time-invariant channel models. This assumption is commonly employed in the analysis of communication systems because it provides a lower bound for the performance. Nevertheless, in the particular case of DMT-based systems over broadband indoor power-line channels, it also happens that the Gaussian supposition is not outlandish. Firstly, because it has been shown in the previous section that the background noise can be considered to be Gaussian. Secondly, because the almost deterministic waveforms of the periodical noise make their spectra to be composed of a set of narrowband components. Hence, the noise term in most of the outputs of the DFT performed at a DMT receiver can be assumed to be Gaussian in most phases of the mains cycle.

2.4 Channel capacity

Channel capacity is a fundamental limit in the performance of a communication system. In an LTI channel it denotes the maximum data rate that can be achieved with an asymptotically small error probability [75]. The maximization is performed with respect to the distribution of the input signal and is subject to different constraints, among which the most common one imposes an average power value on the signal launched into the channel. Under this constraint, the capacity of the classical discrete-time AWGN channel is attained by a Gaussian input [75]. Similarly, in a frequency-selective channel in which the frequency response is known by both the transmitter and the receiver, the capacity is achieved by a Gaussian input with a PSD following the water-filling scheme [62, 76].

The capacity of a linear time-varying (LTV) channel is a more subtle concept, since it depends on the knowledge that the transmitter and the receiver have about the channel response. Moreover, the time-variant nature of the channel gives rise to different capacity definitions, depending on whether it accounts for the maximum constant rate maintained in all channel states or for the maximum rate averaged over all channel states [76]. The case where the transmitter and the receiver have perfect knowledge of the channel, commonly referred to as transmitter and receiver channel state information (TRCSI), upper bounds the remaining situations and, in a memoryless channel with a finite set of states, S, can be obtained by [77]

$$C = \sum_{s \in S} C_s p_s, \tag{2.28}$$

where C_s is the capacity of the channel state s and p_s is the probability or the proportion of time that the channel is in state s. This result can be also extended to infinite sets [78], allowing to derive a closed-form expression for the capacity of a time-varying frequency non-selective channel with AWGN. In these circumstances, a Gaussian input signal in which the instantaneous power is varied according to a water-filling distribution in time achieves the capacity when an average power value is used as a constraint [79, 78].

Unfortunately, there is no closed-form expression for the capacity of a frequency-selective time-varying channel with TRCSI. Channel time variations cause the output signal to have larger bandwidth than the input one. This prevents us from using strategies employed to derive capacity in the LTI case, like channel partitioning based on complex exponentials, which are not eigenfunctions of LTV systems. Nevertheless, simple approximations exist for the case where the channel is underspread [80, 81, 76]. Thus, assuming a cyclostationary Gaussian nature for the noise, results presented in [81] can be generalized to obtain an approximation to the capacity of an indoor power-line channel in the frequency band up to the Nyquist frequency, $f_s/2$, under TRCSI conditions

$$C \approx \max_{S_X(t,f)} \left\{ \frac{1}{T_0} \int_0^{f_s/2} \int_0^{T_0} log_2 \left(1 + \frac{|H(t,f)|^2 S_X(t,f)}{S_U(t,f)} \right) dtdf \right\}, \tag{2.29}$$

where $S_X(t,f)$ and $S_U(t,f)$ are the instantaneous PSD of the transmitted signal and the noise, respectively. Maximizing (2.29) with respect to $S_X(t,f)$ subject to an average power constraint

leads to a water-filling in time and frequency scheme in the presence of AWGN [81]. At the moment of writing this thesis, still there is no regulation in Europe about the maximum average power that can be used for broadband PLC purposes. However, it seems that a PSD mask will be imposed to the transmitted signals in order to avoid EMC problems and that this will be the most restrictive constraint. Consequently, a flat PSD of -20dBm/kHz has been selected in this work as a unique constraint. This value is in accordance with the one employed by main modem manufacturers in this area [22, 64]. The use of a PSD constraint considerably simplifies capacity calculations because there is no need to save power during bad channel states, as the water-filling distribution does. On the other hand, it leads to reduced information rate values, since it is more restrictive condition than the average power one. Nevertheless, performance loss in actual systems have been proven to be small [82].

Approximate capacity values of the cyclic model channels described in the previous sections have been computed by evaluating (2.29) with a flat transmitted PSD of -20dBm/kHz. Fig. 2.22 depicts an estimate of the CDF associated to each scenario and to the overall set of channels. For each of these channels, an equivalent LTI channel has also been obtained by calculating their time-averaged frequency response and noise instantaneous PSD. The estimated CDFs of their resulting capacity values have also been drawn in Fig. 2.22 using dashed lines. As expected, the highest values are achieved in the apartment channels, due to their lower attenuation. Similarly, the lowest values are attained in the university building, especially because of the large noise levels caused by high number of electrical devices connected to the grid. It is worth noting that capacity values of the measured channels are lower than those of the LTI channels, although differences are certainly negligible. This is a well-known result in wireless channels at high SNRs [79, 76] and, surprisingly, it also holds in a cyclostationary noise environment.

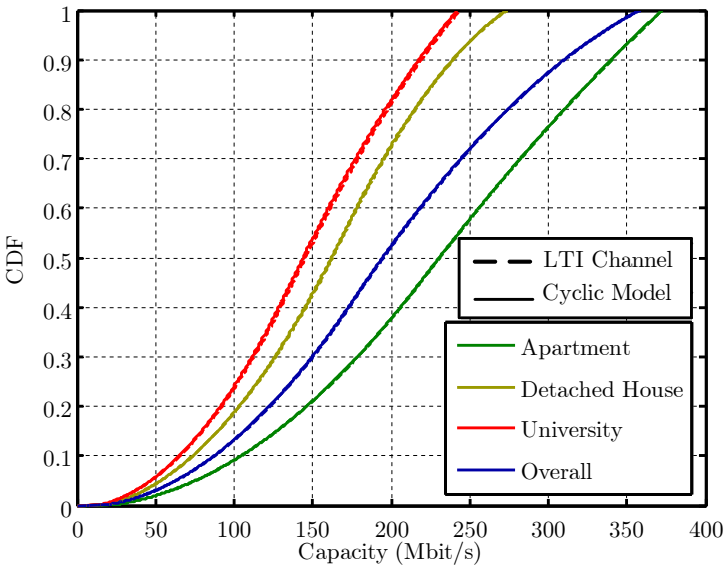

Figure 2.22: CDF of the approximate capacity values of the channels from the cyclic model and of their equivalent LTI channels

Correspondingly, Fig. 2.23 shows the CDF of the capacity values obtained in a set of 56 channels of the time-invariant model presented in the previous section. In order to allow the

comparison with the results displayed in Fig. 2.22 for the apartment site, only the frequency band from 1MHz up to 20MHz has been used. As seen, there is quite good agreement between both CDFs, in particular for CDF values under 0.6.

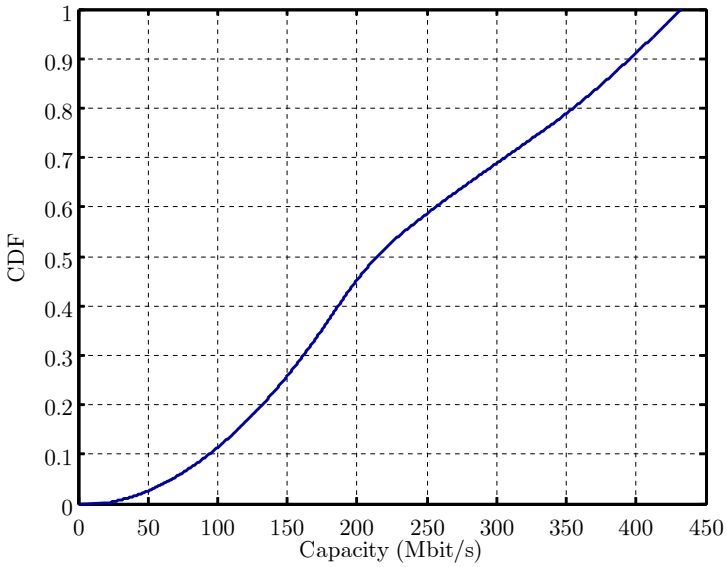

Figure 2.23: CDF of the capacity values for a set of 56 channels of the time-invariant model

Chapter 3

Discrete MultiTone Modulation

3.1 Introduction

The principle behind multicarrier modulations admits a twofold interpretation. From an information theory perspective they can be seen as an attempt to achieve the capacity of a time-invariant frequency-selective channel. By dividing the available bandwidth into a high number of smaller subbands (theoretically infinite) and by proper power allocation, the water-filling distribution may be attained. From a more practical communication point of view, the transmission of the incoming data stream by means of multiple carriers with smaller bandwidth facilitates channel equalization. This fact, along with the adaptation of the carriers constellations according to their particular SNR conditions, allows to accomplish high spectral efficiencies.

The history of multicarrier modulations dates back to 1958, when the Collin's Kineplex modem achieved 3kbit/s by transmitting several carriers at the same time [83]. Although this modem performed more than ten times faster than any other in existence at that time, the hardware complexity of these systems made them impractical until an efficient implementation based on the use of the DFT was proposed in [84]. Another important contribution to development of multicarrier systems was the introduction of the cyclic prefix [85], by which carrier and symbol orthogonality can be retained in time dispersive FIR channels with minimal implementation complexity.

Multicarrier techniques comprise a family of modulations from which OFDM and DMT are their two most common forms. Although both of them are based on the same principle, the term OFDM is usually employed to name the technique in which a digitally generated complex baseband signal is upconverted via analog modulation. In a DMT system, a real baseband signal is converted to analog and launched into the channel. Currently, most popular broadband PLC systems employ OFDM for their physical layer implementation [23, 24]. Nevertheless, since state-of-the-art ADC's easily allows the acquisition of 30MHz signals (the bandwidth allocated by ETSI [15]) with more than 12bits of effective precision, the utilization of DMT modulation

is proposed in this work. By doing so, signal degradation due to frequency offsets and phase noise of the local oscillator used for the downconversion of OFDM signals is avoided [54].

The reduced spectral containment of the OFDM and DMT subchannels is one of their main problems. The use of rectangular pulses with their sinc-shaped spectrum has a double effect. The transmitted signal has considerable out-of-band power, which may produce considerable ICI in case of synchronization errors, when passing through a time dispersive channel or in a non-synchronized FDMA multiuser environment. From the receiver point of view, the low decay of the side lobes of the sinc increases the out-of-band power captured in each subchannel. This certainly worsens the aforementioned problems and, due to the non-white nature of power-line noise, it also increases the received noise power in each carrier. However, it has been shown that by carefully employing non-rectangular windows at the transmitter and at the receiver, these problems can be minimized while retaining the efficient DFT-based structure [84, 86, 56].

Other multicarrier modulation that have aroused considerable interest in the last years are FMT (Filtered Multitone) [87] and DWMT (Discrete Wavelet MultiTone) [88]. The pros and cons of the latter when used in power-line scenarios has been studied in [89]. It is shown that, although DWMT pulses have higher spectral containment, the severe distortion caused by multipath propagation obliges to use very long symbols and a more complex equalization structure than the one employed in OFDM or DMT. In addition, to obtain bit-rates comparable to the ones of these systems, symbols must be overlapped in time, which in turns difficulties synchronization.

The objective of this chapter is to analyze and design some of the main aspects of a single-user DMT system working over indoor power-line channels. To this end, the model of a DMT system is firstly described and an analytical procedure for the estimation of the distortion terms caused by the frequency and time dispersion of the channel is presented. The optimum number of carriers and cyclic prefix length are determined and the benefit provided by the pulse-shaping and windowing techniques is assessed. Afterwards, performance improvements obtained by adapting the constellation transmitted in each carrier along the mains cycle is evaluated. Finally, main conclusions drawn from the chapter are summarized. Most of the results presented in this chapter have been partially published in papers [90], [28], [91] co-authored by the author of this work.

3.2 DMT system model

This section describes the basic elements of a DMT system. It starts with the description of the modulation and demodulation processes and the techniques used for channel equalization. In a first instance, DMT modulation with rectangular pulses is presented. Afterwards, pulse-shaping and windowing principles are also explained. To avoid confusion, from now on the former system will be referred to as conventional DMT, or simply DMT, and the latter as DMT with pulse-shaping and windowing. In addition, fundamentals of the bit-loading procedure, which is in charge of selecting the constellation to be used in each carrier, and the symbol synchronization

process, which determines the exact beginning of the DMT symbols at the receiver, are also discussed. An excellent summary and well referenced introduction to most of these topics can be found in [47].

3.2.1 DMT system with rectangular pulses

The discrete-time model of the ℓ-th symbol of a N-carriers DMT system can be expressed as

$$x_\ell[n] = \sum_{k=-(N-1)}^{N} X_{\ell,k} \cdot p_k[n], \tag{3.1}$$

where $X_{\ell,k}$ are the values that modulate the amplitude of the complex finite duration pulse transmitted in carrier k,

$$p_k[n] = \frac{1}{2N}\, e^{j\frac{2\pi}{2N}kn} w_{2N}[n], \tag{3.2}$$

where $w_{2N}[n]$ denotes a rectangular window with $2N$ samples

$$w_{2N}[n] = \begin{cases} 1 & 0 \le n \le 2N-1 \\ 0 & \text{elsewhere} \end{cases}. \tag{3.3}$$

Symbols transmitted in different carriers overlap both in time and frequency, which results in high spectral efficiency, as shown in Fig. 3.1. Orthogonality is guaranteed by the fact that all carriers frequencies are multiple of the DMT symbol rate,

$$\sum_{n=0}^{2N-1} p_k[n]p_i[n] = \frac{1}{2N}\delta[k-i]. \tag{3.4}$$

The resulting DMT signal,

$$x[n] = \sum_{\ell=-\infty}^{\infty} x_\ell[n-\ell L], \tag{3.5}$$

where $L = 2N$ is the DMT symbol period, is then converted to analog and launched into the channel. Since there is no carrier modulation (as in OFDM) samples of $x_\ell[n]$ must be real valued. To this end, the following hermitical symmetry conditions are imposed

$$\begin{array}{c} X_{\ell,k} = X^*_{\ell,-k} \;\; \text{for } k = 1, 2, ...N-1 \\ X_{\ell,0}, X_{\ell,N} \;\in \Re \end{array}. \tag{3.6}$$

It is interesting to note that expressions (3.1) and (3.5) correspond to a multipulse PAM (Pulse Amplitude Modulation) with $2N$ orthogonal pulses [62]. However, due to the redundancy introduced to make the transmitted samples real valued, the amount of information in a DMT symbol equals only the one conveyed by a sum of N QAM (Quadrature Amplitude Modulation) symbols.

At the receiver, the values transmitted in each carrier can be recovered by employing a bank of matched filters, $q_k[n] = 2N\, p_k[2N-1-n]^*$, as shown in Fig. 3.2.

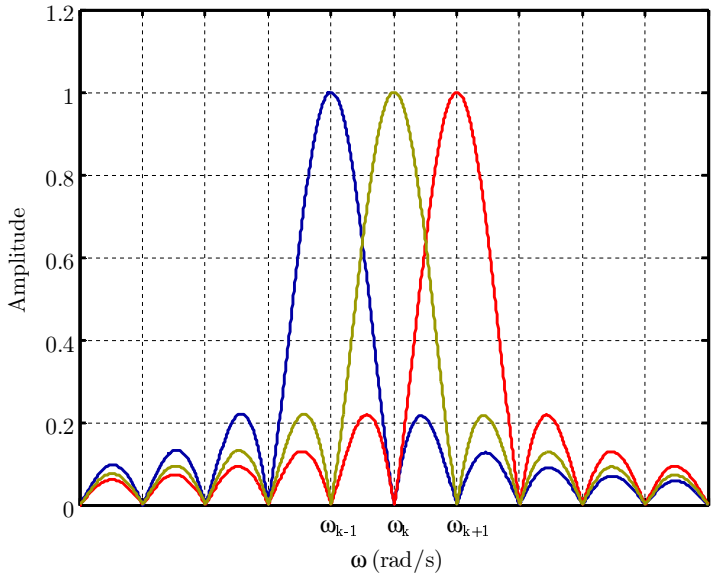

Figure 3.1: Normalized power spectrum of three consecutive carriers

One of the major advantages of DMT comes from the observation that the samples of each transmitted symbol can be obtained by means of an $2N$-point IDFT of the sequence $X_{\ell,k}$ [84]. Similarly, the demodulation of the ℓ-th symbol can be performed by computing a DFT over the $2N$ samples of $x_\ell[n]$. The resulting scheme of the DMT transmitter and receiver is shown in Fig. 3.3. This efficient implementation reduces the $4N^2$ complex products of each filter bank to the $2N\log_2(2N)$ ones needed by Fast Fourier Transform (FFT) algorithms [92].

Equalization

A DMT system with an infinite number of carriers may operate over an LTI channel with a finite impulse response (FIR) without distortion. However, in a system with a practical number of carriers, the transient that appears at the beginning of each symbol is no longer negligible when compared with the DMT symbol length. As a consequence, orthogonality among symbols and carriers is lost. Fig. 3.4 shows this effect in the case of a one-shot transmission. For simplicity, the DMT symbol has been drawn as a set of continuous sinusoids, from which only the first three are shown. The transient is, in fact, the sum of the transients to each of the sinusoids. Hence, ICI will appear after the computation of the DFT. In the case of a continuous transmission, the transient also contains information from past symbols and ISI is also generated. It must be remarked that ICI will appear even if the transmitted symbols are preceded by an empty guard interval.

Equalization of the received signal can be done with a reduced computational cost by using the so-called cyclic prefix. The cyclic prefix is just a periodic extension of the DMT symbol and can be efficiently performed by preceding the original DMT symbol with its last samples, as shown in Fig. 3.5.

A DMT signal with cp samples of cyclic prefix can still be expressed using (3.5) just by setting

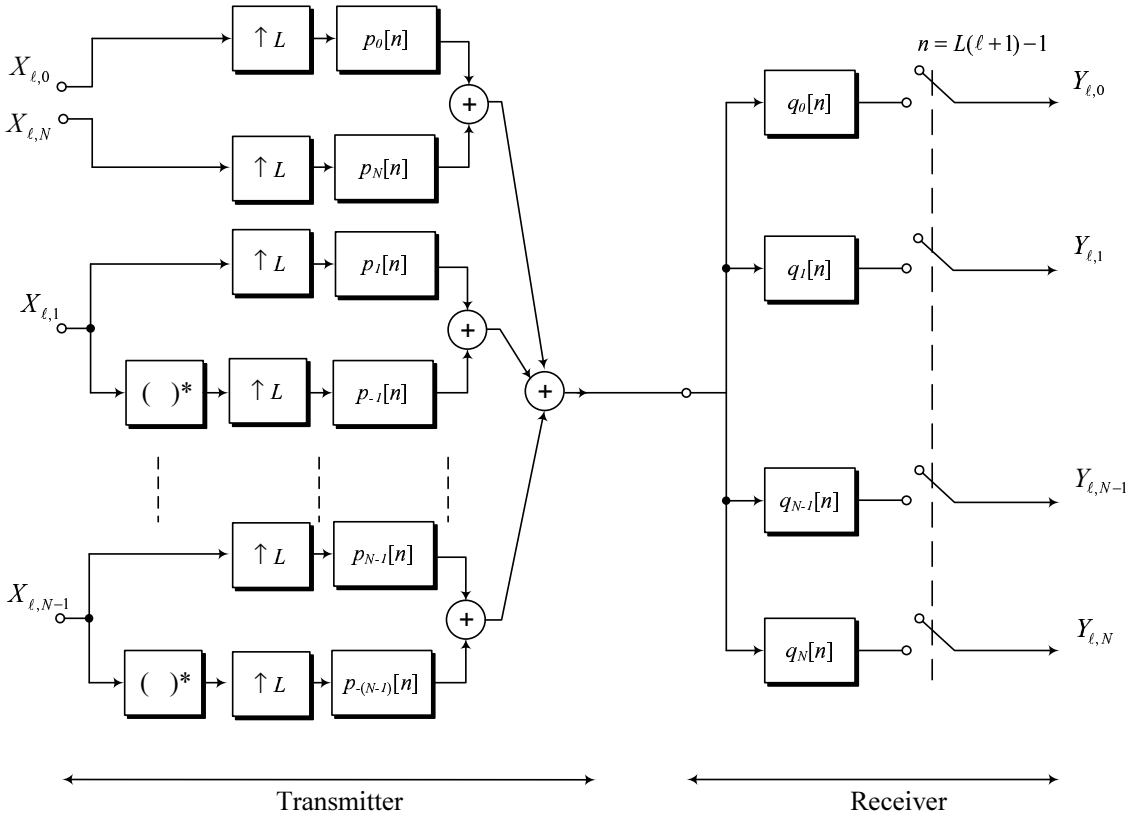

Figure 3.2: Filter bank implementation of a DMT modulator and demodulator

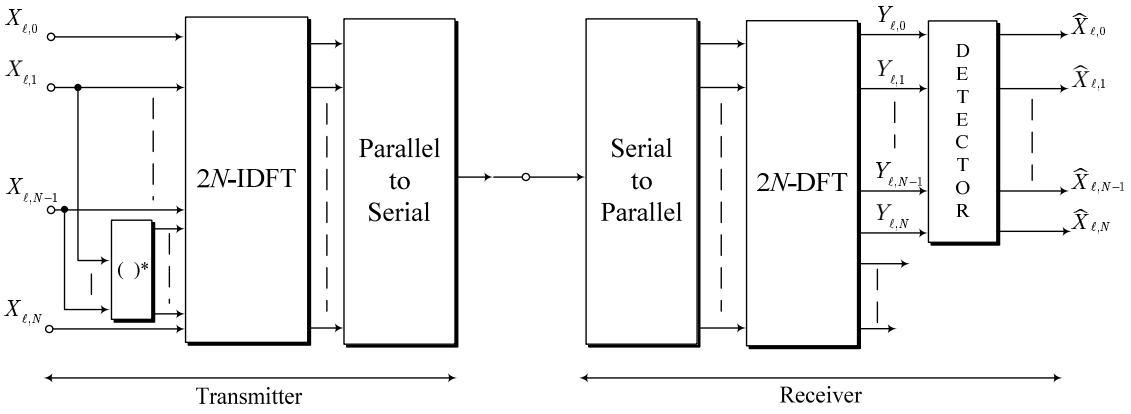

Figure 3.3: DFT-based DMT transmitter and receiver

$L = 2N + cp$ and redefining the transmitted pulses according to

$$p_k[n] = \frac{1}{2N}\, e^{j\frac{2\pi}{2N}k(n-cp)} w_{(2N+cp)}[n]. \tag{3.7}$$

The modulating symbols can be recovered by using a bank of filters matched only to the original DMT symbol,

$$q_k[n] = 2N\, p_k[2N + cp - 1 - n]^*\, w_{2N}[n]. \tag{3.8}$$

The above operation is equivalent to removing the cyclic prefix and performing the already stated DFT demodulation process. Hence, denoting the received signal by $y[n] = x[n] * h[n]$,

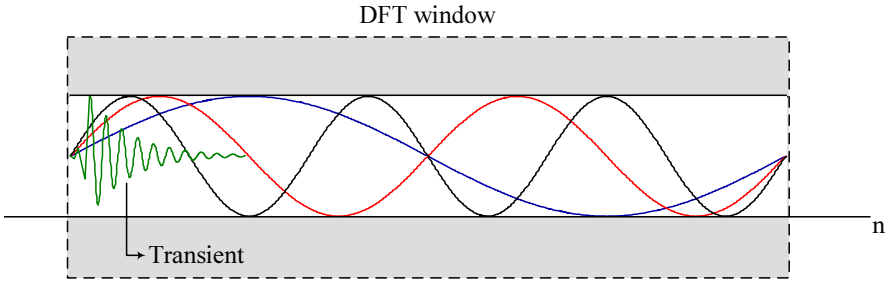

Figure 3.4: Effect of a time dispersive channel over the DMT symbol

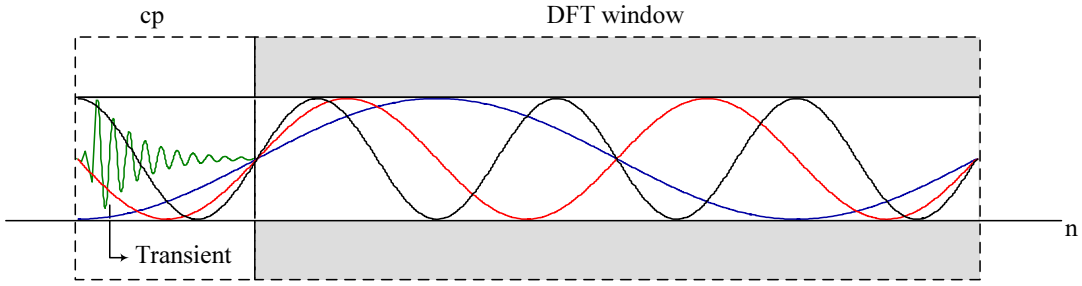

Figure 3.5: DMT equalization by means of the cyclic prefix

where $h[n]$ is the channel impulse response, the ℓ-th values transmitted in each carrier can be extracted by performing a $2N$-point DFT over the rectangularly windowed sequence $y[n+cp+\ell L]$. As long as the cyclic prefix length remains longer than the memory of the channel, i.e. $cp \geq L_h - 1$, where L_h is the channel impulse response length, ICI and ISI are avoided and the outputs of the DFT are given by

$$Y_{\ell,k} = \sum_{n=0}^{2N-1} y[n + \ell L + cp]\, w_{2N}[n]\, e^{j\frac{2\pi}{2N}kn} = H_k X_{\ell,k}, \tag{3.9}$$

where H_k is the value of the channel frequency response at the frequency of carrier k. Therefore, the DMT system behaves as a set of parallel channels whose information can be recovered after compensating for the channel attenuation. This process can be accomplished by means of the FEQ, which in its simplest form is selected according to the *zero-forcing* criterion, $FEQ_k = 1/H_k$.

The use of the cyclic prefix allows the equalization process to be performed with a reduced implementation complexity. However, this simplicity is obtained at the cost of reducing the system performance in two ways. Firstly, the energy available for the detection process is reduced, since the cyclic prefix is discarded before computing the DFT. This lessens the SNR at the detector input by $10\log(1+cp/2N)$dB. Nevertheless, this effect is in most cases negligible, e.g. in the case of $cp = N/2$ this loss is just 0.97dB. Secondly, the symbol period is increased from $L = 2N$ samples to $L = 2N + cp$. This causes a reduction in the symbol rate that may severely degrade the bit-rate in environments with long channel impulse responses. A common technique used in these circumstances is to place a TEQ before the removing of the cyclic prefix. The TEQ is a FIR filter intended for shortening the channel impulse response. The resulting

scheme of the DMT transmitter and receiver with the equalization procedures described up to now is shown in Fig. 3.6.

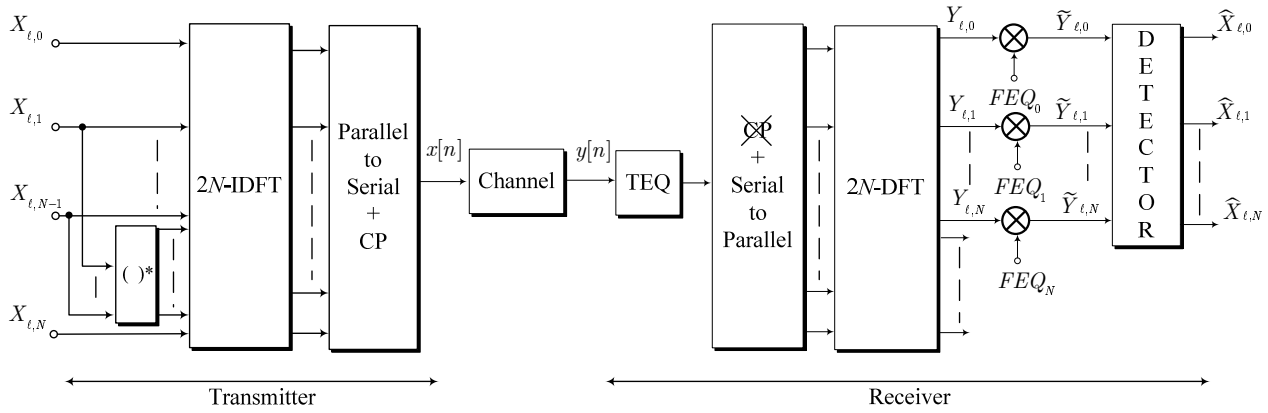

Figure 3.6: DMT system with channel equalization by means of a TEQ, a cyclic prefix and a FEQ

3.2.2 DMT system with pulse-shaping and windowing

Rectangular pulses employed in conventional DMT systems lead to individual power spectra that decay only with $1/f^2$. Its use at the transmitter side difficulties spectrum management [23] and is responsible for an increased ICI in time-dispersive channels, in the presence of synchronization errors and in FDMA multiuser environments [56]. In addition, it increases the out-of-band power captured by the receiver [86]. These effects may be particularly harmful in PLC systems due to the non-white nature of the noise and the highly dispersive character of the channel, which may cause severe ICI. Fortunately, improved spectral containments can be obtained in DMT with reduced implementation complexity. This section describes two of these methods. The first one uses a non-rectangular window at the receiver and is usually referred to as windowing. It was proposed as a way to reduce the effect of RF interferences in VDSL [86]. The second one, known as pulse-shaping, employs a non-rectangular window at the transmitter. It was proposed, before the invention of the equalization by means of the cyclic prefix, as a mean for reducing the ICI in time dispersive channels [84]. It must be emphasized that both methods can be applied independently, e.g. a receiver with windowing can operate over a conventional DMT signal. The main price to be paid in both techniques is the reduction in the symbol rate. Despite this fact, the resulting bit-rate may still be higher than the one achieved by a conventional DMT system, since the distortion and captured noise reduction may compensate for the symbol rate loss.

Windowing

Let's consider an LTI FIR channel whose impulse response length is L_h samples. Although the minimum cyclic prefix length needed to avoid ISI and ICI in these circumstances is $cp = L_h - 1$, the proposed method extends it β samples more, i.e. $cp = L_h - 1 + \beta$. The ℓ-th received symbol,

$y[n+\ell L+cp]$, is delayed $\beta/2$ samples and windowed with $w_{RX}[n]$, which is a non-rectangular window with non-zero samples only in the interval $-\beta/2 \leq n \leq 2N+\beta/2-1$. Fig. 3.7 (a) illustrates this process.

As long as

$$\sum_{r=-\infty}^{\infty} w_{RX}[n-2Nr] = 1, \tag{3.10}$$

the transmitted values can be recovered with neither ICI nor ISI from the samples of the Fourier transform of $y[n+\ell L+cp-\beta/2]w_{RX}[n]$ taken at $\omega_k = \pi k/N$ with $k = -(N-1), ..., N$. It is interesting to note that (3.10) is the time domain counterpart of the well-known frequency domain expression of the Nyquist criterion.

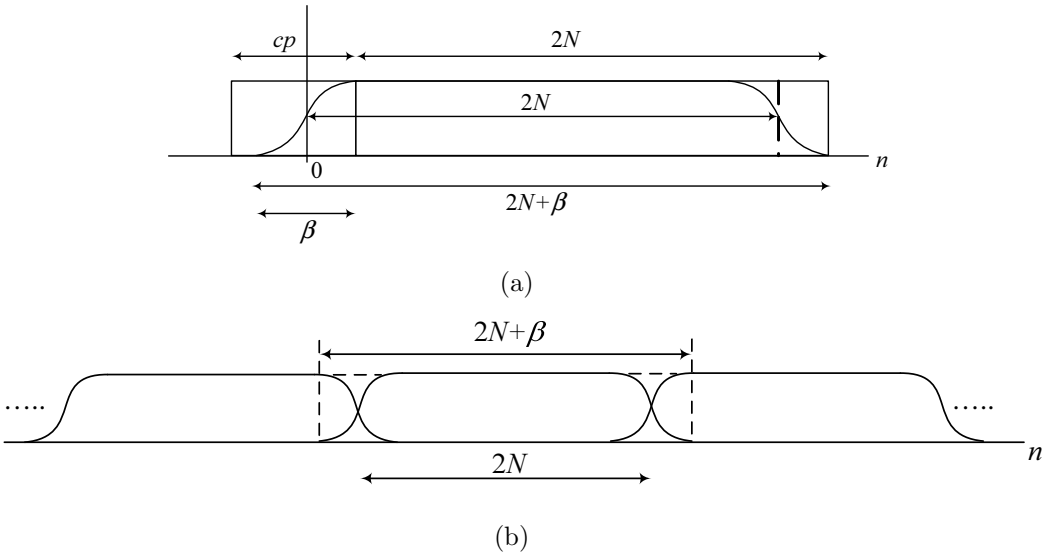

Figure 3.7: Windowing process: (a) applying the window to the received symbol; (b) time aliasing of the symbol before computing the DFT

The advantage of this windowing technique comes from the observation that the IDFT of the $2N$ samples of the Fourier transform of $y[n+\ell L+cp-\beta/2]w_{RX}[n]$ produces the time aliased signal

$$\widetilde{y}[n] = \sum_{r=-\infty}^{\infty} y[n+\ell L+cp-\beta/2-2Nr]\, w_{RX}[n-2Nr], \tag{3.11}$$

since $y[n+\ell L+cp-\beta/2]w_{RX}[n]$ was undersampled in the frequency domain, as shown in Fig. 3.7 (b). Hence, the $2N$ samples of the Fourier transform of $y[n+\ell L+cp-\beta/2]w_{RX}[n]$ can be obtained by computing a $2N$-point DFT of the samples with indexes $0 \leq n \leq 2N-1$ of the signal in (3.11). The resulting values,

$$Y_{\ell,k} = X_{\ell,k}\, H_k\, e^{-j\frac{\pi}{N}(\beta/2)k}, \tag{3.12}$$

experience a phase rotation due to the $\beta/2$ delay introduced at the beginning of the process. However, provided that this effect can be easily compensated by the FEQ, the major drawback of the described method is the reduction in the symbol rate caused by the cyclic prefix extension.

In this work, the raised-cosine window

$$w_{RX}[n] = \begin{cases} \frac{1}{2}\left[1+\cos\left(\frac{\pi(n-\beta/2)}{\beta+1}\right)\right] & -\beta/2 \le n \le \beta/2-1 \\ 1 & \beta/2 \le n \le 2N-\beta/2-1 \\ \frac{1}{2}\left[1+\cos\left(\frac{\pi(n-2N+\beta/2+1)}{\beta+1}\right)\right] & 2N-\beta/2 \le n \le 2N+\beta/2-1 \end{cases}, \quad (3.13)$$

is employed. Fig. 3.8 shows the window spectrum for $N = 1024$, $cp = 200$ and different values of β.

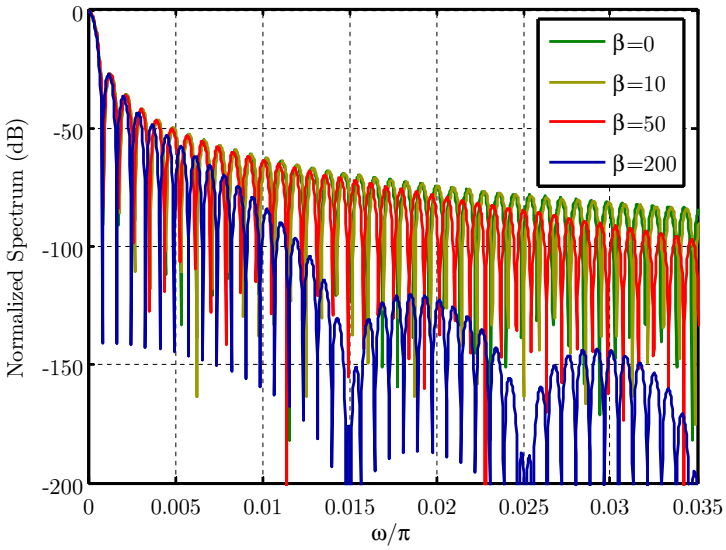

Figure 3.8: Normalized spectrum of the receiver pulse for different values of β

Pulse-shaping

The following procedure can be employed to achieve higher spectral containment in the transmitted signal. DMT symbols, including the cyclic prefix, are extended α samples at both ends and multiplied by a non-rectangular window, $w_{TX}[n]$, as shown in Fig. 3.9 (a). As long as the flat part of the window includes the original DMT symbol and its cyclic prefix, ICI and ISI are avoided. In this work, the raised-cosine window

$$w_{TX}[n] = \begin{cases} \frac{1}{2}\left[1+\cos\left(\frac{\pi(n-\alpha)}{\alpha+1}\right)\right] & 0 \le n \le \alpha-1 \\ 1 & \alpha \le n \le L-1 \\ \frac{1}{2}\left[1+\cos\left(\frac{\pi(n-L+1)}{\alpha+1}\right)\right] & L \le n \le L+\alpha-1 \end{cases}, \quad (3.14)$$

with $L = 2N + cp + \alpha$, is employed. In order to minimize the symbol rate loss, pulse-shaped symbols may be partially overlapped, as shown in Fig. 3.9 (b).

The resulting signal can then be expressed as

$$x[n] = \sum_{\ell=-\infty}^{\infty} \sum_{k=-(N-1)}^{N} X_{\ell,k}\, e^{j\frac{\pi}{N}k(n-cp-\alpha-\ell L)}\, w_{TX}[n-\ell L]. \tag{3.15}$$

Fig. 3.10 shows the resulting PSD of a DMT signal with $N = 1024$ and $cp = 200$ for different values of α. Since the periodical extension and the multiplication by the window have a relatively low computational cost, the major drawback of this technique are the SNR loss (energy allocated to the shaped regions is not available at the detector input) and the symbol rate reduction.

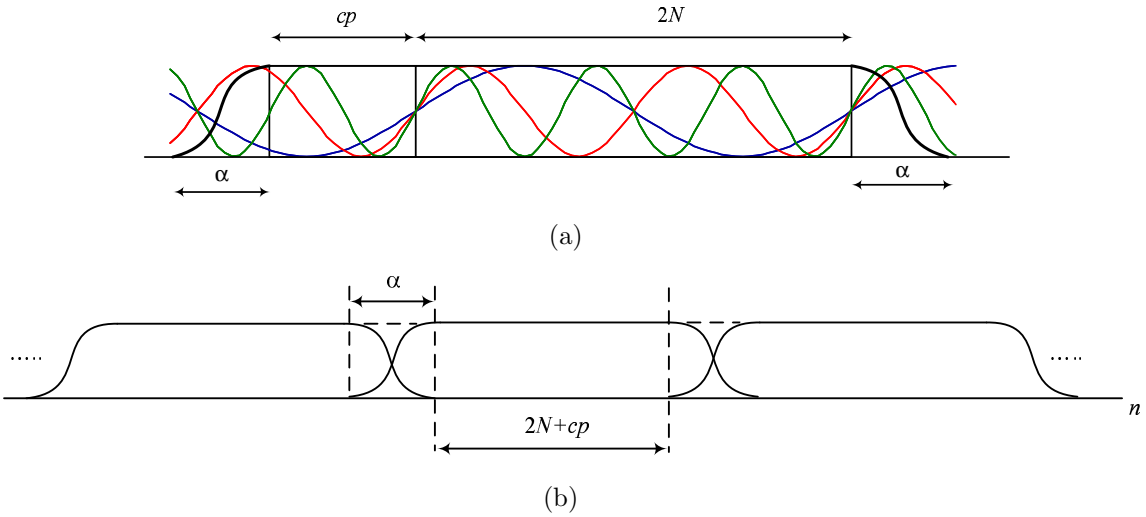

Figure 3.9: Pulse-shaping process: (a) periodical extension of the symbol and shaping; (b) overlapping individual symbols for transmission

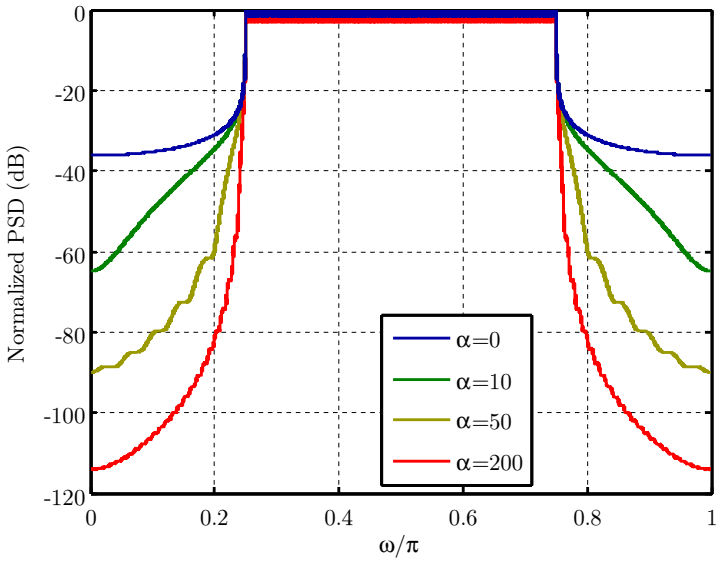

Figure 3.10: Normalized PSD of a pulse-shaped DMT signal for different values of α

3.2.3 Bit-loading

The problem of assigning power and constellations to the carriers of a DMT system is commonly referred to as bit-loading and, in the single-user environment, has been extensively treated in the literature [93, 94, 95]. There are two basic groups of bit-loading algorithms. The first one is called MA (Margin Adaptive) and their objective is to minimize the total energy required to transmit a fixed data rate. In the second one, called RA (Rate Adaptive), the goal is to distribute the available energy among the carriers such that the overall bit-rate is maximized. The optimal solution to the latter problem is the *water-filling* assignment, that leads to non-integer number of bits per symbol. Therefore, this distribution has to be modified when the bit assignment is constrained to be integer. The Hughes-Hartong algorithm [96] achieves the optimal solution to this problem by using a brute force iterative method. In each step, an additional bit is allocated to the carrier that requires the smaller power increment to convey its assigned bits without exceeding the objective error probability. A more efficient solution to this problem was proposed in [94].

As mentioned in section 2.4, a PSD constraint is considered in this work. This notably simplifies the bit-loading problem, since power can be independently distributed among carries. Thus, assuming an LTI channel with impulse response shorter than the cyclic prefix length and a zero-mean Gaussian non-white noise, the k-th output of the DFT for the ℓ-th received symbol is given by

$$Y_{\ell,k} = X_{\ell,k}\, H_k + U_{\ell,k}, \tag{3.16}$$

where $U_{\ell,k}$ is the k-th DFT output of the noise samples corresponding to the ℓ-th received symbol. The SNR in carrier k is then given by

$$SNR_k = \frac{\mathrm{E}[|X_{\ell,k}|^2]|H_k|^2}{\sigma^2_{U_k}}, \tag{3.17}$$

where $\mathrm{E}[\cdot]$ denotes expectation with respect to ℓ and $\sigma^2_{U_k}$ is the noise power at the k-th DFT output. The number of bits per symbol in carrier k is then given by

$$b_k = \left\lfloor \log_2 \left(1 + \frac{SNR_k}{\Gamma_k} \right) \right\rfloor, \tag{3.18}$$

where $\lfloor x \rfloor$ stands for the integer part of x. Γ_k is the so-called *SNR gap* in carrier k, and models the SNR penalty experienced because of the use of a constellation with discrete granularity [62]. The value of the *SNR gap* depends on the symbol error rate (SER) and on the employed constellation. However, for square QAM ones it can be upper bounded by [97]

$$\Gamma = \frac{1}{3} \left[Q^{-1} \left(\frac{\mathrm{SER}}{4} \right) \right]^2, \tag{3.19}$$

where $Q(\cdot)$ is the Marcum Q function [62]. Throughout of this work, BPSK and square QAM constellations with a maximum of 16bits per symbol are employed. Unless otherwise stated, the bit-loading is performed using a SER constraint of 10^{-6}. However, a bit error rate (BER) constraint is also used in situations where a higher degree of accuracy is required. In these

circumstances, the SNR gap of the square QAM constellations is derived from the BER approximation proposed in [82]

$$\Gamma = -\frac{1}{1.6}\ln\left(\frac{\mathrm{BER}}{0.2}\right), \tag{3.20}$$

where Gray coding and BER $\leq 10^{-3}$ is assumed.

When an insufficient cyclic prefix is employed, ISI and ICI are also present. The signal at the k-th output of the DFT can then be expressed as

$$Y_{\ell,k} = X_{\ell,k}\, H_k + U_{\ell,k} + D_{\ell,k}, \tag{3.21}$$

where $D_{\ell,k}$ is the distortion term. However, provided that the ICI is the dominating term in the distortion and that it is due to the sum of a great amount of independent terms, the central limit theorem states that its distribution is approximately Gaussian. Therefore, expression (3.18) can be also used to obtain the number of bits in these circumstances just by substituting the SNR by the signal-to-noise-and-distortion ratio (SNDR) defined as

$$SNDR_k = \frac{\mathrm{E}[|X_{\ell,k}|^2]|H_k|^2}{\sigma^2_{U_k} + \mathrm{E}[|D_{\ell,k}|^2]}. \tag{3.22}$$

The bit-rate of the DMT system is then given by

$$R = \frac{f_s}{L}\sum_{k=0}^{N} b_k, \tag{3.23}$$

where f_s is the digital-to-analog conversion frequency at the transmitter.

It is worth noting that, strictly speaking, the optimum bit-loading requires an iterative process. Using a training sequence, the receiver is able to estimate the distortion power at each carrier. For simplicity, the training sequence should transmit all the carriers with maximum power. Based on this information, the receiver computes the bit-loading. However, since some of the carrier will remain empty after the bit-loading process, the distortion power in the remaining carriers is smaller than the one employed to perform the constellation assignment.

3.2.4 Synchronization

Synchronization of the receiver sampling clock with the incoming data signal is a fundamental issue in digital communications. However, in DMT systems synchronization errors are especially harmful because, in addition to the ISI that appears in single-carrier systems, ICI is also generated. The spectral selectivity of power-line channels makes the need for accurate synchronization particularly important, since it must be ensured that these errors do not limit the performance of those subbands with high SNR.

Two types of synchronization tasks can be distinguished in DMT systems: symbol synchronization and sample synchronization. The former, which is also referred to as coarse synchronization, is in charge of delimiting the symbol boundaries, controlling that the samples that

feed the DFT correspond to a unique DMT symbol. The latter, also called fine synchronization, attempts to guarantee that the correct sampling frequency and phase is being employed. This problem is thoroughly tackled in chapter 4 and, until that moment, is overcome by assuming perfect frequency and phase synchronization. On the contrary, the problem of symbol synchronization is somehow subtler and the idea of *perfect* symbol synchronization is not so straightforward. The main reason is that ISI and ICI are unavoidable when DMT symbols traverse a time dispersive channel with an impulse response longer than the cyclic prefix length. Hence, determining the start of the symbol in these circumstances is not a trivial issue, as shown in Fig. 3.11.

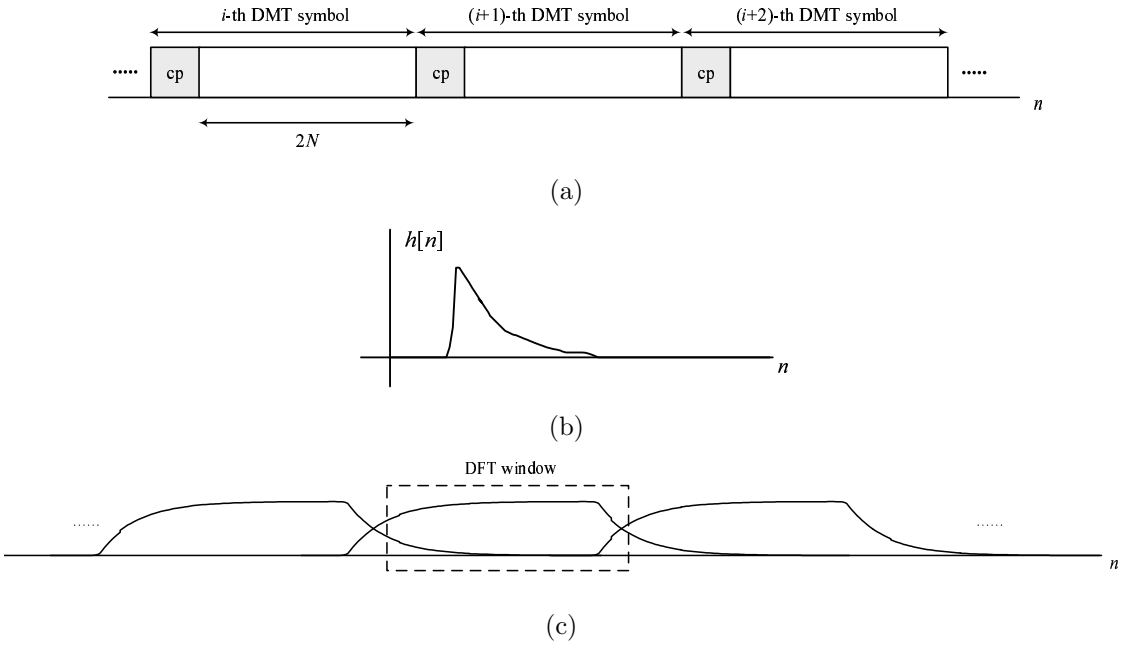

Figure 3.11: Symbol synchronization: (a) original DMT symbols; (b) channel impulse response; (c) received DMT symbols

The ideal symbol synchronizer would be the one that maximizes the bit-rate of the system. However, this criterion leads to complicated algorithms [98]. Therefore, two simpler approaches have been proposed for symbol synchronization. The first one exploits the correlation properties between the original DMT symbol and its cyclic prefix [98]. It has been tested that this algorithm performs poorly in PLC systems. The cause is that the aforementioned correlation does not exhibit a clearly distinguishable peak but, due to the longer cyclic prefixes employed, it presents a flat region that lasts for many samples. The second one requires knowledge of the channel impulse response, and is based on the observation that the power of ICI and ISI caused by a symbol misalignment is essentially due to the energy of the channel impulse response not covered by the cyclic prefix. Thus, finding the beginning of the symbol is equivalent to determining the starting point of the $(cp+1)$-samples window of the impulse response with the largest energy [98]. This is the criterion employed throughout this work.

3.3 Analysis and optimization of DMT in time-invariant channels

In chapter 2 it was shown that the delay spread and the coherence bandwidth of PLC channels are essentially constant along the mains cycle. Therefore, those aspects of a DMT system that depend on the frequency selectivity of the channel can be designed without taking into account the channel time variations. This is clearly the case of the cyclic prefix length and the TEQ. Moreover, even for parameters like the number of carriers, whose optimum value results from the trade-off between frequency and time selectivity of the channel, the analysis accomplished in a LTI channel provides an insight into the problem.

In this section, the performance of a DMT system operating in the channels of the time-invariant model is assessed in terms of the cyclic prefix length and the number of carriers. To this end, an analytical procedure that allows separate estimation of the ICI and ISI is firstly presented. Afterwards, the suitability of the TEQ for PLC scenarios is discussed in terms of bit-rate and the computational load.

3.3.1 Analytical estimation of the distortion due to the frequency selectivity of the channel

The estimation of the distortion caused by the frequency selectivity of a FIR channel is firstly accomplished for the conventional DMT system. Afterwards, expressions for the DMT with pulse-shaping and windowing will be derived. Although the former is a particularization of the latter with $\alpha = \beta = 0$, computationally simpler expressions can be obtained by starting with the already simplified pulses. In addition, the plainer expressions of the conventional DMT systems makes easier to gain deeper knowledge of the ISI and ICI generation process.

The discrete-time model shown in Fig. 3.12 can employed for the analysis of the distortion terms of both DMT systems. The parameter D is the delay provided by the symbol synchronizer according to the criterion stated in section 3.2.4, i.e. the beginning of the $(cp + 1)$-samples window of the impulse response with highest energy.

DMT with rectangular pulses

For the conventional DMT system, the diagram shown in Fig. 3.12 is particularized with $\alpha = \beta = 0$, $L = 2N + cp$ and the transmitter and receiver pulses are given by (3.7) and (3.8), respectively.

$\widetilde{Y}_{\ell,z}$ is composed of the desired and the ISI and ICI signal terms. Fortunately, the calculation of the latter terms is considerably simplified by the fact that the effective length of indoor power-line channels is shorter than the symbol length of DMT systems that employ the band up to 30MHz with a reasonable number of carriers (e.g. $N > 256$). Hence, in the case of a

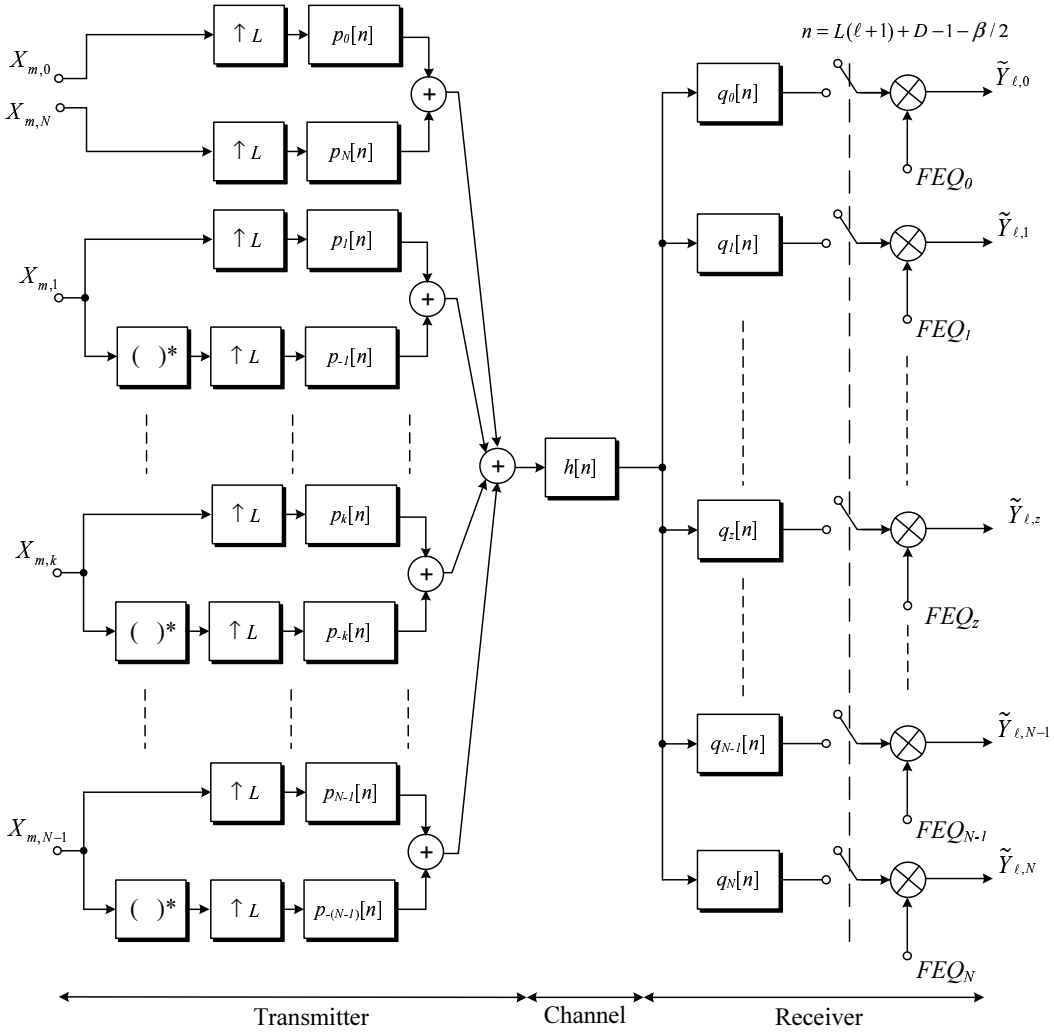

Figure 3.12: Discrete-time model of a DMT system

one-shot transmission with index m, the output of carrier z at $\ell = m$ is only distorted by the preceding, $\ell = m-1$, and subsequent symbols, $\ell = m+1$. Let's denote

$$b_k[n] = p_k[n] * h[n], \tag{3.24}$$

where $*$ is the convolution operator.

The output of carrier z for $\ell = m$ can be expressed as

$$\widetilde{Y}_{m,z} = FEQ_z \sum_{k=-(N-1)}^{N} \left(b_k[n] * q_z[n]\right)\big|_{n=L(m+1)+D-1}, \tag{3.25}$$

Taking into account that $b_k[n] = b_{-k}[n]^*$ and $X_{m,k} = X^*_{m,-k}$ for $k = 1, ..., N-1$ and that for $k = 0$ and $k = N$ both, $b_k[n]$ and $X_{m,k}$, are real valued, (3.25) can be written as

$$\begin{aligned}\widetilde{Y}_{m,z} = 2FEQ_z \sum_{k=0}^{N} \Bigg[& X^I_{m,k} \left(\sum_{n=0}^{2N-1} \Re\left[b_k[n+M_0]\right] e^{-j\frac{\pi}{N}zn} \right) \\ & - X^Q_{m,k} \left(\sum_{n=0}^{2N-1} \Im\left[b_k[n+M_0]\right] e^{-j\frac{\pi}{N}zn} \right) \Bigg],\end{aligned} \tag{3.26}$$

where $\Re[\cdot]$ and $\Im[\cdot]$ denote the real and imaginary part, respectively, $M_0 = cp + D$ and $X^I_{m,k}$ and $X^Q_{m,k}$ are the in-phase and quadrature components of $X_{m,k}$. It is worth noting that the coefficients that multiply the in-phase and quadrature components of the transmitted symbol in (3.26) will not be equal unless a sufficient cyclic prefix is employed. If this is not the case, perfect *zero-forcing* equalization with a one-tap FEQ is not possible, even in the case of a one-shot transmission with only one carrier. It is also interesting to note that the bracketed expressions in (3.26) can be efficiently computed by means of the $2N$-point FFT of the signals $\Re\left[b_k[n + M_0]\right]$ and $\Im\left[b_k[n + M_0]\right]$.

Correspondingly, the output for $\ell = m - 1$ can be expressed as

$$\widetilde{Y}_{m-1,z} = 2e^{j\frac{\pi}{N}zD}\, FEQ_z \sum_{k=0}^{N} \left[X^I_{m,k} \left(\sum_{n=0}^{D-1} \Re\left[b_k[n]\right]\, e^{-j\frac{\pi}{N}zn} \right) - X^Q_{m,k} \left(\sum_{n=0}^{D-1} \Im\left[b_k[n]\right]\, e^{-j\frac{\pi}{N}zn} \right) \right], \tag{3.27}$$

where the bracketed expressions can be also computed by means of the $2N$-point FFT of the signals $\Re\left[b_k[n]\right]$ and $\Im\left[b_k[n]\right]$ with $0 \leq n \leq D-1$ and padded with zeros.

Finally, the output for $\ell = m + 1$ can be written as

$$\begin{aligned} \widetilde{Y}_{m+1,z} = 2FEQ_z \sum_{k=0}^{N} \Bigg[& X^I_{m,k} \left(\sum_{n=0}^{L_h-cp-D-2} \Re\left[b_k[n + M_1]\right]\, e^{-j\frac{\pi}{N}zn} \right) \\ & - X^Q_{m,k} \left(\sum_{n=0}^{L_h-cp-D-2} \Im\left[b_k[n + M_1]\right]\, e^{-j\frac{\pi}{N}zn} \right) \Bigg], \end{aligned} \tag{3.28}$$

where $M_1 = L + cp + D$. Since $L_h < 2N$, the bracketed expressions can also be computed by means of the $2N$-point FFT of the signals $\Re\left[b_k[n + M_1]\right]$ and $\Im\left[b_k[n + M_1]\right]$ with $0 \leq n \leq L_h - cp - D - 2$ and padded with zeros.

The schematic view of $b_k[n]$ and $q_z\left[L(\ell + 1) + D - 1 - n\right]$, shown in Fig. 3.13, provides an interesting insight into the problem. For simplicity, it has been assumed that $k = z$. It can be seen that the *steady state* part of $b_k[n]$, i.e. where it has the form of a complex exponential multiplied by the frequency response of the channel, lasts for $2N + cp - (L_h - 1)$ samples. Since $q_z[n]$ lasts for $2N$ samples, only when $cp \geq L_h - 1$ perfect equalization can be achieved with a one-tap filter. In addition, since in a continuous symbol transmission the initial and final transients introduce ISI and ICI from the previous and subsequent symbols, the trade-off in the selection of D can be clearly observed.

Based on the above results, the input to output relation of the DMT system can be matricially written as

$$\left[\widetilde{Y}_{m,0}\ \widetilde{Y}_{m,1}\ \cdots\ \widetilde{Y}_{m,z}\ \cdots\ \widetilde{Y}_{m,N-1}\widetilde{Y}_{m,N}\right]^T = \mathbf{T} \cdot \left[\mathbf{X}_{m-1} \mid \mathbf{X}_m \mid \mathbf{X}_{m+1}\right]^T, \tag{3.29}$$

where $\widetilde{Y}_{m,z}$ denotes the m-th value received in carrier z and $\mathbf{X}_{m+i}$, with $i = -1, 0, 1$, are vectors with the in-phase and quadrature components of the $(m + i)$-th transmitted values in each carrier

$$\mathbf{X}_{m+i} = \left[X^I_{m+i,0}\ X^Q_{m+i,0}\ X^I_{m+i,1}\ X^Q_{m+i,1}\ \cdots\ X^I_{m+i,k}\ X^Q_{m+i,k}\ \cdots\ X^I_{m+i,N}\ X^Q_{m+i,N}\right], \tag{3.30}$$

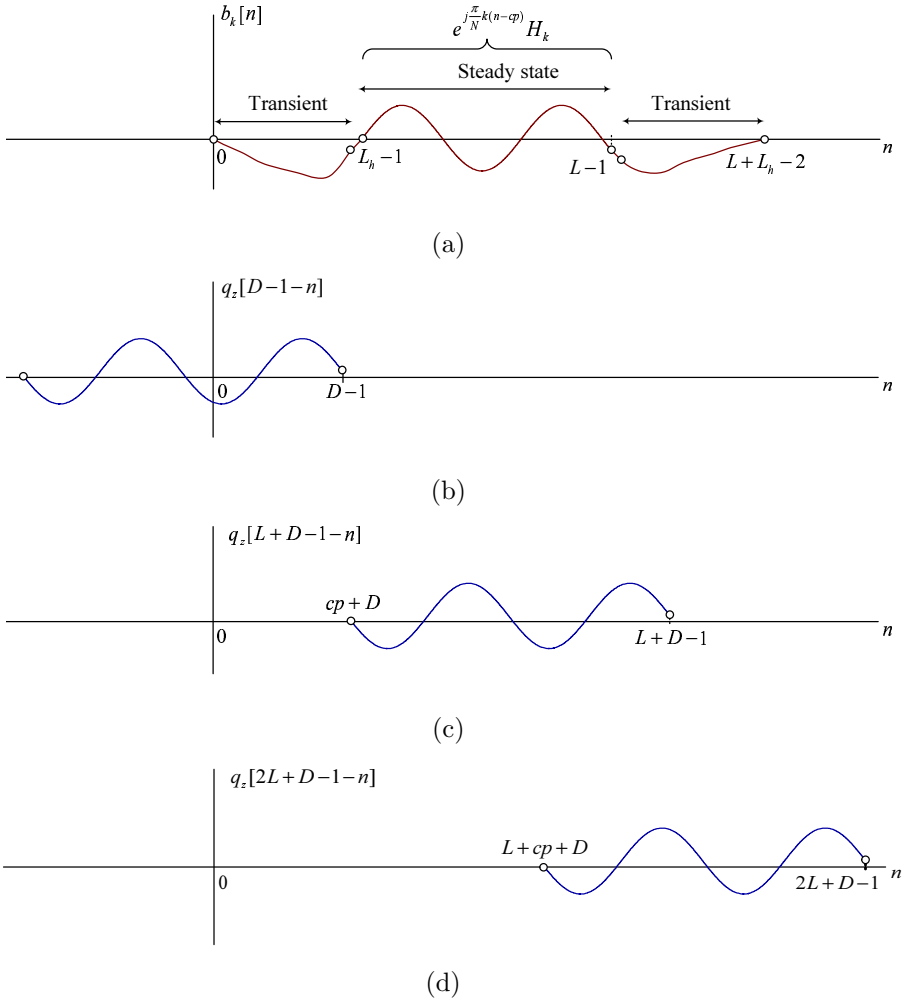

Figure 3.13: Schematic representation of the filtering process at the receiver: (a) $b_k[n]$; (b) filtering with $q_z[n]$ for $\ell = m-1$; (c) filtering with $q_z[n]$ for $\ell = m$; (d) filtering with $q_z[n]$ for $\ell = m+1$

and $\mathbf{T}$ is a transmission matrix that can be written as

$$\mathbf{T} = [\mathbf{T}_{m-1} \mid \mathbf{T}_m \mid \mathbf{T}_{m+1}], \tag{3.31}$$

where $\mathbf{T}_{m-1}$, $\mathbf{T}_m$ and $\mathbf{T}_{m+1}$ are $(N+1) \times 2(N+1)$ submatrices,

$$\mathbf{T}_{m+i} = \begin{pmatrix} T^{0,I}_{m+i,0} & T^{0,Q}_{m+i,0} & T^{0,I}_{m+i,1} & T^{0,Q}_{m+i,1} & \cdots & T^{0,I}_{m+i,k} & T^{0,Q}_{m+i,k} & \cdots & T^{0,I}_{m+i,N} & T^{0,Q}_{m+i,N} \\ T^{1,I}_{m+i,0} & T^{1,Q}_{m+i,0} & T^{1,I}_{m+i,1} & T^{1,Q}_{m+i,1} & \cdots & T^{1,I}_{m+i,k} & T^{1,Q}_{m+i,k} & \cdots & T^{1,I}_{m-i,N} & T^{1,Q}_{m+i,N} \\ \vdots & \vdots & \vdots & \vdots & \vdots & \vdots & \vdots & \vdots & \vdots & \vdots \\ T^{z,I}_{m+i,0} & T^{z,Q}_{m+i,0} & T^{z,I}_{m+i,1} & T^{z,Q}_{m+i,1} & \cdots & T^{z,I}_{m+i,k} & T^{z,Q}_{m+i,k} & \cdots & T^{z,I}_{m+i,N} & T^{z,Q}_{m+i,N} \\ \vdots & \vdots & \vdots & \vdots & \vdots & \vdots & \vdots & \vdots & \vdots & \vdots \\ T^{N-1,I}_{m+i,0} & T^{N-1,Q}_{m+i,0} & T^{N-1,I}_{m+i,1} & T^{N-1,Q}_{m+i,1} & \cdots & T^{N-1,I}_{m+i,k} & T^{N-1,Q}_{m+i,k} & \cdots & T^{N-1,I}_{m+i,N} & T^{N-1,Q}_{m+i,N} \\ T^{N,I}_{m+i,0} & T^{N,Q}_{m+i,0} & T^{N,I}_{m+i,1} & T^{N,Q}_{m+i,1} & \cdots & T^{N,I}_{m+i,k} & T^{N,Q}_{m+i,k} & \cdots & T^{N,I}_{m+i,N} & T^{N,Q}_{m+i,N} \end{pmatrix}, \tag{3.32}$$

whose elements, $T^{z,I}_{m+i,k}$ and $T^{z,Q}_{m+i,k}$, represent the complex coefficients by which the respective in-phase and quadrature components of the $(m+i)$-th transmitted symbol in carrier k appear at the m-th output of carrier z.

Taking into account the observations made about the efficient calculation of (3.26),(3.27) and (3.28), the columns of $\mathbf{T}_{m+i}$ can be efficiently computed by means of the FFT of the signals

$$f_k^{M,P}[n] = \begin{cases} \Re\left[b_k\left[n+M\right]\right] & 0 \le n \le P \\ 0 & \text{otherwise} \end{cases}, \tag{3.33}$$

and

$$g_k^{M,P}[n] = \begin{cases} -\Im\left[b_k\left[n+M\right]\right] & 0 \le n \le P \\ 0 & \text{otherwise} \end{cases}, \tag{3.34}$$

according to

$$T_{m-1,k}^{z,I} = 2\, e^{j\frac{\pi}{N}zD}\; FFT(f_k^{0,D-1}[n], 2N, z)\, FEQ_z, \quad 0 \le z \le N, \tag{3.35}$$

$$T_{m-1,k}^{z,Q} = 2\, e^{j\frac{\pi}{N}zD}\; FFT(g_k^{0,D-1}[n], 2N, z)\, FEQ_z, \quad 0 \le z \le N, \tag{3.36}$$

$$T_{m,k}^{z,I} = 2\, FFT(f_k^{M_0,2N-1}[n], 2N, z)\, FEQ_z, \quad 0 \le z \le N, \tag{3.37}$$

$$T_{m,k}^{z,Q} = 2\, FFT(g_k^{M_0,2N-1}[n], 2N, z)\, FEQ_z, \quad 0 \le z \le N, \tag{3.38}$$

$$T_{m+1,k}^{z,I} = 2\, FFT(f_k^{M_1,L_h-cp-D-2}[n], 2N, z)\, FEQ_z, \quad 0 \le z \le N, \tag{3.39}$$

$$T_{m+1,k}^{z,Q} = 2\, FFT(g_k^{M_1,L_h-cp-D-2}[n], 2N, z)\, FEQ_z, \quad 0 \le z \le N, \tag{3.40}$$

where

$$FFT(x[n], N', z) = \sum_{n=0}^{N'-1} x[n] e^{-j\frac{2\pi}{N'}zn}. \tag{3.41}$$

DMT with pulse-shaping and windowing

In the case of using pulse-shaping and windowing, the diagram shown in Fig. 3.12 is particularized with $L = 2N + cp + \alpha$ and with the pulse waveforms given by

$$p_k[n] = \frac{1}{2N}\; e^{j\frac{\pi}{N}k(n-cp-\alpha)} w_{TX}[n], \tag{3.42}$$

and

$$q_z[n] = e^{j\frac{\pi}{N}z(n+1)} w_{RX}[n], \tag{3.43}$$

where $w_{RX}[n]$ and $w_{TX}[n]$ are respectively given by (3.13) and (3.14). In addition, a term $e^{j\frac{\pi}{N}z\beta/2}$ is included in the FEQ of carrier z to compensate for the delay introduced in the windowing operation, as explained in section 3.2.2.

The analysis with the new pulses leads to the following expressions for the output of carrier z at $\ell = m$

$$\begin{aligned} \widetilde{Y}_{m,z} = 2\, FEQ_z \sum_{k=0}^{N} \Bigg[& X_{m,k}^{I} \left(\sum_{n=0}^{2N+\beta-1} \Re\left[b_k[n+M_0']\right] w_{RX}\left[W_0 - n\right]\; e^{-j\frac{\pi}{N}zn} \right) \\ & - X_{m,k}^{Q} \left(\sum_{n=0}^{2N+\beta-1} \Im\left[b_k[n+M_0']\right] w_{RX}\left[W_0 - n\right]\; e^{-j\frac{\pi}{N}zn} \right) \Bigg], \end{aligned} \tag{3.44}$$

where $M_0' = cp + D + \alpha - \beta$, $W_0 = 2N + \beta/2 - 1$. It is worth noting that, this time, the efficient computation of the bracketed expressions in (3.44) requires a $4N$-point FFT.

Similarly, the output of carrier z at $\ell = m-1$ and $\ell = m+1$ are given by

$$\begin{aligned}\widetilde{Y}_{m-1,z} = 2e^{j\frac{\pi}{N}z(D-\beta)}\, FEQ_z \sum_{k=0}^{N} \Bigg[X^I_{m,k} \left(\sum_{n=0}^{D-1} \Re\left[b_k[n]\right] w_{RX}\left[W_{-1}-n\right]\, e^{-j\frac{\pi}{N}zn} \right) \\ - X^Q_{m,k} \left(\sum_{n=0}^{D-1} \Im\left[b_k[n]\right] w_{RX}\left[W_{-1}-n\right]\, e^{-j\frac{\pi}{N}zn} \right) \Bigg],\end{aligned} \tag{3.45}$$

where $W_{-1} = D - 1 - \beta/2$, and

$$\begin{aligned}\widetilde{Y}_{m+1,z} = 2\, FEQ_z \sum_{k=0}^{N} \Bigg[X^I_{m,k} \left(\sum_{n=0}^{L_h-cp-D+\beta-2} \Re\left[b_k[n+M_0'+L]\right] w_{RX}\left[W_0-n\right]\, e^{-j\frac{\pi}{N}zn} \right) \\ - X^Q_{m,k} \left(\sum_{n=0}^{L_h-cp-D+\beta-2} \Im\left[b_k[n+M_0'+L]\right] w_{RX}\left[W_0-n\right]\, e^{-j\frac{\pi}{N}zn} \right) \Bigg].\end{aligned} \tag{3.46}$$

The coefficients of the transmission matrix can now be computed using the functions

$$f_k^{M,W,P}[n] = \begin{cases} \Re\left[b_k\left[n+M\right]\right] w_{RX}[W-n] & 0 \le n \le P \\ 0 & \text{otherwise} \end{cases}, \tag{3.47}$$

and

$$g_k^{M,W,P}[n] = \begin{cases} -\Im\left[b_k\left[n+M\right]\right] w_{RX}[W-n] & 0 \le n \le P \\ 0 & \text{otherwise} \end{cases}, \tag{3.48}$$

according to

$$T^{z,I}_{m-1,k} = 2\, e^{j\frac{\pi}{N}z(D-\beta)}\; FFT(f_k^{0,W_{-1},D-1}[n], 2N, z)\, FEQ_z, \quad 0 \le z \le N, \tag{3.49}$$

$$T^{z,Q}_{m-1,k} = 2\, e^{j\frac{\pi}{N}z(D-\beta)}\; FFT(g_k^{0,W_{-1},D-1}[n], 2N, z)\, FEQ_z, \quad 0 \le z \le N, \tag{3.50}$$

$$T^{z,I}_{m,k} = 2\, FFT(f_k^{M_0',W_0,2N+\beta-1}[n], 4N, 2z)\, FEQ_z, \quad 0 \le z \le N, \tag{3.51}$$

$$T^{z,Q}_{m,k} = 2\, FFT(g_k^{M_0',W_0,2N+\beta-1}[n], 4N, 2z)\, FEQ_z, \quad 0 \le z \le N, \tag{3.52}$$

$$T^{z,I}_{m+1,k} = 2\, FFT(f_k^{M_0'+L,W_0,L_h-cp-D+\beta-2}[n], 2N, z)\, FEQ_z, \quad 0 \le z \le N, \tag{3.53}$$

$$T^{z,Q}_{m+1,k} = 2\, FFT(g_k^{M_0'+L,W_0,L_h-cp-D+\beta-2}[n], 2N, z)\, FEQ_z, \quad 0 \le z \le N, \tag{3.54}$$

Signal to distortion ratio calculation

The ISI term in carrier z can be computed from

$$ISI_z = \left(\left|T^{z,I}_{m-1,z}\right|^2 + \left|T^{z,I}_{m+1,z}\right|^2 \right) \sigma^2_{z,I} + \left(\left|T^{z,Q}_{m-1,z}\right|^2 + \left|T^{z,Q}_{m+1,z}\right|^2 \right) \sigma^2_{z,Q}, \tag{3.55}$$

where $\sigma^2_{z,I}$ and $\sigma^2_{z,Q}$ denote the average energy of the in-phase and quadrature components of the symbols transmitted in carrier z, which have been assumed to be independent.

Similarly, the ICI term in carrier z can be obtained from

$$ICI_z = \sum_{\substack{k=0 \\ k\neq z}}^{N} \left[\left(\left| T^{z,I}_{m-1,k} \right|^2 + \left| T^{z,I}_{m,k} \right|^2 + \left| T^{z,I}_{m+1,k} \right|^2 \right) \sigma^2_{k,I} + \left(\left| T^{z,Q}_{m-1,k} \right|^2 + \left| T^{z,Q}_{m,k} \right|^2 + \left| T^{z,Q}_{m+1,k} \right|^2 \right) \sigma^2_{k,Q} \right]. \tag{3.56}$$

The signal-to-distortion ratio (SDR) in carrier z, defined as

$$SDR_z = \frac{\mathrm{E}\left[|X_{\ell,z}|^2 \right]}{\mathrm{E}\left[\left| \widetilde{Y}_{\ell,z} - X_{\ell,z} \right|^2 \right]}, \tag{3.57}$$

can then be expressed in terms of the ISI and ICI as

$$SDR_z = \frac{\sigma^2_{z,I} + \sigma^2_{z,Q}}{ISI_z + ICI_z + \left(\left| 1 - T^{z,I}_{m,z} \right|^2 \sigma^2_{z,I} + \left| j - T^{z,Q}_{m,z} \right|^2 \sigma^2_{z,Q} \right)}. \tag{3.58}$$

When the cyclic prefix length is longer than the channel impulse response, $T^{z,I}_{m,z} = 1$ and $T^{z,Q}_{m,z} = j$, and the bracketed terms in the denominator of (3.58) are zero. However, when an insufficient cyclic prefix length is used, these terms account for the aforementioned impossibility of performing a perfect equalization of the channel with a one-tap FEQ.

In order to illustrate the validity of the proposed method, the SDR given by (3.58) is compared with the one obtained by means of simulations. To this end, the PLC channel response shown in Fig. 3.14 (a) is employed. Fig. 3.14 (b) depicts the SDR values corresponding to a DMT system with pulse-shaping and windowing and to a conventional one. In both cases $N = 1024$ and $cp = 25$. The DMT system with pulse-shaping and windowing has been parameterized with $\alpha = \beta = 50$. As seen, there is perfect matching between the values calculated with both procedures.

The implementation complexity of the analytical procedure is essentially that of the N convolutions and the $6N$ FFT's of $2N$ points (slightly higher for the DMT system with pulse shaping and windowing). In a conventional system simulation, the transmission of M symbols requires M convolutions and $2M$ FFT's of $2N$-points. Hence, for $M = N$, the computational load of the proposed method is 2.3 times the one of a system simulation. The amount of memory required to store $\mathbf{T}$ grows with the square of the number of carriers. However, the ISI and ICI can be obtained from the columns of $\mathbf{T}$ without the necessity of storing the whole matrix.

It is worth noting that the presented method can be also used to compute the effect of a frequency mismatch, Δf (ppm), between the transmitter and the receiver clocks in systems that employ a frequency domain timing correction scheme based on a ROTOR [98]. Just by modifying the transmitted pulse according to

$$p_k[n] = \frac{1}{2N}\, e^{j\frac{\pi}{N}k(n(1+\Delta f)-cp-\alpha)} w_{TX}[n(1+\Delta f)], \tag{3.59}$$

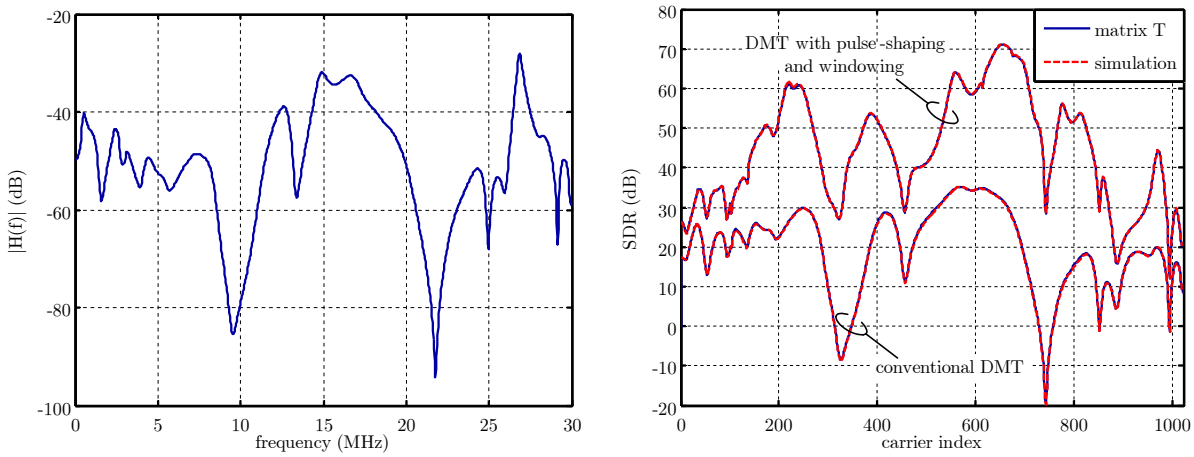

(a) channel amplitude response

(b) signal to distortion ratio

Figure 3.14: Comparison between the SDR calculated using the transmission matrix and by means of simulation

the SDR due to the frequency mismatch can be calculated.

In addition, the analytical method proposed in this section is a powerful tool for the study of carrier allocation strategies, since the ICI caused by a single carrier can be easily computed. This approach becomes particularly useful in multiuser environments where, once the transmission matrices have been computed, the SDR for different carrier assignments can be obtained with a reduced computational load employing expression (3.58).

3.3.2 Determination of the cyclic prefix length

To assess the performance of the DMT system in terms of the cyclic prefix length and the number of carriers, a *best-case channel* and a *worst-case channel* from an apartment environment have been selected. The receiver is placed in a fixed position and the transmitter is placed at about 18m within the same electrical circuit of the indoor power network and at 34m in a different electrical circuit, respectively. Fig. 3.15 (a) shows the frequency responses and the noise PSD of both channels. The PSD of the received noise, depicted in Fig. 3.15 (b), is practically the same in both cases because there are minimal changes in the network configuration (only the transmitter position).

DMT system with rectangular pulses

Bit-rate values obtained in both channels as a function of the cyclic prefix length and the number of carriers are shown in Fig. 3.16. Let's concentrate firstly in the influence of the former parameter. As seen, there is a range in which increasing its value improves the system performance due to the reduction in the ISI and ICI. However, once the distortion power is smaller than the noise one or, even being greater, its reduction does not compensate for the symbol rate loss, enlarging the cyclic prefix is counterproductive. It is also worth noting that

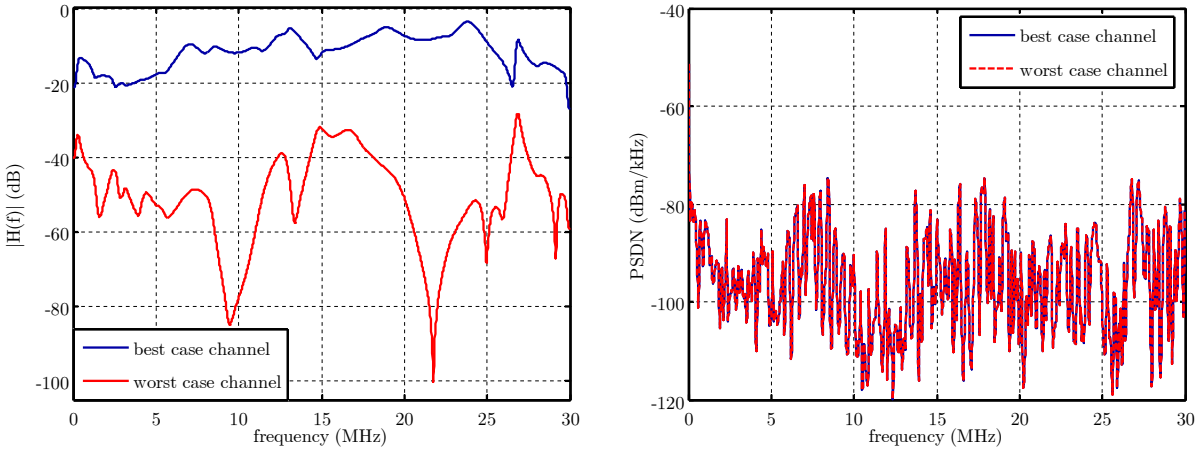

(a) channel frequency response (b) received noise PSD

Figure 3.15: *Best-case* and *worst-case* channels used in the performance assessment

its optimum value depends not only the channel profile and the noise PSD, but also on the number of carriers. This effect has a threefold origin. On the one hand, increasing the number of carriers improves the transmission efficiency because the proportion of time used for the transmission of the cyclic prefix is reduced. In addition, since the bandwidth of each carrier is smaller, distortion is also reduced. On the other hand, increasing the number of carriers enlarges the rectangular window used at the receiver. In a white noise environment this would have no effect, but in a non-white noise scenario this leads to a reduction in the out-of-band noise at the outputs of the DFT. As a conclusion, it can be stated that around 200 samples (at 60MHz) may be an appropriate cyclic prefix length for most channels. Regarding the number

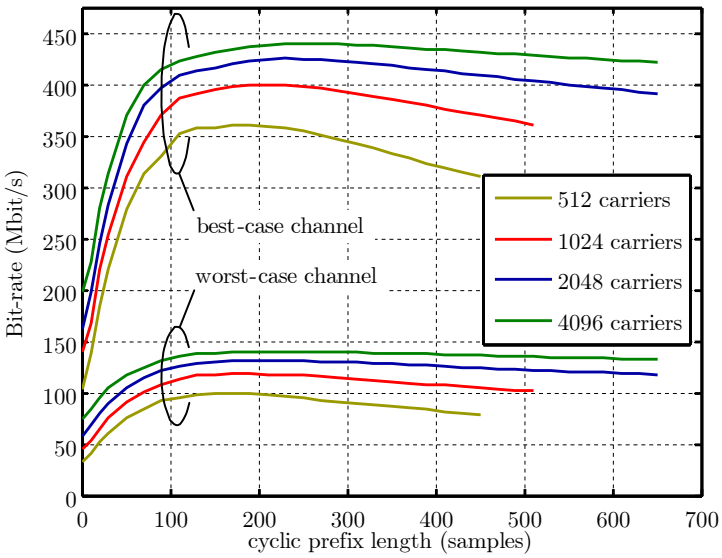

Figure 3.16: Bit-rate in the *best-case* and *worst-case* channels as a function of the cyclic prefix length and the number of carriers

of carriers, increasing its value always improves the performance, due to the reasons stated in

the preceding paragraph. In particular, there are significant gains when going from 512 carriers to 1024. However, for values higher than 2048 gains tend to reduce below 5%.

DMT system with pulse-shaping and windowing

In the analysis of a DMT system with pulse-shaping and windowing it is convenient to distinguish between the two terms that integrate the cyclic prefix, i.e. the one introduced in the windowing process and the one used to absorb the channel impulse response. Thus, the expression cyclic prefix is exclusively used in this subsection to make reference to latter term, although, the cyclic prefix of the system is actually β samples longer.

To assess the performance improvement obtained by means of pulse-shaping and windowing, the following procedure is employed. The number of carrier is varied from 512 to 4096 and the cyclic prefix length from 0 to 300 samples (remember that β is not included here). For each pair of N and cp, the bit-rate is computed for a wide range of α and β values and the maximum bit-rate is selected. This value is expressed as a percentage of the maximum bit-rate achieved by a conventional DMT system with the same number of carriers. Fig. 3.17 depicts the result of this process. Maximum performance gains are obtained by selecting β according to the values shown in Table 3.1, while α must be fixed to zero in all cases. The reason to avoid pulse-shaping is that it only reduces the ICI, while windowing also reduces the power of the non-white noise at the FFT output. Hence, the latter technique provides additional benefits for a given symbol rate reduction.

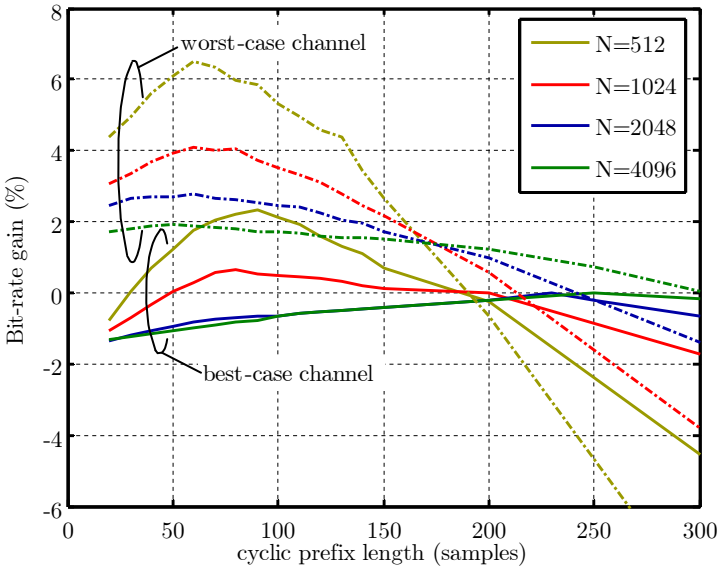

Figure 3.17: Bit-rate gains obtained by using pulse-shaping and windowing in the *best-case* and *worst-case* channels

Table 3.1 shows that, as long as the windowing provides bit-rate gains, the higher the number of carriers, the larger the optimum value of β. This is a consequence of the improvement in the transmission efficiency that occurs as N increases, since the time devoted to transmit the

β samples represents a smaller percentage of the symbol duration. Nevertheless, maximum performance gains are generally fairly modest and trend to zero as the number of carriers is increased. This situation can be clearly observed in the *best-case* channel when $N = 2048$ and $N = 4096$. As shown in Table 3.1, $\beta = 0$ is the optimum value in these circumstances. This is not a surprising result, since the conventional DMT is a channel capacity achieving strategy for $N \to \infty$. In the *worst-case* channel distortion is yet greater even for a relatively high number of carriers. Hence, the ICI reduction achieved by the windowing process still compensates for the symbol rate reduction.

Channel	N**=512**	N**=1024**	N**=2048**	N**=4096**
best-case	60	70	0	0
worst-case	90	130	160	220

Table 3.1: Values of β that maximize the performance of the DMT system with windowing

It is worth noting that bit-rate gains in Fig. 3.17 can not be achieved simultaneously in both channels, since they require different values of β. Consequently, average performance improvements will be lower than the ones in Fig. 3.17. Moreover, it could be even counterproductive if the number of carriers is high. Therefore, conventional DMT will be the only modulation scheme considered in this work until chapter 5, in which the benefits of pulse-shaping and windowing in a multiuser environment will be investigated.

3.3.3 Time equalization

The use of the cyclic prefix is certainly a simple equalization method. However, as mentioned in section 3.2.1, it may result in a significant symbol rate loss when the channel impulse response is of considerable length. One way of reducing the performance degradation is to increase the number of carriers, which increases the end-to-end delay and the implementation complexity. An alternative solution based on shortening the channel impulse response by means of a TEQ was firstly proposed in [57]. After obtaining a MSE pole-zero model for the DSL channel impulse response, the authors propose to place a FIR filter, whose zeroes equal the poles of the channel, before the removal of the cyclic prefix. This design strategy can be categorized within the *zero-forcing* design criterion, in which the objective is to constrain the channel impulse response to $(cp + 1)$ samples. Additional *zero-forcing* schemes based on iterative and block methods have been proposed in [99, 100, 101]. Maximizing the confinement of the channel impulse response does not necessarily maximize the transmission rate. Nevertheless, the design of the TEQ coefficients for true capacity optimization leads to a highly non-linear optimization problem with local minima [102]. This makes it impractical for real-time implementations. Moreover, it has been shown that performance gains over the simpler *zero-forcing* criterion are small [101].

Despite the TEQ design has been around for more than a decade, the problem is still difficult and largely unsolved. Convergence is uncertain in most methods. In particular, it is well-known

that performance obtained with TEQ's designed according to the *zero-forcing* criterion often exhibit a non-monotonic character with respect to the number of coefficients, and a nonsmooth behavior with respect to the beginning of the $(cp+1)$-samples window imposed in the design process [58].

The aim of this section is to evaluate the suitability of employing a TEQ in a PLC environment. To this end, both the performance and implementation complexity of this equalization strategy is analyzed.

Design criterion and performance

The TEQ *zero-forcing* criterion is grounded on the observation that the ISI and ICI are caused by the part of the channel impulse response not absorbed by the cyclic prefix. Hence, the idea is to constrain the composite impulse response of the channel and the TEQ, $h_c[n]$, to $(cp+1)$ samples. Fig. 3.18 illustrates this process, where $h_{teq}[n]$ is the TEQ impulse response.

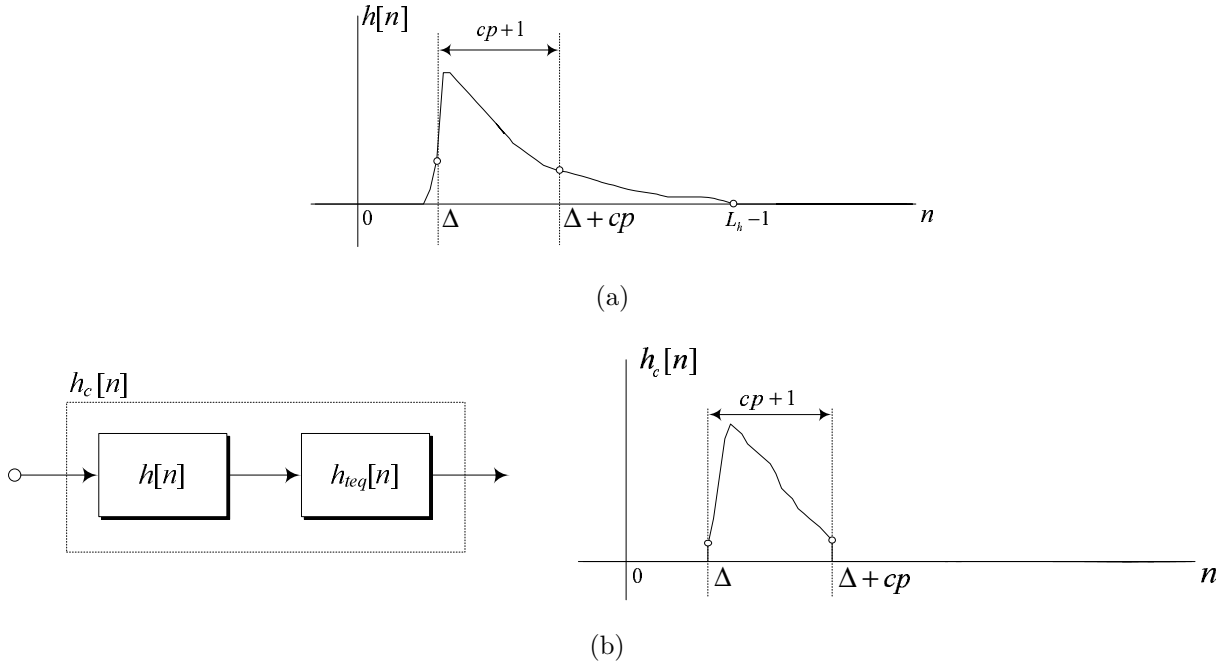

Figure 3.18: Time equalization principle: (a) channel impulse response; (b) composite impulse response

In practice, it is impossible to achieve a perfect shortening of the channel impulse response and the effective length of $h_c[n]$, L_{h_c}, is greater than the cyclic prefix length. The relative magnitude of the energy outside the $(cp+1)$-samples window beginning at Δ, known as confinement,

$$F(\text{dB}) = -10\log\left(\frac{\sum_{n\notin[\Delta,\Delta+cp]} h_c^2[n]}{\sum_{n=0}^{L_{h_c}-1} h_c^2[n]}\right), \tag{3.60}$$

is commonly used as an indicator of the TEQ performance.

In this work, the time-domain TEQ design method proposed in [101] is employed. Denoting by M_{TEQ} the number of TEQ taps, the problem is stated as

$$\sum_{n=0}^{M_{TEQ}-1} h[n-k]h_{teq}[k] = 0 \quad \text{for} \quad 0 \leq n \leq \Delta - 1 \quad \text{and} \quad \Delta + cp + 1 \leq n \leq L_{h_c} - 1, \tag{3.61}$$

subject to

$$\sum_{n=0}^{M_{TEQ}-1} h[n-k]h_{teq}[k] = 1 \quad \text{for} \quad n = \Delta, \tag{3.62}$$

to avoid the trivial solution. The TEQ taps are then obtained by calculating the minimum mean-squared error (MMSE) solution of the resulting overdetermined system of linear equations.

The confinement and the system bit-rate achieved using the above method is highly dependent on the value of Δ imposed in the design process. Fig. 3.19 illustrates this end for the *best-case* channel shown in Fig. 3.15. The blue curves (left axis) represent the confinement, while the green ones (right axis) depict the bit-rate. Both magnitudes are plotted versus $d = \Delta - D$, i.e. the displacement of the confinement window imposed in the design process with respect to the beginning of the $(cp + 1)$-samples window of the channel impulse response with maximum confinement. Fig. 3.19 also corroborates two of the already mentioned characteristics of the TEQ's designed with the *zero-forcing* criterion. First, the nonsmooth behavior of the performance with respect to d and, second, the fact that maximizing the confinement does not maximize the bit-rate (see the case of $cp = 100$ and 17 taps). Finally, it is interesting to note that $\Delta = D$ is an appropriate selection to maximize the system performance.

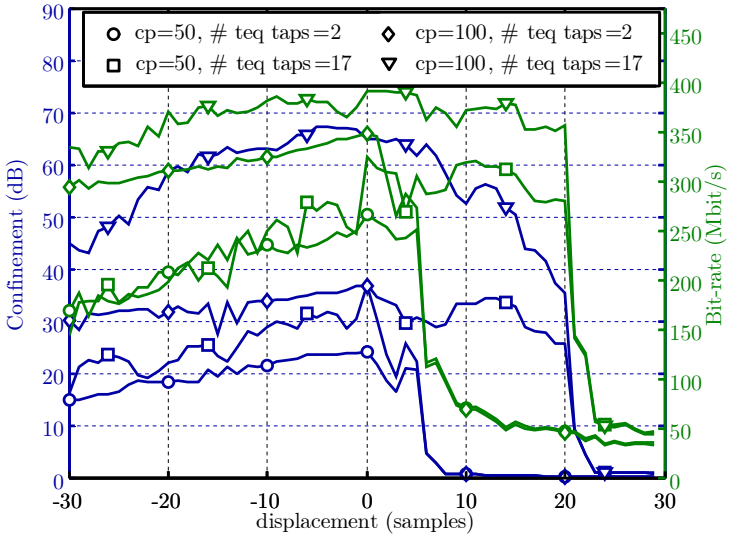

Figure 3.19: Confinement and bit-rate values for the *best-case* channel of Fig. 3.15 for various number of TEQ taps and cyclic prefix lengths

To evaluate the convenience of using a TEQ, the system bit-rate and implementation complexity are compared with the ones obtained by doubling the number of carriers. The *best-case* channel is used for this purpose, since in the *worst-case* one performance is rapidly limited by the noise

and there is little margin for distortion reduction. Fig. 3.20 (a) depicts the confinement values and Fig. 3.20 (b) the corresponding bit-rates for a system with 512 carriers. The maximum bit-rates achieved by a non-equalized system with 512 (black line) and 1024 carriers (brown line) have been also drawn as a baseline. It is interesting to note that the confinement experiences considerable increments with the number of taps only when the cyclic prefix is long. On the contrary, it saturates, or increases very slowly, for shorter cyclic prefixes. Although the system performance does not depend only on the confinement, but also on the distribution of the remaining energy of the impulse response, the observed behavior has a clear reflect in the bit-rate. The correspondence is particularly plain for $cp = 75$, $cp = 50$ and $cp = 25$. In the latter case, the non-monotonic character of the performance with respect to the number of taps can be also observed. For $cp = 100$ and $cp = 150$ the bit-rate saturates rapidly with the number of taps. The reason is that these are nearly optimum cyclic prefix values for the DMT system without TEQ, as shown in Fig. 3.16. Hence, reducing the distortion produces small increments in the system performance, which is nearly dominated by the noise.

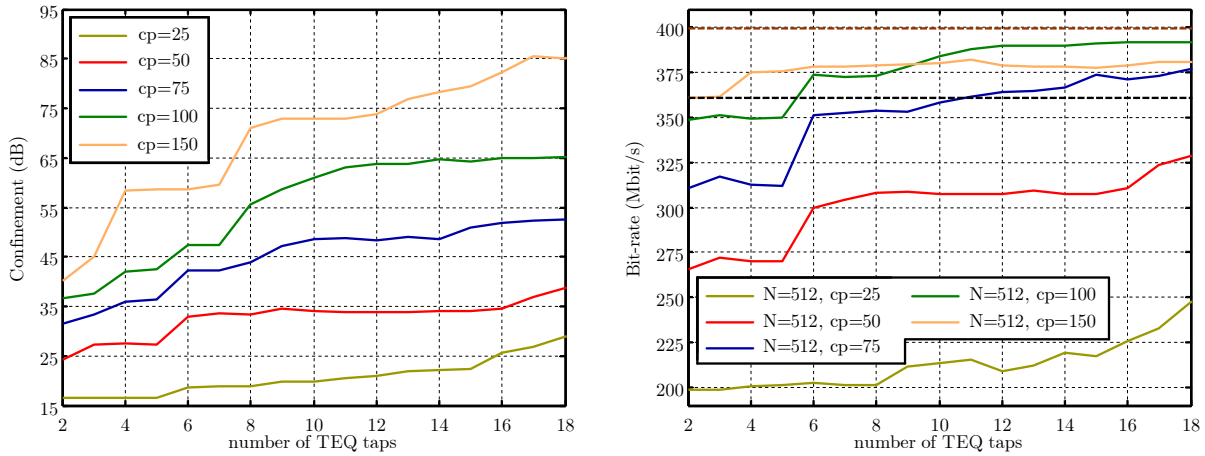

(a) (b)

Figure 3.20: (a) Confinement and (b) bit-rate values attained by using a TEQ in the *best-case* channel

Fig. 3.20 (b) shows that the bit-rate of a DMT system can be improved by using a TEQ, although the performance gain is always smaller than the one obtained by a properly parameterized system with twice the number of carriers. In particular, a system with 1024 carriers and $cp = 210$ outperforms the bit-rate of a 4-taps TEQ system with 512 carriers and $cp = 150$ by approximately 6.7%. However, the computational load of both systems must be compared before taking a decision on the suitability of the TEQ. Table 3.2 displays the number of operations per second required by the FFT and the TEQ filtering of both systems as a function of the sampling frequency, f_s. It has been assumed that the TEQ filtering is performed in the time domain, while a radix-2 algorithm is employed to compute the FFT. As seen, the computational load of the system with 1024 carriers is lower that the one with 512 and a TEQ.

The preceding analysis allows to conclude that the TEQ is not a convenient option for indoor power-line environments, since greater bit-rate improvements can be obtained with reduced computational load alternatives like doubling the number of carriers. This result contrasts

with the good performance exhibited by the TEQ in other wired scenarios like DSL. The discrepancy is grounded in the remarkably low-pass shape of the latter channels, in which the cancellation of a couple of poles increases the confinement by more than 30dB even with short cyclic prefix lengths [101].

System	FFT	TEQ filtering	Total
$N = 512$, $cp = 150$, 4-taps TEQ	$43.61\, f_s$	$7\, f_s$	$50.61\, f_s$
$N = 1024$, $cp = 210$, no-TEQ	$49.89\, f_s$	0	$49.89\, f_s$

Table 3.2: Computational load comparison of a system with 512 carriers employing a TEQ and the optimum system without TEQ and 1024 carriers

3.4 Analysis and optimization of DMT in cyclic channels

In section 3.3, the optimum number of carriers and cyclic prefix length to be used in a DMT system were determined under the assumption of an LTI channel. It was shown that increasing the cyclic prefix length reduces the distortion caused by the frequency selectivity of the channel, but also reduces the transmission efficiency. Regarding the number of carriers, it was concluded that increasing its value always improves the performance because distortion caused the frequency selectivity of the channel is reduced and transmission efficiency is increased. In addition, it reduces the out-of-band power captured by the side lobes of the rectangular pulses employed at the receiver, which is of particular interest in a colored noise environment. However, when a DMT signal traverses a time-variant channel, ICI appears even if the channel impulse response is shorter than the cyclic prefix length. Orthogonality is lost because of the bandwidth enlargement suffered by the carriers after passing through the channel. Hence, augmenting the number of carriers enlarges the symbol length, which makes the system more sensitive to time variations and, consequently, increases the ICI. In the mobile radio environment this problem was firstly tackled by [103], upper bounds for the ICI are given in [104], and a comprehensive analysis can be found in [55].

The objective of this section is to determine the optimum number of carriers and cyclic prefix length to be used when the cyclic short-term variations of the channel are taken into account. To this end, an analytical expression for the ICI caused by the channel time variations is firstly derived. It will be also shown that distortion due to the frequency selectivity of the channel is essentially time-invariant. Both results are used to determine the bit-rate in the channels of the cyclic model.

3.4.1 Analytical estimation of the distortion due to the time selectivity of the channel

The discrete-time expression of a DMT signal with N carriers and cp samples of cyclic prefix can be written as

$$x[n] = \sum_{\ell=-\infty}^{\infty} \sum_{k=-(N-1)}^{N} \frac{1}{2N} X_{\ell,k}\, e^{j\frac{2\pi}{2N}k(n-cp-\ell L)} w_L\left[n-\ell L\right], \tag{3.63}$$

where $L = 2N + cp$, $X_{\ell,k}$ is the ℓ-th complex value transmitted in carrier k and $w_L[n]$ is a rectangular window with non-zero samples in the range $0 \leq n \leq L-1$.

Let's consider an indoor power-line channel sampled with a frequency multiple of the mains one. In the absence of long-term changes its response can modelled as a discrete-time LPTV filter with impulse response $h[n,m]$, where n is the observation time and m is the elapsed time since the impulse is applied. In a noiseless situation, the channel output to the input signal $x[n]$ can be expressed as [105]

$$y[n] = \sum_{m=0}^{L_h(n)-1} h[n,m]x[n-m], \tag{3.64}$$

where $L_h(n)$ is the length of the impulse response observed at time n. However, as measurements presented in chapter 2 showed that $L_h(n)$ is essentially invariant along the mains cycle, from now on it is denoted by L_h. Subsequent expressions can be simplified by separating the impulse response of the channel during the useful part of the ℓ-th symbol in two terms,

$$h[n+\ell L+cp, m] = h_\ell[m] + \Delta h_\ell^n[m] \qquad 0 \leq n \leq 2N-1, \tag{3.65}$$

where $h_\ell[m]$ is the impulse response at the middle of the useful part of the ℓ-th DMT symbol and $\Delta h_\ell^n[m]$ accounts for the time variation of the channel during the n-th sample of the ℓ-th symbol with respect to $h_\ell[m]$. As it will be corroborated later on, for reasonable symbol lengths, the time-variant term can be assumed to have a linear variation,

$$\Delta h_\ell^n[m] = \Delta h_\ell[m] \frac{(n-N+1/2)}{2N} \qquad 0 \leq n \leq 2N-1. \tag{3.66}$$

The first term in (3.65) is time-invariant during each symbol. Hence, it only causes ISI and ICI due to the frequency selectivity of $h_\ell[m]$. On the other hand, the response in the second term is time-variant, which causes ICI. These distortion terms can be estimated by means of simulation with an LTPV filtering, which in this work is performed according to the scheme shown in Fig. 3.21. The structure is based on the *direct form A* described in [105] but with linear interpolation between adjacent filter responses. The number of impulse responses within the mains cycle is fixed to $P = 976$, distributed at regularly intervals of $\upsilon = 1024$ samples [34]. The filter responses, $h_p[n]$, correspond to the channel response at time $n + p\upsilon$ to an impulse applied at time $p\upsilon$, where $0 \leq p \leq P-1$. The values of γ_n are given by

$$\gamma_n = \frac{n}{\upsilon} - \left\lfloor \frac{n}{\upsilon} \right\rfloor. \tag{3.67}$$

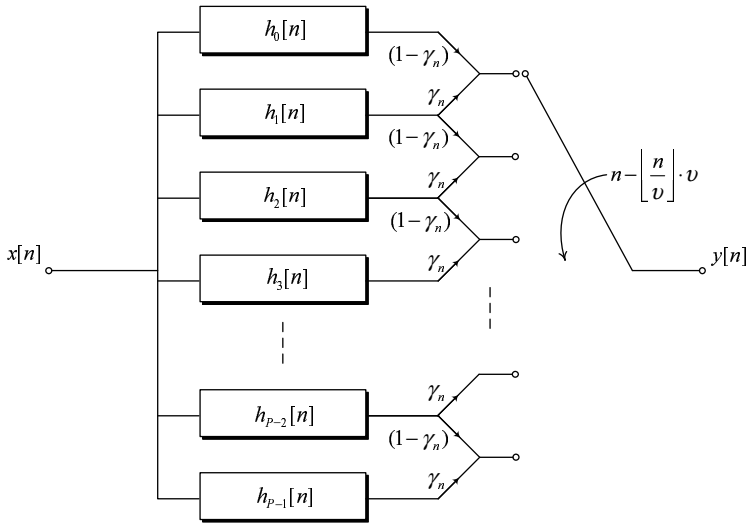

Figure 3.21: Structure of the LPTV filtering implemented in the simulator

LPTV simulations lead to considerable simulation time because, in practice, the computation of each output symbol from the channel requires the use of several filters from the bank. This thesis proposes a much faster and simpler method in which each term is calculated independently with a different procedure.

Distortion due to the channel time variations

To obtain an analytical expression of the ICI caused by the channel time variation, the distortion terms due to the channel frequency selectivity are eliminated by selecting $cp \geq L_h - 1$. Under these circumstances, at the receiver, the ℓ-th output of the DFT in carrier k can be expressed as

$$\begin{aligned} Y_{\ell,k} &= \sum_{n=0}^{2N-1} y[n+\ell L+cp]\, e^{-j\frac{2\pi}{2N}kn} = X_{\ell,k}H_\ell[k] \\ &+ j\frac{1}{4N}\sum_{\substack{i=-(N-1)\\ i\neq k}}^{N} X_{\ell,i}\,\Delta H_\ell[i]\,\frac{e^{-j\frac{\pi}{2N}(i-k)}}{sin\left(\frac{\pi}{2N}(i-k)\right)}, \end{aligned} \tag{3.68}$$

where

$$\begin{aligned} H_\ell[i] &= \sum_{m=0}^{L_h-1} h_\ell[m]\, e^{-j\frac{2\pi}{2N}im}, \\ \Delta H_\ell[i] &= \sum_{m=0}^{L_h-1} \Delta h_\ell[m]\, e^{-j\frac{2\pi}{2N}im}. \end{aligned} \tag{3.69}$$

For the sake of simplicity, a DMT system in which transmissions are synchronized with the mains is considered. Assuming that Q complete DMT symbols can be fitted into each mains period, the symbol index can be expressed as $\ell = q+rQ$, where $0 \leq q \leq Q-1$ and $-\infty < r < \infty$. Due to the periodical character of the channel, $H_{q+rQ}[i] = H_q[i]$ and $\Delta H_{q+rQ}[i] = \Delta H_q[i]$. Thus, fixing the frequency equalizer (FEQ) in carrier k to $H_q^{-1}[k]$ and using equal power constellations,

the signal to distortion ratio (SDR) due to the channel time variations (TV) in carrier k can be expressed as

$$SDR_{TV}(q,k) = \frac{E\left[|X_{q,k}|^2\right]}{E\left[|X_{q,k} - Y_{q,k}H_q^{-1}[k]|^2\right]} = \frac{16N^2\,|H_q[k]|^2}{\sum\limits_{\substack{i=-(N-1)\\ i\neq k}}^{N} \frac{|\Delta H_q[i]|^2}{sin^2\left(\frac{\pi}{2N}(i-k)\right)}}. \tag{3.70}$$

The time variations of the channel during the preceding and subsequent symbols cause additional ICI terms when $cp < L_h - 1$. However, as it will be shown in the next section, their magnitude is negligible compared with the remaining distortion terms.

Expression (3.70) relies on the assumption that the channel time variations have a linear character. To assess the extent of this approximation, one of the cyclic model channel responses in which the time variations are more significant has been selected. The sampling frequency is fixed to 50MHz and no noise is introduced. Fig. 3.22 displays the cyclic amplitude response of the selected channel. The frequency selectivity of the channel can be clearly seen in Fig. 3.23 (a), where the averaged value of the channel attenuation along the mains cycle has been depicted. Similarly, the magnitude of the time variations is clearly manifest in Fig. 3.23 (b), where the time evolution of the amplitude response along the mains cycle at two frequencies is drawn. As seen, there are frequency bands with more than 6dB of amplitude variation.

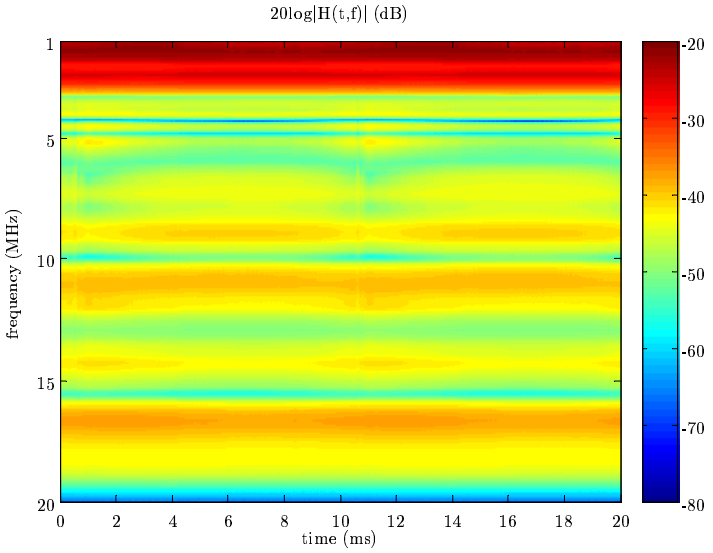

Figure 3.22: Cyclic amplitude response of the example channel

The ISI and ICI due to the channel frequency selectivity are eliminated by fixing the cyclic prefix to the extremely high value of $cp = 1022$ samples, i.e. 20.44μs (see Fig. 2.8). Results given by (3.70) are compared with those obtained by means of an LPTV simulation. Fig. 3.24 shows the time and frequency-averaged SDR values versus the base-two logarithm of the number of carriers obtained employing the two methods. Curve (a) has been obtained using (3.70) and curve (b) by means of the LPTV simulation. As seen, even for $N = 2^{15}$, the error between (a) and (b) is smaller than 3dB.

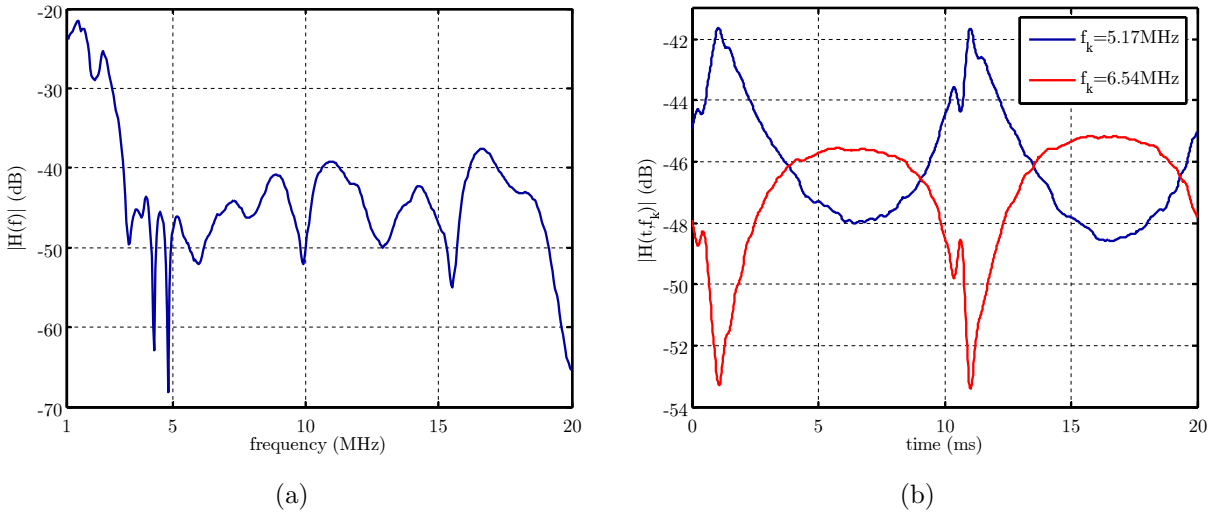

Figure 3.23: (a) Time-averaged value of the attenuation along the mains cycle; (b) Time evolution of the amplitude response along the mains cycle at two frequencies

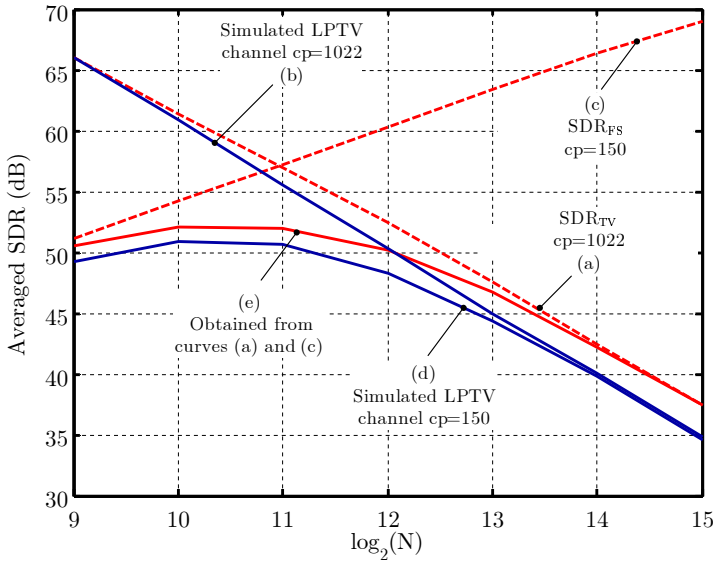

Figure 3.24: Averaged SDR values in the example channel

Distortion due to the channel frequency selectivity

Assuming that the ISI and ICI caused by the channel frequency selectivity are essentially time-invariant, their calculation can be accomplished by means of an LTI simulation using the impulse response at any time within the mains cycle. This end can be confirmed using the example channel employed in the previous subsection with a cyclic prefix of $cp = 150$ samples. This ensures that distortion is mainly due to the channel frequency selectivity (FS) when the number of carriers is low. The signal to distortion ratio, $SDR_{FS}(k)$, is then computed by means of an LTI simulation with an impulse response obtained from the time-averaged impulse response of the LPTV channel. Frequency-averaged values of $SDR_{FS}(k)$ are depicted in curve (c) of Fig. 3.24. SDR values resulting from simulations with the actual LPTV channel are

depicted in curve (d). As seen, for $N = 2^9$, where the distortion due to the channel frequency selectivity is the limiting term, the difference between (c) and (d) is below 2dB, what justifies the initial assumption.

Overall noise and distortion evaluation

Provided that the noise and the two distortion terms are independent, the signal to noise and distortion ratio (SNDR) in carrier k of the p-th transmitted symbol in each mains cycle can be obtained according to,

$$SNDR(q,k) = \left(SDR_{TV}(q,k)^{-1} + SDR_{FS}(k)^{-1} + SNR(q,k)^{-1}\right)^{-1}, \tag{3.71}$$

where $SNR(q,k)$ is the signal to noise ratio.

To corroborate the independence of the two distortion terms, the worst case channel response employed in the previous subsections is considered again in a noiseless situation. The cyclic prefix is fixed to $cp = 150$ samples. Results given by (3.71) are shown in curve (e) of Fig. 3.24. The overall SDR values obtained by means of an LPTV simulation are depicted in curve (d). As seen, except for $N = 2^{15}$, the difference is always smaller than 2dB.

3.4.2 Determination of the number of carriers and the cyclic prefix length

Performance is assessed in terms of the bit-rate, which is calculated from the SNDR under the assumption of an additive Gaussian distribution both for the distortion and the noise. The former is grounded in the central limit theorem and in the high number of carriers considered in the analysis. The latter leads to a lower bound in the performance. Channels from the cyclic model are employed in the analysis. The bit-rate of the m-th measured channel, $R_m(N,cp)$, is computed for different values of N and cp. BPSK and square QAM constellations with up to 16 bits per symbol are selected on a symbol basis subject to a target bit error probability of 10^{-5}. The averaged bit-rate loss over the M considered channels is then computed as

$$R_{loss}(N,cp) = \frac{1}{M}\sum_{m=1}^{M}\left(1 - \frac{R_m(N,cp)}{\max\limits_{N,cp}\{R_m(N,cp)\}}\right). \tag{3.72}$$

Fig. 3.25 (a) depicts the values of (3.72) expressed as a percentage. Detailed results for representative cyclic prefixes are shown in Fig. 3.25 (b). It can be observed that the most appropriate number of carriers is $N = 2^{13}$, which correspond to a symbol length of approximately 300μs (for $cp = 100$ samples), i.e. about 60 DMT symbols per mains period. However, it is worth nothing that the averaged bit-rate loss is still below 3.5% for $N = 2^{12}$. Optimum cyclic prefix lengths are shown in Table 3.3. It is worth noting that there is quite good agreement between these values and the ones derived in section 3.3.2 when an LTI channel was assumed [1]. It is

[1] It must be taken into account that results presented in section 3.3.2 were obtained for a sampling frequency of 60MHz.

also interesting to observe that the influence of the cyclic prefix length on the performance decreases as the number of carriers increases.

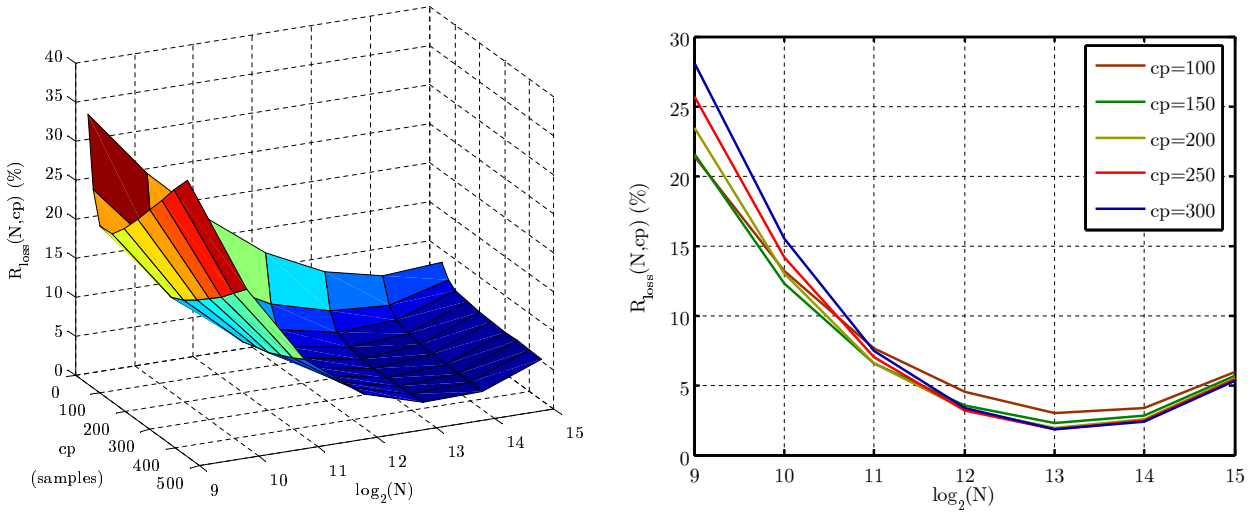

(a) (b)

Figure 3.25: (a) Averaged bit-rate loss in the overall set of measured channels as a function of the number of carriers and the cyclic prefix length; (b) Averaged bit-rate loss for selected cyclic prefix lengths

N	2^9	2^{10}	2^{11}	2^{12}	2^{13}	2^{14}	2^{15}
cp (samples)	100	150	150	250	300	350	400

Table 3.3: Optimum cyclic prefix length as a function of the number of carriers

3.5 Adaptive DMT modulation

The principle behind adaptive transmission is to vary the transmitted power level, the symbol rate, the constellation size, the coding scheme or a combination of these parameters according to the channel state [61]. The objective is to transmit at high data rates when channel conditions are favorable and to reduce the throughput when the channel gets poorer, while guaranteeing a target BER. The bit and power distribution is computed at the receiver and sent by means of a feedback channel to the transmitter. Because of their simplicity, the most common strategies are based on power level and constellation size adaptation, which are usually referred to as adaptive modulation. This strategy has been studied in depth in single-carrier systems for wireless communications, where it has been shown that little performance degradation occurs by adapting just one of these parameters [82]. Adaptive multicarrier modulation in wireless environments has also been analyzed in detail [106, 107, 108]. The common approach is to use a cyclic prefix longer than the channel impulse response and, by neglecting the ICI caused by the channel time variations, consider the multicarrier signal as a set of independent single-carrier modulations [107]. The usual objective is to maximize the bit-rate subject to the constraint of

an instantaneous BER (IBER) or an average BER (ABER) in each carrier [82]. The former is typically employed in data systems, where the frame error is the magnitude of interest, while the latter is commonly used in voice communications. In wired environments, like DSL, constellations size and power levels are also varied with time according to the instantaneous channel conditions. An initial bit-loading is performed according to an RA or MA criterion but, since time variations are expected to be small and to occur very scarcely, adaptation is accomplished by performing a *reloading* algorithm. This leads to a bit distribution with only minor changes with respect to the original one. This technique is usually referred to as dynamic bit-loading [109].

The analysis of adaptive modulation in the indoor power-line scenario has interesting particularities. Firstly, the employed modulation schemes only need to be updated at the rate of long-term changes. Secondly, the cyclic behavior of the channel allows to apply a bit-loading algorithm in the time and frequency dimensions. In this section, the use of adaptive modulation schemes to improve the bit-rate is evaluated. Long-term channel variations are not considered in the study. Information rate of the feedback channel from transmitter to receiver is not analyzed. In a first instance, several bit-loading algorithms subject to IBER and ABER constraints are proposed. Afterwards, performance is assessed over the set of measured channels presented in chapter 2.

3.5.1 System model

An adaptive DMT system synchronized with the mains is considered in this section. It is assumed that Q complete DMT symbols can be fitted in a mains cycle. The receiver has perfect knowledge of the time and frequency-variant channel response, of the noise instantaneous PSD and of the distortion (ISI and ICI) power at each carrier and symbol. Based on this, the receiver determines the constellation size to be employed in each carrier for the Q DMT symbols transmitted in a mains cycle. The bit-loading is computed under the assumption of a Gaussian distribution for the noise and the distortion. Using a feedback channel, this information is sent to the transmitter, which assigns the maximum power level allowed by the PSD constraint to each carrier. From this point on, data transmission starts and the system enters an steady state that lasts until a channel long-term change occurs. In a practical system this will require the execution of a reloading algorithm. However, as previously mentioned, this case is not considered in the presented study.

The periodical behavior of the channel allows to consider the DMT system described above as a set of flat subchannels impaired by an additive and Gaussian disturbance (noise and distortion) and referenced by their time and frequency indexes (q, k), as depicted in Fig. 3.26. Two main BER criteria can then be employed to perform the bit-loading: IBER and ABER. The former obliges to maintain the probability of bit error under an objective value, $\mathrm{BER}_{\mathrm{obj}}$, in all subchannels

$$IBER(q,k) \leq \mathrm{BER}_{\mathrm{obj}} \quad \text{for} \quad 0 \leq q \leq Q-1, \quad 0 \leq k \leq N. \tag{3.73}$$

The ABER criterion is less restrictive and imposes the average BER, which in a general sense

can be defined as

$$ABER = \frac{\mathrm{E}\left[\text{number of bit errors per transmission}\right]}{\mathrm{E}\left[\text{number of bits per transmission}\right]}, \tag{3.74}$$

to fulfil

$$ABER \leq \mathrm{BER}_{obj}. \tag{3.75}$$

To avoid confusion, from now on the BER criterion will be denoted using roman typography (e.g. ABER), while its associated BER magnitude will be denoted in italics (e.g. $ABER$).

Expression (3.74) can be computed over the number of bits transmitted in each single carrier during the data transmission phase, as illustrated in Fig. 3.26. Since the averaging is performed along the time dimension, from now it will be referred to as $\mathrm{ABER_t}$ criterion. Denoting by $b_{q,k}$ the number of bits transmitted in the subchannel (q,k), the magnitude of its associated $ABER$ in carrier k is computed according to

$$ABER_{\mathrm{t}}(k) = \frac{\sum_{q=0}^{Q-1} IBER(q,k)\, b_{q,k}}{\sum_{q=0}^{Q-1} b_{q,k}}. \tag{3.76}$$

This is the standard procedure followed in wireless systems. However, due to the periodical behavior of the indoor power-line channels, expression (3.74) can be interpreted in two additional ways. Hence, it can be calculated by performing the averaging over the frequency dimension (see Fig. 3.26), from now referred to as $\mathrm{ABER_f}$ criterion. Its corresponding $ABER$ is calculated according to

$$ABER_{\mathrm{f}}(q) = \frac{\sum_{k=0}^{N} IBER(q,k)\, b_{q,k}}{\sum_{k=0}^{N} b_{q,k}}. \tag{3.77}$$

Finally, it can be computed over the time and frequency dimensions by taking into account the total amount of bits transmitted in all carriers,

$$ABER_{\mathrm{tf}} = \frac{\sum_{q=0}^{Q-1}\sum_{k=0}^{N} IBER(q,k)\, b_{q,k}}{\sum_{q=0}^{Q-1}\sum_{k=0}^{N} b_{q,k}}, \tag{3.78}$$

as shown in Fig. 3.26.

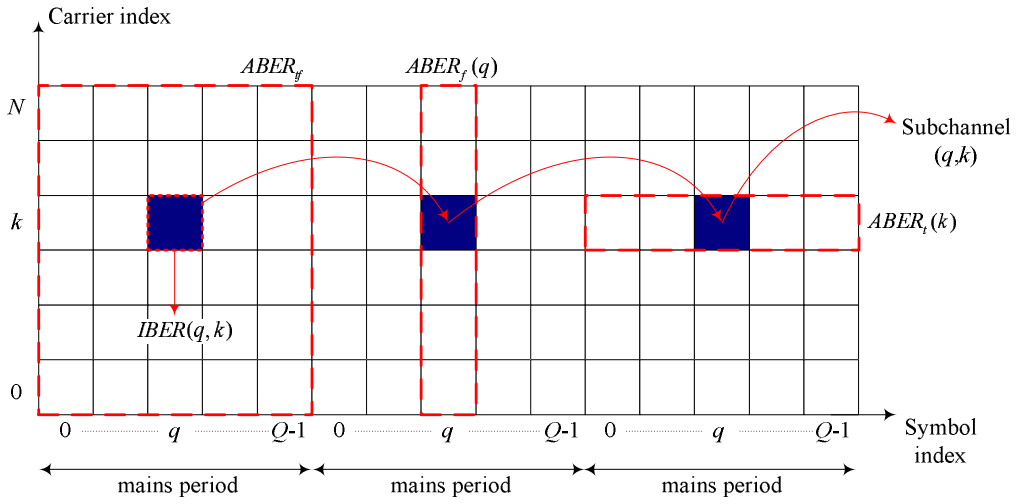

Figure 3.26: Illustration of the different BER criteria

3.5.2 Bit-loading algorithms

To assess the improvement obtained when using an adaptive scheme, several bit-loading algorithms have been developed. They are obtained by combining the above BER criteria with two modulation strategies: adaptive and fixed. While in the former each subchannel can be assigned a different number of bits, in the latter, subchannels with the same frequency index must carry the same number of bits. Algorithms subject to an IBER constraint are trivial in both cases. On the other hand, $\mathrm{ABER_t}$ and $\mathrm{ABER_f}$ criteria can be obtained by particularizing the one subject to the $\mathrm{ABER_{tf}}$ one. Similarly, those with a fixed modulation scheme can be considered as particular cases of the ones employing adaptive strategies. Hence, only the algorithm that uses an adaptive scheme subject to an $\mathrm{ABER_{tf}}$ constraint is described. Due to the high number of subchannels that result in a realistic DMT system, it is not conceivable to implement it in real-time. However, it provides an upper bound for the performance of the remaining ones and, as previously mentioned, constitutes a framework from which derive all other algorithms.

The proposed algorithm has three phases:

1. Determination of an initial bit distribution. Conceptually, the optimum bit distribution can be obtained by means of a simple iterative method in which an additional bit (two bits in case of the square QAM constellations) are assigned to the subchannel that produces the smallest increment in the $ABER_{\mathrm{tf}}$. The process continues while the objective BER is not exceeded. However, provided that millions of bits must be usually allocated, this brute force procedure has a extremely slow convergence. To accelerate the algorithm, an initial bit allocation is determined using an IBER criterion.

2. Transformation of the initial bit allocation into an optimum one. In general, the initial bit allocation performed in the previous stage is not optimum. A bit distribution can be defined as optimum if there is no other bit distribution with the same number of bits and lower $ABER_{\mathrm{tf}}$. An iterative bit swapping process starts by removing bits from those

subchannels that produce the greater reduction in the $ABER_{\text{tf}}$ and placing them in those that produce the smaller increment in the $ABER_{\text{tf}}$. This process continues until no reduction in the $ABER_{\text{tf}}$ can be obtained.

3. Allocation of new bits while the objective BER is not exceeded. At this point we have an optimum bit distribution. However, it usually happens that more bits can still be allocated without violating the BER constraint. An iterative method places additional bits in the subchannels that lead to the smallest increment in the $ABER_{\text{tf}}$. Since the complexity of this phase is proportional to the number of assigned bits, it is very important to start from a distribution with a total number of bits quite close to the optimum one.

Tasks accomplished in the above phases can be summarized as follows:

Phase 1

Let's denote the $Q \times N$ matrix that contains the number of bits assigned to each subchannel, $b_{q,k}$, by $\mathbf{b}$.

1: *Initialize* $ABER_{tf} = 0$

2: *Perform a bit-loading subject to an* IBER *constraint with* $BER(q,k) \leq \lambda \text{BER}_{\text{obj}}$

3: *while* $(ABER_{\text{tf}} < \text{BER}_{\text{obj}})$ {

4: *Update* $\mathbf{b}$

5: $\lambda = \lambda + \Delta\lambda$

6: *Perform a bit-loading subject to an* IBER *constraint with* $BER(q,k) \leq \lambda \text{BER}_{\text{obj}}$

6: *Compute* $ABER_{\text{tf}}$

8: }

The *while* loop implements a simple way of achieving a distribution with $ABER_{\text{tf}} < \text{BER}_{\text{obj}}$ and a large number of bits. Both the initial value of λ and $\Delta\lambda$ can be fixed to 1.

Phase 2

To transform the bit distribution given by the previous phase in an efficient one it is convenient to employ two $Q \times N$ matrices: $\mathbf{ABER}_{\Delta b}$ and $\mathbf{ABER}_{\nabla b}$. Element (q,k) of the former one contains the value of the $ABER_{\text{tf}}$ that results when subchannel (q,k) is assigned the immediately greater constellation. The latter is the equivalent one but when subchannel (q,k) is assigned the immediately smaller constellation. Two scalar variables are also required in this phase: $ABER^c_{\text{tf}}$ and $ABER^p_{\text{tf}}$. They contain the value of $ABER_{\text{tf}}$ computed in the current and previous iteration, respectively. In principle, this phase should be limited to a bit swapping process executed while $ABER^c_{\text{tf}} < ABER^p_{\text{tf}}$ and in which bits subtracted from the subchannel with the greater value of $\mathbf{ABER}_{\nabla b}$ are given to the subchannel with the smallest value of $\mathbf{ABER}_{\Delta b}$. However, in order to obtain an efficient distribution it may be necessary to remove two bits from a given subchannel and to assign one of these bits to one subchannel and the other bit to a different one. This would severely complicate the algorithm, hence, the bit swapping process is allowed to subtract two bits and to assign just one. The price to be paid is an increased number of iterations in this phase and in the next one.

Denoting by $\Delta b_{q,k}$ and by $\nabla b_{q,k}$ the minimum number of bits per symbol that can be added and removed from subchannel (q,k), the pseudocode of this phase can be summarized as

1: *Compute* $ABER^c_{\text{tf}}$, $\mathbf{ABER}_{\Delta b}$ *and* $\mathbf{ABER}_{\nabla b}$

2: *do* {

  3: $ABER^p_{\text{tf}} = ABER^c_{\text{tf}}$

  4: *Find the minimum value in* $\mathbf{ABER}_{\Delta b} \rightarrow (q_{min}, k_{min})$

  5: *Find the maximum value in* $\mathbf{ABER}_{\nabla b} \rightarrow (q_{max}, k_{max})$

  6: *Compute* $ABER^c_{\text{tf}}$ *with temporary values*:
  -$b_{q_{max},k_{max}} \leftarrow b_{q_{max},k_{max}} - \nabla b_{q_{max},k_{max}}$
  -$b_{q_{min},k_{min}} \leftarrow b_{q_{min},k_{min}} + \Delta b_{q_{min},k_{min}}$

  7: *if* $(ABER^c_{\text{tf}} < ABER^p_{\text{tf}})$

    8: *Update the values of* $\mathbf{b}$, $\mathbf{\Delta b}_{q,k}$, $\nabla \mathbf{b}_{q,k}$, $\mathbf{ABER}_{\nabla b}$ *and* $\mathbf{ABER}_{\Delta b}$ *corresponding to subchannels* (q_{max}, k_{max}) *and* (q_{min}, k_{min})

9: }*while* $(ABER^c_{\text{tf}} < ABER^p_{\text{tf}})$

The values of $\mathbf{ABER}_{\Delta b}$ corresponding to subchannels that have already been allocated the maximum number of bits per symbol, i.e. $\Delta b_{q,k} = 0$, are fixed to 1. This prevents from selecting any of these subchannels as the one with minimum $\mathbf{ABER}_{\Delta b}$.

Phase 3

1: *Compute* $ABER_{\text{tf}}$ *and* $\mathbf{ABER}_{\Delta b}$

2: *do* {

3: *Find the minimum value in* $\mathbf{ABER}_{\Delta b} \rightarrow (q_{min}, k_{min})$

4: *Compute* $ABER_{\text{tf}}$ *with temporary value*:
$b_{q_{min},k_{min}} \leftarrow b_{q_{min},k_{min}} + \Delta b_{q_{min},k_{min}}$

5: *if* $(ABER_{\text{tf}} < \text{BER}_{\text{obj}})$

6: *Update the values of* $\mathbf{b}$, $\mathbf{\Delta b}_{q,k}$ *and* $\mathbf{ABER}_{\Delta b}$ *corresponding to subchannel* (q_{min}, k_{min})

7: }*while* $(ABER_{\text{tf}} < \text{BER}_{\text{obj}})$

Once again, the values of $\mathbf{ABER}_{\Delta b}$ corresponding to subchannels that have already been allocated the maximum number of bits per symbol are fixed to 1. This causes the algorithm to end when all subchannels have allocated the maximum number of bits and the $ABER_{tf}$ is still lower than BER_{obj}

3.5.3 Performance evaluation

In this section, the performance of the seven bit-loading algorithms resulting from the combination of the different BER criteria with adaptive and fixed modulation schemes are assessed over the channels of the cyclic model. The algorithms will be denoted by the employed BER criterion and a letter, A or F, that indicates the utilized modulation strategy (adaptive or fixed). The resulting cases are summarized in Table 3.4. The case $\text{ABER}_{\text{f}} - \text{F}$ is not considered because its complexity is similar to the $\text{ABER}_{\text{tf}} - \text{F}$ but it has inferior performance.

Algorithm	BER criteria	Modulation strategy
$\text{ABER}_{\text{tf}} - \text{A}$	ABER in time and frequency	Adaptive
$\text{ABER}_{\text{tf}} - \text{F}$	ABER in time and frequency	Fixed
$\text{ABER}_{\text{t}} - \text{A}$	ABER in time	Adaptive
$\text{ABER}_{\text{t}} - \text{F}$	ABER in time	Fixed
$\text{ABER}_{\text{f}} - \text{A}$	ABER in frequency	Adaptive
IBER – A	IBER	Adaptive
IBER – F	IBER	Fixed

Table 3.4: Summary of the analyzed bit-loading algorithms

Two DMT systems are considered: the first one uses 512 carriers and 100 samples of cyclic prefix and the second employs 8192 carriers and 300 samples of cyclic prefix. The former has been selected because of its simplicity and the latter because it is the optimum one, as it has been shown in section 3.4.2. The sampling frequency is fixed to 50MHz. Distortion terms due to the time and frequency selectivity of the channel are obtained using the method described in section 3.4.1. BPSK and square QAM constellations with a maximum of 16 bits per symbol are employed. Algorithms are executed with an objective bit error probability of 10^{-5}.

In a first instance, the influence of the set of employed constellations on the system performance is evaluated. To this end, bit-rate values obtained with a practical system employing the $\mathrm{ABER_{tf}}-\mathrm{A}$ are contrasted with an ideal one using an $\mathrm{IBER}-\mathrm{A}$ scheme with an hypothetical set of constellations with an SNR gap given by (3.20) but in which the number of bits per symbol can take any real value in the range $[0, 16]$. This allows to evaluate how far to capacity is the practical system performing. Since the $ABER_{\mathrm{tf}}$ of an IBER-A distribution with continuous bit distribution equals the $IBER$, this scheme will be referred to as "$\mathrm{ABER_{tf}}-\mathrm{A}$ Cont" from now on.

Fig. 3.27 shows the CDFs of the bit-rates achieved in the overall set of measured channels for the 512 carriers system. The CDF of the bit-rate loss of the $\mathrm{ABER_{tf}}-\mathrm{A}$ with respect to the "$\mathrm{ABER_{tf}}-\mathrm{A}$ Cont" has also been depicted using the top axis. It can be seen that the achieved bit-rates are approximately half of the capacity values shown in Fig. 2.22. The two main causes for this considerable degradation are the *SNR gap*, which for the objective BER is about 8dB, i.e. around 2 bits per symbol, and the distortion due to the time and frequency selectivity of the channel. In addition, it is worth noting that the use of an improper number of carriers is degrading the bit-rate by about 20%, as shown in section 3.4.2. Regarding the influence of the set of employed constellations, it can be seen that the maximum bit-rate degradation is about 14% and that in approximately 75% of the channels the loss is smaller than 10%. This result indicates that reduced gains can be expected by including QAM constellations with an odd number of bits per symbol. Moreover, their inclusion would increase the running time of the bit-loading algorithm and, in an actual system with channel long-term changes, would also increase the information rate through the feedback channel. This same conclusion applies to the system with 8192 carriers.

To compare the performance of the seven bit-loading strategies, the bit-rate loss with respect to the one obtained with the $\mathrm{ABER_{tf}}-\mathrm{A}$ criterion is employed. Fig. 3.28 shows the CDF computed in the channels of the cyclic model for both DMT systems. Firstly, it is worth noting that the use of an ABER criterion does not seem to be worthwhile when an adaptive modulation strategy is used. Thus, curve of the IBER-A case indicates that the maximum degradation is always below 7%, while implementation complexity is considerably lower. Nevertheless, if an ABER criterion is finally employed, it can be observed that almost all the gain with respect to the IBER one can be obtained by performing the averaging only in the frequency or time dimension. As a reference, differences between the IBER-A and the $\mathrm{ABER_{t}}-\mathrm{A}$ in wireless channels are even smaller [76]. On other hand, the use of a fixed modulation scheme in a wireless scenario has a dramatic impact on the system performance [76], whereas in the indoor power-line it seems to have a much smaller influence. Hence, degradation due to the use of

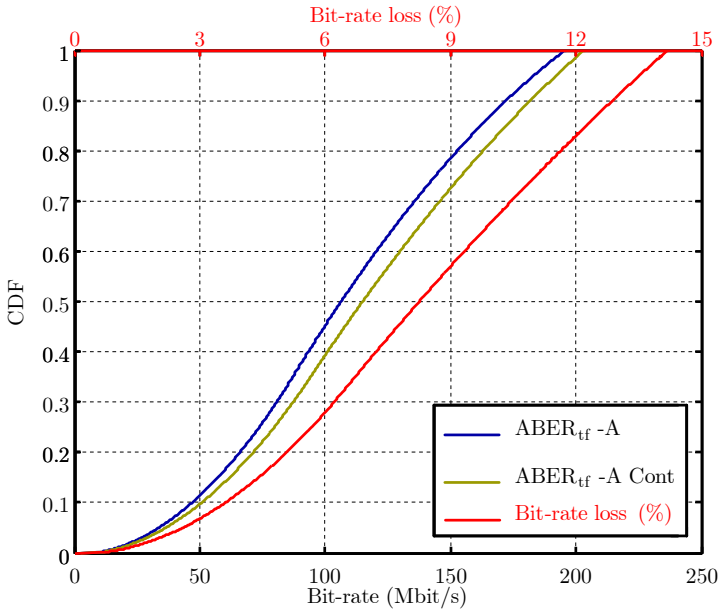

Figure 3.27: CDF of the bit-rate values and of the bit-rate loss obtained with the $\text{ABER}_{\text{tf}} - \text{A}$ with different constellation sets

a fixed modulation strategy is smaller than 10% in 60% of the channels when employing an ABER_{tf} criterion with a 512 carriers systems. Degradation goes up to 15% when employing 8192 carriers. The reason for this reduced influence of the adaptive scheme on the former system is that distortion caused by the frequency selectivity of the channel, which is nearly time invariant, is the limiting term in many channels. On other hand, the maximum performance degradation is larger when using 512 carriers, since its lower spectral resolution makes the system more vulnerable to the notable frequency selective character of the channel time variations.

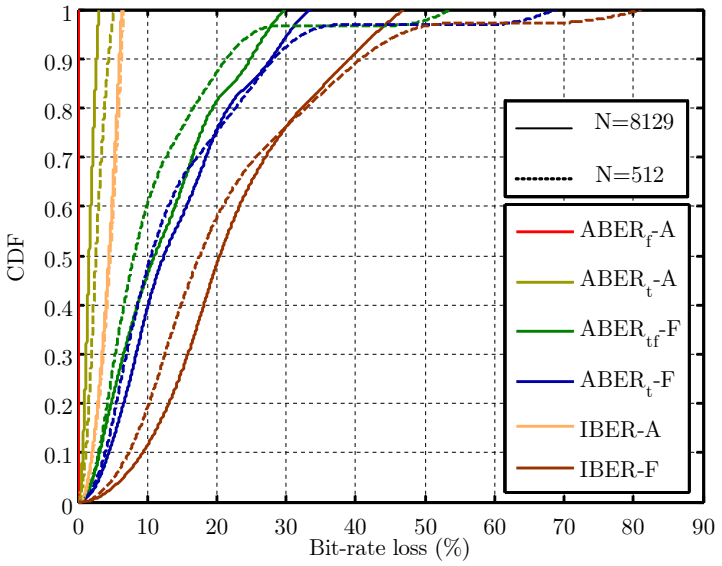

Figure 3.28: CDF of the bit-rate loss with respect to the $\text{ABER}_{\text{tf}} - \text{A}$ for $N = 8192$ and $N = 512$

Percentages in Fig. 3.28 must be handled with care. They represent bit-rate loss and, then,

have been computed taken as a reference the highest magnitude. If bit-rate gains accomplished when moving from a fixed modulation scheme to an adaptive one are computed instead, values at least twice the ones in Fig. 3.28 are obtained. Nonetheless, performance improvements provided by the adaptive modulation scheme are quite modest when compared with the ones achieved in the wireless environment. The main causes to this unexpected low gains are the frequency selectivity of the time variations and the considerably high SNDR values achieved in these channels. Their conjunction cause the additional bits that can be transmitted in a mains cycle when using an adaptive modulation strategy to be concealed by the huge amount of bits allocated to carriers in which channel conditions are nearly invariant.

Although using a fixed modulation scheme produce moderate performance degradations in systems that employ a wide bandwidth, the frequency selective nature of the time variations may cause significant bit-rate loss in systems that use smaller bandwidths. Fig. 3.29 depicts the maximum, minimum and average values of the number of bits per symbol allocated to each carrier with the $\text{ABER}_{\text{tf}} - \text{A}$ scheme in a university environment channel. The number of bits per symbol when employing the $\text{ABER}_{\text{tf}} - \text{F}$ is also drawn.

The bit-rate loss of the $\text{ABER}_{\text{tf}} - \text{F}$ strategy with respect to the $\text{ABER}_{\text{tf}} - \text{A}$ is around 13% when using the whole bandwidth. As an example, let's consider that the 2MHz bandwidth of the system proposed in [110] and the 10MHz bandwidth of the commercial one described in [64] are employed this channel. A system working in the 2MHz bandwidth occupied by carriers 50 to 90 will experience 47% of bit-rate loss, and around 23% when using the 10MHz occupied by carriers 1 to 205.

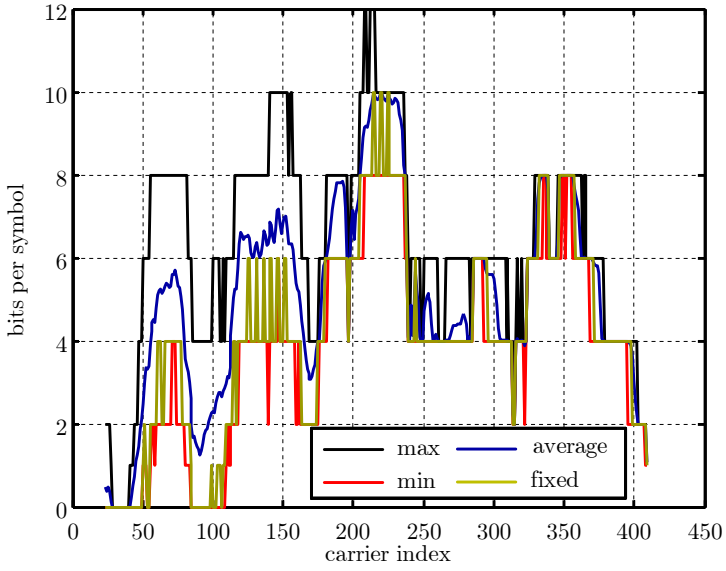

Figure 3.29: Bits per symbol in an university channel with the $\text{ABER}_{\text{tf}} - \text{A}$ and the $\text{ABER}_{\text{tf}} - \text{F}$ schemes

3.6 Conclusions

This chapter has addressed some of the most important aspects of a single-user DMT system working over broadband indoor power-line channels. Main achievements are now summarized:

- Analytical methods for estimating distortion caused by time and frequency selectivity of the channel. An analytical procedure to obtain the ICI and ISI caused by a frequency-selective LTI channel has been proposed. It has been also shown that, in actual channels, the power of these distortion terms is essentially invariant along the mains cycle. The presented method can be also used to compute the effect of timing errors and is a powerful tool for the study of carrier allocation strategies both in single-user and multiuser environments. Similarly, an analytical expression for the ICI due to the channel time variations has been developed. Both methods allow to assess the performance of a DMT system in a much faster and simpler way than by means of conventional simulations employing an LPTV filtering.

- Optimum number of carriers and cyclic prefix length. The optimum number of carriers in a DMT system working over time and frequency selective channels results from the trade-off between reducing distortion due to the frequency selectivity (high number of carriers) and diminishing distortion caused by the channel time variations (low number of carriers). It has been shown that the most appropriate number of carriers for the broadband power-line scenario is about 8192, although minimal performance losses occur when using 4096. The influence of the cyclic prefix decreases as the number of carriers increases. However, its optimum length for a system with 8192 carriers is around 300 samples at a sampling frequency of 50MHz. For a more practical system with 512 carriers, the optimum cyclic prefix length is about 150 samples.

- Performance improvements obtained by employing non-rectangular pulses. Benefits provided by pulse-shaping and windowing techniques that allow to retain the DFT-based structure of the DMT system have been investigated. It has been shown that pulse-shaping is always counterproductive, since distortion lessening does not compensate for the symbol rate reduction. On the other hand, the bit-rate can be increased in most cases by means of windowing. However, averaged gains are below 4% for 512 carriers and practically negligible for 2048 carriers.

- Suitability of time equalization. It has been shown that a large number of taps are required for the TEQ to shorten the channel impulse response significantly. As a consequence, higher bit-rates can be achieved with a reduced computational load by doubling the number of carriers.

- Adaptive modulation. Bit-rate gains obtained by adapting the constellation to the instantaneous channel conditions have been investigated. The cyclic nature of the channel naturally gives rise to ABER criteria in which the averaging can be performed in both the time and frequency dimensions. To exploit this channel behavior,

a set of bit-loading algorithms subject to different BER constraints have been developed for systems with fixed and adaptive modulation schemes. It has been proven that performing the averaging in both the time and frequency dimensions provides minimal gains with respect to the ABER criterion in which the averaging is accomplished only in the frequency or time dimension. It has also been shown that bit-rate losses caused by the use of a fixed modulation scheme are quite modest when the frequency band from 1MHz to 20MHz is employed. On the contrary, the frequency selective character of the channel time variations may cause severe degradation in systems employing narrower bandwidths. Similarly, it has been shown that performance degradation increases with the number of carriers, since distortion caused by the frequency selectivity of the channel, which is basically time invariant, decreases. As a reference, 60% of the channels experience bit-rate losses lower than 10% in a system with 512 carriers subject to an ABER constraint, and lower than 15% when 8192 carriers are used. These values nearly double when the bit-loading is accomplished using an IBER constraint.

Chapter 4

Timing Recovery Techniques for DMT

4.1 Introduction

The study performed up to now has assumed that the transmitter and the receiver were perfectly synchronized. This implies that symbols boundaries at the input of the DFT are correct and that the receiver sampling frequency and phase is synchronized with the incoming signal. Small symbol time misalignments cause ISI and ICI, while sampling (timing) errors cause rotation and attenuation of the constellation symbols, ICI and, if not corrected, may result in a severe drift of the symbol alignment. Main aspects concerning symbol boundary synchronization where presented in section 3.2.4. Hence, this chapter concentrates on sampling synchronization.

Synchronization becomes an important concern when large spectral efficiencies are needed. Nowadays, the most common procedure to accomplish synchronization is by means of a fixed frequency sampling and a digital phase-locked loop (PLL) [111], [98], [101]. Synchronization issues in scenarios with high SNR carriers have been extensively studied in DSL applications [98], [112]. A detailed and well referenced work about most of these topics can be found in [63]. However, it has been shown that when the same strategies are employed in power-line channels, their performance can be seriously degraded. As shown in [91], this inferior performance has a twofold origin: the short-term variations of the channel response and the jitter of the sampling process. Uncompensated cyclic time variations of the channel, with harmonics at multiples of the mains signal frequency, mislead the estimation of the sampling error. The periodical bias in the phase error estimates can be reduced by narrowing the loop bandwidth, but this also reduces the loop's capacity to track the sampling jitter. While the effect of random period instabilities has been extensively studied in the downconversion of OFDM signals [54], its influence on the analog-to-digital conversion has been always neglected. However, when sampling broadband signals, the relative magnitude of the jitter with respect to the sampling period increases and its effects can not be disregarded [91], [113].

In this chapter, a new timing recovery scheme for indoor PLC is proposed. To this end, the shortcomings of the conventional strategies designed for DMT systems that operate in LTI channels are firstly revisited. This analysis suggests two direct improvements. The first one is

to design a phase error estimator that takes into account the magnitude of the cyclic changes in the channel response. The second one is to modify the loop response so that higher attenuation is provided to the harmonics of these cyclic variations. Performance gains and computational complexity of both alternatives are presented and discussed. Finally, main conclusions are summarized. Results presented in this chapter have been partially published in [91] and [114].

4.2 Synchronization procedure

Synchronization procedures are notably dependent on the required accuracy, which in turns depends on the desired spectral efficiency and on the channel characteristics. In DSL systems, for instance, channel conditions allow to achieve higher transmission rates. Hence, synchronization systems must be thoroughly designed to avoid degrading the attainable performance. On the other hand, in wireless scenarios the SNR is generally much lower and a less accurate synchronization procedure suffices.

Synchronization in a DMT system is accomplished in two steps, as shown in Fig. 4.1 [101], [63]. During the former one, known as acquisition phase, coarse symbol and timing synchronization is achieved. Since the receiver still has no time reference, a periodical signal must be transmitted to this end. In principle, the higher number of carriers employed for this purpose, the improved frequency error estimation. However, unsynchronized sampling cause ICI at the DFT output, which in turns degrades the estimation. Hence, the higher number of carrier the higher ICI. Once the coarse frequency error has been estimated, the symbol synchronization task is tackled. Alternatively, in TDMA wireless systems, coarse symbol synchronization is usually accomplished in a first instance. To this end, a preamble consisting in one or more well-known symbols is usually transmitted at the beginning of the data frame, and correlation is used at the receiver to detect the symbol boundaries [115].

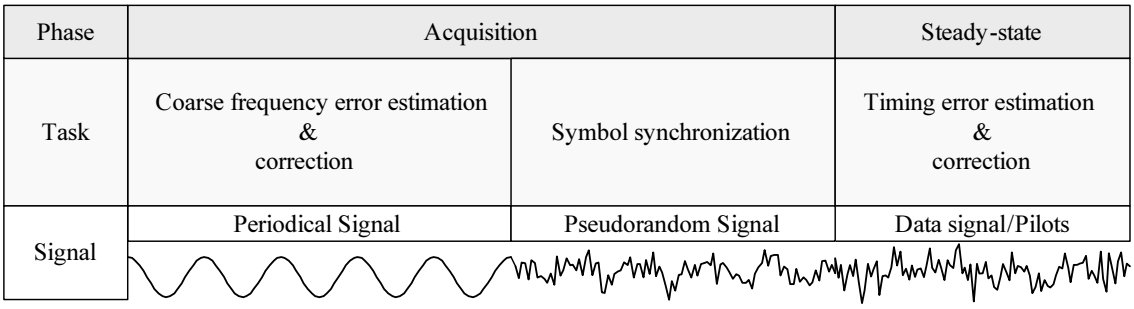

Figure 4.1: Synchronization procedure in a DMT system

Timing synchronization during the steady-state phase can be accomplished using a data-aided (DA) structure or a non-data-aided (NAD) scheme [98]. In the former case, the receiver uses the decided symbols (decision-directed) or a training sequence to estimate the timing error. In the latter case, the synchronizer structure operates independent of the transmitted data. Synchronization in a DA decision-directed system consists of two main tasks: timing recovery and timing correction. The former estimates the phase error of the received symbols and, by

means of a feedback loop, computes the correction to be applied by the latter. Timing error correction can be performed using two main approaches: in the frequency domain or in the time domain. The former is commonly employed in environments with moderate to low SNR. It consists of an skip/duplicate block that, to avoid symbol misalignment, compensates accumulated errors greater than a sample time. The remaining timing error is compensated in the frequency domain by means of a ROTOR [98]. This method is quite simple, but it does not preclude ICI. The time domain error correction scheme is employed when high spectral efficiencies are required. It is based on the digital resampling of a signal by means of an interpolator filter [116]. Interpolator filters introduce higher distortion close to Nyquist frequency, hence, oversampling is needed [63]. However, this increased complexity is compensated by a much higher performance.

This chapter concentrates on the steady-state synchronization phase and, in particular, in the timing recovery task of a DA decision-directed system.

4.3 System model

This section describes the three basic elements of the analyzed system: the channel model, the timing error model and the structure of the utilized DMT receiver.

4.3.1 Channel model

Simulations presented in this chapter have been carried out using the cyclic channel model. In particular, the study concentrates on the residential environment: the apartment and the detached house. Throughout of the work, averaged performance values computed using the overall set of channels are always preceded by qualitative results obtained in one of them. A representative apartment channel has been selected to this end. In Fig. 4.2 the modulus of the frequency response, $H(t,f)$, along the mains cycle have been superimposed (black-left axis). Fig. 4.2 also shows information about phase changes of the frequency response (red-right axis). However, this time no superimposed curves are drawn, and the depicted magnitude is the peak excursion of the phase along a cycle time, defined as

$$\measuredangle H(f)_{pp} = \max_t[\measuredangle H(t,f)] - \min_t[\measuredangle H(t,f)], \tag{4.1}$$

where $\measuredangle H(t,f)$ denotes the angle of $H(t,f)$ and $t \in [0, T_0)$. As observed, there are no significant amplitude changes and, discarding the 4dB that occur in the vicinity of the notch, the maximum variation is about 2.5dB around 1MHz. On the contrary, remarkable phase changes occur in the 1MHz to 3MHz band and in the neighborhood of 5MHz and 9MHz.

Noise in this channel is shown in Fig. 4.3, where the values of the instantaneous PSD measured along a mains cycle have been depicted. It is worth noting that differences exceeding 20dB do occur between 2MHz and 3MHz and about 15dB around 5MHz.

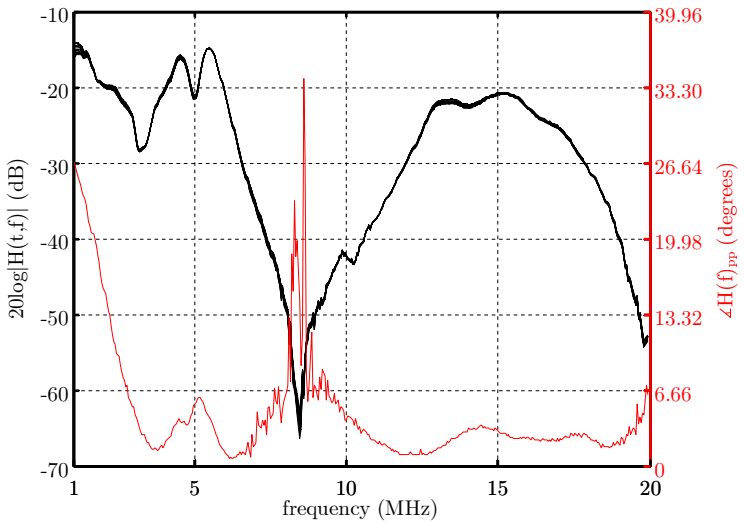

Figure 4.2: Superimposed values of the amplitude channel response along the mains cycle (black). Peak excursion of the channel phase response along the mains cycle (red)

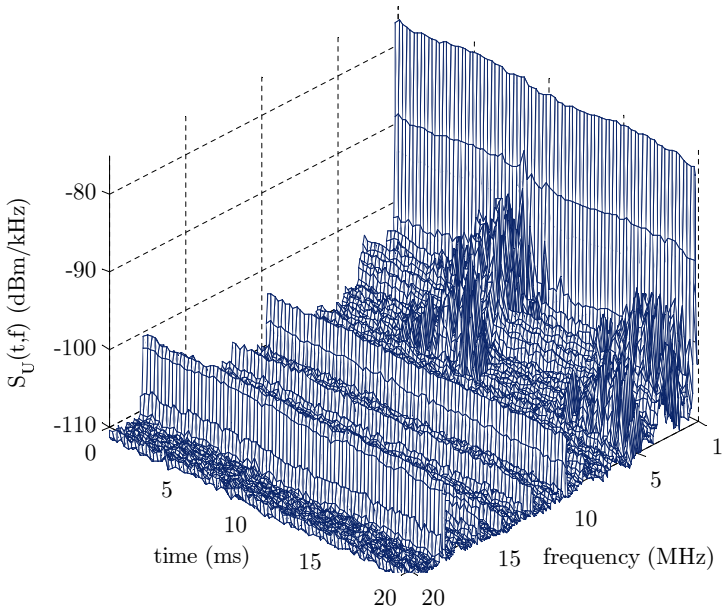

Figure 4.3: Cyclostationary noise instantaneous PSD in the example channel

4.3.2 Analog-to-digital conversion model

The sampling instants of an analog-to-digital conversion process experience two types of deviation from their nominal values. The first is a systematic effect due to the frequency inaccuracy of the clock that drives the ADC. The influence of this phenomenon on the performance of DMT systems have been widely studied [98], [112], and will not be considered in this work unless otherwise stated. The second is a random deviation with two components: one due to the fluctuations of the ADC sampling clock period, the so-called oscillator jitter, and another due

to the uncertainty in the sampling instants introduced by the sample-and-hold (S&H) circuit of the ADC, the so-called aperture jitter [117].

The signal generated by an actual sinusoidal oscillator without amplitude instabilities, has the form

$$s(t) = A\cos(2\pi f_s t + \phi_o(t)), \tag{4.2}$$

where $\phi_o(t)$ is the phase noise that models the random fluctuations caused by the noise sources of the circuit that generates the oscillation [118], [119]. Due to the phase noise, the significant instants of the signal, e.g. zero-crossings, experience a time deviation from their nominal values. This is the so-called timing jitter or simply jitter, $\tau_o(t)$, whose relation with the phase noise can be generally approximated by $\tau_o(t) \approx -\phi_o(t)/2\pi f_s$. Fig. 4.4 illustrates the effect of the oscillator jitter for a square wave [120]. In an ideal oscillator, the spacing between transitions is constant. However, in an actual one, the transition spacing is variable. The time delay between the reference and the observed transition accumulates with time because "any uncertainty in an earlier transition affects all the following transitions, and its effect persists indefinitely" [120].

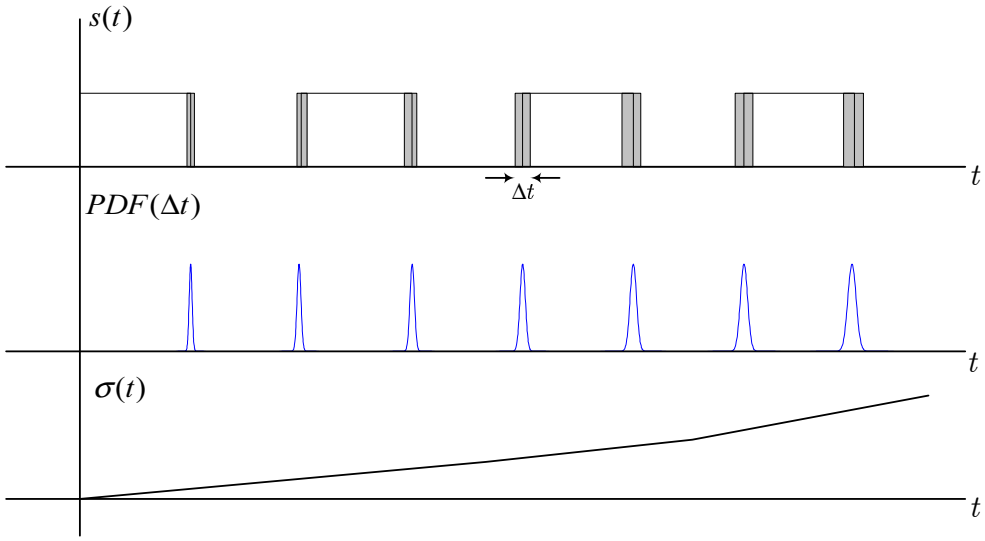

Figure 4.4: Illustrative effect of the timing jitter

It should mentioned that phase noise is still an open subject for theoretical research and, as stated in [118]: "mathematical analysis of phase noise does not rest on a firm theoretical foundation". Moreover, nomenclature found in the literature is sometimes confusing or inadequate.

Random period instabilities can be characterized in the frequency domain by means of the Phase Noise Spectrum, $S_{\phi_o}(f)$ (rad^2/Hz), [118]. For distant frequencies from the carrier, this magnitude is related with the so-called Single-Sideband (SSB) Phase Noise Spectrum

$$\mathscr{L}(f) = 10\log_{10}\left(S_s(f)/A^2\right) \approx 10\log_{10}\left(S_{\phi_o}(f)/2\right) \quad (\text{dBc/Hz}), \tag{4.3}$$

where $S_s(f)$ is the PSD of the signal in (4.2) and dBc/Hz stands for dB below the carrier power in a 1Hz bandwidth. $\mathscr{L}(f)$ is a very popular magnitude because it can be measured in a quite simple way with a spectrum analyzer. However, it should be noted that naming it SSB

Phase Noise Spectrum is a clear example of the aforementioned confusing terminology usually employed in this subject.

In the time domain, the most employed magnitude is the integrated jitter, σ_o, computed as

$$\sigma_o^2 = \frac{1}{(2\pi f_s)^2} \int_{f_L}^{f_H} S_{\phi_o}(f)\, df, \tag{4.4}$$

where f_L is usually fixed to 10Hz and f_H to 20MHz.

Phase noise is accurately characterized by means of a Power-Law model [118], [119]. It approximates $S_{\phi_o}(f)$ by a piece-wise linear function whose slopes are in the range from -40dB/decade to 0dB/decade with 10dB/decade steps. Jitter values employed in this work have been generated by filtering a Gaussian white noise with a cascade of first and second order transfer functions that approximate the different slopes of the phase noise spectrum. Fig. 4.5 shows the curves corresponding to three 100MHz state-of-the-art oscillators with integrated jitter values of 20ps, 10ps and 5ps. When modeling the phase noise of the oscillators employed in the downconversion of OFDM signals, this model is sometimes simplified and only the -20dB/decade slope is considered [54]. This leads to a Lorentzian shape for $\mathscr{L}(f)$ and to an analytically tractable problem. However, it produces excessively optimistic results when used to model the timing jitter of the ADC driving clock.

Even if an ideal oscillator could be used, actual sampling instant would fluctuate due to the aperture jitter, $\tau_a(t)$. The usual method to model these random instabilities is by means of the aperture phase noise PSD, which is assumed to have a Lorentzian shape [117]

$$S_{\phi_a}(f) = 2\pi \frac{\sigma_a^2 f_s^2}{f_s^2/4 + f^2}, \tag{4.5}$$

where σ_a is the aperture jitter rms value. Fig. 4.5 depicts the aperture phase noise PSD of a state-of-the-art 12bit, 100MHz sampling frequency ADC with 5ps of rms aperture jitter. As seen, in the frequency band of interest, it is essentially flat. Provided that the circuit has a well designed layout, oscillator and aperture instabilities can be assumed to be independent. Hence, the PSD of the overall instability, which from now on will be referred to as ADC jitter, can be obtained by summing the PSDs of the oscillator and aperture jitter.

4.3.3 DMT receiver model

The simplified block diagram of an N carrier DMT receiver with an all-digital synchronization scheme is shown in Fig. 4.6. The incoming signal is oversampled with an unsynchronized clock. Timing error correction is carried out in the time domain by means of an interpolator. By using accurate interpolator filters it can be ensured that signal distortion is essentially due to timing recovery errors. As observed, the FEQ that follows the DFT is performed in two stages. The reason is that, according to the statistics of the Doppler Spread bandwidth shown in section 2.2.1, the taps of a one-stage FEQ should be adapted at a rate comparable to that of the synchronization system. This may cause an interaction between both adaptive systems and

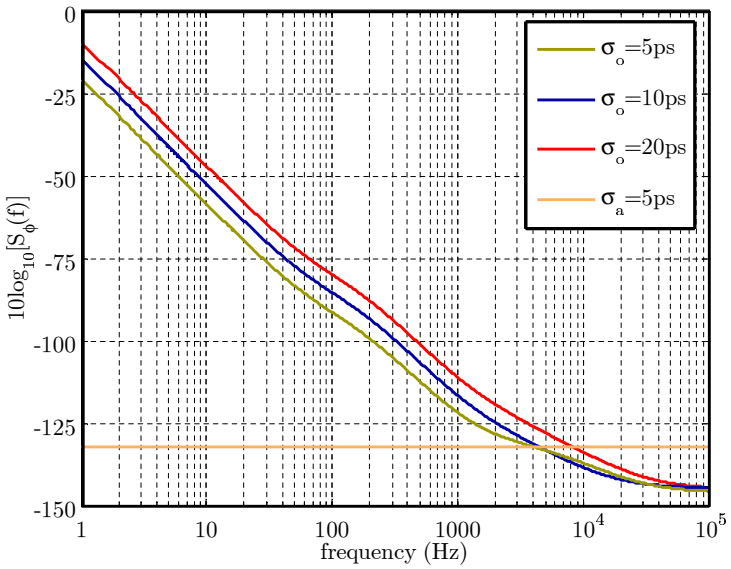

Figure 4.5: Oscillator and aperture phase noise spectra

their eventual divergence [62]. Hence, a long-term FEQ (LFEQ) is firstly used to compensate for the long-term changes in the channel response. Since these changes occur at a rate much slower than the symbol rate, the information needed for timing recovery is taken from the output of this stage. Afterwards, a short-term FEQ (SFEQ), follows the short-term variations of the channel response with respect to its long-term value. Since channels considered in this work do not present long-term changes, the LFEQ compensates for the time-average channel response over the mains cycle. The timing recovery scheme follows the conventional digital PLL structure: an estimator of the phase errors due to the uncorrected timing errors, a loop filter and a numerically controlled oscillator (NCO).

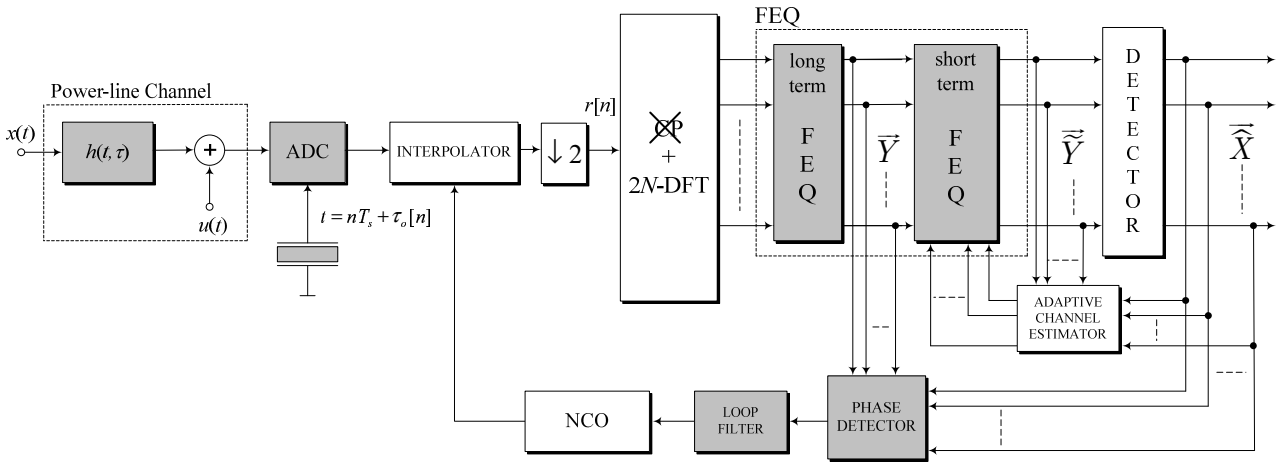

Figure 4.6: Simplified scheme of the DMT receiver

4.4 Conventional timing recovery scheme

In a first instance, this section describes the conventional timing recovery mechanism employed in DMT systems that operate in LTI channels. To this end, the expressions of the most common phase estimator and loop filter employed in time-invariant channels are firstly presented. Afterwards, the effect of the channel cyclic changes over the outputs of the phase estimator and the loop filter are quantified and the performance of the overall timing recovery scheme is assessed.

4.4.1 System description

The timing error in the signal $r[n]$ (see Fig. 4.6) varies from sample to sample due to the uncorrected jitter and frequency offset. Assuming an LTI channel and following a similar approach to the one in [111], [63], it can be shown that in the absence of ISI the expression of the ℓ-th input symbol to the receiver DFT can be expressed as [1]

$$r_\ell[n] = \sum_{k=-(N-1)}^{N} H_k X_{\ell,k} e^{j\frac{\pi}{N}k(n+\tau_\ell[n])} + u_\ell[n], \tag{4.6}$$

where $0 \leq n \leq 2N-1$ and H_k is the channel frequency response for carrier k. $X_{\ell,k}$ denotes the ℓ-th complex value transmitted in carrier k. $\tau_\ell[n]$ is the uncorrected sampling error (relative to the sampling period) for the n-th sample of the ℓ-th symbol and $u_\ell[n]$ is the channel noise term.

The k-th output of the DFT of $r_\ell[n]$ can then be expressed as

$$\begin{aligned} R_{\ell,k} &= \frac{1}{2N}\sum_{n=0}^{2N-1} r_\ell[n]e^{-j\frac{\pi}{N}kn} = \frac{1}{2N}\sum_{n=0}^{2N-1}\sum_{z=-(N-1)}^{N} H_z X_{\ell,z} e^{j\frac{\pi}{N}(z-k)n} e^{j\frac{\pi}{N}z\tau_\ell[n]} + \frac{1}{2N}\sum_{n=0}^{2N-1} u_\ell[n]e^{-j\frac{\pi}{N}kn} \\ &= \frac{1}{2N}H_k X_{\ell,k}\sum_{n=0}^{2N-1} e^{j\frac{\pi}{N}k\tau_\ell[n]} + \frac{1}{2N}\sum_{\substack{z=-(N-1)\\ z\neq k}}^{N}\sum_{n=0}^{2N-1} H_z X_{\ell,z} e^{j\frac{\pi}{N}(z-k)n} e^{j\frac{\pi}{N}z\tau_\ell[n]} + U_{\ell,k}, \end{aligned} \tag{4.7}$$

and the k-th output of the conventional one-tap FEQ, $Y_{\ell,k}$, is given by

$$Y_{\ell,k} = \frac{1}{2N}X_{\ell,k}\sum_{n=0}^{2N-1} e^{j\frac{\pi}{N}k\tau_\ell[n]} + \frac{1}{2N}FEQ_k\sum_{\substack{z=-(N-1)\\ z\neq k}}^{N}\sum_{n=0}^{2N-1} H_z X_{\ell,z} e^{j\frac{\pi}{N}(z-k)n} e^{j\frac{\pi}{N}z\tau_\ell[n]} + U_{\ell,k}FEQ_k. \tag{4.8}$$

where $FEQ_k = H_k^{-1}$ is the k-th tap of a zero-forcing FEQ. The first term in (4.8) is the desired symbol, which is attenuated and phase shifted, the second term represents the ICI. Provided

[1] For simplicity, the effect of the cyclic prefix is not considered because it does not change the essence of the analysis.

that the timing error variation along a DMT symbol is small, the attenuation of the desired symbol and the ICI term can be neglected. Hence, $Y_{\ell,k}$ can be approximated by

$$Y_{\ell,k} \approx X_{\ell,k} e^{jk\theta_\ell} + U_{\ell,k} FEQ_k, \tag{4.9}$$

where θ_ℓ is the phase error caused by the timing errors occurred during the ℓ-th symbol [101],

$$\theta_\ell \approx \frac{\pi}{2N^2} \sum_{n=0}^{2N-1} \tau_\ell[n]. \tag{4.10}$$

To verify the validity of the approximation in (4.9), the SDR at the detector input, defined as

$$SDR_k = \frac{\mathrm{E}\left[|X_{\ell,k}|^2\right]}{\mathrm{E}\left[|X_{\ell,k} - Y_{\ell,k}|^2\right]}, \tag{4.11}$$

has been computed using the expression for $Y_{\ell,k}$ given in (4.8) and the one in (4.9). For simplicity, a DMT system with 512 carriers working in a noiseless flat channel and impaired by an uncorrected sampling frequency offset of 10ppm is considered. Results are depicted in Fig. 4.7. As seen, the phase shift is the dominating term in nearly all carriers. The difference between both curves is lower than 1.2dB except for the low carriers region. However, it should be taking into account that most of the carriers in this latter zone can not be used because they fall within the reject band of the coupling circuit used to protect the receiver from the mains. Moreover, all the carriers in which the difference between both curves is higher than 2dB, experience SDR values higher than 60dB. Hence, the channel noise, and not the ICI, will be the limiting term in these carriers.

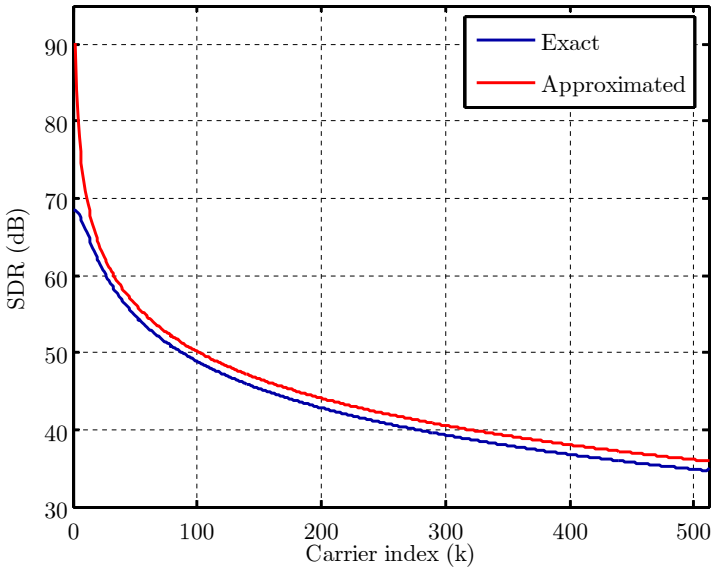

Figure 4.7: SDR values computed by taking into account the ICI and the desired symbol attenuation (exact) or only the phase shift (approximated)

The phase detector can estimate θ_ℓ based on the decided symbols (decision-directed) or using one or more predefined carriers designated as pilots. Pilot-based schemes do not seem to be

appropriate for indoor power-line environments due to their larger variance and to the unknown position of the channel frequency response notches. Hence, the former approach has been selected in this work. The maximum likelihood (ML) is probably the most widely employed estimator for this purpose. Assuming correct decisions and Gaussian noise, its expression can be approximated by [58]

$$\widehat{\theta}_\ell \approx \frac{\sum_{k\in K}\left(\Im[Y_{\ell,k}\widehat{X}^*_{\ell,k}]k/\left[|FEQ_k|^2\sigma^2_{U_k}\right]\right)}{\sum_{k\in K}k^2SNR_k}, \tag{4.12}$$

where $\widehat{X}^*_{\ell,k}$ is the complex conjugate of the detector output and SNR_k is the signal-to-noise ratio experienced by carrier k. K is the set of carrier indexes utilized in the estimation and $\sigma^2_{U_k}$ is the noise power in the band of carrier k.

The output of the phase detector is fed to a loop filter, whose transfer function,

$$L(z) = \alpha + \frac{\beta}{1-z^{-1}}, \tag{4.13}$$

is selected so that a second order type II PLL results [62]. The output of this filter is supplied to the NCO, which computes the timing adjustment to be applied to each sample of the next received symbol.

In order to analyze the performance of the ML estimator calculated according to (4.12) in an LPTV channel with cyclostationary noise, it is convenient to express the symbol index, ℓ, in terms of the channel and the noise instantaneous PSD period. Denoting by $Q = T_0/T_{DMT}$, where T_{DMT} is the DMT symbol period, $\ell = q + rQ$, where $0 \leq q \leq Q-1$ and r is the cycle index. Assuming that the slow-variation approach holds, the output of the LFEQ at the frequency of carrier k during the q-th interval of the r-th cycle, $Y^r_{q,k}$, can be expressed as

$$Y^r_{q,k} \approx X^r_{q,k}|H_{q,k}|e^{j\measuredangle Hq,k}\, e^{jk\theta^r_q} LFEQ_k + U^r_{q,k}LFEQ_k, \tag{4.14}$$

where $H_{q,k}$ denotes the frequency response of the channel at the frequency of carrier k during the q-th symbol and $U^r_{q,k}$ is the noise value in carrier k at the output of the q-th DFT performed in the r-th cycle. The LFEQ only compensates for the time-averaged value of the frequency response, $LFEQ_k =< H_{q,k} >^{-1}$, where $< \cdot >$ denotes averaging over the variable q. Hence, the output of the phase detector in (4.12) would be misled by the cyclic changes of the channel.

4.4.2 Performance

This subsection analyzes the performance of the above synchronization scheme when employed in the apartment and detached house channels. Qualitative results in the example channel shown in Fig. 4.2 and Fig. 4.3 are firstly presented. Throughout the work, the following system parameters apply unless otherwise stated. A DMT with 512 carriers distributed in the frequency band up to 25MHz is employed. However, only carriers with indexes $2 \leq k \leq 409$,

i.e. in the band from approximately 1MHz to 20MHz, are finally used. The sampling frequency is fixed to $1/T_s = 100$MHz. The cyclic prefix length, cp, has been fixed to 226 samples at $1/(2T_s)$, which ensures that the power of ISI and ICI due to the spectral distortion of the channel will be much lower than the channel noise level. This cyclic prefix length also makes the DMT symbol length a submultiple of the mains period, $T_0/T_{DMT} = 800$, which simplifies the subsequent analysis. An ideal equalization is accomplished, i.e. the LFEQ and SFEQ are provided with the actual frequency response values. The transmitter PSD is fixed to -20dBm/kHz. BPSK and square QAM constellations subject to an instantaneous bit error probability criterion of Pe=10^{-5} and a maximum of 16bits/symbol have been used. A system margin of 6dB is employed. The loop filter is configured for the overall PLL response to be critically dumped.

Fig. 4.8 shows the loop filter output when the only non-ideal effect introduced by the ADC is a frequency offset of 20ppm. The equivalent noise bandwidth of the loop is set to 510Hz. As seen, periodical components caused by the LPTV nature of the channel are manifest at the filter output. They can be diminished by reducing the loop bandwidth. However, this leads to longer convergence times and, therefore, to a reduction in the capacity of the loop to follow timing fluctuations like the ones shown in Fig. 4.5.

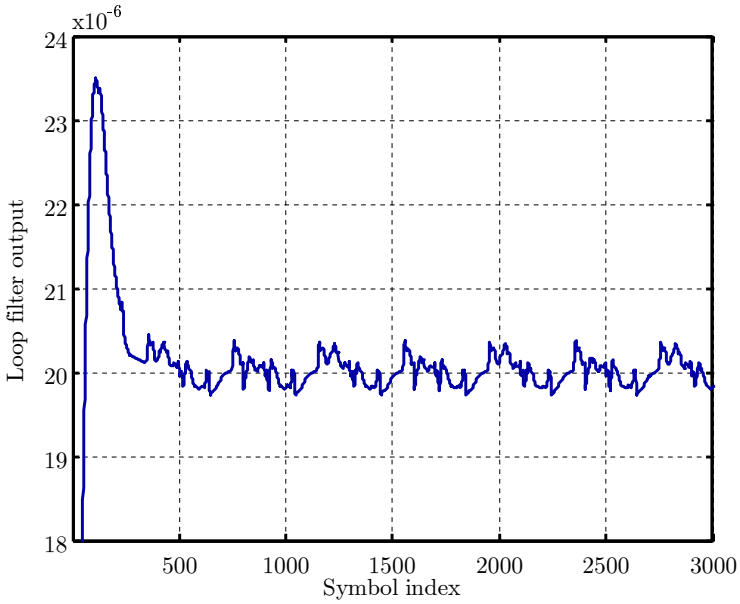

Figure 4.8: Loop filter output in example channel for a frequency error of 20ppm

To illustrate the reduced tracking capacity of narrowband loops, Fig. 4.9 depicts the loop output for a 3Hz sinusoidal input jitter. An LTI channel has been used. As shown, there are no significant amplitude differences for the three considered bandwidths. Moreover, for 10Hz and 30Hz the output amplitude is even greater than for 125Hz. This is due to the unavoidable peaking that appears in the frequency response of a critically dumped second order type II PLL [62]. On the other hand, it is worth noting the remarkably delay increment that occurs for 10Hz. When the loop bandwidth is large, the group delay is high in frequencies where the

$S_{\phi_o}(f)$ of an actual jitter is very small. As the loop bandwidth is reduced, the delay becomes larger in the low frequency region, where the jitter has its most significant components.

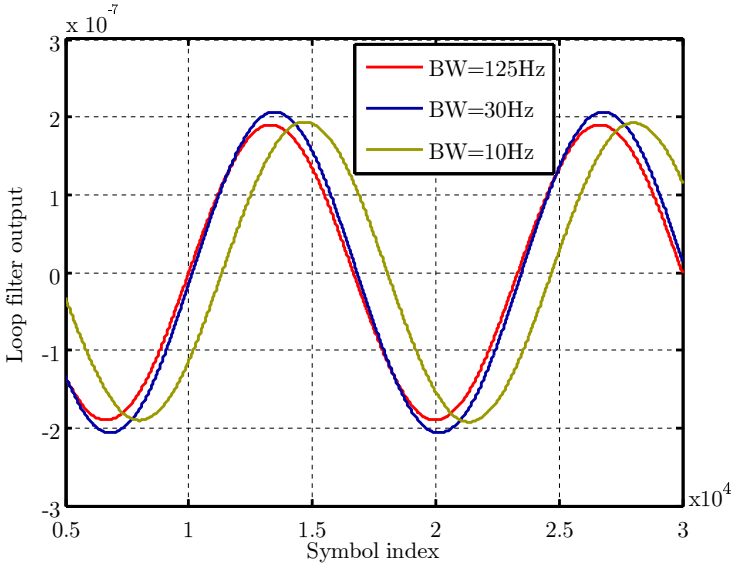

Figure 4.9: Loop filter output for a 3Hz sinusoidal input jitter in an LTI channel

Performance of the timing recovery procedure is characterized in terms of the SDR at the detector input and the achievable bit-rate. For small timing errors, the SDR experienced by carrier k in the q-th interval of each cycle can be expressed as

$$SDR_{q,k} = \frac{\mathrm{E}\left[|X^r_{q,k}|^2\right]}{\mathrm{E}\left[|X^r_{q,k} - X^r_{q,k}\, e^{jk\theta^r_q}|^2\right]} = \frac{1}{\mathrm{E}\left[|1 - e^{jk\theta^r_q}|^2\right]}, \tag{4.15}$$

where the expectation is performed over r.

It is worth noting that the distortion term in the denominator of (4.15) is not additive. Hence, contrary to what happens with the SNR, the effect of a certain SDR value on the error probability depends on the symbol energy. This can be clearly appreciated in Fig. 4.10, where the effect of a phase shift on QAM symbols is depicted. As seen, a symbol error occurs for a phase shift θ_2 but not for a greater one, θ_1.

Estimated values of the SDR experienced by the last used carrier ($k = 409$) in the example channel as a function of the loop bandwidth have been obtained by means of simulations. Results obtained with the ADC jitters depicted in Fig. 4.5 are shown in Fig. 4.11. Although curves are labeled according to the oscillator integrated jitter values, a 5ps aperture jitter is also included in all cases. No frequency offset exists. Two additional curves have been depicted to highlight the individual effect of channel cyclic variations and ADC jitter in the system performance. One of them shows the SDR values obtained when the 20ps oscillator is employed in an LTI channel obtained by means of a time averaging of the LPTV one displayed in Fig. 4.2. The other depicts the SDR values obtained when the time-variant example channel characterized in Fig. 4.2 and Fig. 4.3 is employed but no jitter is introduced by the ADC. Curves in Fig. 4.11 illustrate a clear trade-off in the selection of the loop bandwidth. For larger

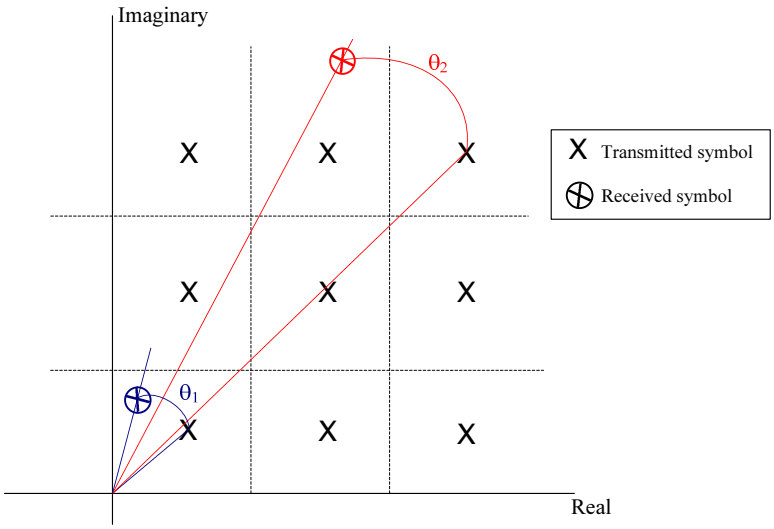

Figure 4.10: Effect of a phase shift on QAM symbols

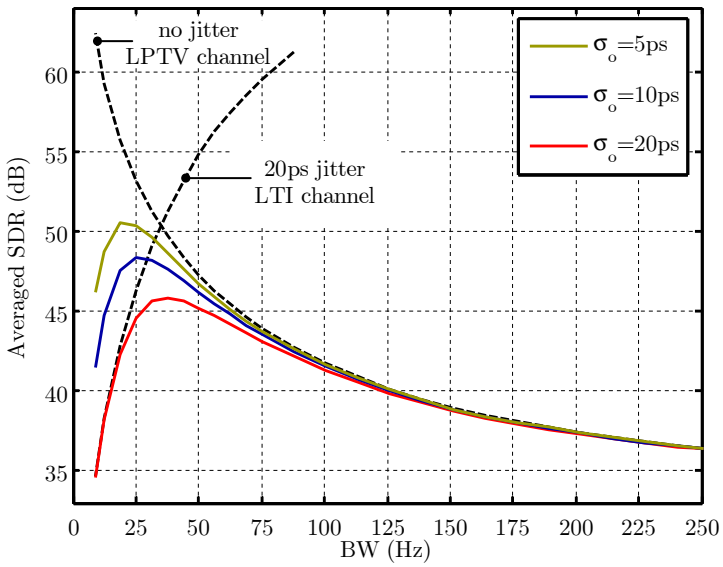

Figure 4.11: SDR in the last used carrier in different situations

loop bandwidths the SDR is low because phase error estimates are strongly misled by the cyclic time variations of the frequency response (the cyclostationary noise has much less influence). As the loop bandwidth is reduced, the SDR increases because channel time variations are attenuated. This process continues until the loop is not able to follow the ADC jitter. From this point on, distortion caused by this phenomenon becomes the dominating term and the SDR degrades very fast.

The ultimate system performance parameter is the achievable bit-rate. However, its exact computation under the considered circumstances is a difficult task. Moreover, values calculated in this way may not reflect the bit-rate attained by an actual system. A practical procedure to determine the bit load of each carrier in a real receiver would estimate the signal-to-noise-and-distortion ratio (SNDR). According to the usual assumption of an additive Gaussian noise

and distortion, the most appropriate constellation for each carrier is obtained by means of a predefined look-up table. Fig. 4.12 depicts the bit-rate values obtained with this procedure in the example channel. Two different modulation strategies have been considered: fixed and adaptive. In the fixed one, the same constellation is employed in each carrier throughout the mains period, while in the adaptive one it is adjusted according to the instantaneous conditions to make the most of the periodically-varying behavior of the channel.

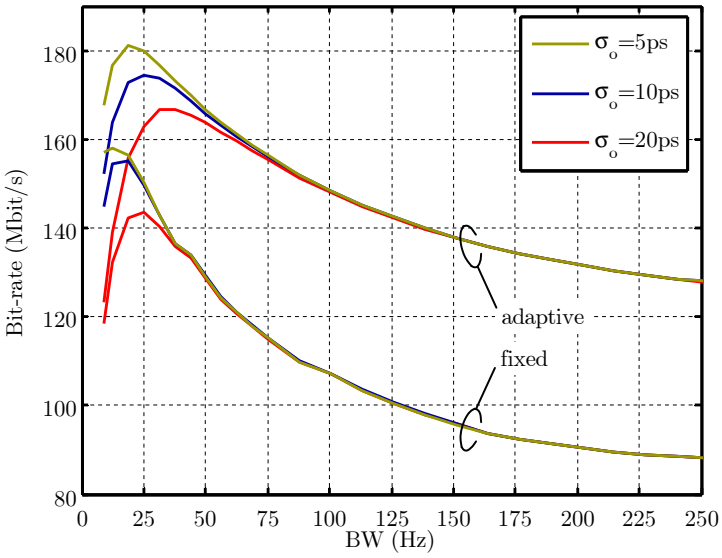

Figure 4.12: Bit-rates estimated from SNDR values and a look-up table

It can be observed that differences between the bit-rates shown in Fig. 4.12 experience a considerably increment when the loop bandwidth is enlarged. For instance, when the 5ps case is considered, the bit-rate gain obtained with the adaptive system for a 19Hz bandwidth is about 16% greater than the one provided by a fixed scheme. When a 160Hz bandwidth is employed, this gain goes up to about 45%. The reason is that, the wider the loop bandwidth, the larger the magnitude of the channel time variations at the output of the phase detector and, consequently, the greater the dispersion in SDR values. Fig. 4.12 also shows the great sensitivity of the bit-rate with respect to the bandwidth, especially in the jitter-limited region. Thus, a small bandwidth reduction over the optimum values for the 5ps case, may reduce the performance of both, the adaptive and the non-adaptive systems, to nearly the ones of the 20ps case. Hence, the investment in a better oscillator is not always productive.

It should be noticed that achieving the highest bit-rate values shown in Fig. 4.12 requires very narrow loop bandwidths. This cause a significant reduction of the capacity for tracking frequency errors, as can be observed in Fig. 4.13, where the settle time of the timing loop is displayed versus the loop bandwidth. The settle time is measured as the delay spread of the loop impulse response. The corresponding settle time for a 25Hz loop bandwidth is so large that convergence is at serious risk. To avoid this end, two distinct loop bandwidths should be employed: a broader one during the acquisition phase and a narrower one during the steady-state phase. This is common practice also in DSL DMT systems, where loop bandwidths between 70Hz and 300Hz are usually employed [63].

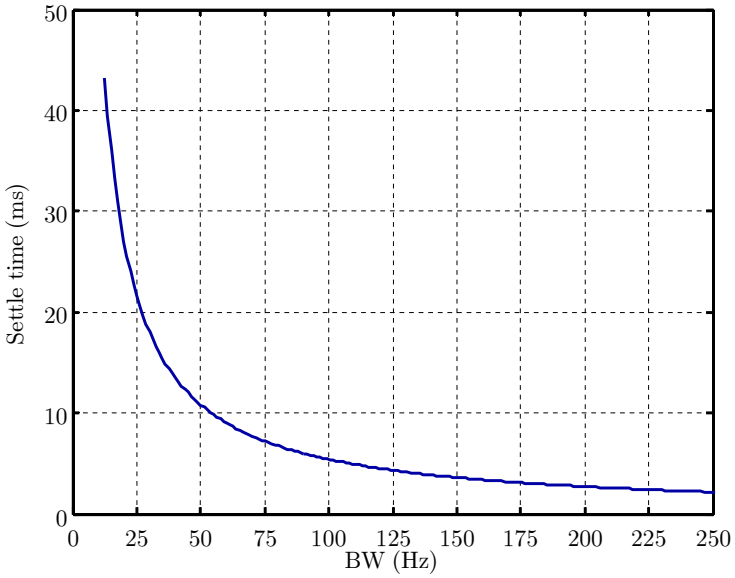

Figure 4.13: Settle time of the timing recovery loop

So far, qualitative effects of the jitter and cyclic time variations in the timing recovery mechanism have been presented. Statistical values of the performance degradation computed in the overall set of channels are now given. To this end, the bit-rate loss experienced in both scenarios with each oscillator and modulation strategy is computed. Bit-rates obtained in each channel under perfect synchronization conditions are taken as reference for the comparison. The bandwidth employed in all the channels is fixed for each modulation strategy and oscillator. These bandwidths values are computed by averaging the optimum bandwidths of all the channels in the selected configuration. Results are shown in Table 4.1. As seen, considerable performance degradation occurs in the apartment channels, especially when the constellation remains fixed throughout the mains cycle. Bit-rate losses are smaller in the detached house due to the inherently worse characteristics of these channels, which are established over longer and more branched links than in the apartment.

Scenario	$\sigma_o = 20$**ps**	$\sigma_o = 10$**ps**	$\sigma_o = 5$**ps**
Apartment (adaptive)	13.9	10.9	8.4
Apartment (fixed)	22.9	20.4	17.5
Detached house (adaptive)	3.2	2.1	1.3
Detached house (fixed)	6.6	5.3	4.2

Table 4.1: Average Bit-rate loss (%) in each scenario when the optimum loop bandwidth (on average) is employed in all the channels

Exact values of the performance degradation depend on the set of available constellations, the objective bit error probability and the system margin [121]. However, the only way to reduce the remarkable bit-rate losses experienced in the apartment channels is to modify the timing recovery scheme.

4.5 Modified timing recovery scheme

The conventional synchronization scheme admits two direct improvements when used in indoor power-line scenarios. Firstly, the phase detector can be matched to the particularities of the problem. This can be accomplished by taking into account the magnitude of the channel time variations before combining the estimates of the phase error obtained in the different carriers. Secondly, the loop filter can be modified to achieve higher attenuation at the harmonics of the mains frequency. This could be done by means of a higher order loop. However, due to the periodical nature of the estimation bias, the introduction of notch filters is a more suitable solution.

4.5.1 Phase estimator

Since the probability density function of the channel cyclic time variations is not precisely known, a weighted least-squares (LS) estimator is proposed. Let's denote by $\phi^r_{q,k}$ the phase error measured in carrier k during the q-th symbol of the r-th cycle, computed according to

$$\phi^r_{q,k} = \arctan\left(\frac{\Im\left[Y^r_{q,k}\widehat{X}^{r^*}_{q,k}\right]}{\Re\left[Y^r_{q,k}\widehat{X}^{r^*}_{q,k}\right]}\right) = k\theta^r_q + \measuredangle\widetilde{H}_{q,k} + \varphi^r_{q,k}, \tag{4.16}$$

where $\Re[\cdot]$, denotes the real part, $\widehat{X}^r_{q,k}$ is the q-th decided symbol of the r-th cycle in carrier k, $Y^r_{q,k}$ is the output value of the LFEQ given in (4.14), $\varphi^r_{q,k}$ is the phase noise due to the additive channel noise, $U^r_{q,k}$, and whose power can be approximated by $\sigma^2_{\varphi_{q,k}} \approx 1/(2SNR_{q,k})$, provided that $SNR_{q,k} \gg 1$ [30]. $\measuredangle\widetilde{H}_{q,k}$ is the difference between the channel phase and the LFEQ phase experienced by the q-th received symbol in carrier k. The weighted LS estimator of θ^r_q is selected according to

$$\widehat{\theta}^r_q = \arg\min_{\widetilde{\theta}^r_q}\left\{\sum_{k\in K}\frac{|\phi^r_{q,k} - k\widetilde{\theta}^r_q|^2}{\left(\measuredangle\widetilde{H}^2_{q,k} + \sigma^2_{\varphi_{q,k}}\right)}\right\} = \frac{\displaystyle\sum_{k\in K}\frac{k\phi^r_{q,k}}{\left(\measuredangle\widetilde{H}^2_{q,k} + \sigma^2_{\varphi_{q,k}}\right)}}{\displaystyle\sum_{k\in K}\frac{k^2}{\left(\measuredangle\widetilde{H}^2_{q,k} + \sigma^2_{\varphi_{q,k}}\right)}} \tag{4.17}$$

The selection of the carriers to be employed in the phase estimation is a difficult task, as the mean-squared error (MSE) in (4.18) reveals,

$$MSE^r_q = \mathrm{E}\left[|\widehat{\theta}^r_q - \theta^r_q|^2\right] = \frac{1}{\displaystyle\sum_{k\in K}\frac{k^2}{\left(\measuredangle\widetilde{H}^2_{q,k} + \sigma^2_{\varphi_{q,k}}\right)}}\left[\left(\sum_{k\in K}\frac{k\measuredangle\widetilde{H}_{q,k}}{\left(\measuredangle\widetilde{H}^2_{q,k} + \sigma^2_{\varphi_{q,k}}\right)}\right)^2 + \right.$$
$$\left.\sum_{k\in K}\frac{k\sigma^2_{\varphi_{q,k}}}{\left(\measuredangle\widetilde{H}^2_{q,k} + \sigma^2_{\varphi_{q,k}}\right)} + 2\theta^r_q\left(\sum_{k\in K}\frac{k\measuredangle\widetilde{H}^r_{q,k}}{\left(\measuredangle\widetilde{H}^2_{q,k} + \sigma^2_{\varphi_{q,k}}\right)}\right)\left(\sum_{k\in K}\frac{k^2}{\left(\measuredangle\widetilde{H}^2_{q,k} + \sigma^2_{\varphi_{q,k}}\right)}\right)\right] \tag{4.18}$$

The influence of the channel phase variations and the noise on (4.18) is evident. However, the first and second terms in the square bracket also highlight the importance of the carrier index, since a given channel variation is more harmful in carriers with higher indexes. Similarly, the third term shows that the estimation error depends on the magnitude to be estimated, θ_q^r, which, in turns, is also determined by the loop response.

The computation of (4.17) involves two main difficulties. Firstly, it requires $\|K\|+1$ divisions, where $\|\cdot\|$ denotes the size of the set, or alternatively, the storage of the $Q\|K\|$ values of $\left(\measuredangle \widetilde{H}_{q,k}^2 + \sigma_{\varphi_{q,k}}^2\right)^{-1}$. This excessively high complexity can be reduced by replacing the instantaneous values of $\left(\measuredangle \widetilde{H}_{q,k}^2 + \sigma_{\varphi_{q,k}}^2\right)$ by their time-averaged values. Secondly, these time-averaged values are still unknown and must be estimated. In this work, an exponential averaging of the squared magnitude of $\phi_{q,k}^r$ is employed to perform the estimation. The resulting LS estimator will be referred to as simplified LS from now on.

Fig. 4.14 compares the SDR values experienced by the last carrier in the example channel when using the LS estimator in (4.17) and the simplified LS. The conventional estimator in (4.12) is included as a reference. A 20ps oscillator jitter is used in all cases. As expected, there are no SDR differences in the region in which distortion is limited by the jitter. On the contrary, the proposed estimators provide considerable gains in the region where the channel variations limit the performance. In addition, it is worth noting that the SDR becomes less sensitive to the loop bandwidth. The steady-state computational load of the modified LS estimator is equal to that of the conventional one and, as shown in Fig. 4.14, it performs less than 2dB worse than the LS in a quite wide region. Therefore, it has been selected for the subsequent analysis.

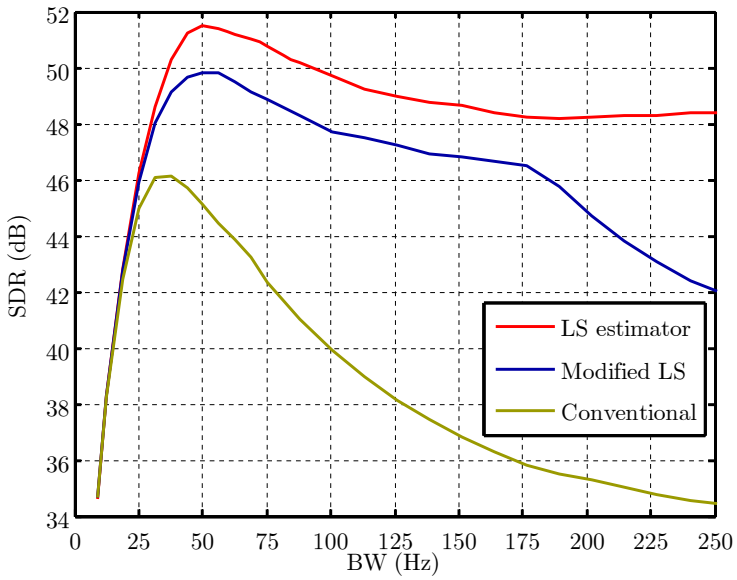

Figure 4.14: SDR values of the proposed and conventional phase error estimators

4.5.2 Loop filter

The modified LS estimator considerably reduces the magnitude of the channel variations in the phase detector output. Additional attenuations can be introduced before supplying the interpolator with the timing adjustment values. Two equivalent methods can be employed to achieve this objective. The first one is to estimate the most important harmonics of phase error signal, e.g. by means of the Goertzel algorithm, and to cancel them before entering the NCO. The second one is to eliminate these harmonics by placing notch filters in the loop. Both strategies offer equal performance but, due to the easiest stability analysis, the latter one has been selected. The modified loop filter is given by

$$L(z) = \left(\alpha + \frac{\beta}{1 - z^{-1}}\right) \prod_{i=1}^{M} H_i(z), \tag{4.19}$$

where $H_i(z)$ are the transfer functions of notch filters obtained by applying the bilinear transform to the continuous-time second-order prototypes

$$H_i(s) = \frac{s^2 + \omega_{z,i}^2}{s^2 + 2\xi\omega_{0,i}s + \omega_{0,i}^2}, \tag{4.20}$$

with $\omega_{z,i} = 100\pi i$ (rad/s). Up to three notch filters ($M = 3$) are employed in this study. Filter parameters have been heuristically selected to minimize the unavoidable resonance that appears in the passband and to achieve narrowband notches. As a result, ξ_i is fixed to 0.1 in all filters and $\omega_{0,i} = \omega_{z,i}k(\alpha)$, where

$$k(\alpha) = \begin{cases} 1 & 0 \leq \alpha \leq 4 \cdot 10^{-3} \\ \sqrt{1.1} & 4 \cdot 10^{-3} < \alpha \leq 6 \cdot 10^{-3} \\ \sqrt{1.2} & 6 \cdot 10^{-3} < \alpha \leq 10^{-2} \end{cases}. \tag{4.21}$$

The introduction of the notch filters considerably reduces the stability range of the overall loop filter. Fig. 4.15 depicts the modulus (in dB) of the open-loop timing recovery loop frequency response, denoted by $H(\Omega)$, versus the phase of this same function. This representation, known as Nichols chart [118], is useful for determining the stability range of a feedback system. Thus, for the closed-loop system to be stable, the 0dB gain crossings of the Nichols chart must occur at phase values greater than -180º. As shown in Fig. 4.15, for $M = 3$ the loop is stable only for $0 < \alpha < 2.15 \cdot 10^{-2}$. However, for $\alpha > 10^{-2}$ (BW > 130Hz) the peaking that appears in the passband of the filter [62] experiences an enormous growing that invalidates the resulting frequency response.

Performance obtained with the modified loop is firstly assessed in terms of the SDR. Fig. 4.16 depicts the SDR values experienced by the last carrier in the example channel for different values of M and a 20ps oscillator jitter. The conventional loop, $M = 0$, has been included as a reference. As observed, gains obtained by using just one notch filter are rather small, while considerable improvement is obtained for $M = 2$. This is due to the 100Hz periodicity exhibited by the example channel. It is worth noting that the introduction of the notch filters ease the selection of the loop bandwidth, since the SDR is monotonically increasing for $M \geq 2$

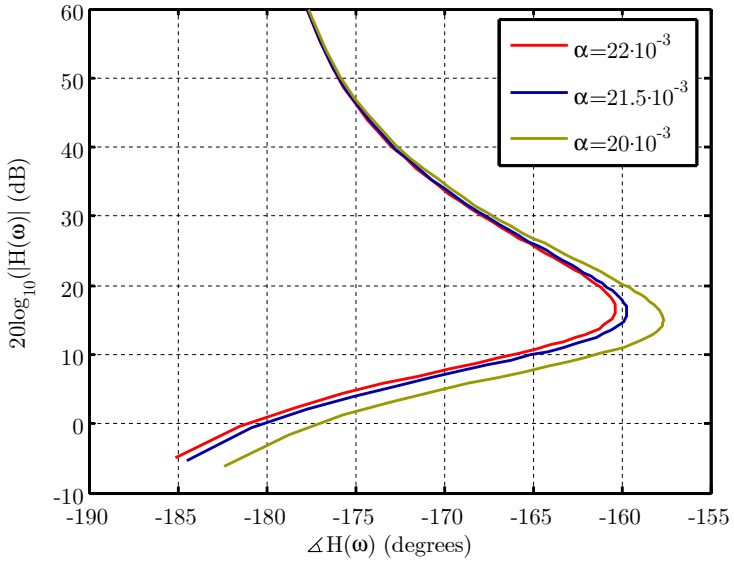

Figure 4.15: Nichols chart of the open-loop timing recovery loop frequency response

in the selected range. Although not shown in Fig. 4.16, small gains are obtained for $M > 3$, specially in the apartment channel, in which more than 90% of the system carriers experience less than 150Hz of Doppler Spread.

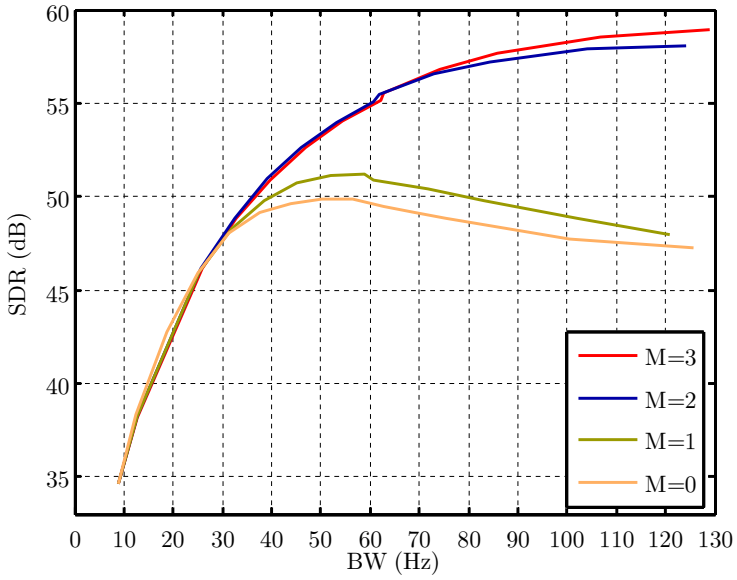

Figure 4.16: SDR obtained with the modified LS estimator for several number of notch filters

Bit-rates corresponding to $M = 3$ and different oscillator jitters are shown in Fig. 4.17. Values have been computed using the SNDR and a look-up table. The new timing recovery scheme provides remarkable gains with respect to the conventional one (see Fig. 4.12). The maximum bit-rate values obtained with the new system are, at least, 13% higher than those obtained with the latter. This gain goes up to 24.5% when the oscillator jitter is 20ps and a fixed

modulation strategy is employed. In addition, the bandwidth selection problem is now easier, since performance is less sensitive to this parameter.

Statistical values of the bit-rate loss computed over the whole set of residential channels are now given. The procedure employed for the calculation is analogous to the one employed with the conventional timing recovery scheme. Results are shown in Table 4.2. As observed, performance degradation is considerably reduced in the apartment channels, especially when an adaptive modulation strategy is used, and practically eliminated in the detached house ones. These significant improvements are particularly interesting when the reduced increment in the computational load is taken into account. Thus, the steady-state complexity of the modified LS estimator is equivalent to that of the conventional one, and the six-order filtering of the modified loop is performed only at symbol rate.

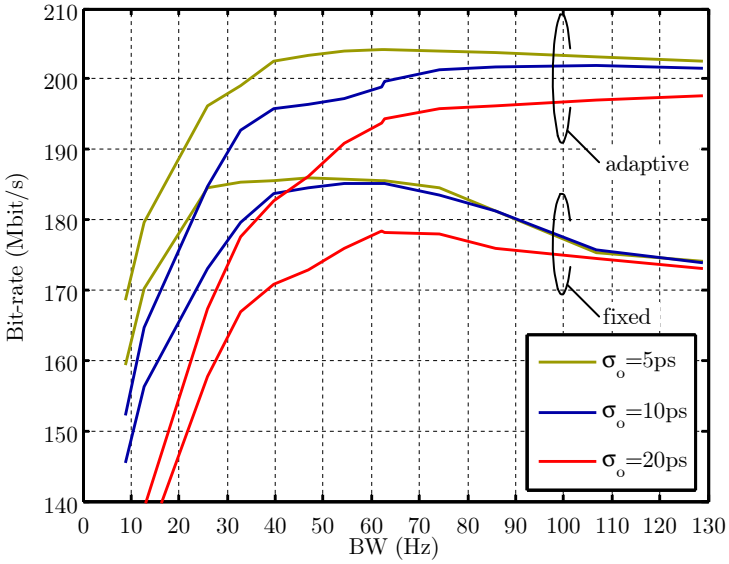

Figure 4.17: Bit-rate values obtained with the modified LS estimator and $M = 3$

Scenario	$\sigma_o = 20$**ps**	$\sigma_o = 10$**ps**	$\sigma_o = 5$**ps**
Apartment (adaptive)	1.9	1.1	0.6
Apartment (fixed)	4.6	3.7	3.6
Detached house (adaptive)	0.1	0.1	< 0.05
Detached house (fixed)	0.1	0.1	< 0.05

Table 4.2: Average Bit-rate loss (%) in each scenario with the modified LS estimator and $M = 3$ when using the optimum loop bandwidth (on average)

4.6 Conclusions

This chapter has studied timing synchronization in DMT over indoor power-lines. In particular, it has focused on the timing recovery problem of a DA decision-directed system. Main conclusions are now summarized:

- Analog-to-digital conversion model. When dealing with synchronization issues, non-idealities in the analog-to-digital conversion are usually restricted to frequency and phase errors. This model is appropriate when the sampling frequency is relatively low. However, it has been shown that when sampling broadband signals, the relative magnitude of the clock jitter with respect to the sampling period can not be neglected.

- Two-stage frequency equalization. In order to track the cyclic time variations of the frequency response, the classical FEQ used in DMT must be adapted at a rate comparable to that of the synchronization system. This may cause interaction between them and their eventual divergence. To overcome this pitfall, a two-stage frequency equalizer has been proposed. The first one compensates for the long-term changes in the channel response and, the second one, tracks the short-time variations experienced by the channel with respect to its long-term value. The timing recovery scheme takes information from the output of the long-term FEQ. The price to be paid is that the cyclic time variations of the channel, with harmonics at multiples of the mains signal frequency, mislead the estimation of the sampling error.

- Performance of timing recovery schemes designed for LTI channels. The two main causes that limit the performance of this scheme have been identified. One is the periodical bias introduced by the channel time variations in the phase error estimates. The other is the timing jitter introduced in the analog-to-digital conversion process. The former can be reduced by using a narrower loop bandwidth, but this also reduces the loop ability to track the sampling jitter. Simulations have revealed that performance is extremely sensitive to the loop bandwidth in the jitter limited region. It has been shown that, even with the optimum loop bandwidth value, the averaged bit-rate loss in residential channels can be up to 20%.

- Modified phase estimator and loop filter. Two modifications have been proposed to overcome the shortcomings of the conventional scheme. The first one is to reduce the influence of the channel cyclic time variations on the estimates of the phase error. To this end, an LS estimator that takes into account the magnitude of these variations has been designed. With similar implementation complexity, the proposed estimator notably outperforms the classical estimator designed for LTI channels.

  The second modification is intended for providing additional attenuation of the channel time variations by means of a modified loop filter. Based on the periodical nature of these variations, instead of using a higher filter order, a series of notch filters tuned to the harmonics of the mains frequency are included in the loop. It has been determined that, since a large number of channels exhibit a 100Hz periodicity, at least

two notches have to be employed. On the other hand, increasing the number of notch filters difficulties the design process, reduces the stability region of the overall timing recovery scheme and provides minimal improvements. It has been shown that the combined use of the proposed LS estimator and a loop filter with three notches lead to negligible performance degradation in most channels.

Chapter 5

DMT-FDMA Multiple Access

5.1 Introduction

The main aspects related to single-user DMT systems have been studied in the previous chapters. Now, the problem of sharing the indoor power-line network among different users is addressed. The straightest multiple access approach is to employ a kind of contention scheme, like the CSMA/CA adopted in the IEEE 802.11 wireless LAN standards. However, contention strategies do not take into account the channel characteristics of the different users, which may be quite different. Moreover, they are not appropriate to provide the latency, jitter and guaranteed bandwidth needed by some streaming applications [48]. These quality of service requirements can be fulfilled by using centralized TDMA or FDMA schemes. In these techniques, a central manager dynamically modifies the time slots or the frequency bands assigned to each user in order to guarantee the requested quality parameters.

In TDMA, the number of time slots assigned to each user is determined according to its QoS necessities. During these slots, which last several DMT symbols, only one user occupies the available bandwidth. Since unused carriers in one link, because of their low signal-to-noise ratio (SNR), may experience acceptable SNR in other links, this strategy may result in a waste of capacity. To overcome this pitfall, hybrid TDMA-FDMA schemes have been proposed [49].

The signaling rates needed for the users to communicate to the central manager the bit-rate that can be attained in each available resource (time slot or frequency band) are also an important consideration for the selection of a multiple access strategy. In a time-invariant channel this is one of the points in favor of TDMA, since just one bit-rate value per user is required. However, due to the short-time changes of indoor PLC channels, users must divide the mains cycle into several regions and indicate the bit-rate achieved in these regions to the central manager. This fact considerably reduces the signaling rates differences between TDMA and FDMA.

In FDMA the available bandwidth is shared among the different users. This process results particularly efficient when employing a DMT modulation, since the bands assigned to the different users overlap. Moreover, as in FDMA the protocol data units length is no longer

limited by the time slots duration, the transmitted overhead is reduced. On the other hand, it requires symbol and frequency synchronization of all terminals to avoid MAI among users [50], [56]. Nevertheless, in environments like VDSL it has been demonstrated that symbol synchronization can be avoided by using pulse-shaping, windowing and tone-grouping [56].

In DMT systems the desired carriers can be recovered without the need for an analog filtering by means of the receiver DFT. On the other hand, this digital band separation increases number of bits required in the ADC. When a TDD technique is employed the input to the ADC is comprised of the desired and interferer signals. Provided that the latter term may have much higher power than the former one, either severe clipping or quantization errors are unavoidable. In a FDD scheme the situation is even worse because the wide range of impedance values presented by the network makes very difficult to obtain more than 5dB of isolation from transmitter to receiver. As a reference, in the DMT implementation of VDSL the digital duplexing operation requires a 12-bits ADC [53].

TDMA-TDD is the multiple access scheme implemented in the current generation of broadband power-line modems [23], [64], probably due to its simplicity. However, to the author's knowledge, there is no comprehensive study about the use of a DMT-FDMA scheme in an indoor power-line scenario. The aim of this chapter is to analyze the performance of this strategy. Firstly, the effects of the channel dispersion and the symbol and frequency asynchrony on the system performance are assessed. Afterward, the utilization of a DMT modulation with pulse-shaping and windowing as a mean for reducing the above effects is also studied. The influence of the carrier allocation strategy on the system performance is evaluated in both cases. Finally, the number of bits required in the ADC in both the TDD and the FDD cases is analyzed. Results presented in this chapter have been partially published in [121].

5.2 DMT-FDMA system model

In a centralized DMT-FDMA multiple access scheme, the N carriers of the DMT system are dynamically distributed among the M links by a central entity. Fig. 1 shows a simple network with two unidirectional active links. As seen, only one direction of the communication is assessed, i.e. simplex operation is considered. This is done to separate the multiple access problem from the duplexing one. It is assumed that there is a central manager entity that assigns carriers to users. In practice, the first node entering the network plays the central manager role.

For simplicity, the LTI channel model is employed throughout the study. The validity of this simplification for the analysis of an FDMA scheme is grounded in two facts. The first one is that, provided that the number of carriers is kept smaller than 2048, the effect of the ICI and the MAI due to the channel short-term variations is negligible, as it has been shown in 3.4.1. Hence, the dominant distortion term is due to the channel frequency selectivity, which can be obtained using an LTI channel response. The second one is that in an FDMA technique users are permanently assigned a given set of carriers. Since each user experiences all the cyclic

changes of the channel, performance is measured in terms of the average bit-rate achieved in a mains cycle. This value can be approximated by the bit-rate obtained in the LTI channel that results from the time-averaging of the cyclic one. It should be noted that the LTI channel model is not acceptable for the analysis of a TDMA scheme because the bit-rate achieved by each user depends on the position of the assigned time slots within the mains cycle.

Users and impulse responses are named on a link basis. Thus, $h_{ij}[n]$ denotes the impulse response of the channel seen from the transmitter of user 1-link i to the receiver of user 2-link j. From now on, $h_{ij}[n]$ would be referred to as interfered channels and $h_{ii}[n]$ to as desired channels. The reverse directions of the links can be also described in terms of the above impulse responses, since it is a well-known fact that indoor power-line channel responses are symmetric [122]. Correspondingly, $n_i[n]$ represents the noise at the receiver of user 2-link i

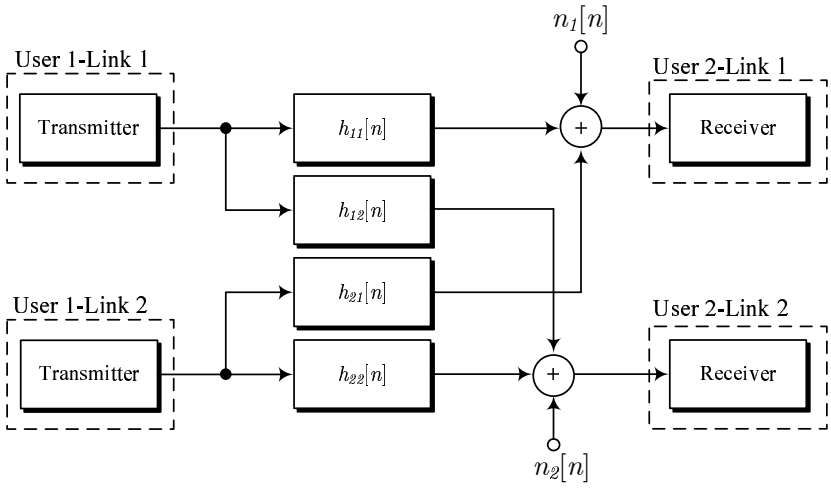

Figure 5.1: Simplified discrete-time multiuser environment with two links

5.2.1 Multiple access interference

Multiple access interference is the main cause of performance degradation in a DMT-FDMA system. It may have three different origins: frequency selectivity of the channel, misalignment between the desired and interferer symbols at the input of the desired receiver DFT and frequency offsets between the interferer transmitter and the desired receiver clocks. It should be noticed that channel short-term variations cause an additional MAI term. However, when the number of carriers is lower than 2048, as it will be the case in this study, its magnitude is much smaller that the one due to the frequency selectivity. A brief description of the significant MAI components is now given.

Effect of the frequency selectivity of the channel

MAI caused by the frequency selectivity of the interferer channel can be easily overcome in a synchronized DMT system by using a cyclic prefix length longer than the channel impulse

response. However, as shown in chapter 3, due to the long impulse responses of indoor power-line channels, a shorter cyclic prefix must be selected and some residual MAI will exist. This type of distortion delimits the upper bound for the performance of the DMT-FDMA strategy. The power of this type of MAI depends on several factors: the frequency separation between the interferer and interfered carriers; the difference between the attenuation of the interferer channel and the desired one; the frequency selectivity of the interferer channel and the shape of the pulses used in the DMT system. Assigning groups of tones instead of individual carriers is a common technique used to reduce this type of MAI [56].

Effect of the symbol and frequency desynchronization

Even when the impulse responses of the interferer channel are shorter than the cyclic prefix, MAI will appear if the desired and interferers symbols are not aligned at the desired receiver or if their clock frequencies are not identical. In an FDMA scheme with no specific synchronization method, the transmissions of the different users are synchronized only when the central manager performs a new carrier distribution. From that point on, offsets between the clock frequencies of the interferer and interfered users will cause a time-varying symbol asynchrony. In an indoor power-line scenario this is the main cause of symbol misalignment, since small propagation delay differences are expected among the links of a specific site due to the short distances involved. In order to quantify the respective influence of both asynchronies, this study analyzes separately the performance degradation caused by a fixed symbol misalignment, Δn (samples), and by a clock frequency offset, $\Delta f(ppm)$.

As indicated in section 3.2.4, symbol boundaries in a single-user environment are usually determined by searching the $cp + 1$ window of the impulse response that has maximum energy. In a multiuser scenario this selection leads to the situations shown in Fig. 5.2, where a time advanced (b) and delayed (c) interferer have been also depicted. Whereas most of the distortion caused by a positive offset Δn is expected to be absorbed by the cyclic prefix, as shown in Fig. 5.2 (c), the situation is rather distinct for a sample offset in the opposite direction. As depicted in Fig. 5.2 (b), MAI due to the transients in the interferer's symbols will be much greater in these circumstances. This example illustrates that when considering a multiuser environment, it may be interesting to modify the symbol synchronizer criterion in order to benefit from the robustness provided by the cyclic prefix against small symbol time misalignments. The price to be paid is the reduced performance in the case of no interferers.

Let's now consider an indoor network in which users are synchronized by means of periodical beacons transmitted by the central manager. Symbol misalignment can be constrained to one sample just by transmitting beacons at a sufficiently high rate. In these circumstances terminals adjust the phase of their clocks after the reception of the beacon. However, since there is no frequency adjustment, offsets between the interferer and interfered clocks will cause MAI. Hence, the broadcasting of a continuous reference signal for synchronization is the only solution to completely avoid MAI.

The power of the MAI due to symbol or frequency offset depends on the frequency separation

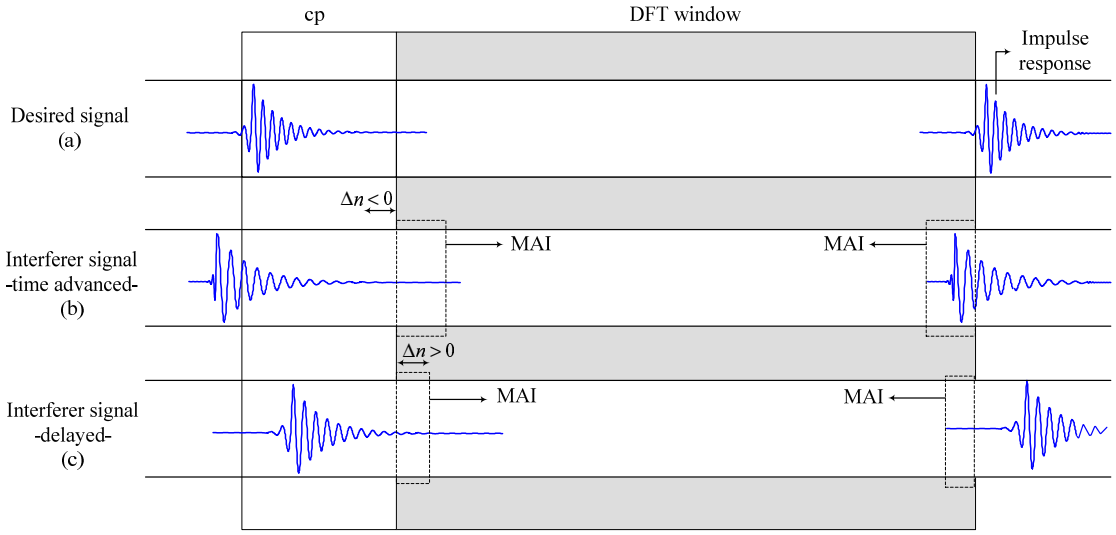

Figure 5.2: Illustration of symbol misalignment situations

between the interferer and interfered carriers; on the difference between the attenuation of the interferer channel and the desired one; on the value of the symbol or frequency offset and on the shape of the pulse used in the transmitter and the receiver.

5.2.2 Carrier allocation strategies

The resource allocation problem is one of the critical tasks in any multiple access scheme. First of all, a *fair* optimality criterion must be established [123]. Secondly, the optimization problem must be solved. The optimal carrier allocation strategy in a frequency-selective environment is the solution to a non-linear optimization problem which is usually approximated by means of linear or integer programming [52]. In principle, achieving the desired solution with the latter methods requires an iterative procedure. The reason is that the ICI and the MAI make the SNDR experienced by each carrier to depend on the assignation of the remaining carriers. However, this study is mainly concerned with the performance degradation due to the MAI. Hence, the important issue is whether carriers are assigned individually or on a group basis, but not the optimality criterion employed for neither the allocation process nor the grade in which the achieved solution satisfied this criterion.

Two strategies are used for assigning carriers to users in this work. In the first one carriers are assigned individually, while in the second one they are distributed on a group basis. In this latter scheme, usually known as tone-grouping, the available bandwidth is divided into 16, 32 and 64 subbands. The individual carrier assignment problem is solved by means of linear programming (LP) [124]. The optimality criterion is to maximize the aggregate bit-rate of the two links subject to the restriction that each of them must achieve, at least, a certain percentage, p (%), of the bit-rate that they would attain in a single-user scenario. This constraint is included in the optimization process to avoid all carriers to be assigned to the link with the best transmission characteristics. Let's denote by b_k^i the number of bits that can be allocated to carrier k when used in link i. These values are estimated in each link by

transmitting a training sequence. Only one transmitter is active at a time. Once the values corresponding to the M links have been received at the central manager, it solves the following LP optimization problem, in which c_k^i denotes whether carrier k is assigned to link i, $c_k^i = 1$, or not, $c_k^i = 0$,

$$\max \sum_{i=1}^{M} \sum_{k=0}^{N} b_k^i c_k^i, \tag{5.1}$$

subject to

$$\sum_{k=0}^{N} b_k^i c_k^i \geq \frac{p}{100} \sum_{k=0}^{N} b_k^i \quad \text{for } i = 1...M. \tag{5.2}$$

In addition, and to make each carrier to be assigned only to one link, the following constraint is also imposed

$$\sum_{i=1}^{M} c_k^i = 1 \quad \text{for } k = 0...N. \tag{5.3}$$

In practice, condition (5.3) does not prevent these coefficients to be non-integer values in the range $[0, 1]$ and the obtained c_k^i must be rounded. In fact, this is the common situation when the transmission characteristics of the involved links are quite similar.

Two strategies have been used to perform the subband allocation process. The first one employs integer programming (IP) with the same optimality criterion and constraint employed in the individual carrier assignment. The second one allocates adjacent subbands to different users (interleaved). Since the MAI depends on the distance between the interferer and the interfered carriers, this latter scheme is used to obtain a worst case scenario from the MAI perspective. Table 5.1 shows a summary of the number of subbands and carrier allocation strategies employed in the study.

For simplicity, only two links are assumed to be active at the same time, $M = 2$. This implies no loss of generality, since the important issue from the MAI perspective is whether adjacent carriers or subbands are assigned to the own user or to a different one. Accordingly, the constraint in the LP optimization problem has been fixed to $p = 40$ (%).

Number of subbands	**Allocation strategy**
16	Integer Programming & Interleaved
32	Integer Programming & Interleaved
64	Integer Programming & Interleaved
N	Linear Programming

Table 5.1: Summary of the number of subbands and carrier allocation strategies employed

5.2.3 Digital band separation: analog-to-digital converter requirements

The DFT performed at the DMT receiver provides a straight method for extracting the desired carriers without the need for an analog filtering. Let's consider the diagram shown in Fig. 5.3. The coupling circuit is a bandpass filter that protects the transceiver circuitry from the mains and also acts as a reconstruction and antialiasing filter for the transmitted and received signals, respectively. The directional coupler acts as duplexor that isolates the transmitted and received signals. However, the wide range of impedance values presented by the network makes very difficult to obtain more than 5dB of isolation. The received signal level is conditioned to the dynamic range of the ADC by means of an automatic control gain (AGC).

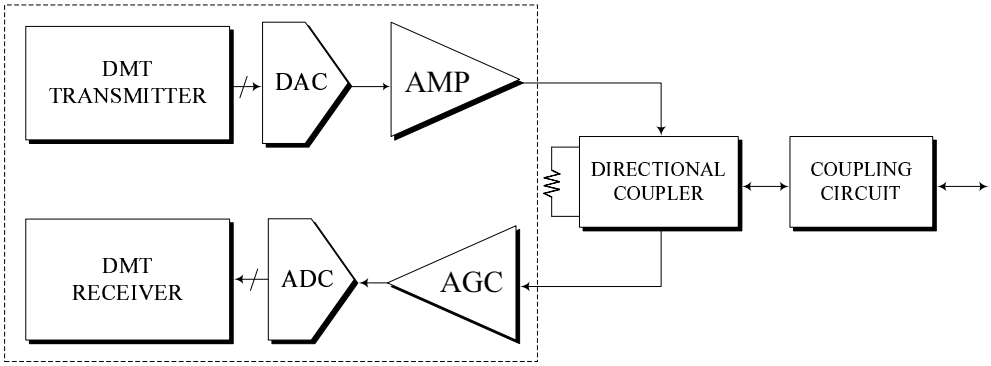

Figure 5.3: Simplified block diagram of the considered transceiver

The output signal from the directional coupler is composed of the sum of N carriers modulated with independent symbols. According to the central limit theorem, its amplitude can be assumed to have a Gaussian distribution. In a TDD scheme this input signal is composed of the desired and interferer terms. The former one is expected to have much less power than the latter one. Firstly, because in a network with M active links, the desired one would be generally allocated only $1/M$ of the available bandwidth. Secondly, because some of the $M-1$ interferer channels may be less attenuated than the desired one. In these circumstances, a large AGC gain is required to minimize the quantization noise, but this severely increases the clipping noise [125]. In an FDD scheme the situation is even worse because the large signal from the transmitter is coupled to the receiver through the low loss directional coupler.

From the distortion point of view, the analog-to-digital conversion of a signal $x(t)$ can be modelled as the cascade of two processes. The first one limits the amplitude of the input signal to the dynamic range of the ADC, $[-X_l, X_l]$, and the second one quantizes the clipped signal, $y(t)$, that results from the previous stage. While the error introduced by the limiting process, $e_l(t)$, depends on the relation between the the dynamic range of the ADC and the power of the input signal, the error introduced by the quantization process, $e_q(t)$, is exclusively dependent on the number of bits of the ADC.

Assuming a bandlimited Gaussian input signal, the limiter output can be written as

$$y(t) = \alpha x(t) + e_l(t). \tag{5.4}$$

According to [126], $x(t)$ and $e_l(t)$ are uncorrelated for $\alpha = \text{erf}\left(\frac{\mu}{\sqrt{2}}\right)$, where $\mu = \frac{X_l}{\sigma_x}$. The power of $e_l(t)$ is then given by [125]

$$\sigma_{e_l}^2 = \sigma_x^2 \left[(1+\mu)^2 \,\text{erfc}\left(\frac{\mu}{\sqrt{2}}\right) + \sqrt{\frac{2}{\pi}} \mu e^{-\frac{\mu^2}{2}} \right]. \tag{5.5}$$

The PSD of $e_l(t)$ falls outside the band occupied by $x(t)$. Hence, aliasing in the sampling process is unavoidable unless a low pass filtering is previously performed. This low pass filtering also reduces the power of the discrete-time error signal. However, it is not considered in this work because it has been proven that it gives minimal performance improvement [125]. For reasonable clipping values, it holds that the PSD of $e_l(t)$ is essentially flat well beyond the bandwidth of $x(t)$. This striking feature is independent of the PSD of the input signal [127]. Based on this fact, and provided that a low oversampling factor is employed, the resulting discrete-time random process is approximately white.

On the other hand, the quantization noise can be assumed to be uniformly distributed with a white PSD and a power given by the well-known expression

$$\sigma_{e_q}^2 = \frac{X_l^2}{3 \cdot 2^{2B}}, \tag{5.6}$$

where B is the number of bits of the ADC. The SDR of the limiting and quantization processes can then be expressed as

$$SDR_l = \frac{\alpha^2 \sigma_x^2}{\sigma_{e_l}^2}, \tag{5.7}$$

and

$$SDR_q = \frac{\alpha^2 \sigma_x^2}{\sigma_{e_q}^2}. \tag{5.8}$$

In addition to the classical trade-off in the selection of the input signal power, it is worth noting that the problem in an FDMA network is that the input signal is composed of two terms (desired and interferer) with difference levels of tenths dB. In these circumstances, $\sigma_{e_l}^2$ and $\sigma_{e_q}^2$ are still determined by the input signal, but the numerators of (5.7) and (5.8) only include the power due to the desired signal term. To illustrate this end, Fig. 5.4 shows the SDR values given by (5.7) and (5.8) for $X_l = 5$. The overall SDR of the quantization and limiting processes that can be achieved with $B = 12$ in a single-user scenario is also depicted. As seen, the maximum value is above 60dB. Now, let's consider a multiuser scenario in which the input signal, $x(t)$, is composed of a desired and an interferer term. The overall SDR that results when the power of interferer component is 20dB higher than the one of the desired term is depicted in Fig. 5.4. It can be observed that the performance of the analog-to-digital conversion process is now much worse than in a single-user environment.

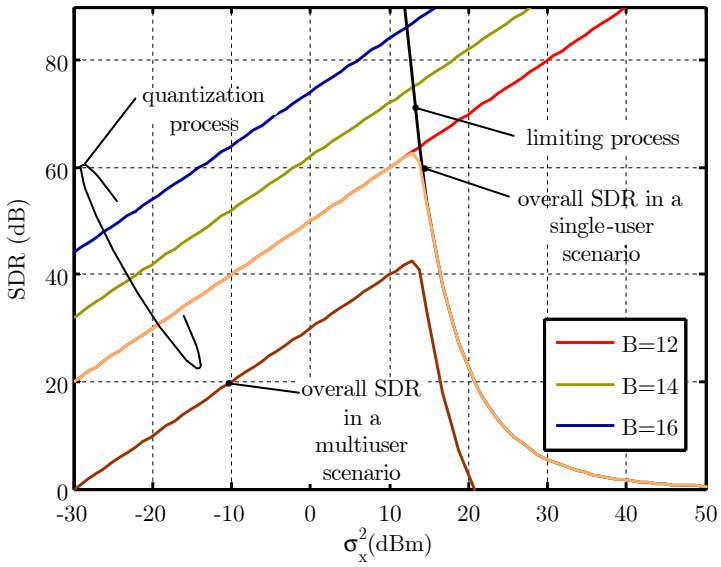

Figure 5.4: SDR of the quantization and limiting processes

5.3 Performance evaluation

In order to asses the performance of the DMT-FDMA scheme, three transmitters and three receivers have been distributed in the apartment employed for generating the channels of the time-invariant model described in section 2.3. The approximate plan of the apartment is shown in Fig. 5.5. Receivers have been numbered 1, 3 and 5, while 2, 4 and 6 have been used for transmitters. Numbers have been assigned according to the estimated physical length of the main path between transmitter and receiver, e.g. the main path between receiver 1 and transmitter 2 is much shorter than the one between receiver 1 and transmitter 6. Three MAI scenarios, each one with two unidirectional links have been defined. Table 5.2 shows the transmitters and receivers positions of each one.

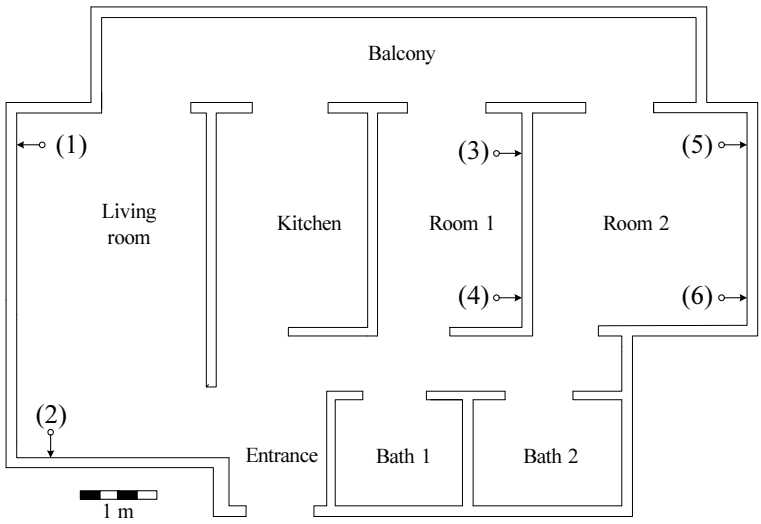

Figure 5.5: Approximate plan of the apartment site

Desired link Transmitter/receiver position	MAI category scenario
6/5 2/1	*Best*
4/5 6/3	*Intermediate*
6/1 2/5	*Worst*

Table 5.2: Definition of MAI scenarios

Fig. 5.6 (a) and (b) show the frequency responses of the desired and interferer channels in the *best* and *intermediate* MAI scenarios. As seen, the best scenario presents lowly attenuated desired channels and highly attenuated interferer channels. Desired channels of the *worst* scenario are the same as the interferer ones of the *best* MAI scenario and viceversa. The noise PSD at the receivers' site is depicted in Fig. 5.6 (c). It can be observed that, except for some minor differences, values for receivers 3 and 5, are practically equal.

The system performance is assessed in terms of the achievable bit-rate, which is calculated under the assumption that the noise and distortion terms are independent and Gaussian distributed. This is a reasonable assumption, since the ICI and the MAI are caused by the contribution of a high number of independent sources. Under these premises, the SNDR in carrier k of the desired receiver is computed using the analytical method proposed in section 3.3.1. Let's denote by $\mathbf{T}$ and $\widetilde{\mathbf{T}}$ the transmission matrices corresponding to the desired and interferer channels of the evaluated link, respectively. Similarly, K denotes the set of carriers employed in the desired link and $\widetilde{K}$ the set of carriers assigned to the interferer one. Provided that the in-phase and quadrature components of the complex values transmitted in all carriers are independent with power $\sigma^2_{k,I}$ and $\sigma^2_{k,Q}$, the SNDR in carrier k of the desired link can be expressed as

$$SNDR_k = \frac{\sigma^2_{k,I} + \sigma^2_{k,Q}}{ISI_k + ICI_k + \left(\left| 1 - T^{k,I}_{m,k} \right|^2 \sigma^2_{k,I} + \left| j - T^{k,Q}_{m,k} \right|^2 \sigma^2_{k,Q} \right) + MAI_k + \sigma^2_{U,k}}, \tag{5.9}$$

where $k \in K$; $\sigma^2_{U,k}$ is the noise power at the k-th output of the DFT performed in the desired receiver and ISI_k and ICI_k are the ISI and ICI terms given by (3.55) and (3.56), respectively. MAI_k is the MAI experienced in carrier k of the desired link, computed according to

$$MAI_k = \sum_{z \in \widetilde{K}} \left[\left(\left| \widetilde{T}^{k,I}_{m-1,z} \right|^2 + \left| \widetilde{T}^{k,I}_{m,z} \right|^2 + \left| \widetilde{T}^{k,I}_{m+1,z} \right|^2 \right) \sigma^2_{z,I} + \left(\left| \widetilde{T}^{k,Q}_{m-1,z} \right|^2 + \left| \widetilde{T}^{k,Q}_{m,z} \right|^2 + \left| \widetilde{T}^{k,Q}_{m+1,z} \right|^2 \right) \sigma^2_{z,Q} \right]. \tag{5.10}$$

DMT system parameters are shown in Table 5.3. The number of carriers and the cyclic prefix length have been selected according to the results presented in section 3.3.2. No coding is used. The DMT system with pulse-shaping and windowing also employs the parameters in Table II, except for the cyclic prefix length, which is β samples longer. Optimum values of α and β are strongly dependent on the dominating type of MAI. Hence, their selection is carried out separately for the cases of symbol misalignment and frequency asynchrony.

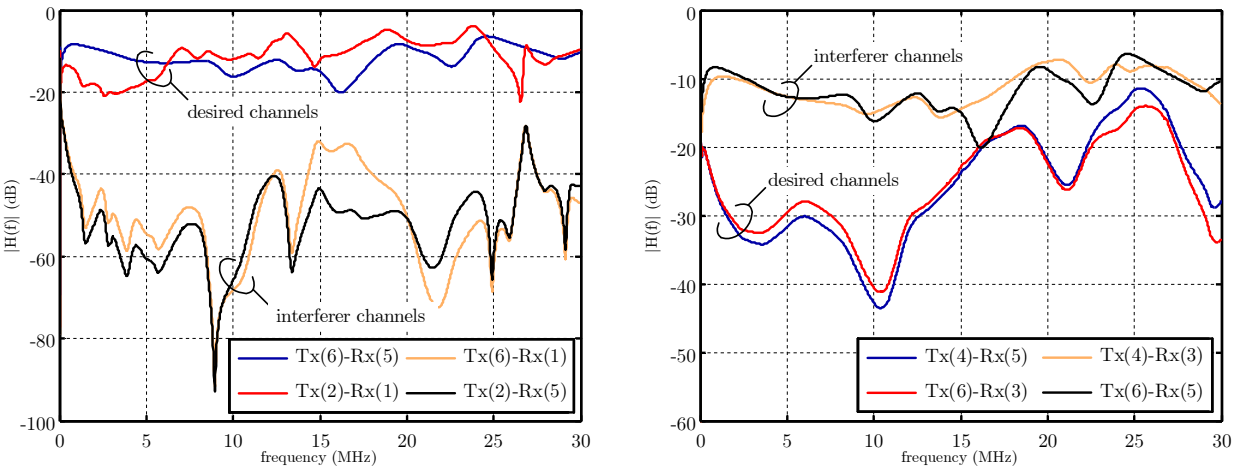

Figure 5.6: Amplitude response of the channels in the (a) *best* MAI scenario; (b) *intermediate* MAI scenario. (c) Noise PSD at the three receivers' site

Parameter	Value
Sampling frequency (f_s)	60MHz
Number of carriers (N)	1024
Cyclic prefix (cp)	228
Constellations	BPSK and square QAM
Maximum number of bits per QAM symbol	16
Objective symbol error probability	10^{-6}

Table 5.3: DMT system parameters

5.3.1 Degradation caused by symbol misalignment

In the case of an integer symbol displacement, increasing α and β reduces the ICI and the MAI at the receiver, but the symbol rate and the available energy for the detection process is

also reduced. MAI is minimum in the case of symbol synchronization, where it is exclusively due to channel dispersion, and maximum when the misalignment between the desired and interferer symbols is about one half of the symbol length. Therefore, the selection of α and β is performed in the latter situation. To this end, the bit-rate of the six links has been evaluated for the different carrier assignments. In scenarios in which the pulse-shaping and the windowing improve the performance, it has been observed that the bit-rate is maximized when $\alpha \approx \beta$. As an example, Fig. 5.7 shows the bit-rate values obtained in the link (4/5) of the intermediate MAI scenario for a carrier assignment consisting of 16 interleaved subbands. It can be also observed that for small values of α and β, small increments in these parameters result in considerable bit-rate improvements. On the other hand, when the reduction in the MAI power, which allows to use denser constellations, does not compensate for the reduction in the symbol rate, the bit-rate decreases when α or β are increased.

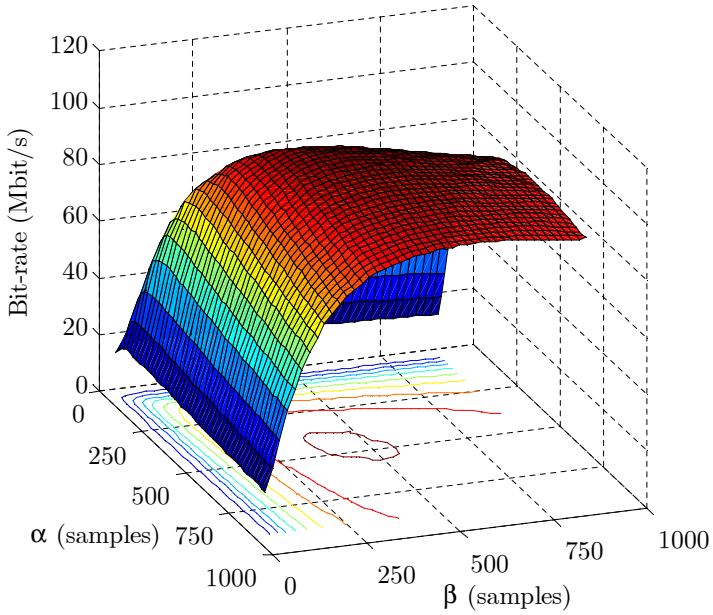

Figure 5.7: Bit-rate for a link of the intermediate MAI scenario with 16 interleaved subbands

To select the most appropriate values for α and β, the interleaved subbands carrier assignments schemes have been selected, since they provide upper bounds for the MAI. Fig. 5.8 depicts the aggregate bit-rate of each MAI scenario for the 16 and 64 interleaved subbands schemes when $\alpha = \beta$ and a *worst* symbol misalignment situation. As a reference, an additional curve labeled as "bit-rate loss asymptote" is drawn. It has been obtained by summing the bit-rates obtained by both users in this scenario without taking into account the MAI, and scaling the symbol rate with the corresponding values of α and β. It is worth noting that in the *best* MAI scenario pulse-shaping and windowing is nearly always counterproductive, since the MAI is very small. This fact is reinforced by noting that the bit-rate for the 16 interleaved subbands scheme is nearly coincident with the bit-rate asymptote due to symbol rate loss. This result also reveals the comparatively reduced influence of the SNR loss due to the pulse shaping and windowing on the bit-rate (energy allocated to the extended parts of the symbols is not available at the detector input). It can be also observed that the bit-rate loss in the intermediate and *worst*

MAI scenarios has a very similar behavior. In the 16 interleaved subbands scheme there is an optimum value for α and β around 500 samples. On the contrary, in the 64 interleaved subbands case, the MAI is so strong that increasing α and β in the analyzed range always improves the performance. Fig. 5.8 shows that $\alpha = \beta = 500$ samples would be an appropriate trade-off for most situations. Consequently, these have been the selected values for the pulse-shaping and windowing.

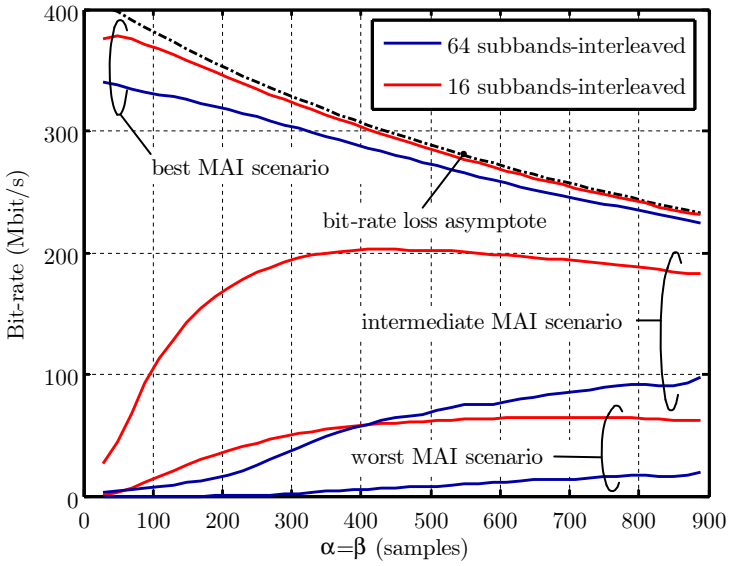

Figure 5.8: Aggregate bit-rate of each MAI scenario as a function of α and β

The performance of the pulse shaped and windowed DMT parameterized with $\alpha = \beta = 500$ is now compared with that of the conventional DMT. To this end, the aggregate bit-rate achieved with both systems in each scenario has been obtained as a function of the symbol misalignment, Δn. Fig. 5.9 depicts the bit-rate loss for the *worst* MAI scenario. The sum of the individual bit-rates obtained by the conventional DMT system in the same scenarios with only one active link at a time is taken as reference. It is interesting to note that the effect of a time advance ($\Delta n < 0$) in the interferer symbol is much harmful than a delay of the same magnitude. The reason is that in the latter situation, the interferer's symbol transitions occurs within the cp of the desired symbol, which absorbs part of the generated MAI. It can be also observed that the performance of the conventional DMT system is extremely sensitive to small symbol misalignments. This suggests that in order to relax the requisites of an FDMA network synchronization system, the displacement of the symbol synchronizers with respect to their optimum position in a single-user environment may be an interesting option. Fig. 5.9 also reveals that performance degradation due to the frequency selectivity of the channel is negligible in a synchronized conventional DMT system. Regarding the DMT system with pulse-shaping and windowing, it is shown that the bit-rate loss is around 25% in a symbol synchronized situation. However, in the presence of symbol misalignment, the bit-rate becomes much more resilient to the MAI. It is also important to note the impact of the carrier assignment in the performance degradation. Thus, whereas in the case of 16 subbands assigned with IP the loss can be up to 30%, in the case of 64 interleaved subbands the communication system can be nearly on outage.

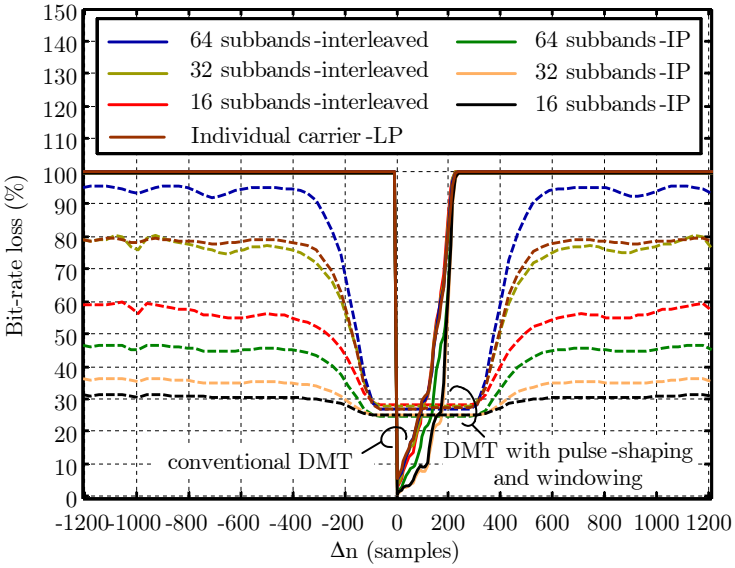

Figure 5.9: Bit-rate loss for the *worst* MAI scenario as a function of the symbol misalignment

The corresponding values for the bit-rate loss in the *best* MAI scenario are shown in Fig. 5.10. This time, the MAI is so small that pulse-shaping and windowing are always counterproductive. However, even with a 30% loss, the aggregate bit-rate achieved in this scenario is over 250Mbit/s.

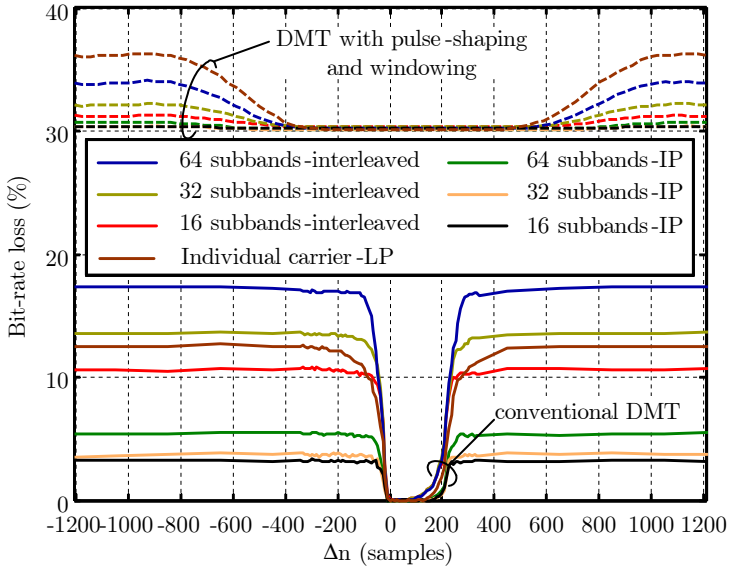

Figure 5.10: Bit-rate loss for the *best* MAI scenario as a function of the symbol misalignment

At this point, it is interesting to compare the performance of the different carrier allocation schemes in the synchronized case. To this end, Fig. 5.11 depicts the bit-rate obtained by the conventional DMT system in each channel (labelled as R1 and R2) of the three MAI scenarios with the 16 subbands (IP) and the individual carrier (LP) assignment strategies. For the sake of clarity, bit-rate values corresponding to channels of the same MAI scenario have been linked with a line. The aggregate bit-rate values are shown in Table 5.4. According to it,

performance is quite similar in both cases. However, as displayed in Fig. 5.11, the rounding of the c_k^i coefficients provided by the LP may lead to a severe unbalancing of the channels bit-rate. Moreover, it makes the obtained solution to violate the constraints imposed in the optimization process. This is clearly shown by the circular markers displayed in Fig. 5.11, which correspond to 40% of the bit-rate value achieved in each channel in a single-user environment. As seen, the individual carrier scheme does not fulfill the corresponding constraints in two MAI scenarios, with particularly harmful results in the intermediate one. On the other hand, the IP method has a much higher implementation complexity and longer running times.

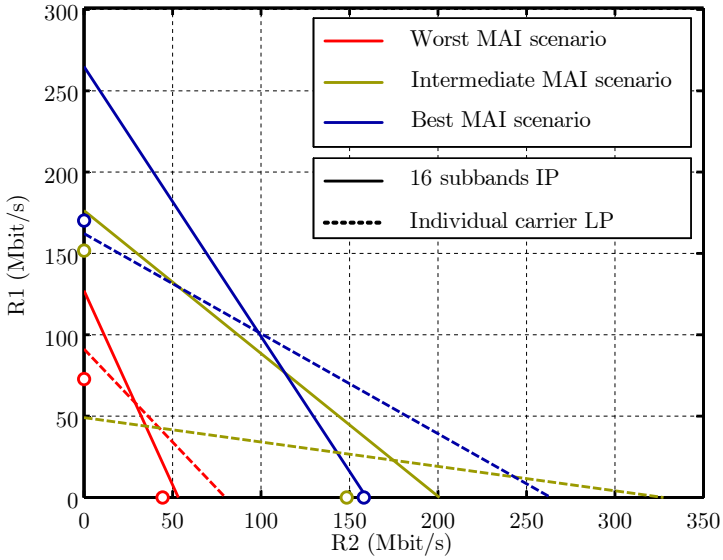

Figure 5.11: Bit-rate obtained in each channel of the three MAI scenarios with the 16 subband and the individual carrier assignment schemes

MAI scenario	Individual carrier (LP)	16 subbands (IP)
Best	425.96	424.59
Intermediate	376.77	376.87
Worst	170.75	180.00

Table 5.4: Aggregate values of the bit-rate shown in Fig. 5.11

5.3.2 Degradation caused by frequency errors

In this section, symbol misalignment is assumed to be kept less than one sample by using the aforementioned synchronization scheme based on periodical beacons sent at a proper rate. Terminals adjust the phase of their clocks after the reception of the beacon. However, in the interval between two consecutive synchronization beacons, users' frequency drift cause MAI. In these circumstances, pulse-shaping at the transmitter is nearly always counterproductive, since it only reduces the MAI caused by channel dispersion. Hence, only windowing is considered from now on ($\alpha = 0$). This is clearly shown in Fig. 5.12, where the bit-rate values obtained in the link (4/5) of the intermediate MAI scenario for a carrier assignment consisting of 16 interleaved subbands are displayed.

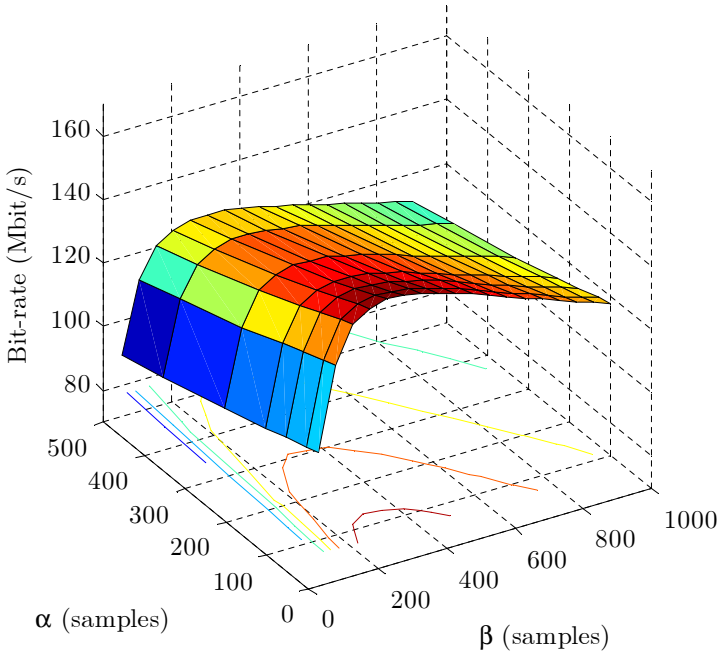

Figure 5.12: Bit-rate for a link of the intermediate MAI scenario with 16 interleaved subbands

In order to determine the most appropriate value for β, the aggregate bit-rate of the three scenarios have been estimated for a frequency mismatch of $\Delta f = 25$ppm. Fig. 5.13 depicts the bit-rate values for the 16 and 64 interleaved subbands schemes. As observed, the behavior is quite similar to the one seen in the case of symbol asynchrony (see Fig. 5.8). In the *best* MAI scenario windowing is always counterproductive and in the remaining ones it improves the bit-rate. A trade-off value of $\beta = 480$ has been selected for the subsequent analysis.

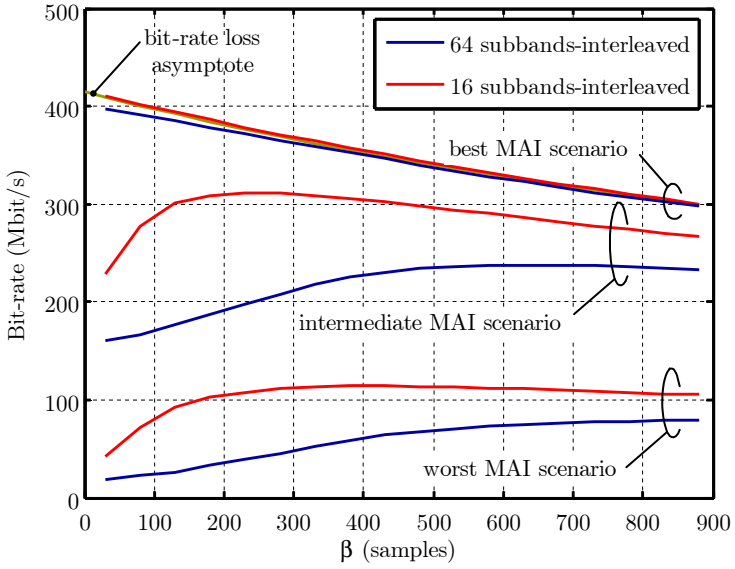

Figure 5.13: Aggregate bit-rate of each MAI scenario as a function of β

Fig. 5.14 depicts the bit-rate loss attained in the *best* and *worst* MAI scenarios as a function

of the frequency mismatch. The sum of the individual bit-rates obtained by the conventional DMT system in the same scenarios with only one link active at a time are taken as reference. It can be observed that in the *best* MAI scenario the performance of the conventional DMT system is nearly unaffected by the frequency mismatch. Although not shown in the figure, the bit-rate loss of the windowed DMT system in this scenario in the analyzed range is around 15%. On the other hand, in the *worst* MAI scenario, the performance of the conventional DMT is seriously degraded even for small frequency offsets. Similarly, the bit-rate loss of the windowed DMT may also be considerable for some carrier assignments even for a frequency mismatch of 30ppm. For frequency errors smaller than 2ppm, the bit-rate loss is below 30%, which ensures more than 110Mbit/s.

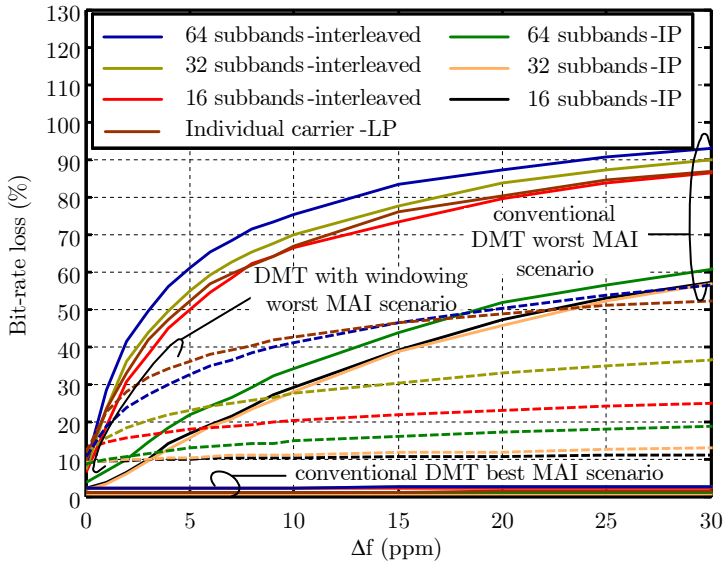

Figure 5.14: Bit-rate loss in the *worst* and *best* MAI scenarios as a function of the frequency mismatch

5.3.3 Degradation caused by the analog-to-digital conversion

The study performed up to now has neglected the performance degradation caused by the errors introduced in the analog-to-digital conversion. This situation is only feasible if an infinite resolution ADC is employed or, alternatively, if an analog filtering is employed to feed a high resolution ADC only with the desired signal. In this section, bit-rate loss experienced in a synchronized network with digital band separation due to the errors introduced by the ADC is assessed. Both FDD and TDD are analyzed.

The worst case in a TDD scheme occurs when the number of active users is very high and the desired link has been allocated only small bandwidth. To simulate these circumstances, the available bandwidth is divided into 16 subbands and the desired link is allocated only the one in which it achieves the highest bit-rate. Fig. 5.15 depicts the bit-rate loss in the three MAI scenarios as a function of the AGC gain for various ADC resolutions. In all cases $X_l = 5$ and the bit-rate achieved in an ideal situation, i.e. no ADC errors, is taken as a reference for the

percentage calculation. As seen, regions limited by the quantization and limiting errors are clearly manifest. In the latter zone, performance is extremely sensitive to the AGC gain. It is worth noting that in order to keep the bit-rate loss below 10% in all scenarios, an ADC with at least 16bits is required. Fig. 5.15 has displayed the worst case for a TDD scheme. In a situation in which the desired link is allocated half of the available bandwidth, minimum bit-rate loss values improve by approximately 10%. Hence, the previous conclusion is not substantially modified, since at least a 14-bits ADC would be needed.

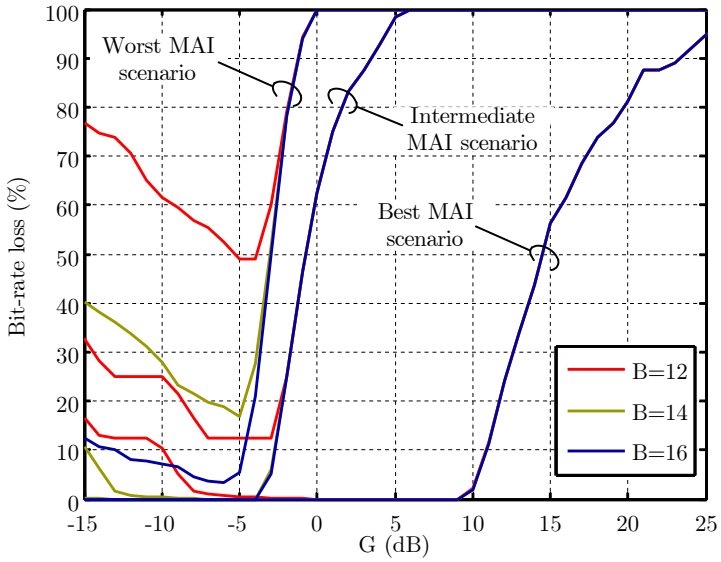

Figure 5.15: Bit-rate loss with a TDD scheme as a function of the AGC gain for various ADC resolutions

In an FDD scheme the input to the ADC is composed of three terms: the desired signal, the interferer one and the signal from the own transmitter. Assuming that the directional coupler provides only 5dB of isolation between transmitter and receiver, the worst case arises when only the desired link is active and, in addition, the traffic is highly asymmetric. However, this work considers the more practical situation with two active links and symmetric traffic distribution. Hence, the desired link is allocated half of the available bandwidth, which is then divided in two equal subbands, one for transmitting and one for receiving. It can be observed that at least 16bits are required to keep the bit-rate loss below 10%.

It is interesting to compare results shown in Fig. 5.16 with the ones in Fig. 5.15. As seen, performance degradation in the *worst* MAI scenario is very similar in both cases. The reason is that the attenuation of the interferer channel is similar to the one introduced by the directional coupler. In the *best* MAI scenario, the attenuation of the desired channel is similar to the one of the directional coupler. Since the interferer signal power is negligible, the input to the ADC is composed of two terms with nearly equal power. Hence, the penalty in the FDD case is very small. On the other hand, in the *intermediate* MAI scenario the signal coming from the own transmitter dominates, and differences between the FDD and the TDD techniques is 15% for a 12-bits ADC, and about 10% for a 14-bits ADC.

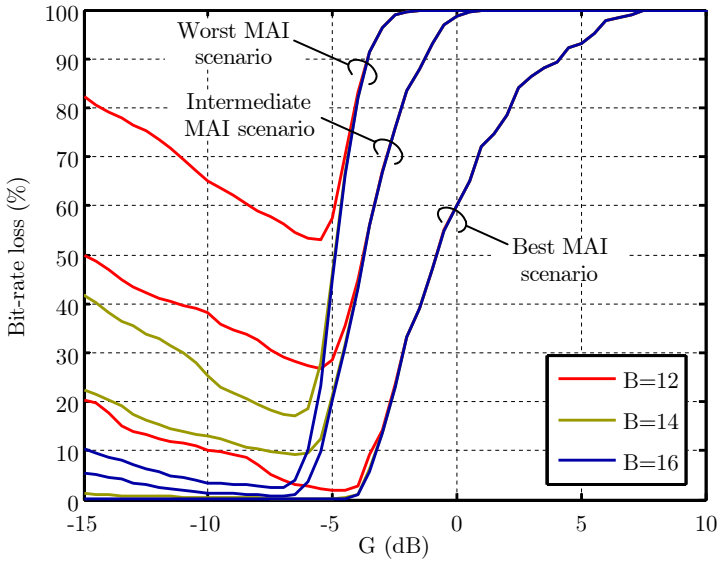

Figure 5.16: Bit-rate loss with an FDD scheme as a function of the AGC gain for various ADC resolutions

5.4 Conclusions

This chapter has analyzed the performance of a DMT-FDMA scheme for indoor broadband PLC. The number of carriers has been fixed to 1024, which is in the range of the values employed by current commercial systems [64], [23]. Under these circumstances, distortion due to the channel short-term variations is negligible and MAI is caused by three phenomena: the frequency selectivity of the channel; the misalignment between the desired and the interferer symbols and the frequency asynchrony between user's clocks. Performance degradation caused by each of these sources has been quantified. Benefits obtained by using a DMT system with pulse-shaping and windowing in the presence of symbol and frequency asynchrony have been assessed. The influence of the carrier assignment scheme has also been evaluated. Finally, the required resolution of the ADC in an FDD and a TDD scheme with digital band separation has been determined. Main achievements are now summarized:

- Influence of the different MAI sources. It has been shown that MAI due to the frequency selectivity of the channel is negligible in a symbol and frequency synchronized network. It has been also verified that performance degradation caused by symbol misalignment due to differences in the propagation delay is minimal. However, the conventional DMT system has proven to be extremely sensitive to additional symbol displacements. In this sense, it has been corroborated that the effect of a time advance in the interferer symbols is much harmful than a delay of the same magnitude, since in the latter situation the cyclic prefix absorbs part of the generated MAI. Based on this observation, it has been suggested that the displacement of the symbol synchronizers, with respect to their optimum position in a single-user environment, can be employed to relax the requisites of an FDMA network synchronization system. Performance is

also enormously sensitive to frequency errors. Thus, system outage may occur even for a frequency mismatch of 40ppm.

- Performance of a DMT system with pulse-shaping and windowing. It has been proven that pulse-shaping and windowing are useful techniques for mitigating the effect of small symbol misalignments. The bit-rate is maximized by selecting $\alpha \approx \beta$, but their particular values result from the trade-off between MAI reduction and symbol rate reduction. Under significant symbol misalignment, performance is extremely dependent on the carrier allocation procedure. Even by using tone-grouping, the bit-rate loss can be up 95% when employing 64 subbands. It has also been shown that pulse-shaping is counterproductive in the presence of frequency errors, since it only reduces MAI caused by the channel frequency selectivity. On the contrary, windowing has proven to be an effective way of reducing performance degradation in these circumstances. Nevertheless, bit-rate loss can be up to 50% for a frequency mismatch of 20ppm.

- Influence of the carrier assignment strategy and the number of users. It has been verified that using an allocation scheme in which carriers are individually assigned to users is always counterproductive in the presence of symbol and frequency asynchrony because the MAI is significantly increased. Moreover, it has been shown that even in a synchronized network, the necessary rounding of the solution given by the LP method causes severe bit-rate unbalancing. In some cases this leads to a violation of the constraint imposed in the optimization process. The combined use of tone-grouping, pulse-shaping and windowing can be used to implement an asynchronous DMT-FDMA environment with a small number of users. However, bit-rate loss with respect to a synchronous network can be up to 60% for a network with 16 users.

- ADC requirements. It has been determined that, in order to avoid the use of an analog filtering and to accomplish the band separation using the receiver DFT, the employed ADC must have, at least, 16bits. This ensures that the bit-rate loss is always below 5%, both in an FDD and a TDD scheme. In case a 14-bits ADC is employed, the bit-rate loss can be up to 18% in both schemes.

Chapter 6

Conclusions

6.1 Achievements

This thesis has studied the utilization of DMT modulation for indoor broadband power-line communications. The presented analysis has addressed some of the major aspects concerned with this transmission technique: selection of modulation parameters, equalization, synchronization and multiple access schemes. Main achievements are now summarized:

- Channel characterization. Although the thesis has been focused on digital communication systems aspects, rather than in channel characterization ones, novel results have also been given in three particular matters: relation between the delay spread and the channel coherence bandwidth, analysis of the channel response time variations and discussion of the noise amplitude distribution. Regarding the first issue, an analytical expression that relates both parameters has been determined. Concerning the second one, a sort of Doppler spread has been defined to characterize the rate of change of the channel response. By measuring the spectral broadening suffered by a sinusoid after traversing the channel, it has been determined that output bandwidths higher than 100Hz occur in 50% of the cases. In addition, it has been shown that time variations are quite frequency selective. In reference to the noise amplitude distribution, it has been demonstrated that the Gaussian assumption is appropriate only for the background noise. In those time instants with impulsive components, the probability of high amplitude noise samples is higher than in a normally distributed variable. All these results have been obtained by performing a statistical analysis over a representative set of more than 50 actual channels measured in three different scenarios (apartment, detached house and university building).

- Analytical computation of the distortion caused by an LPTV channel. Distortion caused by the power-line channel response can be separated in two terms. One is due to the frequency selectivity of the channel and the other is caused by its time variation. An analytical method has been developed to compute both components. The proposed procedure allows a much faster computation than conventional simulations employing an

LPTV filtering. In addition, it has been shown that distortion due to the frequency selectivity is essentially invariant along the mains cycle.

- Optimum number of carriers and cyclic prefix length. It has been determined that performance of the DMT system in a single-user environment is maximized by employing 8192 carriers and around 300 samples of cyclic prefix at a sampling frequency of 50MHz. While selecting a higher number of carriers increases the ICI caused by the channel time variations, using a lower one increases the ISI and ICI due to the channel frequency selectivity.

- Time equalization. The utilization of a TEQ in a multiuser environment is not straightforward because different taps are required for each link. However, it has been also verified that its use is not justified from a performance gain perspective. Hence, higher bit-rates can be obtained with a reduced computational complexity by doubling the number of carriers. The reason for the poorer performance of the TEQ in power-line scenarios is that these channels do not match the classical pole-zero model of DSL channels, in which the cancellation of a couple of poles increases the confinement of the impulse response by more than 30dB.

- Adaptive modulation. Benefits obtained with an adaptive modulation system in which the constellation employed in each carrier is selected according to the instantaneous channel conditions have been assessed. To this end, bit-loading algorithms for adaptive and fixed modulation systems subject to ABER and IBER constraints have been developed. It has been shown minimal performance degradation occurs if the bit-loading is performed according to an ABER criterion but just in one dimension or, even more, according to an IBER criterion. In general, bit-rate losses caused by the use of a fixed modulation scheme are relatively modest when a wide band is employed, e.g. from 1MHz to 20MHz. On the other hand, the frequency selective character of the channel time variations may cause severe degradation in systems employing narrower bandwidths. It has been also proven that performance degradation in a fixed modulation system increases with the number of carriers, since distortion caused by the frequency selectivity of the channel, which is basically time invariant, decreases.

- Analysis and design of timing recovery schemes. The conventional DA decision-directed timing recovery scheme used in other scenarios with high SNR values has been adapted to the peculiarities of indoor PLC channels. Thus, a two-stage FEQ has been proposed to avoid interaction between the equalization and synchronization blocks. One of these stages compensates for the long-term changes in the channel response, and the other tracks the short-time variations experienced by the channel with respect to its long-term value. The timing recovery scheme takes information from the output of the long-term FEQ. The price to be paid is that the cyclic variations of the channel, with harmonics at multiples of the mains signal frequency, mislead the estimation of the sampling error. This error can be reduced by using a narrower loop bandwidth, but this also reduces the loop ability to track the sampling jitter. This latter non-ideality is usually neglected when sampling relatively narrowband signals. However, it has been shown that its effect

is particularly important in the considered problem. In fact, simulations have revealed that performance is extremely sensitive to the loop bandwidth in the jitter limited region.

Two modifications have been proposed to overcome the aforementioned shortcomings. The first one is to reduce the influence of the channel cyclic time variations on the estimates of the phase error. To this end, an LS estimator that takes into account the magnitude of these variations has been designed. With similar implementation complexity, the proposed estimator notably outperforms the classical one designed for LTI channels. The second modification increases the attenuation of the channel time variations by placing a series of notch filters in the PLL loop. It has been shown that the combined use of the proposed LS estimator and three notch filters, tuned to the three first harmonics of the mains, lead to negligible performance degradation in most channels.

- Analysis of DMT-FDMA as a multiple access scheme. A DMT-FDMA network employing a number of carriers similar to the one currently in use by commercial system is impaired by three MAI sources: the frequency selectivity of the channel, the misalignment between the desired and the interferer symbols and the frequency errors between the clocks of the different users. It has been shown that the former has a negligible effect in a synchronized network, and that the influence of the second one can be reduced by using pulse-shaping and windowing. Similarly, distortion caused by frequency errors can be reduced by means of windowing. However, even with optimum parameterization of the pulse-shaping and windowing techniques, performance degradation is so severe that an asynchronous DMT-FDMA network is only feasible when the number of users is small.

  It has been shown that carrier allocation schemes in which carriers are individually assigned to users are always counterproductive in the presence of symbol and frequency asynchrony because the MAI is significantly increased. Moreover, it has been verified that even in a synchronized network, the necessary rounding of the solution given by the LP methods causes severe bit-rate unbalancing which, in some cases, also violate the constraint imposed in the optimization process.

- Digital band separation in a DMT-FDMA network. It has been determined that at least a 16-bits ADC is required to accomplish the band separation by means of the receiver DFT. This ensures that the bit-rate loss is always below 10% both in FDD and TDD. It has been also shown that for a 12-bits ADC, the performance degradation with the former duplexing technique is, at most, 15% worse than with the latter.

6.2 Suggestions for further work

Research in PLC is only in an embryonic state, hence, there is still much work to do. One of the open fields is channel characterization and modeling. However, focusing on transmission techniques issues, and in particular on multicarrier modulations, results presented in this thesis can be used as the starting point for further studies. Some of the straightest ones are now summarized:

- Frequency equalization. This issue was not particularly interesting when the channel was assumed to be LTI. However, the short-term variations of the channel have made it a two-dimensional problem with especially challenging aspects: the cyclostationary character of the received noise; the periodic and frequency-selective nature of the channel time variations and the remarkable phase changes of the frequency response along the mains cycle. A preliminary study has already been undertaken at the moment of writing this thesis [60]. Results show that some classical estimators may have considerable problems to track phase changes. It has been also noticed that the influence of the cyclostationary noise can be somehow masked by the frequency-selective character of the instantaneous PSD changes. Performance losses of up to 50% have been registered when employing an estimator that only takes into account the frequency correlation of the channel. Nevertheless, the work accomplished up to now has been limited to adapt techniques that are known to perform well in other environments. Ad-hoc strategies based on series decomposition of the channel in terms of periodical functions should be explored.

- Analysis of the TDMA scheme. In a first instant, a simplified study can be tackled by assuming perfect synchronization and frequency equalization. Then, the selection of the optimum time slot duration can be done. A short time slot increases the amount signaling exchanged between the users and the central node. In addition, it also reduces the transmission efficiency, since overhead introduced by the layers increases. On the other hand, a long time slot increases the delay and the system complexity. This issue has recently been studied in [128], although the considered scenario is too simplistic. Similarly, the resolution required in the ADC when using the TDMA-TDD and the TDMA-FDD schemes must be determined. Nevertheless, results presented in this thesis point out that about 12bits would suffice in the former case and that 16bits would be required in the latter.

  The aforementioned analysis is appropriate for a first approach to the problem. However, the adoption of a TDMA technique has strong implications in the synchronization and equalization tasks. TDMA systems employ a preamble at the beginning of each slot for synchronization and channel estimation purposes. This overhead may reduce the transmission efficiency considerably. In addition, the duration of the time slot is closely related to the convergence time of the timing recovery loop and of the equalization procedure. Faster convergence implies higher residual errors and, consequently, lower achievable bitrates.

- Channel coding. In a fist instance, performance gains obtained by the classical concatenation of convolutional and block codes can be assessed. The interleaving depth must also be investigated. This analysis should also cover the use of joint coding and modulation techniques. However, exploiting the cyclic nature of the channel, and particularly the cyclostationary character of the received noise, is by far the most interesting study. Adapting the code rate or even the coding scheme along the mains cycle seems to be an appropriate way of increasing the system throughput.

- Performance evaluation of other multicarrier modulations. Implementation of an asynchronous FDMA scheme would be desirable from a complexity point of view. How-

ever, when using DMT this is only feasible for a small number of users. Performance degradation is driven by the MAI due to the symbol and frequency asynchrony. Alternative multicarrier modulations with higher spectral containment, like Filtered MultiTone (FMT) [87], must be evaluated. Its performance in a multiuser environment has been recently presented in [129]. Nevertheless, still there is much work to do in aspects like modulation parameterization, synchronization and equalization issues, etc.

Appendix A

Resumen en español

A.1 Introducción

La utilización de las redes de distribución de electricidad como medio de transmisión de información se remonta a los inicios del siglo XX [1]. Durante muchos años su uso ha estado restringido a sistemas de banda estrecha: en exteriores para la lectura remota de contadores y telecontrol y en interiores para aplicaciones domóticas [2],[3]. La mayor parte de estos sistemas hacen uso de esquemas de modulación relativamente simples y en Europa utilizan la denominada banda CENELEC (*Comité Européen de Normalisation Electrotechnique*), que se extiende desde los 3kHz hasta los 148.5kHz [4]. Sin embargo, el empleo de estas redes para aplicaciones de banda ancha ha sido tradicionalmente desestimado por considerar que el canal era demasiado ruidoso e impredecible.

El final de los monopolios de las telecomunicaciones en Europa a finales de los años noventa, junto con los nuevos avances en la transmisión digital, abrieron nuevas expectativas de negocio para las comunicaciones por la red eléctrica, o más comúnmente PLC (*Power-Line Communications*). En primera instancia se propuso emplear la red eléctrica que se extiende desde los transformadores de media-baja tensión hasta las instalaciones de usuario como medio de acceso a redes de comunicaciones de área extensa. Sin embargo, en los países desarrollados, la fuerte competencia de los servicios DSL (*Digital Subscriber Loop*) ofrecidos por las compañías telefónicas y de cable hacen que el número de clientes no esté respondiendo a las expectativas iniciales. Así pues, parece que son los países en vías de desarrollo donde esta aplicación de las PLC tienen un futuro más prometedor.

Al mismo tiempo, la creciente demanda de conectividad en los denominados entornos SOHO (*Small Office-Home Office*) ha despertado el interés por las PLC en interiores. El objetivo de estos sistemas es utilizar las líneas eléctricas del interior de los edificios a modo de red de área local. Esta red de área local no se restringe a la conexión de ordenadores, sino que incluye a los equipos multimedia de entretenimiento como reproductores DVD o televisores de alta definición. En cualquier caso, también en este entorno las PLC tienen que competir con

sistemas sólidamente implantados, como es el caso de *Ethernet* en zonas de negocios y con los inalámbricos en las residenciales [9].

El rango de frecuencias actualmente asignado por el ETSI (*European Telecommunications Standards Institute*) a las PLC de banda ancha se extiende desde 1.6MHz hasta 30MHz [15]. En lo que respecta a la normativa de emisiones conducidas aplicables, a día de hoy los únicos límites existentes en Europa para la frecuencias superiores a los 500kHz son los indicados en la EN-55022 [13]. Esta norma de compatibilidad electromagnética (EMC-*Electromagnetic Compatibility*) impone unos valores máximos excesivamente restrictivos para el funcionamiento de las PLC, ya que está pensada para emisiones no intencionadas. Sin embargo, pese a que un comité conjunto del ETSI PLT (*Power Line Telecommunications*) y CENELEC lleva varios años trabajando con mandato de la Comisión Europea en la definición de una norma específica, aún no existen límites ni sobre la potencia inyectable en la red ni sobre la densidad espectral de potencia (DEP) de transmisión.

Además de las citadas aplicaciones, en los últimos tiempos están cobrando fuerza nuevas propuestas para las PLC. Una de ellas plantea emplear las líneas de distribución de energía existente en los vehículos como medio de transmisión de información [10]. El objetivo es comunicar el cada vez mayor número de dispositivos electrónicos (computadora de a bordo, sensores, equipos multimedia, etc.) usando los mismos cables por los que estos reciben la alimentación de la batería. De esta forma se consigue una considerable reducción de peso del vehículo. Otro de los recientes proyectos consiste en utilizar las líneas de contacto empleadas para el suministro de energía a trenes, metros y tranvías como canal de comunicaciones para aplicaciones de automatización y control [11].

A.1.1 Estado actual de la cuestión

La investigación en el campo de las PLC de banda ancha comienza de forma efectiva en la segunda mitad de la década de los noventa. Desde entonces, el interés por las mismas ha venido creciendo de forma ininterrumpida. Buena prueba de ello es que la conferencia internacional sobre el tema que, con carácter monográfico, se celebra anualmente, el *International Symposium on Power Line Communications and its Applications*, está desde 2006 auspiciada por la *Communications Society* del IEEE (*Institute of Electrical and Electronic Engineering*). Además, en los últimos años han aparecido cuatro números específicos dedicados a las PLC en revistas de reconocido prestigio [1].

La mayor parte del esfuerzo investigador realizado en el ámbito de las PLC en estos últimos años se ha concentrado en la caracterización y modelado de canal [29], [32], [33], [39], [40], [34]. La topología de estas redes, aunque varía de unos países a otros, tiene generalmente una disposición arborescente [28]. Esta estructura ramificada está formada por cables de distintas secciones interconectados entre sí y terminados en circuitos abiertos o en dispositivos eléctricos. La

[1] *IEEE Communications Magazine* e *International Journal on Communications Systems* en 2003, *IEEE Journal on Selected Areas on Communications* en 2006 y *EURASIP Journal on Advances in Signal Processing* que aparecerá en 2007

notable variación de impedancia que presentan los aparatos eléctricos, junto a la desadaptación que se produce en las uniones entre cables, da lugar a un fenómeno de propagación multicamino que confiere a la respuesta de estos canales una marcada selectividad en frecuencia [29]. Además de esto, la respuesta en frecuencia experimenta variaciones temporales de dos tipos. Por un lado, existe una variación a largo plazo debida a la conexión y desconexión de los aparatos eléctricos [33]. Por otro, una variación a corto plazo, síncrona con la tensión de la red, y que se debe a la dependencia que presenta la impedancia de algunos dispositivos eléctricos con el valor instantáneo de la tensión de la red [34].

En lo que respecta al ruido, los canales de la red eléctrica interior presentan características sumamente interesantes. En gran medida, el ruido es generado por los dispositivos conectados a la propia red, aunque parte del mismo también puede resultar de acoplamientos por conducción o radiación. Su naturaleza es tal que no resulta aplicable el clásico modelo de ruido blanco aditivo y Gaussiano. De hecho, en él pueden distinguirse cuatro componentes [65], [41]. La primera está formada por interferencias de banda estrecha. La segunda es una componente cicloestacionaria, síncrona con la tensión de la red, causada por la diferencia de comportamiento que los dispositivos eléctricos presentan con el valor instantáneo de la tensión de la red. Generalmente adopta la forma de impulsos casi-periódicos. Este carácter cicloestacionario es conocido desde hace años [35], y sistemas de banda estrecha como el X10 [2] lo explotan para aumentar la robustez de las transmisiones. La tercera es una componente no-estacionaria y asíncrona con la tensión de red causada generalmente por la conexión y desconexión de aparatos. Finalmente, existe un ruido de fondo estacionario cuya DEP decrece con la frecuencia.

A pesar del esfuerzo realizado en los últimos años, aún no existen canales de referencia como en DSL, ni acuerdo entre la comunidad científica sobre un modelo estadístico de canal. En esta tesis doctoral se adopta el modelo propuesto en [41]. Según este, dejando al margen las componentes de ruido asíncrono impulsivo, una red sin cambios en su configuración (esto es, sin variaciones temporales a largo plazo) puede modelarse mediante un sistema lineal y periódicamente variante con el tiempo (LPTV-*Linear Periodically Time-Variying*) y un término de ruido cicloestacionario.

Para hacer frente a las perturbaciones de los canales de la red eléctrica interior se han valorado distintas técnicas de transmisión [42]. Las más inmediatas son las modulaciones monoportadora. Sin embargo, su uso no resulta apropiado por dos razones fundamentales. La primera es que la gran selectividad en frecuencia del canal produce una considerable interferencia entre símbolos (ISI-*Intersymbol Interference*), lo que obliga a usar complejas estructuras de igualación. Además, los reducidos períodos de símbolo inherentes a la transmisión a alta velocidad hacen a estas modulaciones muy vulnerables frente al ruido impulsivo. La segunda, y más importante, es que parece claro que el cumplimiento de la futura normativa de EMC impondrá zonas no utilizables dentro del rango de frecuencias asignado a las PLC en [15], lo que limitará seriamente el ancho de banda disponible de forma contigua.

Las modulaciones de espectro ensanchado y su técnica de acceso múltiple consustancial, CDMA (*Code Division Multiple Access*), también han suscitado un interés considerable en los últimos años [43], [44], [45]. De hecho, actualmente existen productos comerciales basados en esta

modulación [46]. La baja DEP de la señal trasmitida le permite cumplir fácilmente los límites de EMC. Además, su mayor inmunidad frente a los desvanecimientos multicamino (comparadas con las modulaciones monoportadora) la hacen una candidata apropiada para las PLC. Sin embargo, estas modulaciones no explotan la selectividad espectral del canal, cuyas diferencias de relación señal a ruido (SNR-*Signal to Noise Ratio*) entre bandas pueden llegar a los 40dB. Además, requieren esquemas de igualación complejos, códigos ortogonales y sincronía entre los terminales para combatir el efecto cerca-lejos que aparece en entornos multiusuario.

A día de hoy, las modulaciones multiportadora son consideradas las técnicas de transmisión más adecuadas para las comunicaciones por la red eléctrica [42]. No en vano, los principales productores de módems para PLC basan su capa física en OFDM (*Orthogonal Frequency Division Multiplexing*), que junto a DMT (*Discrete MultiTone*) es una de las dos estrategias multiportadora más extendidas [23], [24]. Estas técnicas dividen el espectro disponible en subbandas. Así, el canal selectivo en frecuencia se transforma en un conjunto de canales planos cuya igualación puede realizarse de forma sencilla mediante un igualador en frecuencia de un único coeficiente denominado FEQ (*Frequency Equalizer*). Además, mediante el uso del denominado *bit-loading*, la constelación empleada en cada subbanda puede elegirse de forma independiente conforme a sus condiciones particulares de transmisión. Aquellas bandas con límites muy restrictivos de emisiones pueden dejarse sin usar. De esta forma, las modulaciones multiportadora hacen un uso eficiente de los recursos espectrales, incluso cuando están dispersos. Además, como consecuencia de la división en subbandas, el tiempo de símbolo aumenta, lo que los hace más resistentes frente a la ISI y al ruido impulsivo.

Actualmente, las dos técnicas de acceso múltiple más utilizadas con OFDM y DMT son TDMA (*Time Division Multiple Access*) y FDMA (*Frequency Division Multiple Access*). La implementación más simple de la primera es la basada en el acceso por contienda. Sin embargo, este esquema es incapaz de garantizar los parámetros de calidad de servicio requeridos por ciertas aplicaciones multimedia. Para solucionar el problema se han propuesto estrategias centralizadas [48]. Por otra parte, el acceso múltiple FDMA resulta especialmente eficiente cuando se usa OFDM o DMT, ya que las subbandas asignadas a cada usuario se solapan y pueden separarse, sin necesidad de usar filtros analógicos, mediante la Transformada Discreta de Fourier (DFT-*Discrete Fourier Transform*). Este proceso, conocido como separación digital de bandas, se hace a costa de aumentar el número de bits necesarios en el conversor analógico digital (ADC-*Analog to Digital Converter*) [53]. No obstante, la estrategia FDMA implementada de esta forma tiene algunos inconvenientes. En primer lugar, requiere que los terminales estén sincronizados para evitar la interferencia de acceso múltiple (MAI-*Multiple Access Interference*).

Cualquiera de los dos esquemas de acceso múltiple citados puede combinarse con una técnica de duplexación en tiempo (TDD-*Time Division Duplexing*) o en frecuencia (FDD-*Frequency Division Duplexing*). Tradicionalmente, TDD permitía una gestión más flexible de las asimetrías en el tráfico de usuario. Sin embargo, el uso la separación digital de bandas confiere a FDD una capacidad similar.

A.1.2 Objetivos

Las prestaciones de los sistemas de comunicaciones por la red eléctrica interior han experimentado significativos avances en los últimos tiempos. Sin embargo, aún existen elementos de los mismos que son adaptaciones de soluciones tomadas de otros entornos, pero que no se ajustan a las particularidades de este escenario. Además, como se ha comentado, la mayor parte del esfuerzo investigador realizado en el ámbito académico hasta el momento se ha concentrado en el modelado y caracterización del canal [36], [37].

Por todo ello, el **objetivo fundamental** de esta tesis es realizar un **estudio** de los principales aspectos relacionados con el empleo **de la modulación DMT para comunicaciones** de banda ancha **por la red eléctrica en el interior de los edificios**. Este objetivo general se concreta en los siguientes objetivos parciales:

- Caracterización del canal. Aunque las características del canal han sido ampliamente tratadas en la literatura [29], [32], [65], [41], esta tesis se plantea profundizar aún más en el conocimiento del mismo. En concreto, en la determinación de parámetros que resulten de interés para el diseño de sistemas de comunicaciones.

- Número de portadoras de la modulación DMT. Los valores empleados en la actualidad por los sistemas comerciales parecen haber sido elegidos bajo criterios de implementación más que de optimalidad. Por tanto, uno de los objetivos será determinar el valor más apropiado para este parámetro.

- Tipos de pulsos. Los pulsos rectangulares habitualmente empleados en la modulación DMT dan como resultado un reducido confinamiento espectral que no es apropiado para las características de los canales de la red eléctrica. Esto hace que la parametrización y evaluación de prestaciones que pueden conseguirse con otros tipos de pulsos sea otro de los objetivos de la presente tesis.

- Igualación. En aplicaciones DSL ha resultado exitosa la utilización de un igualador temporal para aumentar el confinamiento de la respuesta al impulso y, de esta forma, reducir la longitud del prefijo cíclico. Sin embargo, no existen, en conocimiento del autor, estudios sobre su eficacia en aplicaciones PLC. Así pues, la determinación de la idoneidad de este tipo de igualador y del valor óptimo del prefijo cíclico son otros de los objetivos de la tesis.

- Modulación adaptativa. La adaptación de la constelación transmitida a las condiciones instantáneas del canal es una estrategia ampliamente utilizada en canales de radio móvil. Las variaciones temporales de los canales de la red eléctrica interior los convierten en candidatos interesantes para el uso de estas técnicas. Además, el carácter periódico de las mismas añade al problema interesantes perspectivas cuyos beneficios deben ser ponderados.

- Sincronización. La sincronización en PLC tiene dos características distintivas de gran interés. Por un lado, se pueden alcanzar SNRs bastante elevadas, lo que obliga a un diseño

minucioso del sistema de sincronización que evite la degradación de prestaciones. Por otra parte, el canal presenta variaciones temporales relativamente rápidas [34]. Esta tesis se centra en la tarea de la recuperación del sincronismo de muestra. En concreto, el objetivo es identificar los problemas de las estrategias más habituales y proponer soluciones adaptadas a las características del canal.

- Acceso múltiple. A pesar de los potenciales beneficios de la combinación DMT-FDMA, no existen, en conocimiento del autor, estudios sobre su uso en aplicaciones PLC. Por tanto, esta tesis se plantea también un estudio detallado de todos los aspectos relacionados con esta estrategia: evaluación de las fuentes de MAI, influencia de los esquemas de asignación de portadoras, efecto de las asincronías de símbolo y frecuencia y número de bits necesarios en el ADC.

La presentación de los resultados obtenidos se ha organizado en cuatro capítulos. Tras la introducción, en el capítulo 2 se presenta la caracterización del canal y los modelos que se emplearán en el resto del trabajo. El capítulo 3 introduce los aspectos básicos de la modulación DMT y aborda la determinación del número óptimo de portadoras, el estudio de los tipos de pulsos, la idoneidad de la igualación temporal y el valor óptimo del prefijo cíclico y el análisis de la modulación adaptativa. El capítulo 4 se concentra en los aspectos relacionados con la sincronización y el capítulo 5 en los relativos al acceso múltiple DMT-FDMA. Finalmente, se presentan de forma resumida las conclusiones más importantes que se derivan de la investigación realizada.

A.2 Desarrollo y resultados

A.2.1 Caracterización del canal

Antecedentes

Hasta fechas relativamente recientes se había considerado que las únicas variaciones temporales que experimentaba la respuesta de los canales de la red eléctrica interior eran las que se producían a largo plazo. Respecto al ruido, si bien existían trabajos que postulaban su naturaleza cicloestacionaria, estos se limitaban a la banda por debajo de los 450kHz [74]. Es en [41] donde se presenta un riguroso estudio que pone de manifiesto que la respuesta en frecuencia de estos canales presenta variaciones temporales a corto plazo síncronas con la tensión de red. Asimismo, confirma la existencia de componentes de ruido cicloestacionarias en la banda de frecuencias de 1MHz hasta 20MHz.

Aportaciones

El elemento de partida de las aportaciones presentadas en esta tesis en el ámbito de la caracterización de canal es una amplia campaña de medidas llevada a cabo en tres escenarios residenciales (un apartamento, una casa independiente y en laboratorios y despachos universitarios) en la

banda de 1MHz hasta 20MHz. El conjunto total está formado por más de 50 canales, incluyendo las correspondientes DEP instantáneas de ruido, y será usado a lo largo de toda la tesis para obtener resultados representativos.

Desde el punto de vista del diseñador de un sistema de comunicaciones digitales, y en particular de aquellos que emplean DMT, existen tres parámetros del canal que resultan especialmente interesantes. El primero de ellos es el denominado *delay spread*, que proporciona una medida de la duración efectiva de la respuesta al impulso y cuyo valor está íntimamente relacionado con la longitud del prefijo cíclico. El segundo es el ancho de banda de coherencia, que de forma coloquial puede definirse como el ancho de banda en el que el canal puede considerarse aproximadamente constante. Por último, el ancho de banda Doppler caracteriza la rapidez de las variaciones temporales del canal. Estos dos últimos parámetros resultan de interés para la determinación del número de portadoras. El primero para garantizar que el canal que experimenta cada una de ellas sea plano, y el segundo para asegurar que el canal permanece prácticamente invariante durante el período de símbolo.

En esta tesis se ha determinado una expresión analítica que relaciona el valor medio del ancho de banda de coherencia en el ciclo con el correspondiente valor del *delay spread*. Además, de las medidas realizadas se concluye que 50kHz es una cota inferior para el ancho de banda de coherencia, lo que en un ancho de banda de 25MHz obligaría a usar un sistema DMT con al menos 500 portadoras.

Respecto al ancho de banda Doppler, se ha definido un procedimiento de cálculo basado en el desarrollo en series de Fourier de la respuesta en frecuencia del canal. Los resultados obtenidos demuestran que en el 50% de las frecuencias el ancho de banda Doppler es mayor de 100Hz, y que en el 10% llega a incluso a superar los 400Hz. Además, se ha utilizado el valor RMS del ancho de banda Doppler, calculado sobre las frecuencias de cada canal, para medir el carácter selectivo en frecuencia de las variaciones temporales. Esto ha puesto de manifiesto que las variaciones temporales a corto plazo del canal tienen una notable selectividad en frecuencia. Así, no hay canal en que el valor RMS del ancho de banda Doppler no sea de al menos el 40% del valor medio. Más aún, en el 50% de los canales su valor llega al 140%.

En lo que respecta al ruido, se ha investigado su función densidad de probabilidad. Se ha determinado que su distribución no es en absoluto Gaussiana cuando se ignora su naturaleza cicloestacionaria. Este era un resultado previsible teniendo en cuenta la forma casi determinista de las componentes de ruido impulsivo síncrono. Sin embargo, cuando la función densidad de probabilidad se calcula sobre muestras tomadas en una misma fase del ciclo de red, la aproximación Gaussiana resulta apropiada para todas aquellas fases en las que no existan componentes de ruido impulsivo.

Parte de las aportaciones realizadas en este apartado han sido publicadas en [28], [31], [66] y [34].

A.2.2 La modulación DMT

Los sistemas comerciales actualmente existentes para PLC emplean la modulación OFDM. Sin embargo, en esta tesis se propone el uso de DMT porque la tecnología de ADCs existentes en el mercado permite la adquisición de señales en la banda asignada por el ETSI con precisiones superiores a los 12 bits. De esta forma, se evita la degradación provocada por los errores de frecuencia y el ruido de fase de los osciladores que realizan la conversión de frecuencia en OFDM [54].

Cálculo analítico de la distorsión causada por un canal LPTV

Antecedentes

Cuando la señal DMT atraviesa un canal selectivo en frecuencia sufre distorsión en forma de ISI e ICI. De forma similar, cuando atraviesa un canal con variaciones temporales experimenta distorsión en forma de ICI. En los canales de la red eléctrica interior, debido a la periodicidad de las variaciones temporales, la potencia de esta ICI también lo es. A día de hoy no existen, en conocimiento del autor, métodos analíticos para el cálculo de cada una de estas distorsiones.

Aportaciones

En primer instancia se aborda la determinación de la distorsión que sufre la señal DMT al ser filtrada por un sistema lineal e invariante con el tiempo (LTI- *Linear Time-Invariant*). Para resolver este problema se propone un método analítico que da como resultado una matriz de transmisión cuyos coeficientes representan la contribución de los símbolos transmitidos en cada portadora a la salida del sistema DMT. Gracias a su implementación eficiente basada en la FFT (*Fast Fourier Transform*), la obtención de esta matriz tiene un coste computacional similar al de la simulación cuando el número de portadoras está en torno al millar.

El método propuesto tiene importantes ventajas. Una de ellas es que, una vez que se ha determinado la matriz de transmisión, los términos de ISI e ICI creados por una portadora sobre otra pueden obtenerse de forma simple e independiente. Este último hecho hace del método una herramienta muy útil para el estudio de algoritmos de asignación de portadoras. Además, mediante una sencilla modificación, el método desarrollado también puede usarse para calcular la distorsión ocasionada por los errores en la frecuencia de muestreo.

Por su parte, el cálculo de la distorsión causada por la variación temporal del canal se hace considerando que esta tiene un carácter aproximadamente lineal a lo largo de cada símbolo DMT. De esta forma se obtiene una expresión analítica sencilla para la ICI causada por cada portadora. Se ha comprobado que, incluso para 32768 portadoras, el error en el cálculo de la ICI debido a la aproximación lineal es inferior a 3dB.

Estas aportaciones han sido parcialmente publicadas en [121].

Determinación del número de portadoras y prefijo cíclico óptimos

Antecedentes

Los dos parámetros clave en la modulación DMT son el prefijo cíclico y el número de portadoras. Aumentar el prefijo cíclico reduce la distorsión causada por la selectividad en frecuencia, pero también la tasa de símbolo. En lo que respecta al número de portadoras, aumentar su valor reduce la distorsión causada por la selectividad en frecuencia del canal, mejora la eficiencia en la transmisión y reduce el ruido de fuera de banda captado en el receptor. Sin embargo, también provoca un aumento de la distorsión causada por la variación temporal del canal. Este efecto ha sido estudiado en entornos de radio móvil [103],[55], pero no en PLC, donde la periodicidad de las variaciones del canal y la naturaleza coloreada del ruido añaden una interesante dimensión al problema.

Aportaciones

Para llevar a cabo la optimización se propone un método mucho más eficiente que las simulaciones LPTV. El punto de partida es la suposición, corroborada a posteriori, de que las distorsiones causadas por la selectividad espectral y temporal del canal son independientes, lo que permite su cálculo de forma separada.

En primera instancia se determina la distorsión causada por la selectividad en frecuencia. En principio, puesto que la respuesta del canal varía de forma cíclica, también deberían hacerlo la ISI y la ICI. Sin embargo, los valores de *delay spread* presentados en el capítulo 2 muestran que esta magnitud es esencialmente invariante a lo largo del ciclo de red. Esta observación da pie a la hipótesis, de nuevo verificada a posteriori, de que la distorsión causada por la selectividad en frecuencia también es invariante con el tiempo. Con todo ello, la cuestión queda reducida a la determinación de la ISI y la ICI provocada por un canal LTI. Ambos términos pueden calcularse con el procedimiento analítico resumido en el apartado anterior o bien mediante simulación con un canal LTI. Por su parte, la ICI causada por las variaciones temporales del canal se obtiene utilizando el método analítico descrito en el apartado anterior.

Una vez determinados todos los términos de distorsión se calcula el régimen binario en función del número de portadoras, N, y de la longitud del prefijo cíclico en muestras, cp. Este cálculo se lleva a cabo en cada uno de los 50 canales cuya caracterización estadística se muestra en el capítulo 2. Finalmente, se determinan los valores de N y cp que maximizan el régimen binario promedio del conjunto de canales. Se ha determinado que el número de portadoras óptimo es $N = 8192$, si bien la pérdida para un valor más práctico como $N = 4096$ es pequeña. El valor óptimo del prefijo cíclico para $N = 8192$ es $cp = 300$ (a 50MHz), aunque su influencia en las prestaciones es pequeña y se reduce aún más conforme aumenta el número de portadoras.

Parametrización y análisis de prestaciones con distintos tipos de pulso

Antecedentes

Los pulsos rectangulares comúnmente empleados en DMT dan lugar a un espectro que decae solo a razón de $1/f^2$. Esto dificulta la gestión del espectro disponible y provoca un aumento de la ICI en canales selectivos en frecuencia [23], en presencia de errores de frecuencia y en entornos multiusuario con acceso FDMA [56]. Además, también ocasiona un aumento de la potencia de fuera de banda captada por el receptor [86]. Afortunadamente, empleando las técnicas conocidas como *pulse-shaping* [56] y *windowing* [86] es posible utilizar otro tipo de pulsos en transmisión y recepción, respectivamente. Todo ello se consigue sin necesidad de abandonar las eficientes estructuras de modulación y demodulación basadas en la DFT. El principal precio que debe pagarse es la reducción de la tasa de símbolo.

Esta tesis se plantea como objetivo determinar la idoneidad de las técnicas de *pulse-shaping* y *windowing* para aplicaciones PLC. El estudio se lleva a cabo, en primer lugar, en entornos monousuario, siendo el caso multiusuario tratado en el capítulo 4.

Aportaciones

Para evaluar las prestaciones en esta nueva situación se ha desarrollado una extensión del procedimiento analítico para el cálculo de la distorsión que experimenta la señal DMT convencional de forma que pueda aplicarse también cuando se usan estas técnicas. Los pulsos empleados tanto en transmisión como en recepción son de tipo coseno alzado. El análisis se ha llevado a cabo en un entorno residencial, donde se ha seleccionado un canal con buenas características de transmisión, que podría considerarse como caso mejor, y otro que por su fuerte selectividad espectral podría representar el caso peor.

Los resultados muestran que el empleo de *pulse-shaping* en entornos monousuario siempre degrada las prestaciones del sistema. Por el contrario, el uso de la técnica de *windowing* puede reportar ganancias de régimen binario. Este resultado se debe a que, mientras que los pulsos no rectangulares en el transmisor solo reducen la ICI, su utilización en receptor disminuye, además, el ruido de fuera de banda. No obstante, la ganancia de régimen binario que puede obtenerse respecto al DMT con pulsos rectangulares es generalmente pequeña. A modo de ejemplo, en un sistema con 512 portadoras la ganancia máxima es de aproximadamente el 6% en el canal peor y del 2% en el mejor. Estos valores se reducen conforme aumenta el número de portadoras. Además, no pueden obtenerse en ambos canales de forma simultánea, ya que requieren pulsos con distintos valores de *roll-off*. Por tanto, puede concluirse que el uso de las estrategias de *pulse-shaping* y *windowing* en un entorno monousuario no está justificado desde el punto de vista de la mejora de prestaciones.

Igualación temporal

Antecedentes

El prefijo cíclico es una técnica extremadamente sencilla de igualación, pero puede ocasionar una reducción considerable en la tasa de símbolo en canales con respuestas al impulso de gran duración. Una forma de reducir esta pérdida es empleando un igualador en el dominio del tiempo (TEQ) colocado a la entrada del receptor. El objetivo es que la respuesta al impulso del sistema equivalente compuesto por el canal y el igualador tenga una longitud menor que la respuesta original. Esta técnica fue inicialmente propuesta para aplicaciones en entornos DSL [57], donde un igualador de apenas dos coeficientes aumenta el confinamiento de la respuesta al impulso en más de 30dB [101]. Pese a ser un problema sobre el que se ha estado trabajando durante más de una década, el problema de diseño del TEQ sigue siendo complejo y sin convergencia asegurada con buena parte de los métodos [58].

Aportaciones

Para determinar la conveniencia de usar un TEQ se han calculado tanto la ganancia de prestaciones que este reporta, como el incremento de coste computacional que conlleva. Los coeficientes del TEQ se han obtenido siguiendo el criterio *zero-forcing* propuesto en [101]. Se ha comprobado que el confinamiento experimenta un crecimiento extremadamente lento con el número de coeficientes del TEQ. En términos generales, un TEQ de menos de cinco coeficientes no produce incremento apreciable en el régimen binario. De hecho, se ha mostrado que duplicando el número de portadoras pueden conseguirse mayores ganancias de régimen binario con un menor coste computacional. Todo ello permite concluir que el TEQ no es una opción apropiada para los escenarios PLC. Parte de estas aportaciones han sido publicadas en [90].

Modulación adaptativa

Antecedentes

El principio de la modulación adaptativa es ajustar la constelación y el nivel de potencia transmitido a las condiciones instantáneas del canal [61]. Esta técnica ha sido ampliamente estudiada en entornos de radio móvil [106, 107, 108], donde su uso produce una importante ganancia de prestaciones. Formalmente, el objetivo es maximizar el régimen binario sujeto a una restricción de tasa de error de bit (BER-*Bit Error Rate*) instantánea (IBER-*Instantaneous BER*) o de tasa de error de bit media (ABER-*Average BER*) [82]. En el primer caso se busca que la tasa de error esté siempre por debajo de un determinado valor objetivo, independiente del estado del canal. En el segundo caso, menos restrictivo, el propósito es que sea el valor medio de la tasa de error el que se encuentre por debajo de un umbral. En el caso de los canales de la red eléctrica interior, el carácter periódico de las variaciones temporales de la respuesta en frecuencia y la naturaleza cicloestacionaria del ruido añaden nuevas dimensiones al problema.

Aportaciones

El procedimiento seguido para evaluar las prestaciones que se obtienen con las técnicas de modulación adaptativa en los canales de la red eléctrica interior es el siguiente. En primer lugar, se ha desarrollado un amplio conjunto de algoritmos de *bit-loading* que contemplan tanto las estrategias habitualmente empleadas en radio móvil, como otras especialmente adaptadas a las particularidades de los canales de la red eléctrica. Una vez hecho esto, se han determinado las ganancias de régimen binario proporcionadas por cada uno de ellos en sistemas con distinto número de portadoras y ancho de banda de transmisión.

Como base del estudio se considera un sistema DMT en el que las transmisiones están sincronizadas con el ciclo de red. El receptor tiene un conocimiento perfecto de la respuesta del canal y de los niveles de ruido y distorsión en cada instante de tiempo. Durante una fase inicial, este determina la constelación más apropiada para cada portadora y símbolo. Mediante un canal de retorno esta información es comunicada al transmisor. Una vez comenzada la transmisión el sistema entra en un régimen permanente que solo sería alterado por las variaciones a largo plazo del canal. Sin embargo, este tipo de variaciones no se contemplan en el análisis realizado.

La periodicidad de las variaciones del canal permiten modelar el sistema DMT como un conjunto de subcanales independientes indexados en tiempo y frecuencia con las variables (q, k). La asignación de bits a cada subcanal puede hacerse conforme a los criterios de IBER o ABER. En este último caso el promediado se calcula habitualmente sobre el conjunto de bits transmitidos en cada una de las portadoras, lo que da lugar a un criterio que puede denominarse $\mathrm{ABER_t}$, donde el subíndice t indica que el promediado se realiza sobre la variable temporal. Sin embargo, este promediado puede realizarse de dos modos adicionales: sobre la variable espectral, $\mathrm{ABER_f}$, y sobre ambas variables $\mathrm{ABER_{tf}}$.

Para evaluar las prestaciones que pueden conseguirse con cada uno de los criterios anteriores se han desarrollado siete algoritmos de *bit-loading*. Cada uno de ellos se obtiene como combinación de los criterios de IBER y ABER con dos esquemas de modulación: adaptativo y fijo. Mientras en el primero de ellos cada subcanal puede tener asignado un número distinto de bits, en el segundo, todos los subcanales con el mismo índice espectral transportan el mismo número de bits.

Las prestaciones obtenidas con estos algoritmos se han evaluado empleando dos sistemas que emplean la banda de 1MHz a 20MHz: uno con 512 portadoras y 100 muestras de prefijo cíclico (a 50MHz) y otro con 8192 portadoras y 300 muestras de prefijo cíclico. El primero se ha elegido por su baja complejidad de implementación y el segundo por ser el óptimo, según se muestra en el capítulo 3. Se ha comprobado que la pérdida de régimen binario es menor en el sistema que emplea 512 portadoras. Esto se debe a que, en este caso, la distorsión causada por la selectividad en frecuencia del canal, que es esencialmente invariante, es el término dominante. Del mismo modo, la pérdida de prestaciones con un algoritmo IBER respecto al $\mathrm{ABER_{tf}}$ (ambos con modulación adaptativa), es de solo el 7%, mientras que su complejidad de implementación es notablemente inferior. En general, se ha comprobado que la degradación causada por el empleo de un esquema de modulación fijo es relativamente modesta en comparación, por ejemplo, con

la que se da en entornos de radio móvil. Las razones para ello son, por un lado los elevados valores de relación señal a ruido y distorsión que se alcanzan en este tipo de canales, y por otro la marcada selectividad en frecuencia de las variaciones temporales de los canales. La conjunción de ambas hace que los bits adicionales que pueden transmitirse con un esquema adaptativo queden enmascarados por el gran número de bits transmitidos en subcanales en los que las condiciones son prácticamente invariantes. Este hecho es de gran importancia, ya que en un sistema que emplee una banda menor, resultado de trabajar por ejemplo en un entorno multiusuario FDMA, la degradación de prestaciones sí puede ser muy significativa.

A.2.3 Técnicas de sincronización para DMT

Antecedentes

La sincronización en un sistema DMT comprende dos tareas fundamentales: la sincronización de símbolo y la sincronización de muestra [98]. Dado que la primera de ellas no presenta una problemática especial en los canales de la red eléctrica interior, esta tesis se centra en la segunda. El objetivo de la sincronización de muestra es que la frecuencia y la fase del reloj empleado en el muestreo de la señal recibida sean las adecuadas. Los errores de sincronización de muestra provocan la atenuación y giro de los símbolos de la constelación, ICI y, si no se corrigen, errores en el sincronismo de símbolo.

En sistemas con una relación señal a ruido elevada, como es el caso que nos ocupa, es habitual realizar la sincronización de muestra mediante un muestreo no sincronizado y un PLL (*Phase-Locked Loop*) todo-digital [111]. Este PLL consta de un sistema de recuperación de sincronismo y un sistema de corrección [101]. El primero realiza una estima del error de fase experimentado por los símbolos recibidos y, mediante un lazo de realimentación, calcula la corrección que debe ser aplicada por el último. En entornos donde se necesitan eficiencias espectrales elevadas la corrección suele llevarse a cabo mediante un interpolador [63].

Las técnicas de sincronización en escenarios con relaciones señal a ruido elevadas han sido ampliamente estudiadas para aplicaciones DSL [98], [111], [101]. Con respecto a este tipo de canales, los existentes en la red eléctrica interior presentan dos peculiaridades. Por un lado, el canal es variante con el tiempo, y por otro el ancho de banda utilizado es mayor. La variación temporal del canal se produce, además, a un ritmo comparable al del envío de símbolos. Esto obliga a actualizar el FEQ con una frecuencia comparable a la del sistema de sincronización, lo que puede ocasionar la interacción entre ambos y su posible divergencia [62]. El mayor ancho de banda empleado hace que el efecto del *jitter* del oscilador que dirige el proceso de conversión analógico-digital se ponga de manifiesto y pueda llegar a limitar severamente las prestaciones del sistema. Esta tesis analiza la influencia de estos dos elementos distintivos y plantea soluciones originales que palían la degradación que ocasionan.

Aportaciones

En este trabajo se ha considerado un esquema de sincronización basado en un muestreo no

sincronizado y un PLL todo-digital. La estima del error de fase se efectúa empleando una estrategia ayudada por la decisión. Para evitar la interacción entre el FEQ y el sistema de sincronismo se propone un esquema de igualación en dos etapas. En la primera se compensan las variaciones a largo plazo del canal y en la segunda las variaciones periódicas. La información utilizada por el sistema de recuperación de sincronismo para la estima del error de fase se toma a la salida del primer bloque, que tendrá una frecuencia de actualización muy baja. El problema de esta solución es que dicha estima se verá sesgada por las variaciones cíclicas del canal.

Entre las no-idealidades del proceso de conversión analógico-digital se han incluido las desviaciones aleatorias de los instantes de muestreo. Estas son debidas al ruido de fase del oscilador del ADC, y en el dominio del tiempo dan lugar al conocido *jitter*. El efecto del ruido de fase del oscilador empleado en la traslación de banda de los sistemas OFDM ya ha sido tratado en la literatura [54]. Sin embargo, no existen, en conocimiento del autor, estudios sobre su influencia en el proceso de conversión analógico-digital. En esta tesis se ha utilizado el modelo *Power-Law* para el *jitter* del oscilador [118], [119]. Además, también se ha incluido un término que modela el *jitter* de apertura del ADC [113], que se ha representado siguiendo la caracterización propuesta en [117].

Empleando la estructura anterior se han analizado en primer lugar las prestaciones que se obtienen cuando se utiliza el estimador de fase y el lazo de sincronismo habitualmente usados en sistemas DSL [98], [111], [101]. Se ha comprobado que, cuando el ancho de banda del lazo es grande, las prestaciones están limitadas por las variaciones temporales del canal. Conforme el ancho de banda del lazo se reduce, estas variaciones periódicas se atenúan y las prestaciones mejoran. Sin embargo, la reducción del ancho de banda del lazo también disminuye la capacidad de seguimiento del *jitter*, llegando un momento en que las prestaciones decaen rápidamente. Este compromiso dificulta la elección del ancho de banda más apropiado. Más aún, se ha determinado que incluso empleando el ancho de banda óptimo, la distorsión causada por los errores de sincronización provoca importantes pérdidas de régimen binario en los canales residenciales.

En esta tesis se proponen dos modificaciones para reducir las pérdidas anteriores. La primera consiste en diseñar un estimador del error de fase que tenga en cuenta las variaciones cíclicas del canal. Puesto que la función densidad de probabilidad de estas variaciones no es conocida, el diseño emplea el criterio LS (*Least Squares*). Sin embargo, el estimador resultante tiene un elevado coste computacional. Para reducirlo se proponen una serie de simplificaciones que, con una degradación mínima de prestaciones, consiguen que su complejidad sea finalmente similar a la del estimador habitualmente empleado en las aplicaciones DSL [98].

La segunda modificación consiste en aumentar la atenuación que el lazo introduce sobre las componentes de error inducidas por las variaciones del canal a la salida del estimador de fase. Debido al carácter periódico de este error, en lugar de aumentar el orden del filtro, resulta más conveniente introducir filtros banda-eliminada en el lazo. Estos filtros se obtienen a partir de prototipos analógicos empleando la transformación bilineal. Se ha comprobado que la inclusión de más de tres de estos filtros apenas mejora las prestaciones y, por contra, reduce notablemente el rango de estabilidad del sistema. La inclusión del nuevo estimador y un lazo con tres

filtros banda-eliminada consigue acabar, prácticamente por completo, con la pérdida de régimen binario del esquema de sincronización convencional.

Estas aportaciones han sido parcialmente publicadas en [91] y [114].

A.2.4 Acceso múltiple DMT-FDMA

Antecedentes

Una vez que se han estudiado buena parte de los principales aspectos relacionados con la modulación DMT, se aborda el problema del uso compartido de la red eléctrica interior entre múltiples usuarios. Para conseguir los requisitos de calidad de servicio (QoS) que requieren algunas aplicaciones multimedia, los sistemas PLC comerciales actuales utilizan un esquema TDMA centralizado. En estos, la asignación de recursos es realizada por un elemento que actúa como maestro [23], [64]. Cada usuario recibe un número de intervalos temporales conforme a sus requisitos de QoS. Durante dichos intervalos el usuario dispone de forma exclusiva de todo el ancho de banda. Puesto que las portadoras no usadas en un determinado enlace por su baja SNR pueden tener valores aceptables de SNR en otros enlaces, esta estrategia conlleva un desperdicio de capacidad de transmisión.

La técnica de acceso múltiple FDMA evita el problema de infrautilización de los recursos espectrales de los esquemas TDMA, ya que aquellas subbandas con malas características de transmisión para un usuario pueden ser asignadas a otro usuario. Tradicionalmente, FDMA requería el empleo de filtros analógicos, lo que además reducía la flexibilidad en la asignación de bandas. Sin embargo, cuando se usa DMT este proceso puede realizarse de forma digital en la DFT. El coste es un aumento en el número de bits requeridos en el ADC [53]. En el lado negativo, el uso de FDMA requiere sincronización de símbolo y frecuencia en las transmisiones de los usuarios para evitar la aparición de una fuerte MAI [50], [56]. No obstante, en entornos DSL se ha demostrado que estos dos requisitos pueden obviarse mediante el empleo de *pulse-shaping*, *windowing* y la asignación a cada usuario de grupos de portadoras contiguas, lo que se conoce como *tone-grouping*.

En lo que respecta a la duplexación, TDD es la técnica actualmente usada por los sistemas comerciales [23], [64]. Sin embargo, no existen, en conocimiento del autor, trabajos sobre el número de bits necesarios en el ADC, ni tampoco estudios que justifiquen cuantitativamente el descarte de FDD.

Aportaciones

Esta tesis realiza un estudio detallado del esquema DMT-FDMA. En primer lugar, se analizan las causas de la MAI y su importancia relativa en las prestaciones de un sistema DMT con pulsos rectangulares. Aunque el uso combinado de *pulse-shaping*, *windowing* y *tone-grouping* reduce los efectos de la MAI, también disminuye la tasa de símbolo. Por tanto, deben determinarse los posibles beneficios obtenidos con estas técnicas. Finalmente, se calculará el número de bits necesarios en el ADC cuando se utiliza DMT-FDMA tanto con duplexación TDD como FDD.

Conforme a los resultados obtenidos el capítulo 3, la ICI causada por la variación temporal del canal puede considerarse despreciable siempre que el número de portadoras sea menor que 2048. En estas condiciones, un sistema DMT-FDMA experimenta dos fuentes de MAI. La primera es causada por la selectividad en frecuencia del canal y podría eliminarse aumentando la longitud del prefijo cíclico. Sin embargo, esto conllevaría una enorme reducción de la tasa de símbolo. La segunda fuente de MAI se da cuando no existe sincronización entre los distintos terminales de la red. Esta asincronía entre terminales puede ser de símbolo o de frecuencia. La primera ocurre cuando los símbolos procedentes del transmisor deseado y de los interferentes no están alineados a la entrada de la DFT del receptor deseado. La segunda se produce cuando, incluso existiendo alineación entre los símbolos deseados e interferentes a la entrada de la DFT, existen errores de frecuencia entre los relojes de los terminales.

Se ha comprobado que la MAI causada por la selectividad en frecuencia del canal es prácticamente despreciable. Por contra, el efecto de la asincronía de símbolo tiene un efecto devastador sobre las prestaciones de un esquema DMT-FDMA con pulsos rectangulares, llegando a impedir por completo la comunicación. Del mismo modo, los efectos causados por la asincronía de frecuencia pueden llegar a ser también dramáticos. Así, un error de frecuencia de 20ppm entre los terminales de la red puede provocar una pérdida de régimen binario, respecto a la situación de sincronismo perfecto, de hasta el 90%. Como forma para reducir la magnitud de la MAI se han evaluado estrategias de asignación de portadoras de tipo *tone-grouping*. Sin embargo, cuando se emplean pulsos rectangulares la mejora obtenida es pequeña o nula.

A continuación se han investigado los beneficios proporcionados por las técnicas de *pulse-shaping* y *windowing*. Se ha realizado un análisis para determinar los parámetros más apropiados de ambas técnicas en cada una de las situaciones. Se comprobado que el empleo de *pulse-shaping* y *windowing* reduce la MAI debida a la asincronía de símbolo. Sin embargo, el uso de *pulse-shaping* es siempre perjudicial en presencia de asincronía de frecuencia. En ambas situaciones la asignación de portadoras de tipo *tone-grouping* ofrece considerables incrementos de régimen binario. En cualquier caso, los resultados obtenidos muestran que estas técnicas solo logran contener el efecto de la MAI cuando el número de subbandas es pequeño, lo que limita el número de posibles usuarios de la red.

En última instancia se aborda el estudio de las técnicas de duplexación. La problemática de la cuestión reside en que, tanto en TDD como en FDD, la señal de entrada al ADC estará compuesta por un término de señal deseada y por otro interferente proveniente del resto de usuarios de la red. Esto hace que el tradicional compromiso entre ruido de cuantificación y ruido de sobrecarga sea aún más acusado. En el análisis realizado se ha determinado la pérdida de régimen binario que ocurre como consecuencia del ruido introducido en el proceso de conversión analógico-digital. Se ha comprobado que el empleo de un ADC de 16 bits hace que esta pérdida sea inferior al 5%. Este valor sube hasta el 18% cuando se emplea un ADC de 14 bits. En ambos casos, las diferencias existentes entre una y otra técnica no llegan al 10%.

Las aportaciones aquí presentadas han sido parcialmente publicadas en [121].

A.3 Conclusiones

A.3.1 Aportaciones

En esta tesis doctoral se ha estudiado la utilización de la modulación DMT para comunicaciones de banda ancha por la red eléctrica del interior de los edificios. El análisis realizado ha abarcado los principales elementos relacionados con esta técnica de transmisión: selección de los parámetros de la modulación, igualación, sincronización y acceso múltiple. A continuación se resumen brevemente las principales aportaciones realizadas:

- Caracterización del canal. Se han realizado tres aportaciones en el ámbito de la caracterización de canal: relación entre el *delay spread* y el ancho de banda de coherencia, caracterización de las variaciones temporales y discusión de la distribución de probabilidad del ruido. En lo que concierne a la primera, se ha determinado una expresión analítica que relaciona ambos elementos. Sobre la segunda, se definido una figura similar al ancho de banda Doppler para caracterizar la velocidad de las variaciones temporales y se han calculado valores estadísticos del mismo sobre un conjunto de más de 50 canales medidos. En lo que respecta a la función densidad de probabilidad del ruido, se ha concluido que la distribución Gaussiana es valida para aquellas fases del ciclo de red en la que no existan componentes de ruido periódico impulsivo.

- Cálculo analítico de la distorsión causada por un canal LPTV. Se ha mostrado que la distorsión causada por los canales de la red eléctrica puede separarse en dos componentes independientes: la debida a la selectividad en frecuencia del canal y la debida a las variaciones temporales. Además, se ha mostrado que la primera de ellas es esencialmente invariante a lo largo del ciclo de red. Se ha propuesto un método analítico que permite el cálculo de ambas de una forma mucho más eficiente que las simulaciones LTPV.

- Determinación del número de portadoras y prefijo cíclico óptimos. Se ha determinado que en un entorno monousuario las prestaciones de un sistema DMT se maximizan empleando 8192 portadoras y un prefijo cíclico de 300 muestras (a 50MHz). Un mayor número de portadoras aumenta la distorsión creada por las variaciones temporales del canal y uno menor aumenta la distorsión debida a la selectividad en frecuencia.

- Igualación temporal. Se ha demostrado que el uso de un igualador temporal no está justificado desde el punto de vista de la ganancia de prestaciones, ya que pueden conseguirse mejores resultados con otras alternativas de menor coste computacional como doblar el número de portadoras. Este resultado contrasta con las buenos resultados de estos igualadores en canales DSL. La razón de esta diferencia estriba en que los canales de la red eléctrica no se ajustan al clásico modelo polo-cero de estos entornos, donde la cancelación de un par de polos aumenta el confinamiento de la respuesta al impulso en más de 30dB.

- Modulación adaptativa. Se han analizado las ganancias de régimen binario que pueden obtenerse cuando la constelación empleada en cada portadora se adapta a las condiciones

instantáneas del canal. Para ello se ha desarrollado un conjunto de algoritmos de *bit-loading* que resuelven el problema de la asignación de constelaciones bajo los criterios de tasa de error instantánea (IBER) y de tasa de error media (ABER). Se ha comprobado que el empleo de un criterio IBER produce una pérdida de régimen binario mínima con respecto al caso ABER. Además, la pérdida de prestaciones causada por el uso de un esquema de modulación fijo cuando se emplea la banda de 1MHz a 20MHz es, en general, pequeña. Sin embargo, puede ser considerable en sistemas que empleen una banda más estrecha. Se ha mostrado también que la degradación de prestaciones es menor en sistemas con un menor número de portadoras, ya que en este caso la distorsión dominante es la causada por la selectividad en frecuencia del canal, que es esencialmente invariante con el tiempo.

- Análisis y diseño de esquemas de recuperación de sincronismo. Se han analizado las prestaciones que pueden obtenerse con los esquemas de recuperación de sincronismo ayudados por la decisión empleados habitualmente en entornos con elevadas relaciones señal a ruido. Como consecuencia de las rápidas variaciones del canal surge el problema de la interacción entre los bloques de igualación y sincronización. Para evitarlo se ha propuesto un FEQ en dos etapas: la primera compensa las variaciones a largo plazo del canal y la segunda las variaciones cíclicas. Las prestaciones del sistema resultante están limitadas por dos elementos. Para anchos de banda grandes, por las variaciones periódicas del canal, que sesgan la estima del error de fase. Y para anchos de banda estrechos por la capacidad del lazo para seguir el *jitter* del proceso de muestreo. Se ha demostrado que esta última no-idealidad, que es tradicionalmente despreciada, representa un papel muy importante en este caso.

  Para mejorar las prestaciones se han propuesto dos modificaciones. La primera es un nuevo estimador de fase que tiene en cuenta las variaciones cíclicas del canal. La segunda es la inserción en el lazo de seguimiento de una serie de filtros banda-eliminada sintonizados a la frecuencia de los armónicos de las variaciones del canal. El sistema resultante conseguir eliminar, prácticamente por completo, la pérdida de régimen binario ocasionada por la distorsión introducida por el sistema de sincronización.

- Acceso múltiple DMT-FDMA. Se ha investigado la viabilidad de un esquema de acceso múltiple FDMA que emplee un número de portadoras del orden de los usados por los sistemas comerciales actuales. Se han identificado las dos fuentes principales de interferencia: la causada por la selectividad en frecuencia del canal y la asincronía de símbolo y frecuencia entre los terminales. La primera tiene un efecto despreciable en una red sincronizada. La segunda hace inviable el uso de esta estrategia de acceso múltiple cuando se emplea un sistema DMT con pulsos rectangulares. Incluso cuando se usan las técnicas de *pulse-shaping*, *windowing* y *tone-grouping*, una red DMT-FDMA asíncrona solo es factible para un número de terminales reducido.

- Separación digital de bandas. Se he comprobado que para llevar a cabo la separación digital de bandas en una red DMT-FDMA sincronizada se necesita un ADC de, al menos, 16 bits. De esta forma se asegura que la pérdida de régimen binario es inferior al 5% tanto usando duplexación en tiempo como en frecuencia. Además, se ha comprobado que el

uso de FDD produce, en media, una degradación de prestaciones inferior al 15%, incluso cuando se usa un ADC de 12 bits.

A.3.2 Líneas futuras de trabajo

En lo que respecta a las técnicas de transmisión multiportadora, algunas de las líneas de continuación más directamente relacionadas con los aspectos tratados en esta tesis son los siguientes:

- Igualación en frecuencia. Las variaciones cíclicas del canal hacen de este un tema realmente interesante cuyo estudio ya ha sido iniciado. Los resultados preliminares se han limitado al análisis de técnicas empleadas en otros entornos [60]. Sin embargo, son las estrategias basadas en la descomposición de la respuesta del canal en términos de funciones periódicas las que parecen ofrecer más posibilidades.

- Análisis de un esquema de acceso múltiple TDMA. El empleo de una estrategia de acceso múltiple por división en tiempo tiene importantes implicaciones en partes esenciales del sistema como la sincronización y la igualación. Sin embargo, dejando al margen estos elementos, resulta también interesante determinar las prestaciones y complejidad de implementación de este esquema y compararlas con las ya obtenidas para FDMA.

- Codificación de canal. El objetivo es estudiar la ganancia de prestaciones que se obtiene al adaptar periódicamente la tasa del código, o incluso el propio esquema de codificación, a las condiciones instantáneas del canal.

- Evaluación de otras técnicas multiportadora. En esta tesis se ha mostrado que la viabilidad de un esquema DMT-FDMA viene limitada por la interferencia de acceso múltiple. Se trata, pues, de analizar las prestaciones que se obtienen cuando se emplea una modulación multiportadora con mayor confinamiento espectral, como es el caso de FMT (*Filtered MultiTone*).

References

[1] C. R. Loubery, "Einrichtung zur elektrischen zeichengebung an die theilnehmer eines starkstromnetzes," Kaiserlichen Patenamt, March 1901.

[2] X10 Technology Transmission Theory. [Online]. Available: www.x10.com/technology1.htm, Last visited 19-02-2007.

[3] A. Sanz, J. I. García, I. Urriza, and A. Valdovinos, "A complete node for the power line medium of european home systems specifications," in *Proceedings of the International Symposium on Power Line Communications and its Applications (ISPLC)*, 2001, pp. 53–58.

[4] CENELEC, "Signalling on low-voltage electrical installations in the frequency range 3 kHz to 148.5 kHz," *EN 50065*, 1991.

[5] PLC Utilities Alliance, "Powerline an alternative technology in the local loop," 2004. [Online]. Available: http://www.ieee802.org/802_tutorials/march04/plc-040308_IEEE_V4.pdf, Last visited:19-02-2007.

[6] El País, "Endesa cierra en Zaragoza el servicio piloto de acceso a internet a través del enchufe," February 2006. [Online]. Available: http://www.elpais.com/articulo/portada/Endesa/cierra/Zaragoza/servicio/piloto/acceso/Internet/traves/enchufe/elpcibpor/20060202elpcibpor_1/Tes, Last visited 20-02-2007.

[7] Iberdrola PLC: http://www.plciberdrola.com/, Last visited 19-02-2007.

[8] Korea Now (Biweekly Magazine), "Information technology enhances electricity sector," March 2005. [Online]. Available: http://koreanow.koreaherald.co.kr, Last visited: 19-02-2007

[9] The Wi-Fi Alliance. [Online]. Available: http://www.wifi.org, Last visited: 19-02-2007.

[10] V. Degardin, P. Laly, M. Lienard, and P. Degauque, "Impulsive noise on in-vehicle power lines: Characterization and impact on communication performance," in *Proceedings of the IEEE International Symposium on Power Line Communications and its Applications (ISPLC)*, March 2006, pp. 222–226.

[11] P. Karols, K. Dostert, G. Griepentrog, and S. Huettinger, "Mass transit power traction networks as communication channels," *IEEE Journal on Selected Areas on Communications*, vol. 24, no. 7, pp. 1339–1350, July 2006.

[12] Federal Communications Commission, "Code of Federal Regulations Title 47 Telecommunication: Chap- ter I FCC Part 15 - Radio Frequency Devices," Washington DC, USA, 10-1- 98-Edition, pp. 635-680.

[13] CENELEC, "Limits and methods of measurement of radio disturbance characteristics of information technology equipment," *EN 55022*, 1994.

[14] International Electrotechnical Commission (IEC), "CISPR 22: Information Technology Equipment-Radio Disturbance Characteristics-Limits and Methods of Measurement," Third Edition, 1997.

[15] ETSI, "Powerline Telecommunications (PLT). Coexistence of Access and In-House Powerline Systems," *TS 101 867 V1.1.1*, 2000.

[16] K. Dostert, "EMC aspects of high speed powerline communications," in *Proceedings of the 15th International Wroclaw Symposium and Exhibition on Electromagnetic Compatibility*, June 2000, pp. 98–102.

[17] M. Götz, M. Rapp, and K. Dostert, "Power line channel characteristics and their effect on communication system design," *IEEE Communications Magazine*, vol. 42, pp. 78–86, April 2004.

[18] T. Sartenaer, "Multiuser communications over frequency selective wired channels and applications to the powerline access network," Ph.D. dissertation, Faculté des Sciences Appliquées, Université Catholique de Louvain, September 2004.

[19] IEEE P1775, "Standard for powerline communication equipment: electromagnetic compatibility (EMC) requirements: testing and measurement methods." [Online]. Available: http://grouper.ieee.org/groups/bpl, Last visited: 19-02-2007.

[20] Electronic Industries Alliance, "Power line physical layer and medium specification (CE-Bus standard)," *EIA-600.31*, 1995.

[21] PolyTrax Information Technology. [Online]. Available: http://www.polytrax.com/3tech/3poly.html, Last visited: 19-02-2007.

[22] M. Lee, R. Newman, H. Latchman, S. Katar, and L. Yonge, "Homeplug 1.0 powerline communication LANs-protocol description and performance results," *International Journal of Communication Systems*, vol. 16, no. 5, pp. 447–473, May 2003.

[23] Homeplug, "HomePlug AV White Paper," Homeplug, Tech. Rep., 2005.

[24] Design of Systems on Silicon (DS2): www.ds2.com, Last visited 19-02-2007.

[25] HomePlug Powerline Alliance. [Online]. Available: http://www.homeplug.com, Last visited 19-02-2007.

[26] IEEE P1901, "Draft standard for broadband over power line networks: medium access control and physical layer specifications." [Online]. Available: http://grouper.ieee.org/groups/1901, Last visited: 19-02-2007.

[27] S. Galli and T. C. Banwell, "A deterministic frequency-domain model for the indoor power line transfer function," *IEEE Journal on Selected Areas on Communications*, vol. 24, no. 7, pp. 1304–1316, July 2006.

[28] F. J. Cañete, J. A. Cortés, L. Díez, and J. T. Entrambasaguas, "Modeling and evaluation of the indoor power line channel," *IEEE Communications Magazine*, vol. 41, no. 4, pp. 41–47, Apr 2003.

[29] H. Philipps, "Performance measurements of power-line channels at high frequencies," in *Proceedings of the International Symposium on Power Line Communications and its Applications (ISPLC)*, 1998, pp. 229–237.

[30] J. G. Proakis, *Digital Communications*. McGraw-Hill, 1995.

[31] J. A. Cortés, F. J. Cañete, L. Díez, and J. T. Entrambasaguas, "Characterization of the cyclic short-time variation of indoor power-line channels response," in *Proceedings of the International Symposium on Power Line Communications and its Applications (ISPLC)*, 2005, pp. 326–330.

[32] D. Liu, E. Flint, B. Gaucher, and Y. Kwark, "Wide band AC power line characterization," *IEEE Transactions on Consumer Electronics*, vol. 45, no. 4, pp. 1087–1097, November 1999.

[33] F. J. Cañete, L. Díez, J. A. Cortés, and J. T. Entrambasaguas, "Broadband modelling of indoor power-line channels," *IEEE Transactions on Consumer Electronics*, pp. 175–183, Feb 2002.

[34] F. J. Cañete, J. A. Cortés, L. Díez, and J. T. Entrambasaguas, "Analysis of the cyclic short-term variation of indoor power line channels," *IEEE Journal on Selected Areas on Communications*, vol. 24, no. 7, pp. 1327–1338, July 2006.

[35] O. Ohno, M. Katayama, T. Yamazato, and A. Ogawa, "A simple model of cyclo-stationary powerline noise for communication systems," in *Proceedings of the International Symposium on Power Line Communications and its Applications (ISPLC)*, 1998, pp. 115–122.

[36] IEEE Journal on Selected Areas on Communications. Special Issue on Power Line Communications, Vol. 25, Issue. 7, July 2006.

[37] International Symposium on Power Line Communications and Its Applications (ISPLC) home page: www.isplc.org.

[38] H. Philipps, "Modelling of power line communication channels," in *Proceedings of the International Symposium on Power Line Communications and its Applications (ISPLC)*, 1999, pp. 14–21.

[39] M. Zimmermann and K. Dostert, "A multipath model for the powerline channel," *IEEE Transactions on Communications*, vol. 50, no. 4, pp. 553–559, April 2002.

[40] F. R. Esmailian, T. Kschischang and P. G. Gulak, "In-building power lines as high-speed communication channels: channel characterization and a test channel ensemble," *International Journal of Communications*, vol. 16, pp. 381–400, June 2003.

[41] F. J. Cañete, "Caracterización y modelado de redes eléctricas interiores como medio de transmisión de banda ancha," Ph.D. dissertation, ETSI de Telecomunicación, Universidad de Málaga, 2004.

[42] E. Biglieri, "Coding and modulation for a horrible channel," *IEEE Communications Magazine*, vol. 41, no. 4, pp. 92–98, May 2003.

[43] T. Sartenaer, F. Horlin, and L. Vandendorpe, "Multiple access techniques for wideband upstream powerline communications: CAP-CDMA and DMT-FDMA," in *Proceedings of the IEEE International Conference Communications (ICC)*, June 2000, pp. 1064 – 1068.

[44] W. Hachem, P. Loubaton, S. Marcos, and R. Samy, "Multiple access communication over the power line channel: a CDMA approach," in *Proceedings of the IEEE Global Telecommunications Conference (Globecom)*, November 2001, pp. 420–424.

[45] G. Mathisen and A. M. Tonello, "WireNet: An experimental system for in-house power line communication," in *Proceedings of the International Symposium on Power Line Communications and its Applications (ISPLC)*, March 2006, pp. 137–142.

[46] Yitran Communications. [Online]. Available: http://www.itrancomm.com, Last visited 19-02-2007.

[47] O. Edfors, M. Sandell, J. Van de Beek, D. Landström, and F. Sjöber, *An introduction to orthogonal-frequency division multiplexing.* Research Report , Division of Signal Processing, Luleå University of Technology, September 1996.

[48] D. Ruiz, A. Salas, A. Badenes, D. Arlandis, V. Romero, and J. C. Riveiro, "In-home AV PLC MAC with neighboring networks support," in *Proceedings of the International Symposium on Power Line Communications and its Applications (ISPLC)*, April 2005, pp. 17–21.

[49] P. G. Flikkema, "On multiple access and capacity in frequency-selective channels," in *Proceedings of the IEEE International Conference on Information Technology, Coding and Computing*, 2001, pp. 178–182.

[50] J. J. van de Beek, P. O. Börjesson, M. L. Boucheret, D. Landström, J. Martinez Arenas, P. Ödling, C. Östherg, M. Wahlqvist, and S. K. Wilson, "A time and frequency synchronization scheme for multiuser OFDM," *IEEE Journal on Selected Areas in Communications*, vol. 17, no. 11, pp. 1900–1914, November 1999.

[51] C. Y. Wong, R. S. Cheng, K. B. Letaief, and R. D. Murch, "Multiuser OFDM with adaptive subcarrier, bit, and power allocation," *IEEE Journal on Selected Areas in Communications*, vol. 17, no. 10, pp. 1747–1457, October 1999.

[52] W. Yu and J. M. Cioffi, "FDMA capacity of gaussian multiple-access channels with ISI," *IEEE Transactions on Communications*, vol. 50, no. 1, pp. 102–111, January 2002.

[53] J. M. Cioffi et al., "ADC precision contributions," *See BOTH ANSI T1E1.4 contributions 99-274R2 (June, 1999, Ottawa) and 99-274R3 (August, 1999 Baltimore).*

[54] T. Pollet, M. Bladel, and M. M., "BER sensitivity of OFDM systems to carrier frequency offset and Wiener phase noise," *IEEE Transactions on Communications*, vol. 43, no. 2/3/4, pp. 191–193, 1995.

[55] H. Steendam and M. Moeneclaey, "Analysis and optimization of the performance of OFDM on frequency-selective time-selective fading channels," *IEEE Transactions on Communications*, vol. 47, no. 12, pp. 1811–1819, 1999.

[56] F. Sjöberg, R. Nilsson, M. Isaksson, P. Ödling, and B. P. O., "Asynchronous Zipper," in *Proceedings of the IEEE International Conference on Communications (ICC)*, 1999, pp. 231–235.

[57] J. S. Chow, J. C. Tu, and J. M. Cioffi, "A discrete multitone transceiver system for HDSL applications," *IEEE Journal on Selected Areas on Communications*, vol. 9, no. 6, pp. 895–908, 1991.

[58] T. Pollet, M. Peeters, M. Moonen, and L. Vandendorpe, "Equalization for DMT-based broadband modems," *IEEE Communications Magazine*, vol. 38, no. 5, pp. 106–113, May 2000.

[59] R. Garaluz, "Estudio de algoritmos de procesado de señal aplicados a la transmisión sobre la red eléctrica." Master's thesis, ETSIT, Universidad de Málaga, 2004.

[60] J. A. Cortés, A. Tonello, and L. Díez, "Comparative analysis of pilot-based channel estimators for DMT systems over indoor power-line channels," in *Proceedings of the IEEE International Symposium on Power Line Communications and its Applications (ISPLC)*, March 2007.

[61] A. Goldsmith and S. Chua, "Variable-rate variable-power MQAM for fading channels," *IEEE Transactions on Communications*, vol. 45, no. 10, pp. 1218–1230, October 1997.

[62] E. Lee and D. Messerschmitt, *Digital Communication.* Kluwer Academic Publishers, 1994.

[63] E. Martos Naya, "Optimización de técnicas de sincronización en sistemas de transmisión multiportadora," Ph.D. dissertation, ETSI de Telecomunicación, Universidad de Málaga, 2005.

[64] D. Gutierrez, L. M. Torres, F. Blasco, J. Carreras, and J. C. Riveiro, "In-home PLC ready for triple play," in *Proceedings of the International Symposium on Power Line Communications and its Applications (ISPLC)*, 2005, pp. 366–370.

[65] M. Zimmermann and K. Dostert, "Analysis and modeling of impulsive noise in broadband powerline communications," *IEEE Transactions on Electromagnetic Compatibility*, vol. 44, no. 1, pp. 249–258, February 2002.

[66] F. J. Cañete, J. A. Cortés, L. Díez, J. T. Entrambasaguas, and J. L. Carmona, "Fundamentals of the cyclic short-time variation of indoor power-line channels," in *Proceedings of the International Symposium on Power Line Communications and its Applications (ISPLC)*, 2005, pp. 157–161.

[67] ETSI, "Powerline telecommunications PLT; hidden node review and statistical analysis," *TR 102 269 V1.1.1 (2003-12)*, 2003.

[68] W. A. Gardner, *Introduction to Random Processes*. MacMillan, 1986.

[69] S. Stein, "Fading channels issues in system engineering," *IEEE Journal on Selected Areas on Communications*, vol. 5, no. 2, pp. 68–89, February 1987.

[70] M. Babic, M. Hagenau, K. Dostert, and J. Bausch, "D4: Theoretical postulation of PLC channel model," Opera, Tech. Rep., 2005.

[71] S. J. Howard and K. Palavan, "Doppler spread measurements of indoor radio channel," *Electronics Letter*, vol. 26, no. 2, pp. 107–110, 1990.

[72] V. Degardin, M. Lienard, and P. Degauque, "Transmission on indoor power lines: from a stochastic channel model to the optimization and performance evaluation of multicarrier systems," *International Journal of Communication Systems*, vol. 16, no. 5, pp. 363–379, June 2003.

[73] H. Meng, Y. L. Guan, and S. Chen, "Modeling and analysis of noise effects on broadband power-line communications," *IEEE Transactions on Power Delivery*, vol. 20, no. 2, pp. 630–637, April 2005.

[74] M. Katayama, T. Yamazato, and H. Okada, "A mathematical model of noise in narrowband power line communication systems," *IEEE Journal on Selected Areas on Communications*, vol. 24, no. 7, pp. 1267–1276, July 2006.

[75] C. E. Shannon, "A mathematical theory of communication," *The Bell System Technical Journal*, vol. 27, pp. 379–423, 623–656, July, October 1948.

[76] A. Goldsmith, *Wireless Communications*. Cambridge University Press, 2005.

[77] J. Wolfowitz, *Coding Theorems of Information Theory*. Springer-Verlag, 1964.

[78] A. Goldsmith and P. Varaiya, "Capacity of fading channels with channel side information," *IEEE Transactions on Information Theory*, vol. 43, no. 6, pp. 1986–1992, November 1997.

[79] E. Biglieri, J. Proakis, and S. Shamai, "Fading channels: Information-theoretic and communications aspects," *IEEE Journal on Information Theory*, vol. 44, no. 6, pp. 2619–2692, October 1998.

[80] S. Diggavi, "Analysis of multicarrier transmission in time-varying channels," in *Proceedings of the IEEE International Conference on Communications (ICC)*, vol. 3, June 1997, pp. 1191–1195.

[81] S. Barbarossa and A. Scaglione, "Optimal precoding for transmissions over linear time-varying channels," in *Proceedings of the Global Telecommunications Conference (Globecom)*, vol. 5, December 1999, pp. 2545 – 2549.

[82] S. T. Chung and A. J. Goldsmith, "Degrees of freedom in adaptive modulation: A unified view," *IEEE Transactions on Communications*, vol. 49, no. 9, pp. 1561–1571, September 2001.

[83] M. L. Doelz, E. T. Heald, and D. L. Martin, "Binary data transmission techniques for linear systems," *Proceedings IRE*, vol. 44, pp. 656–661, 1957.

[84] S. B. Weinstein and P. M. Ebert, "Data transmission by frequency-division multiplexing using de discrete fourier transform," *IEEE Transactions on Communications*, vol. 19, no. 5, pp. 628–634, Oct 1971.

[85] A. Peled and A. Ruiz, "Frequency domain data transmission using reduced computational complexity algorithms," in *Proceedings of the IEEE Internatonal Conference on Acoustics, Speech, Signal Processing*, 1980, pp. 964–967.

[86] P. Spruyt, P. Reusens, and S. Braet, "Performance of improved DMT transceiver for VDSL," Tech. Report T1E1.4/96-104, ANSI, Colorado Springs, CO, Apr., Tech. Rep., 1996.

[87] G. Cherubini, E. Eleftheriou, S. Ölçer, and J. M. Cioffi, "Filter bank modulation techniques for very high-speed digital subscriber lines," *IEEE Communications Magazine*, vol. 38, no. 5, pp. 98–104, 2000.

[88] S. D. Sandberg and M. A. Tzannes, "Overlapped discrete multitone modulation for high speed copper wire communications," *IEEE Journal on Selected Areas on Communications*, vol. 13, no. 9, pp. 1571–1585, 1995.

[89] J. Abad, L. M. Torres, and J. C. Riveiro, "OFDM and wavelets performance comparison in power line channels," in *Proceedings of the International Symposium on Power-Line Communications and its Applications (ISPLC)*, 2005, pp. 341–345.

[90] J. A. Cortés, L. Díez, F. J. Cañete, and J. T. Entrambasaguas, "System parameters effect on DMT-based broadband indoor power line communications," in *International Symposium on Power-Line Communications and its Applications (ISPLC)*, 2002, pp. 48–52.

[91] J. A. Cortés, L. Díez, E. Martos, F. J. Cañete, and J. T. Entrambasaguas, "Analysis of timing recovery for DMT systems over indoor power-line channels," in *Proceedings of the IEEE Global Telecommunications Conference (Globecom)*, November 2006.

[92] A. Oppenheim and R. Schafer, *Tratamiento de señales en tiempo discreto*. Prentice Hall, 2000.

[93] P. S. Chow, J. M. Cioffi, and A. C. Bingham, "A practical discrete multitone transceiver loading algorithm for data transmission over spectrally shaped channels," *IEEE Transactions on Communications*, vol. 43, no. 2/3/4, pp. 773–775, 1995.

[94] J. Campello, "Practical bit loading for DMT," in *Proceedings of the IEEE International Conference on Communications (ICC)*, 1999, pp. 801–805.

[95] J. A. Cortés, L. Díez, F. J. Cañete, and J. T. Entrambasaguas, "Bit-loading algorithm for DMT broadband indoor power line communications," in *Proceedings of the IASTED International Conference on Communications Systems and Networks*, 2002, pp. 278–282.

[96] D. Hughes-Hartogs, "Ensemble modem structure for imperfect transmission media," U.S. Patent 4 679 227, July 1987.

[97] I. Kalet, "The multitone channel," *IEEE Transactions on Communications*, vol. 37, no. 2, pp. 119–124, 1989.

[98] T. Pollet and M. Peeters, "Synchronization with DMT modulation," *IEEE Communications Magazine*, vol. 37, no. 4, pp. 80–86, 1999.

[99] J. S. Chow, J. M. Cioffi, and J. A. C. Bingham, "Equalizer training algorithms for multicarrier modulation systems," in *Proceedings of the IEEE International Conference on Communications*, vol. 2, May 1993, pp. 761–765.

[100] P. J. W. Melsa, R. C. Younce, and C. Rohrs, "Impulse response shortening for discrete multitone transceivers," *IEEE Transactions on Communications*, vol. 44, no. 12, pp. 1662–1672, December 1996.

[101] J. López Fernández, "Procedimientos de igualación, sincronización y medida para la transmisión digital asimétrica de alta velocidad por bucles de abonado," Ph.D. dissertation, ETSIT, Universidad de Málaga, 2001.

[102] N. Al-Dhahir and J. M. Cioffi, "Optimum finite-length equalization for multicarrier transceivers," *IEEE Transactions on Communications*, vol. 44, no. 1, pp. 56–64, August 1996.

[103] M. Russel and G. L. Stüber, "Interchannel interference analysis of OFDM in a mobile environmnent," in *Proceedings of the IEEE VTC*, 1995, pp. 820–824.

[104] Y. Li and L. J. Cimini, "Bounds on the interchannel interference of OFDM in time-varying impairments," *IEEE Transactions on Communications*, vol. 49, no. 3, pp. 401–404, 2001.

[105] S. M. Phoong and P. P. Vaidyanathan, "Time-varying filters and filter banks: Some basic principles," *IEEE Transactions on Signal Processing*, vol. 44, no. 12, pp. 2971–2987, December 1996.

[106] T. Keller and L. Hanzo, "Adaptive multicarrier modulation: a convenient framework for time-frequency processing in wireless communications," *Proceedings of the IEEE*, vol. 88, no. 5, pp. 611 – 640, May 2000.

[107] M. C. Aguayo, "Modulación multiportadora adaptativa para canales selectivos en frecuencia con desvanecimientos," Ph.D. dissertation, ETSI de Telecomunicación, Universidad de Málaga, 2001.

[108] B. Canpolat and Y. Tanik, "Performance analysis of adaptive loading OFDM under Rayleigh fading," *IEEE Transactions on Vehicular Technology*, vol. 53, no. 4, pp. 1105–1115, July 2004.

[109] J. Cioffi, *Lecture notes for Advanced Digital Communications, Stanford University*, Fall 2001.

[110] M. Crussière, J. Baudais, and J. Hélard, "Adaptive spread-spectrum multicarrier multiple-access over wirelines," *IEEE Journal on Selected Areas on Communications*, vol. 24, no. 7, pp. 1377–1388, July 2006.

[111] T. N. Zogakis and J. M. Cioffi, "The effect of timing jitter on the performance of a discrete multitone system," *IEEE Transactions on Communications*, vol. 44, no. 7, pp. 799–808, July 1996.

[112] E. Martos, J. López, L. Díez, M. C. Aguayo, and J. T. Entrambasaguas, "Optimized interpolator filters for timing error correction in DMT systems for xDSL applications," *IEEE Journal on Selected Areas on Communications*, vol. 19, no. 12, pp. 2477–2485, December 2001.

[113] R. H. Walden, "Analog-to-digital converter survey and analysis," *IEEE Journal on Selected Areas on Communications*, vol. 17, no. 14, pp. 539–550, April 1999.

[114] J. A. Cortés, L. Díez, E. Martos, F. J. Cañete, and J. T. Entrambasaguas, "Analysis and design of timing recovery schemes for DMT systems over indoor power-line channels," *EURASIP Journal on Advances in Signal Processing*, vol. 2007, article ID 48931, 11 pages, 2007. doi:10.1155/2007/48931.

[115] B. Yang, K. B. Letaief, R. S. Cheng, and Z. Cao, "Timing recovery for OFDM transmission," *IEEE Journal on Selected Areas in Communications*, vol. 18, no. 11, pp. 2278–2291, November 2000.

[116] F. M. Gardner, "Interpolation in digital modems-Part I: Fundamentals," *IEEE Transactions on Communications*, vol. 3, no. 3, pp. 501–507, March 1993.

[117] H. Kopmann, "A generalised parametric error model of ultra-wideband analogue-to-digital conversion," in *Proceedings of the 3rd Karlsruhe Workshop on Software Radios, Karlsruhe*, March 2004, pp. 101–110.

[118] F. M. Gardner, *Phaselock Techniques*, 3rd ed. Wiley, 2005.

[119] IEEE-SA Stardard Board, "IEEE 1139-1999: Standard Definitions of Physical Quantities for Fundamental Frequency and Time Metrology-Random Instabilities," 1999.

[120] A. Hajimiri, S. Limotyrakis, and T. H. Lee, "Jitter and phase noise in ring oscillators," *IEEE Journal on Solid-State Circuits*, vol. 34, no. 6, pp. 790–804, June 1999.

[121] J. A. Cortés, L. Díez, F. J. Cañete, and J. T. Entrambasaguas, "Analysis of DMT-FDMA as a multiple access scheme for broadband indoor power-line communications," *IEEE Transactions on Consumer Electronics*, vol. 52, no. 4, pp. 1184–1192, November 2006.

[122] T. Banwell and S. Galli, "On the symmetry of the power line channel," in *Proceedings of the International Symposium on Power Line Communications and its Applications (ISPLC)*, April 2001.

[123] T. Sartenaer, L. Vandendorpe, and J. Louveaux, "Balanced capacity of wireline multiuser channels," *IEEE Transactions on Communications*, vol. 53, no. 12, pp. 2020–2042, December 2005.

[124] D. G. Luenberger, *Linear and Nonlinear Programming*. Addison-Wesley, 1984.

[125] D. J. G. Mestdagh, P. Spruyt, and B. Biran, "Analysis of clipping effect in DMT-based ADSL systems," in *Proceedings of the IEEE International Conference on Communications (ICC)*, vol. 1, May 1994, pp. 293–300.

[126] D. R. Morgan, "Finite limiting effects for a band-limited gaussian random process with applications to A/D," *IEEE Transactions on Acoustics, Speech and Signal Processing*, vol. 36, no. 7, pp. 1011–1016, July 1988.

[127] J. E. Mazo, "Asymptotic distortion spectrum of clipped,dc-biased, gaussian noise," *IEEE Transactions on Communications*, vol. 40, no. 8, pp. 1339–1344, August 1992.

[128] S. Katar, B. Mashburn, K. Afkhamie, H. Latchman, and R. Newman, "Channel adaptation based on cyclo-stationary noise characteristics in PLC systems," in *Proceedings of the IEEE International Symposium on Power Line Communications and its Applications (ISPLC)*, March 2006, pp. 16–21.

[129] A. Tonello and F. Pecile, "A filtered multitone (FMT) modulation modem with an efficient digital implementation for multiuser powerline communications," in *Proceedings of the IEEE International Symposium on Power Line Communications and its Applications (ISPLC)*, March 2007.